

Forschungszentrum Karlsruhe

in der Helmholtz-Gemeinschaft

Wissenschaftliche Berichte

FZKA 6800

Humic Substances in Performance Assessment of Nuclear
Waste Disposal: Actinide and Iodine Migration in the Far-Field

First Technical Progress Report

G. Buckau (Editor)

Institut für Nukleare Entsorgung

Forschungszentrum Karlsruhe GmbH, Karlsruhe
2003

Impressum der Print-Ausgabe:

**Als Manuskript gedruckt
Für diesen Bericht behalten wir uns alle Rechte vor**

**Forschungszentrum Karlsruhe GmbH
Postfach 3640, 76021 Karlsruhe**

**Mitglied der Hermann von Helmholtz-Gemeinschaft
Deutscher Forschungszentren (HGF)**

ISSN 0947-8620

Project partner:

Partner No. 1 (Coordinator): Forschungszentrum Karlsruhe GmbH (FZK/INE), D

Partner No. 2: Forschungszentrum Rossendorf (FZR-IfR), D

Partner No. 3: GSF-National Research Center for Environment and Health (GSF), D

Partner No. 4: Commissariat à l'Energie Atomique (CEA-DPC), F

Partner No. 5: University of Nantes - Presidency (U-Nantes), F

Partner No. 6: University of Manchester (U-Manch), UK

Partner No. 7: Technical University of Prague (CTU), Cz

**Partner No. 8: Fodor Jozsef National Center of Public Health, Frederic Joliot-Curie
National Research Institute of Radiobiology and Radiohygiene (FJC), HU**

Partner No. 9: University of Cyprus (UCY), Cy

Temporary contributor:

Francis Claret, FZK/INE through EC Marie-Curie Fellowship (MCFI-2001-01983)

Duration of the project:

11.2001 – 10.2004

Foreword

The present report describes progress within the first year of the EC-project “Humic Substances in Performance Assessment of Nuclear Waste Disposal: Actinide and Iodine Migration in the Far-Field”. Without being a formal requirement of the Commission or co-funding bodies, this report documents results in great technical detail and make the results available to a broad scientific community.

The report contains an executive summary written by the coordinator. More detailed results are given as individual contributions in the form of 11 annexes. Not all results are discussed or referred to in the executive summary report and thus readers with a deeper interest also need to consult the annexes.

The report also reflects the successful integration of a temporary contributor via a Marie-Curie Fellowship (MCFI-2001-01983) (Annex 11). Integration of this activity extends the scope of the project to a new potential source of humic substances in clay.

Results of the coming two years of the project will be published in the same form, i.e. as open FZKA reports.

Content	<u>Page</u>
Executive summary report (G.Buckau, FZK/INE)	1
<u>Annexes</u>	
1. Isotope exchange and spectroscopic study on kinetic modes of An(III)/Ln(III) humate complexes, J.M. Monsallier, R. Artinger, M.A. Denecke, F.J. Scherbaum, G. Buckau and J.I. Kim (FZK/INE)	25
2. Origin and mobility of groundwater humic colloids from wetland recharge in the Gorleben aquifer system, G. Buckau, M. Wolf, S. Geyer, R. Artinger and J.I. Kim (FZK/INE)	39
3. Synthetic humic acid model substances with specific functional properties for the use in complexation and sorption experiments with actinides, S. Sachs, K.H. Heise and G. Bernhard (FZR-IfR)	51
4. Determination of structural parameters for Th(IV), Np(IV), Np(V) and Pu(III) humate complexes by means of XAFS spectroscopy, K. Schmeide, S. Sachs, T. Reich, K.H. Heise and G. Bernhard (FZR-IfR)	65
5. Uranium Mining Waste Rock Pile No. 250 in the Region Schlema/Alberoda (Saxony, Germany), K. Schmeide, G. Geipel, K.H. Heise and G. Bernhard (FZR-IfR)	79
6. Chemical data on iodine-natural organic matter interaction, P. Reiller and V. Moulin (CEA)	99
7. Characterization of humic wafers by AFM, TOF-SIMS, ATR-FTIR. Development of new synthesis routes, C. Barbot, J. Pieri, J.P. Durand, F. Goudard, M. Plaschke, G. Buckau, J.I. Kim, W. Szymczak, M. Wolf and O. Bouloussa (U-Nantes, FZK/INE, GSF)	115
8. An experimental and modeling study of metal ion/humate non-exchangeable binding, N.D. Bryan, D.M. Jones, R. Keepax, P. Warwick, S. Stephens and J.J.W. Higgo (U-Manchester)	145
9. Electrophoretic determination of the degree of Eu complexation by humic acid: Analysis and assessment of experimental error, J. Mizera, P. Benes and G. Masnerova (CTU)	191
10. Preliminary results for determination of conditional stability constant for Pu(IV)-humate using immobilized humic acid on silica gel, G. Szabo, J. Gucci, T. Miyajima and A. Bulman (FJC)	203
11. Alkaline conversion of clay organic matter as a potential additional source for humic substances, F. Claret, Th. Schaefer, A. Bauer and G. Buckau (Marie-Curie Grant MCFI-2001-01983)	215

EXECUTIVE SUMMARY

HUMIC SUBSTANCES IN PERFORMANCE ASSESSMENT OF NUCLEAR WASTE DISPOSAL: ACTINIDE AND IODINE MIGRATION IN THE FAR-FIELD (HUPA)

FIRST TECHNICAL PROGRESS REPORT

**EC Contract No.: FIKW-CT-2001-00128
(Work period 11.01-10.02)**

**G. Buckau
(FZK/INE)**

Content of executive summary

	<u>Page</u>
INTRODUCTION	5
1. OBJECTIVES	6
2. PARTNERS AND PROJECT STRUCTURE	7
3. OBJECTIVES OF AND PROGRESS WITHIN INDIVIDUAL WORK PACKAGES	7
3.1 WP 1 (Critical assessment of experimental methods)	8
3.2 WP 2 (Generation and characterization of humic material)	10
3.3 WP 3 (Radionuclide humate interaction data by designed system investigations)	13
3.4 WP 4 (Characterization of radionuclide humate complexes)	14
3.5 WP 5 (Natural chemical analogue studies)	15
3.6 WP 6 (Radionuclide transport experiments)	18
3.7 WP 7 (Model development)	19
3.8 WP 8 (PA)	21
4. REFERENCES	24

INTRODUCTION

The present project is one in a series of research activities supported by the European Commission on the role of humic substances for the long-term safety of nuclear waste disposal. These activities started in the mid eighties within the MIRAGE project (MIgration of RAditionuclides in the GEosphere) with the most recent project being “Effects of humic substances on the migration of radionuclides: Complexation and transport of actinides (HUMICS)” (FI4W-CT96-0028). The HUMICS project was conducted within the fourths framework of the European Commissions research program. It started January 1997 and had a duration of three years. The results of the HUMICS project can be found in three open technical progress reports and a final report [1-4]. In analogy with the HUMICS project, the present project makes use of annual technical progress reports where individual results are published as papers in the form of annexes. By this approach, results rapidly become available to interested parties in a compact form before their publication in various scientific journals and conference proceedings. Furthermore, some of the more preliminary and/or detailed results are not likely to appear in scientific journals and proceedings.

The present project is conducted within the fifths framework of the European Commissions research program. It started November 2001 and has a duration of three years. The present report covers the first project year, i.e. November 2001 to September 2002. The project is divided into eight different work packages. These are (i) “Critical assessment of experimental methods”, (ii) “Generation and characterization of humic substances”, (iii) “Radionuclide humate interaction data by designed system investigations”, (iv) “Characterization of radionuclide humate complexes”, (v) “Natural chemical analogue studies”, (vi) “Radionuclide transport experiments”, (vii) “Model development”, and (viii) “Performance assessment”. Division of work into specified work packages sometimes is not straight forward. This is also reflected in the structure of the report. The executive summary report follows the project work package structure. The annexes focus on scientific results without reference to specific work packages. Following this approach, the reader can get an overview over the overall progress by the executive summary report. Detailed information on scientific results and the respective originators is found in the annexes. It should also be noted that some results presented in the executive summary report originate from presentations and communication within the project without being presented as an annex paper. Further information on such results can be obtained through the editor.

The overall approach of the project is to provide process understanding resting on a solid scientific ground, rationalizing the developed state of knowledge in the form of models, and visualization of the impact of humic colloid mediated actinide and iodine transport via migration cases. Application of the knowledge developed within the project to specific radioactive waste disposal strategies is the task of responsible national organizations and not within the scope of this project. The basis for application to specific disposal strategies is the

models including the required background information being provided, amongst others through the technical progress reports.

The present project builds on the long foregoing development of experience and scientific basis. It distinguishes itself from previous activities by, amongst others, inclusion of iodine next to the highly radiotoxic and long-lived actinides. As the key role of kinetics became obvious, the past project experienced a strong shift in work deviating from initial intentions. This is also reflected in the present project where a main objective is clarification of processes responsible for the wide range of dissociation kinetics observed. Access to and continuous development of advanced analytical methods is a key element in providing for continued progress. One example is x-ray spectroscopy becoming a key element in determining the coordination of humate bound actinide ions. Development and application of advanced mass spectroscopy techniques appears very promising for obtaining detailed information about processes and for the characterization of humic substances and their complexes. The time resolved laser fluorescence spectroscopy continues to be a corner stone in providing detailed process information. Finally, a main objective is to develop a thermodynamic approach reflecting the different experimental observations, contrary to the present situation where different “models” are argued for in the scientific community. Existing models reflect some aspects of available experimental data but fail to enclose other aspects and experimental observations. If this endeavor will succeed will not become clear until towards the end of the project.

1. OBJECTIVES

Nuclear energy is an important element in the energy supply in Europe. Continued use of nuclear energy contributes to a stable socio-economic development and contributes to the overall European strategic objective of lowering dependency on energy import. A key objective of the Commissions support for research in this field is providing for continued acceptance of nuclear energy by demonstrating that residues can be managed appropriately, including providing trust in the capability of safe disposal. The present project contributes to this overall objective by establishing a trustworthy scientific basis for predicting the impact of humic substances on the mobility of long-lived actinide ions and iodine in case of release from a repository in a distant future.

The direct objective of the project is to develop tools for quantification, or justification for exclusion of humic colloid mediated radionuclide migration in performance assessment (PA). It falls within the overall objective of decreasing uncertainty in long-term safety assessment of nuclear waste disposal. For this purpose, the necessary data and adequate process understanding for the radionuclide humic colloid interaction and mobility of humic colloids in natural aquatic systems is developed. The impact of humic colloid mediated radionuclide migration on PA of nuclear waste disposal is visualised by predictive modelling on real site

migration cases. The project focuses on radionuclides relevant for the long-term safety of radioactive waste disposal, i.e. the actinides and iodine.

2. PARTNERS AND PROJECT STRUCTURE

The project has 9 partners from 6 European countries (Table 1). In addition, a Marie-Curie fellowship is providing for a temporary contributor, reporting through the present project. The project structure is based on eight work packages (Table 2). Six of these work packages are of experimental character. Work package No. 7 is model development where knowledge is rationalized for application to various systems and conditions. Work package No. 8 is aiming at visualizing the impact of humic colloid mediated actinide and iodine transport under three different specified conditions, defined as three different migration cases. There is no work package specifically dealing with the origin of humic substances. Analysis of natural aquifer systems and the conversion of clay organic matter show that this is an issue that still needs considerable attention. This issue is dealt with within work package No. 8.

Table 1: Project partner

Partner No.	Partner
1	Forschungszentrum Karlsruhe GmbH (FZK/INE), D (Coordinator)
2	Forschungszentrum Rossendorf (FZR-IfR), D
3	GSF-National Research Center for Environment and Health (GSF), D
4	Commissariat à l'Energie Atomique (CEA-DPC), F
5	University of Nantes - Presidence (U-Nantes), F
6	University of Manchester (U-Manch), UK
7	Technical University of Prague (CTU), Cz
8	Fodor Jozsef National Center of Public Health, Frederic Joliot-Curie National Research Institute of Radiobiology and Radiohygiene (FJC), HU
9	University of Cyprus (UCY), Cy
Temporary contributor:	
Francis Claret, FZK/INE through EC Marie-Curie Fellowship (MCFI-2001-01983)	

3. OBJECTIVES OF AND PROGRESS WITHIN INDIVIDUAL WORK PACKAGES

The progress within the individual work packages is discussed below. Frequent overlap of activities between individual work packages is mirrored by the numerous cross-references between the different work packages.

Table 2: Project structure

Work package	Title (Partner No. (cf. Table 1))	Lead contractor
1	Critical assessment of experimental methods	7
2	Generation and characterization of humic material	2
3	Radionuclide humate interaction data by designed system investigations	4
4	Characterization of radionuclide humate complexes	1
5	Natural chemical analogue studies	1
6	Radionuclide transport experiments	2
7	Model development	6
8	Application to Performance Assessment	6

3.1 WP 1 (Critical assessment of experimental methods)

< Objectives >

Intercomparison of experimental methods is conducted for different purposes. Recognition of possible experimental artifacts is used to ensure access to appropriate complexation data, including data from critical evaluation of published results. Furthermore, comparison of different experimental methods and understanding of individual processes may help in identifying important issues of the complexation process.

< Summary of results >

Experimental methods used for complexation studies may be divided into three different types:

- Separation of different species by size, charge, ... Examples are dialysis, ultrafiltration, (ultra-)centrifugation, size exclusion chromatography and electrophoresis. Examples of potential problems arising are shift in equilibrium, insufficient species separation and loss of species.
- Indirect speciation via additional complexing agents, ion exchange or ion selective electrodes. Examples of potential experimental problems are complexity of data analysis relying on additional input data, generation of additional unintended species and unintended processes that may influence equilibrium.

- Direct speciation via spectroscopy has a limited sensitivity range. In the case of fluorescence spectroscopy, the behavior of excited states may deviate from that of the ground state and photodynamic processes need to be well understood.

In order to have a common basis for the intercomparison of different experimental methods, one batch of Aldrich humic acid is used. Purification and the thorough characterization are documented well in order to establish a good basis for intercomparison within the exercise as well as comparison with well documented published data. Contributions to the intercomparison study may fall within the following conditions:

- Room temperature (18-25 °C)
- pH 4 or 6
- I = 0.1 or 0.01 mol/L (NaClO₄)
- Humic acid concentrations: 10 – 500 mg/L
- Metal ion to humic acid loading: 1, 10 or 50 % of one third of proton exchange capacity (reference to charge neutralization model applied to trivalent metal ions)
- Equilibration time: 24 h or 1 week

Two different batches were prepared in order to generate information on reproducibility of the purification. The two different batches showed Ba exchange capacity in alkaline medium of 7.00 ± 0.01 and 8.62 ± 0.11 meq/g. These results justify the use of one well characterized batch for intercomparison studies.

Potentiometric titration of the batch with a Ba exchange capacity of 7 meq/g was fitted by three pKa values, resulting in the respective following amounts:

pKa₁ of 3.30: 2.416 meq/g

pKa₂ of 5.80: 2.141 meq/g

pKa₃ of 10.98: 2.444 meq/g

The pKa values may be denoted as two types of acidities in the range of carboxylic groups and the highest value in the range of phenolic groups.

Ash content is determined to be 1.8 % by weight, which is in the range of other well purified humic acids. FTIR spectroscopy shows typical features of humic acid and thus underlines the successful purification.

Results at this early stage of the project may be summarized as follows:

Dialysis: Different membranes were used with different material and nominal cut-off of 500, 1000 and 10,000 Dalton. General trends expected for the complexation were observed, namely that the free metal ion concentration decreases with increasing pH, with decreasing

ionic strength and humate ligand loading. Depending on the experiment, the free metal ion concentration decreases or does not change with increasing equilibration time. The following problems were identified for different systems. With a 10,000 Dalton nominal cut-off membrane, humic acid was transported across the membrane. In general, slow establishment of equilibrium and large sorption of the metal ion.

Cation exchange: Amberlite IR-120 was used. A non-linear equilibrium isotherm for the Eu^{3+} ion was obtained, making interpretation of this third system element impact difficult. The expected increase in the free metal ion concentration with decreasing pH was obtained. Contrary to expectations, the free metal ion concentration also increased with decreasing ionic strength, indicating the difficulty to adequately regard the interaction with the third system element, i.e. the cation exchanger. The effect of pre-equilibration is small and variable. The kinetic behavior of europium humate as reported in the literature was verified.

Electrophoresis: Free liquid moving boundary electrophoresis was used for determination of the Eu^{3+} ion mobility under different experimental conditions, including progressive loading of the humate ligand. As expected, the ligand capacity of humic acid increases with increasing pH (pH 4 \rightarrow pH 6). Problems arise through sorption of europium ion and the humate complex. The analytical window is relatively narrow and the method is not sensitive close to humate ligand saturation.

Size exclusion chromatography: Sephadex G15 column was used in combination with UV/Vis detector for humic substances. The total europium concentration in different fractions was determined by AAS and/or OES. A large number of experimental problems are found, including the narrow humic acid metal ion loading window applicable. Other problems are related to poor separation of humate complex and non-complexed europium ions, also influenced by charge exclusion through ionic medium and the buffer (citric acid). Furthermore, pH and degree of humate ligand loading influence sorption of humic acid. Evaluation relies on data for the generation of complexes with the buffer used.

In summary, a large number of critical issues have been identified for a number of experimental methods and conditions. Additional data and application of further experimental methods will follow.

3.2 WP 2 (Generation and characterization of humic material)

< Objectives >

The objectives of this work package are to ensure availability of appropriately purified and well characterized natural humic and fulvic acids and generate humic material with specified properties for certain purposes. The latter includes humic acid where specified functional groups are blocked, synthetic humic substances with designed properties and silica wafer and

other minerals coated, especially with covalently bound humic acid. The purpose of generating material with specified properties is to enable specific insight in metal ion interaction processes.

< *Summary of results* >

One reference batch of Aldrich humic acid was purified within the humate complexation intercomparison exercise (WP1). Basic characteristic properties show that purification is successful. Further characterization is under progress and will become part of final characterization documentation.

Humic and fulvic acids from the Gorleben groundwater Gohy-573 has been used within the EC activities in this field since the start of the MIRAGE project (cf. "Introduction"). A large number of complexation data has been generated over the past many years. The original material has been used up and new batches are under preparation. These two new batches are expected to be available within the next time. These two new well characterized batches will enable continuation of generation of complexation data with humic and fulvic acids from this particular source.

Synthetic humic substances have been generated with distinct redox properties in order to study the influence of humic acid on the behavior of redox sensitive actinide ions. Variation of the starting material is done by no addition of amino acids, addition of glycine and addition of glutamic acid to synthesis of humic acid with high hydroquinone content. The redox capacity is determined by reduction of Fe(III) to Fe(II). The redox capacity for the designed humic substances is considerably higher than that of Aldrich humic acid as well as the synthetic humic acid M42. At pH 9 the redox capacity of the specifically designed ones is around 35 meq/g. The corresponding number for Aldrich humic acid and M42 is around 10-15 meq/g. Initial investigations show that phenolic groups are strongly involved in the redox processes, however, the effect is more pronounced than what would be obtained for a simple oxidation of phenolic OH groups. Further studies will be conducted in order to obtain insight in the nature of redox reactions by humic substances. This will be an essential part of detailed process understanding providing the ground for trust in predictions on the impact of humic substances on the geochemical behavior of actinide ions.

Characterization of humic material is done by a large number of methods. One characteristic property is the hydrodynamic size, measured by the diffusion in liquid media. Analytical methods frequently used for this purpose are size exclusion chromatography (SEC) and field flow fractionation (FFF). Evaluation is normally based on comparison with a series of standards of known molecular mass. In the past there has been a debate on the comparability of different standards and humic acid with respect to the size to mass ratio. This should also include the respective response to changes in pH and ionic strength. Finding a set of standards with similar mass to size ratio as humic acid could be an indication towards the nature of humic acid. Comparison was done of the hydrodynamic size of humic and fulvic acid on one

hand, and a number of “simple” organic acids on the other hand. These simple organic acids were (molecular masses) (malic acid (134), benzene-1,3-dicarboxylic acid (166), citric acid (192), benzene-1,2,4,5-tetracarboxylic acid (254), EDTA (292) and DEPTA (393). For comparison also polyacrylic acids (1250 and 2925 molecular mass) have been used, as well as the frequently used polystyrene sulphonates.

The mass distribution of humic and fulvic acids has become accessible in recent years by application of new mass spectroscopy approaches (MALDI-TOF, ESI-MS and TOF-SIMS) and Overhauser-NMR, showing that humic and fulvic acids comprise of a mixture of relatively small molecules. First results are very encouraging. Comparison of the size distribution of the simple organic acids and humic acid, shows that size to mass ratios are comparable. This may be of importance for the necessary reconsideration of the metal ion humic acid complexation process. Further investigations, however, are necessary in order to investigate the respective response to variation in physico-chemical conditions.

Silica wafer surfaces are used for covalent attachment/binding of humic acid via a number of different approaches. This is done for two different reasons. Such humic acid coated silica wafer surfaces provide the possibility for studying metal ion humate coordination by a large number of surface sensitive/selective methods (for example grazing incidence x-ray spectroscopy, flat angle total reflection laser induced fluorescence spectroscopy and TOF-SIMS). Another reason for generation of such material is that interaction data can be obtained for systems where phase separation is difficult and direct speciation methods are not applicable. This is especially the case with tetravalent actinide ions. The transferability of such data from surface bound to dissolved humic acid still needs to be verified or deviations determined. In the latter case, such deviations need to be related to physico-chemical differences between surface bound and dissolved humic acid.

The principle process for generating such surface coated material can be divided into different steps. The first step is activation of the silica surface by partial hydrolysis of the surface oxygen atoms. The second step is attachment of spacer molecules that with one end are bound to the surface silanol groups and on the other end carry desired functional groups for the final step. The third and final step is attachment of humic acid molecules to the spacer molecules. Throughout the process it must be ensured that surfaces are kept clean. For this purpose a number of different cleaning steps are applied. In order to follow the process and characterize the intermediates, different analytical techniques are used. In the present studies FTIR, TOF-SIMS and AFM have been used together with chemical analysis. U-Nantes has used two different processes and FJC four. Considerable problems have been identified. The main problem found is that the spacer molecules do not attach as monomers to the silica surface, providing the dense homogeneous “carpet” required. Instead, the spacer molecules polymerize and large structures sorb on the surface. This inhomogeneous distribution of large polymerized spacer material has been demonstrated by a combination of AFM and TOF-SIMS.

Based on the present experiences, modified processes are under investigation. The outcome of different optimizations will guide further work. For this reason, characterization of complexed actinide ions will commence at a later stage, given that the required homogeneous surface coating of humic acid molecules can be obtained.

3.3 WP 3 (Radionuclide humate interaction data by designed system investigations)

< Objectives >

The objectives are to ensure accessibility to metal ion humate interaction data for different metal ions and metal ion complexes (generation of ternary complexes) required for providing the basis for adequate understanding of the interaction process. The former approach of providing data for direct application to geochemical transport modeling is partly obsolete because of the finding that kinetic data need to be applied. The data from “equilibrium investigations”, nevertheless, are required for definition and selection of kinetic data and are a prerequisite for adequate process understanding. Therefore, metal ions and metal ion complexes are investigated over a broad range of physico-chemical conditions under defined laboratory conditions with characterized humic material. The characterized humic material also includes synthetic humic acid and humic acid with designed properties.

< Summary of results >

The complexation of pentavalent neptunium has been studied at pH 7 and 8. In order to obtain an insight in the complexation mechanism, Aldrich humic acid was used before and after modification by blocking “phenolic” OH groups. The stability constant remains uninfluenced of both pH and blocking of the phenolic groups. The loading capacities, however, show not only the expected decrease with decreasing pH but also with blocking of the phenolic groups. The mechanism for the decrease in the loading capacity is not yet well understood. These studies, however, are important contributions in providing information for the necessary progress in the complexation process understanding.

Initial results on the complexation of plutonium with humic acid have been obtained by application of humic-coated silica gel. Assuming that plutonium forms a 1:1 complex with binding sites of the humic gel, a conditional stability constant is evaluated to be $\log\beta=7.4$ (L/mol). In order to validate results and characterize complexes formed, access to humic-coated silica wafers under development is essential.

The interaction of iodine with humic substances has been studied. Quantification of humic bound species is done by ultrafiltration. Furthermore, UV/Vis spectroscopic quantification of tri-iodide (I_3^-) is used also for determination of kinetics. It was shown that the iodine under reducing conditions, i.e. present as iodide ion, does not complex with humic acid. The humic acid, however, has an influence on the reduction of iodine species and thus have an influence

on the geochemical behavior. The investigations show that the influence of humic acid is different from that of simple defined phenols and that non-linear processes are involved. Further evaluation of the process is desired in order to ensure that the influence of humic substances on the geochemical behavior of iodine is adequately understood.

3.4 WP 4 (Characterization of radionuclide humate complexes)

< Objectives >

The objective is to provide the basis for adequate process understanding of the metal ion humate interaction process. Metal ion humate complexes are characterized by a large number of analytical approaches, aiming at determining both the local binding environment and changes in the overall structure of humic acid. Numerous advanced analytical methods are applied and further developed within this work package.

< Summary of results >

X-ray absorption spectroscopy (XANES and EXAFS) has been applied to determine the local binding environment of humate bound actinides of different oxidation states (Pu(III), Th(IV), Np(IV) and Np(V)). In order to obtain additional information, also humic acid with blocked phenolic groups was studied. The obtained structural parameters were compared to data on actinide hydrates, Bio-Rex 70 actinide complexes (cation exchange resin with only carboxylic groups) and crystallographic data of actinide complexes with organic ligands from the literature. The results may be interpreted as dominance of monodentate carboxylic coordination to the actinide ions. These results are of great importance for delineation of the effective humate ligand function under different physico-chemical conditions and the obviously very invariant coordination environment. It is also reflected in the invariant stability constants obtained if the effective humate ligand concentration under given physico-chemical conditions is regarded. Nevertheless, final conclusions on the coordination of humic complexed metal ions require further studies and the application of additional analytical methods.

It is well documented that the actinide humic acid complexation is subject to comparably slow kinetics. The kinetics is frequently divided into two or more kinetic modes, based on fitting of complex association/dissociation data. One important question is to which extent such kinetic modes are real or merely reflect parameters that suffice for fitting the overall behavior of a gradual transition without distinct individual kinetic modes. Another question is to which extent the kinetics, and the overall interaction behavior, is significantly different between flocculated humate complex and dissolved/dispersed entities. Comparison was done of the dissociation kinetics between, on one hand low metal ion loading by scavenging of dissociated metal ions with a cation exchanger and, on the other hand isotope exchange between metal ion humic acid flocculate and non-complexed metal ions. No principle

difference was seen, justifying the common approach of inclusion of humate flocculate into the amount/concentration of humate complex for the purpose of evaluating complexation constants.

EXAFS spectroscopy and time resolved laser fluorescence spectroscopy (TRLFS) was conducted on humate complexes, consisting of two different kinetic modes. The spectroscopic studies verify that these kinetic modes are different in their binding environment. The reversible exchange between the different kinetic modes was also verified by TRLFS. A shift in the fluorescence spectrum is obtained if fast dissociating metal ions are removed. Leaving the solution for five days, the original spectrum is obtained again. The magnitude in difference between the different kinetic modes is seen by a shift in emission wavelength from around 600.5 nm for the “slow” dissociation mode to around 602.8 nm for the “fast” dissociation mode. The Tb(III) oxygen distance in the “slow” dissociation mode is evaluated to be 2.33 Å. The distance of the “fast” dissociation mode is estimated to be around 2.41 Å. These findings will be essential for the necessary refinement of the actinide humate interaction process understanding.

Understanding fundamental properties of humic acid under different physico-chemical conditions is required for adequate description of the humic acid ligand function. This includes the size and density under different physico-chemical conditions as a possible key for understanding, amongst others the slow interaction kinetics with different distinguishable modes. For this reason the electrophoretic mobility of humic acids is studied under variation of pH and ionic strength. Data are analyzed with respect to average electrophoretic mobility as well as the distribution under the different physico-chemical conditions. The data show that various evaluation approaches can be used. Depending on the mass distribution and the possibility for association of individual molecules, the outcome changes with respect to variations in size and accompanying possible changes in the ternary structure. Further evaluation of the data accompanied by testing different approaches will give essential input to the required understanding of the overall physico-chemical behavior of humic acid. Theoretical evaluation of different possible humic-humic association mechanisms is an important contribution to this issue (cf. below, WP 7, modeling).

3.5 WP 5 (Natural chemical analogue studies)

< Objectives >

The behavior of natural humic bound trace metal ion inventory differs considerably compared to metal ions added under laboratory conditions. The aim of the present work package is to determine the chemical behavior of natural humic bound trace metal ion inventory and anthropogenic contaminants in comparison to metal ions added under laboratory conditions. The purpose is to determine whether or not actinide ions in the real system will mimic the

behavior of the humic bound natural trace metal ion inventory, especially in regard of relevant chemical conditions and time spans.

< Summary of results >

Most information on the kinetic behavior of the metal ion humate interaction originates from designed laboratory studies where metal ions are added to more or less well defined systems. Most frequently the kinetics is studied between metal ions and purified humic acid under defined pH and electrolyte (ionic strength) conditions. A large number of studies have also been conducted in natural (ground-)water, either under controlled atmosphere representing deep groundwater conditions or in contact with air. The behavior of the natural metal ion inventory and radionuclides from fall-out has also been studied aiming at determining the influence of humic substances on the bioavailability of these elements. Few studies have been conducted on the chemical behavior of chemical analogues to the actinide ions. The key question arising from comparison of the outcome of these individual studies is to which extent actinide ions in long contact with a natural system will mimic the behavior of the natural inventory of natural actinide ions, including natural chemical analogues, or if the description of their behavior can be extrapolated from laboratory studies. For this reason the chemical behavior of americium and plutonium is studied on samples from the bank of Esk Esturia, West Cumbria, UK National Grid Reference SD113964. The anthropogenic inventory originates mainly from releases around 30 years ago.

The samples contain americium and plutonium mainly originating from releases from the Sellafield plant at 10-12 miles distance. The ^{241}Am activity (and ^{152}Eu added to the samples) is measured by gamma ray spectroscopy and the sum of ^{239}Pu and ^{240}Pu is determined by alpha spectroscopy. Soil/mud samples (approximately 50 cm x 15 cm) are found to have homogeneous distribution of ^{241}Am . Humic acid was isolated by alkaline extraction. After adjustment to $\text{pH } 6.0 \pm 0.1$, the cellulose phosphate cation exchanger is added in the sodium form and samples were stored at $25\text{ }^\circ\text{C}$ (in a thermostated water bath). After different time intervals, the ^{241}Am and $^{239,240}\text{Pu}$ activities in the supernatant solution are determined. Following removal of the main part of the desorbing fraction of the anthropogenic inventory of americium and plutonium, ^{241}Am and ^{152}Eu is added and the samples conditioned for seven days (in absence of the cation exchanger). Thereafter, the desorption kinetics is determined for these added radionuclides in an equivalent fashion as for the anthropogenic inventory. Parallel samples showed very comparable results.

There are two principle possibilities responsible for the slow dissociation kinetics. One is related to changes in the humic acid structure, for example self-association and protonation/complexation mediated humic-humic association, conformational changes by coiling of linear structures or development of hydrophobic regions. In this case the kinetics is an inherent property of the humic substances and should show only minor differences between different metal ions of comparable humic structure impact. In the case of association, the humic acid concentration should show a significant impact. Another principle possibility is that the

kinetics is governed by the coordination of complexed metal ions, i.e. different metal ions should show distinct differences. A combination of both is also possible.

The results of the dissociation studies are shown in Table 3. For interpretation, different quantities are relevant, amongst others, (i) the fraction of rapidly dissociating metal ions, (ii) the dissociation rate of slowly dissociating metal ions and (iii) the potential for a fraction with a dissociation rate too slow to be quantified (“quasi-irreversible” binding). The fraction of rapidly dissociating ions is significantly higher for the radionuclides added in the laboratory compared to the anthropogenic contaminants. This may reflect either a higher population of the “slow dissociation mode” or generation of quasi-irreversibly bound ions with the very long contact time for anthropogenic contaminants.

Table 3: Concentrations of radionuclides, the fractions of them showing rapid desorption, the first order desorption rate constants for the “slow desorption” fraction and calculated/ hypothetical time required for desorption until 1 % of the radionuclides remain bound (assuming no fraction with slower dissociation kinetics than given in the table). Radionuclides are $^{241}\text{Am}_{\text{anthr.}}$ and $^{239,240}\text{Pu}_{\text{anthr.}}$ (anthropogenic contaminants), and $^{241}\text{Am}_{\text{lab.}}$ and $^{152}\text{Eu}_{\text{lab.}}$ (radionuclides added in the laboratory and samples conditioned for seven days).

Radio-nuclide(s)	Concentration (10^{-12} mol/L)	Fraction with rapid dissociation (%)	Dissociation constant (years^{-1}) / (2σ error)	Dissociation time for 1 % remaining bound (years)
$^{241}\text{Am}_{\text{anthr.}}$	1.8	72	1.9 / (18 %)	1.8
$^{239,240}\text{Pu}_{\text{anthr.}}$	53-194*	56	1.9 / (40 %)	2.0
$^{241}\text{Am}_{\text{lab.}}$	160	86	1.5 / (11 %)	1.7
$^{152}\text{Eu}_{\text{lab.}}$	10	93	1.5 / (26 %)	1.3

*: Depending on the assumed ratio between the two plutonium isotopes.

The dissociation rates of the anthropogenic radionuclide contaminants do not show a significant difference between each other. The same is true for the addition in the laboratory with seven days of conditioning time. The anthropogenic contaminants, however, show a slightly higher dissociation rate compared to addition in the laboratory followed by the seven days of conditioning. The dissociation rates from laboratory experiments with purified humic substances under controlled physico-chemical conditions are typically around 3.2 years^{-1} , i.e. around two times higher than for the radionuclides added in the laboratory in the present study. There is no significant difference in conditioning time between laboratory addition in the present study and the laboratory studies with purified samples under controlled physico-chemical conditions. Consequently, the conditioning time does not appear to be the reason for differences in the dissociation kinetics of the fraction affected. A significant difference, however, is that laboratory investigations under controlled physico-chemical conditions are generally conducted with humic acid concentrations in the range of about 10 mg/L. Contrary

to this, the present studies with radionuclides added is done with a humic acid concentration around 300 mg/L. This observation would favor a strong impact of the humic acid concentration, i.e. a strong impact of inherent humic acid association properties. This is also supported by the indistinguishable dissociation kinetics of anthropogenic plutonium and americium.

Extrapolation beyond the observation window is connected with great uncertainty. After around 80 days of dissociation, about 18 % of anthropogenic americium, about 10% of americium added in the laboratory, and about 5 % of europium added in the laboratory is still bound to the humic acid. These amounts of bound metal ions may continue to dissociate according to the kinetics of the slowest component identified. Application of the deduced dissociation constants yield that around two years are required for dissociation until 1 % of the metal ions remain bound. The time for europium added in the laboratory is somewhat lower, reflecting the lower complexed amount. Despite the fact that it is questionable to extrapolate beyond the observation range, the dissociation kinetics shows a picture according to which there is no sign for a residue of quasi-irreversibly bound anthropogenic contaminants. Further studies will be conducted to provide safer evidence for the existence or non-existence of such a fraction.

3.6 WP 6 (Radionuclide transport experiments)

< Objectives >

The transport of radionuclides in the laboratory under near-natural conditions (batch and column experiments on natural sediments and groundwater) has been studied extensively in the foregoing HUMICS project (cf. “Introduction”). The results delivered the input for key process understanding and data for the successful development and implementation of the kinetic concept. In the present project these investigations will continue both with respect to refinement of data for radionuclides already investigated and for investigations on radionuclides where data are scarce or missing. Emphasis is on specified investigations aiming at adding to the process understanding.

< Summary of results >

The transport of cobalt with fulvic acid solution has been studied on porous sediment as well as with humic acid on intact sandstone block columns. The porous sediment system was not preconditioned prior to experiments, whereas the sandstone system had experienced considerable equilibration with solutions used. The porous sediment system was investigated by pulse addition and the sandstone system by continuous addition of solution containing humic acid and the cobalt ions, followed by flushing with humic and cobalt ion free solution. Both systems show that cobalt and humic/fulvic acid are co-eluted. No cobalt break-through was found if no humic/fulvic acid was added.

A mixture of reactions sufficiently close to equilibrium and reactions that require kinetics to be regarded describes the cobalt fulvic acid interaction. Also fulvic acid showed interaction with the sediment. This interaction is described by an equilibrium approach. No improvement in description of the elution profiles was obtained where the option for kinetics was included in the fulvic acid sediment interaction. The results show that fulvic acid sorption needs to be regarded for sediments that have not been preconditioned with humic substances and where there are humic substance concentration gradients.

For the sandstone column experiments, results were more complex. The description of the elution profiles required regard of more than one sediment surface site, i.e. the heterogeneity present in all sediments also need to be regarded for transport interpretation. In addition to elution profiles, the distribution along the column was also determined. Comparison between the two sources of information highlights a general problem in extracting/determining the relevant processes from available information. The column distribution profiles could not be well reproduced by the description deduced from analysis of the elution profiles. There are indications, that the problem is the deficient description of the cobalt ion interaction directly with the sandstone sediment. Nevertheless, the general problem remains with the extrapolation of data beyond the range of observation and beyond the type of information actually regarded/available.

In summary, the level of detail in understanding column experiments is increasing, however, under particular laboratory conditions. It is very questionable to apply the models and parameters for blind prediction to the field-scale. One may consider the need for field-scale experiments in order to provide the required confidence in predictive modeling.

3.7 WP 7 (Model development)

< Objectives >

The objective is development of scientifically sound and justified models for the radionuclide interaction with humic colloids. For this purpose results from "radionuclide interaction data", "complex characterization", "natural chemical analogue studies" and "radionuclide transport experiments" (cf. above) are implemented into models reflecting detailed process understanding. This is an absolute necessity in order to generate the required tools trustworthy predictive modelling.

< Summary of results >

Model development is progressing along with progressing availability of data from above described investigations. There is no change in the principle basis of present models compared to before commencement of the project. One issue finding progressive interest is the mechanisms and consequences of humic-humic association. This association is expected both as a self-association but also induced by protonation and metal ion complexation. The

end-state of protonation and metal ion complexation is flocculation of humic acid and drastic increase in fulvic acid light scattering. In order to further develop process understanding of the association processes, also theoretical analysis of possible mechanisms is performed.

Another important aspect is that humic-humic association may be a key process resulting in the distribution of complexed metal ions between different kinetic modes. Based on such an approach the humic-humic association/dissociation rates should be related to the kinetics of transfer between metal ions complexed in different kinetic modes and the bulk solution. General observations to the kinetics of metal ion humate complexation may be summarized as follows:

1. All metal ions show comparable transfer rates between different kinetic modes.
2. There is one distinct fraction with a discrete, single first order desorption rate constant.
3. These rates are insensitive to total metal ion concentration and humate to metal ion ratio.
4. The distribution of metal ions between different kinetic modes varies. Metal ions with high cation charge to a larger extent occupy slow dissociation modes. This observation is independent of the metal ion concentration.
5. With increasing humic acid concentration, the amount of metal ions in the slow dissociation mode increases, the dissociation rates, however, do not change significantly.
6. In batch experiments, the distribution between slow and fast dissociation modes reaches a maximum at intermediate ionic strength. The slow dissociation rate, however, is virtually independent of ionic strength, except for $I=1$ M where there is a slight decrease from around $5 \times 10^{-7} \text{ s}^{-1}$ to $2 \times 10^{-7} \text{ s}^{-1}$.
7. There is very little impact of pH on association and dissociation rates.

The basic mechanism for humic-humic association regarded in the present initial approach leads to qualitative agreement in the trends with some experimental observations. In other cases, the qualitative predictions are not reflected in experimental data. Furthermore, the calculated association/dissociation rates are far from realistic in absolute terms. In the present form the description of association processes is not capable to provide a mechanistic basis for the observed metal ion association/dissociation kinetics. Extension of the approach by inclusion of additional mechanisms will be required. One such example could be regarding the impact of complexation or protonation as triggers for association by changing the charge and functional group properties. Further development will show to which extent the basic idea of association as a possible mechanism responsible for the metal ion humic acid interaction kinetics is feasible.

3.8 WP 8 (PA)

< Objectives >

The objective is to provide scientifically justified simplifications of detailed process understanding and associated models. These scientifically justified simplifications are tailored for direct application in PA codes. Application to real sites in the form of three migration cases is used for visualisation of the impact of humic colloid mediated radionuclide transport on PA. Origin, stability and mobility of humic substances is also treated within this work package.

< Summary of results >

Three migration cases are applied for visualization of the impact of humic colloid mediated actinide transport. One of these migration cases is the far-field of the Gorleben aquifer system. Over the past decades, the Gorleben aquifer system has been extensively studied within the German program to disposal of high-level waste by a large number of methods. The Gorleben migration case was formulated within the past EC-HUMICS project and preliminary calculations on the humic colloid mediated actinide transport were conducted. Some open questions, however, remained with respect to the degree/velocity of vertical groundwater exchange. Furthermore, despite the findings concerning ideal tracer behavior of humic substances in deep groundwater, additional sources could not be excluded and the mobility of aquatic humic substances in the upper part of the aquifer remained an open issue. The hydrological situation in the southeast part of the aquifer system has been investigated by a combination of chemical data, isotope-geochemical/hydrological data and historical data with respect to changes in the land-use.

Until the year 1710, part of the surface in the southeast area was a wetland. Between 1710 and 1750 this wetland was drained. Groundwater recharge from wetland has a different isotopic composition (^{18}O and ^2H) than recharge from non-wetland. This provides a tool for identifying groundwater from these different recharge conditions and couples the information with the historical time-marker. Part of deep groundwater is shown to originate from recharge from the previous wetland. After drainage, about 70 meters of the upper groundwater layer has been exchanged by recharge from the present non-wetland conditions. This justifies the high rates used for vertical groundwater exchange used in the preliminary formulation of the Gorleben migration case. More important, the ^{14}C content in the deep groundwater originating from wetland recharge is higher than in the overlying non-wetland recharge groundwater. This has previously resulted in speculations on reversal of groundwater flow. The present study shows that this simply reflects the higher source term in wetland due to higher turnover of organic matter. Furthermore, calculation of the ^{14}C concentration in recharge dissolved inorganic carbon (DIC) via standard assumptions on the ^{13}C content is shown to be incorrect. The ^{13}C concentration of DIC is shifted to higher values due to microbiologically mediated methane generation in wetland. This further verifies the origin of deep groundwater from previous wetland.

Correlation of DIC content of biogenic origin with the humic and fulvic acid concentration shows that the aquatic humic substances in the deep groundwater originate from wetland recharge as the result of microbiological processes. These humic and fulvic acids migrate like ideal tracers without retention or decomposition over several hundred years. This underlines the correctness of basic assumption applied for transport modeling under natural groundwater conditions, namely that aquatic humic and fulvic acids are stable in solution and that there is no indication for decomposition or retention by interaction with sediment surfaces. The transport properties of humic substances in geochemical gradients such as in the transition from the near- to the far-field still needs to be investigated.

An additional important aspect of the present study is that the groundwater recharge and thus flow conditions are very sensitive to comparable marginal changes in land-use. Higher impacts can be expected from changes in vegetation via climatic changes. Consequently, specification of a very detailed groundwater flow situation over long time periods is not applicable for sandy sediment aquifers like the one in Gorleben. This supports the basic approach of using average values, as presently done, instead of trying to identify a specific flow part with well defined properties valid only for a short window in time.

Another migration case is mining and milling rock pile. In order to provide input data for this transport case, laboratory investigations are conducted on mining and milling material under specified conditions. Interaction with the rock material will be governed by material from the small size fraction due to higher surface to mass ratio and available surface sites on such weathered material. For this purpose, material from the rock pile No. 66, Schlema (Saxony, Germany) has been sampled and characterized. The size fraction < 1 mm was collected directly in the field. Characterization shows that it mainly consists of chlorite, muscovite, quartz, hematite/goethite, ankerite with a negligible fraction of clay minerals and virtually no expandable clay minerals. The carbon content is 1.96 % with about 13 % inorganic carbon (0.26 % of the total carbon). The BET surface is around $11.8 \text{ m}^2/\text{g}$.

The elemental composition of the sampled rock material is shown in Table 4. An example for the composition of a typical seepage water from this rock pile is shown in Table 5. These materials provide the basis for determination of relevant data for the humic colloid mediated actinide transport within the mining and milling rock pile migration case.

Identification of all relevant sources for humic substances is one important question for determination of the impact of humic colloid mediated actinide transport and the application to PA. In various disposal concepts, cement is foreseen as a constituent of waste packages and/or as linings and part of engineered structures. Dissolution of cement leads to high pH solutions. Organic rich clay from four different depths (447 to 516 m) of the Meuse Haute Marne (MHM) site (Bure) was kept in contact with alkaline solution simulating conditions expected from cement dissolution under such near-field conditions. Original organic material in the clay consists mainly of aliphatic hydrophobic compounds basically without oxygen containing functional groups. After contact with “solid young fluid” (mimicking cement

dissolution, initial pH 13.22) for around one and a half years, high concentrations of hydrophilic organic matter are found (243 to 354 mg DOC/L, Table 6).

Table 4: Elemental composition of the size fraction < 1 mm from the uranium mining and milling rock pile No. 66, Schlema, Saxony, Germany.

Element	($\mu\text{g/g}$)						
Li	108	Mn	3120	Nb	22.2	Hg	2.02
Be	4.76	Co	83	Mo	5.56	Al	29600
B	89.2	Ni	208	Ag	4.46	Ti	1.87
Na	2440	Cu	238	Cd	1.04	Pb	91.8
Mg	3120	Zn	235	In	0.29	Bi	11.2
K	20400	Ga	91.0	Sn	15.5	Th	1.91
Ca	10400	As	954	Sb	9.4	U	57.8
Ti	8310	Rb	30.4	Cs	10.9	Sc	66.6
V	280	Sr	73.5	Ba	2300	Nd	4.38
Cr	120	Y	3.72	Ce	11.0	Eu	1.16
Fe	62400	Zr	141	Ta	1.54	Ho	0.204

Table 5: Seepage water composition from the rock pile No. 66, Schlema, Saxony, Germany.

		(mmol/L)		(mmol/L)		(mmol/L)	
pH	7.8	Na	0.54	Fe	0.001	Cl ⁻	0.166
Eh	449 mV	K	0.40	Si	0.07	SO ₄ ²⁻	26.6
Cond.	3.38 mS/cm	Mg	17.5	As	0.007	NO ₃ ⁻	0.051
O ₂	10.8 mg/L	Ca	10.0	U	0.011	HCO ₃ ⁻	2.58
DOC	0.92 mg/L						

Table 6: Sum of humic and fulvic acid estimated from UV/Vis spectroscopy, measured DOC content and the fraction of DOC identified as humic and fulvic acid.

Clay horizon (No.)	Sum of HA and FA from estimation by UV/Vis spectroscopy (mg C/L)	DOC (measured) (mg C/L)	Fraction of DOC as HA+FA (%)
1	349	299	116.9
2	219	260	84.3
3	222	243	91.3
4	242	267	90.8
5	266	270	98.4
6	258	252	102.5
7	342	354	96.7
8	322	324	99.4
			Mean value: 97.5 \pm 9.7

Characterization by solubility behavior, UV/Vis absorption, IR and fluorescence properties show that the dissolved hydrophilic organic matter has the characteristic features of humic and fulvic acids. Estimation of humic and fulvic acid content via UV/Vis spectroscopy results in 97.5 (± 9.7) % of DOC being humic and fulvic acid (Table 6). Quantification of the humic and fulvic acid content is based on comparison between the specific UV/Vis absorption and the UV/Vis absorption ratio between 300 and 400 nm. This approximate method is used because of the small sample volumes. The results show that this process could provide for an important additional source of humic substances that need to be regarded for PA. Further studies are conducted in order to provide for additional characterization data and obtain an insight in the chemical conversion mechanisms. Furthermore, larger samples are required for a better quantification of the humic and fulvic acids generated.

4. REFERENCES

1. G. Buckau (Editor) "Effects of Humic Substances on the Migration of Radionuclides: Complexation and Transport of Actinides, First Technical Progress Report", Report: FZKA 6124, August 1998.
2. G. Buckau (Editor) "Effects of Humic Substances on the Migration of Radionuclides: Complexation and Transport of Actinides, Second Technical Progress Report", Report: FZKA 6324, June 1999.
3. G. Buckau (Editor) "Effects of Humic Substances on the Migration of Radionuclides: Complexation and Transport of Actinides, Third Technical Progress Report", Report: FZKA 6524, Research Center Karlsruhe, October 2000.
4. G. Buckau (Editor) "Effects of Humic Substances on the Migration of Radionuclides: Complexation and Transport of Actinides (Final Report)", Report EUR 19610 EN, 2000.

Annex 1

Isotope Exchange and Spectroscopic Study on Kinetic Modes of An(III)/Ln(III) Humate Complexes

**J.M. Monsallier, R. Artinger, M.A. Denecke, F.J. Scherbaum,
G. Buckau and J.I. Kim**

Forschungszentrum Karlsruhe, Institut für Nukleare Entsorgung (FZK/INE)

Isotope Exchange and Spectroscopic Study on Kinetic Modes of An(III)/Ln(III) Humate Complexes

Jean-Marc Monsallier, Robert Artinger, Melissa A. Denecke, Franz J. Scherbaum, Gunnar Buckau and Jae-Il Kim

*Forschungszentrum Karlsruhe, Institut für Nukleare Entsorgung,
P.O. Box 3640, 76021 Karlsruhe, Germany*

Abstract

Humic acid-metal ion interaction shows a complex kinetic behavior. Dissociation kinetics reported in the literature range from hours to basically irreversibility. Different suggestions for the responsible mechanisms have been made. One possibility is variations in the metal ion-humate complex environment. The dissociation kinetics of Eu(III)/Tb(III)/Cm(III)-humate complexes is investigated with purified humic acid solution (Gohy-573(HA), pH=6.0, I=0.1 M (NaClO₄)) and a humic rich groundwater (Gohy-532, pH=7.5). Different kinetic modes are separated by scavenging of dissociated metal ions by an cation exchanger added after different metal ion-humic acid contact times. The metal ion-humate complex environment is studied by time resolved laser-induced laser fluorescence spectroscopy (TRLFS) and extended X-ray absorption fine structure (EXAFS). Both methods show that there is a considerable difference between metal ions bound in slow and fast dissociation modes. TRLFS also shows that these different kinetic modes are in exchange equilibrium with each other. Furthermore, isotope exchange investigations verify that humic acid/Eu(III)- flocculate is not a separate chemical phase but behaves like dissolved/dispersed humate complexes.

Introduction

Metal ion humic acid interaction shows a complex kinetics. The overall picture is that metal ions associate with humic acid, followed by slow rearrangement, gradually populating slow dissociation binding modes. Dissociation is much slower than association and, in several cases, quantitative dissociation is not achieved. Frequently, sequential kinetic modes are found that show exchange with each other. The transition from fast to slow dissociation mode is mainly entropic, including increase in particle size where complexed metal ions are bound. In addition, very slow dissociation is observed for natural trace metal ions located mainly in large particles.

A number of processes may be responsible for the different kinetic binding modes of humate complexed metal ions. Assuming that humic substances undergo association-dissociation of small primary entities, the kinetics observed in laboratory time scales could be the result of exclusion of metal ions from the bulk solution. Such an association would be enhanced by humic-humic association induced by metal ion complexation. Such an approach is in agreement with some experimental observations. Another approach is to assume different inherent binding environments with differences in their dissociation rate. If the slower dissociation modes are associated with larger entities, increase in size and slow dissociation from large entities could be the result of redistribution with time. Further approaches include migration between surface and inner volume (gel phase) and rearrangement of the humic molecule by coiling around the complexed metal ion. For irreversibly bound metal ions observed particularly for the natural trace element inventory as well as for fall-out plutonium from nuclear atmospheric testing inclusion of inorganic structures may play a role.

The present study is conducted in order to determine the possible relation between the coordination environment of humic acid complexed trivalent actinide and lanthanide ions and the dissociation kinetics. The Eu(III) dissociation kinetics is studied by scavenging dissolved metal ions by an added cation exchanger after different conditioning times of the metal ions with humic acid. Furthermore, isotope exchange between humic bound and non-complexed Eu(III) is done under conditions where the total concentration of complexed ions does not change significantly during the experiment. The fluorescence behavior of humic acid complexed Cm(III) is investigated by time resolve laser induced fluorescence spectroscopy (TRLFS). Finally, Tb(III)-humic acid is characterized by extended X-ray absorption fine structure (EXAFS) as a mixture of both slow and fast dissociation modes as well as after stripping off the fast dissociating mode by cation exchange. Purified humic acid (Gohy-573(HA) at pH 6.0 in 0.1 M NaClO₄ is studied together with a humic rich natural groundwater (Gohy-532, pH 7.5), both from the Gorleben aquifer system.

Experimental

Humic acid and natural groundwater samples

The purified natural humic acid investigated, Gohy-573(HA), originates from a 139 m deep groundwater of the Gorleben aquifer system in Northern Germany. The isolation, purification and detailed characterization of this humic acid is described elsewhere (Kim et al. 1990). The natural groundwater investigated, Gohy-532, originates from 65 m depth at a different location of the same aquifer system. The groundwater is equilibrated with a sandy sediment under Ar atmosphere with 1 % CO₂, according to the procedure described by Artinger et al. 1998. The physico-chemical properties and major chemical constituents are shown in Table 1.

Table 1: Physico-chemical data and chemical composition of the Gorleben groundwater sample Gohy-532, equilibrated with sandy sediment for three months under inert gas (Ar + 1% CO₂).

pH	7.5	Na	(mmol/L) 9.54
Eh (mV)	-160	Mg	0.002
Conductivity (mS/cm)	0.95	Ca	0.026
DOC (mgC/L)	49.1	Fe	0.057
HA (% of DOC)	≈ 70	Cl	3.87
FA (% of DOC)	≈ 20	HCO ₃ ⁻	5.27

Complex dissociation experiments

Dissociating metal ions are scavenged by Chelex 100 cation exchanger. The concentration of humate complexed metal ion is represented by the concentration in solution. The experimental conditions before contacting with Chelex are the following: pH=6.0, 10⁻³ mol/L MES buffer, 0.1 mol/L ionic strength (NaClO₄), 10 mg/L Gohy-573(HA), and 10⁻⁷ mol/L Eu³⁺. After 1 hour and 120 hours conditioning time, an excess of resin (10 g/L Chelex) is added to the solution. After varying time periods, an aliquot sample is removed and analyzed for remaining humate bound metal ion concentration.

Isotope exchange

3.5x10⁻⁹ and 13.8x10⁻⁹ mol/L of ¹⁵²Eu labeled Eu(III) is added to solutions with final humic acid concentrations of 10 and 100 mg HA/L, respectively (pH=6.0 and I=0.1 M (NaClO₄)). Samples are prepared and stored under anoxic conditions. After different storage times (1 hour, 2 days and 1 month), an excess of ionic Eu³⁺ (twice the loading/complexation capacity of the humic acid under these conditions) is added. The humic acid flocculates due to the excess Eu(III) concentration. After different time periods, the samples are centrifuged and an aliquot of the supernatant is sampled. The absence of significant amounts of humic acid in the supernatant was verified by UV/Vis spectroscopy. Prior to further storage, samples are shaken in order to redisperse the Eu(III)/humate-flocculate. Part of the Eu(III) in the ¹⁵²Eu spiked complexed humate will be displaced by the addition of non-labeled Eu(III). Thereafter, the labeled and non-labeled Eu(III) will be slowly exchanged, reflecting the kinetically hindered dissociation of humate bound ¹⁵²Eu. In order to follow this exchange process, the concentration of ¹⁵²Eu in the supernatant is determined by β -counting.

TRLFS experiments

The Cm(III) fluorescence emission and its lifetime is measured. All experiments are performed under Ar atmosphere at room temperature (24 ± 2 °C). For the fluorescence measurements, ^{248}Cm ($t_{1/2} = 350,000$ years) is used. $^{248}\text{Cm(III)}$ concentrations are determined by alpha counting. 5.4×10^{-7} mol/L $^{248}\text{Cm(III)}$ is added to the humic rich groundwater and pH adjusted to the initial equilibrated groundwater pH value (pH=7.5) by addition of small aliquots of 0.1 mol/L NaOH. The sample with purified humic acid contains 10 mg/L humic acid and 2.5×10^{-7} mol/L $^{248}\text{Cm(III)}$. Under these conditions, the concentration of free Cm^{3+} ions can be estimated to be around 4 %. The Cm(III) fluorescence is measured after different conditioning times. In addition, the Cm(III) fluorescence is measured after 5 hours of contact with Chelex resin as well as three days after removal of the resin.

EXAFS measurements

Tb(III) humate samples for EXAFS measurements is prepared as follows: 100 mg purified humic acid is dissolved in 100 mL 0.1 mol/L NaOH, followed by acidification to pH 1 after about 10 min by addition of concentrated HClO_4 . 5.0 mL of 40.6 mmol/L Tb(III) are then added and the pH adjusted to 5.0 by addition of 0.1 mol/L NaOH. The sample is shaken periodically for 8 weeks. During preparation and storage, the sample is kept under an Ar atmosphere at room temperature. In addition, samples are stored in the dark. Immediately prior to the EXAFS measurements, about 0.5 mL of Tb(III)/humate-flocculate in wet-paste form are obtained by centrifugation. The EXAFS spectra of the wet paste samples are then measured. Two different samples are measured. These are the (i) the original sample after 8 weeks of contact time, and (ii) after 5 hours of contact with Chelex 100 resin in order to remove comparably fast dissociating humate complexed Tb(III).

Results and discussion

Dissociation measurements with Chelex

Fig. 1 shows the dissociation kinetics of Eu(III)-humate for the two different metal humic acid conditioning/storage times. After less than two hours of contact with Chelex resin, slow dissociation is observed (straight lines in Fig. 1). With increasing conditioning time, the fraction of Eu(III) in the slowly dissociating binding mode increases. After around 300 h contact with the Chelex resin, the dissociation slows down considerably and a concentration of humate bound Eu(III) of around 5 % is observed. The results show a rapid metal ion uptake, followed by a rearrangement associated with a relatively slow shift of complexed ions to slower dissociation kinetic modes, with small amounts of complexation modes with very slow dissociation kinetics remaining, frequently reported as “irreversible” binding.

Isotope exchange

The kinetic behavior of metal ion humate complexes is verified by isotope exchange between Eu(III) in the bulk solution and $^{152}\text{Eu(III)}$ /humate-flocculate. The isotope exchange is measured as the difference between ^{152}Eu recovered in the supernatant of centrifuged $^{152}\text{Eu(III)}$ -humates, with 10 and 100 mg/L humic acid and conditioned for 1 hour, 2 days and

1 month, following addition of excess of non-labeled Eu(III). At around 300 hours of isotope exchange, samples with 1 hour conditioning time show no further isotope exchange; ^{152}Eu concentrations in the supernatant scatter around a mean value. All experimentally determined ^{152}Eu concentration data points are normalized by these two mean values for the two humic acid concentrations and the results are shown in Fig. 2.

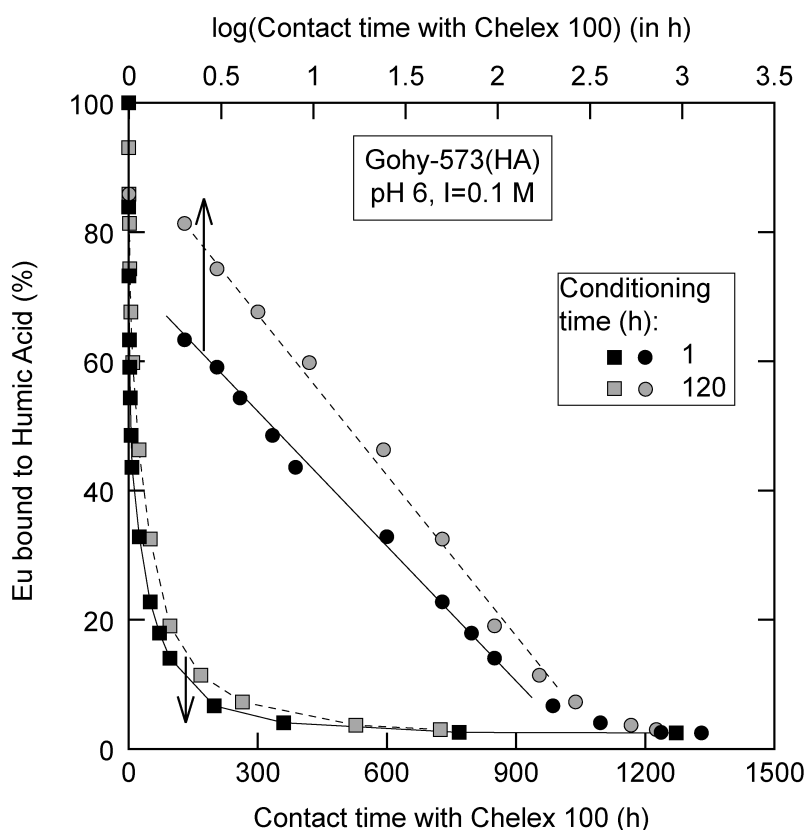


Fig. 1: Dissociation of Eu(III) complexed with Gohy-573(HA) at pH 6.0 ($I=0.1\text{ M NaClO}_4$) after conditioning for 1 and 120 hours. Dissociated Eu(III) is scavenged by the cation exchanger Chelex 100. The upper and lower scales refer to logarithmic and linear scales for the contact time with the cation exchanger, i.e., the Eu(III)-humate complex dissociation time.

One hour after addition of the non-labeled Eu(III), the degree of isotopic dis-equilibrium is found to be higher with higher humic acid concentration and longer conditioning time with ^{152}Eu labeled Eu(III). An exception is observed for the samples with 10 mg/L humic acid concentration, where the difference between 2 days and 1 month conditioning time is negligible. After addition of the non-labeled Eu(III), different initial isotope exchange kinetics are observed as indicated by the straight lines in Fig. 2. Irrespective of the conditioning time, however, this initial exchange kinetics is comparable for the same humic acid concentration (same line slopes).

The differences between the two dissociation kinetics experiments through cation exchange and isotope exchange are (i) that the total Eu(III) concentration in the isotope exchange

experiment is much higher and Eu(III)/humate-flocculate is generated, and (ii) that the degree of metal ion complexation of humic acid decreases along with the cation exchange contact time whereas conditions remain constant during isotope exchange. Despite these different experimental approaches, both experiments show comparable results. The comparable results between isotope exchange between Eu(III)/humate-flocculate and bulk solution on one hand, and dissociation of dissolved Eu(III)-humate by ion exchange, shows that Eu(III)/humate-flocculate may not be seen as a separate chemical phase. They results also provide the basis for preparation of samples with metal ions that to a large extent are in specified dissociation modes.

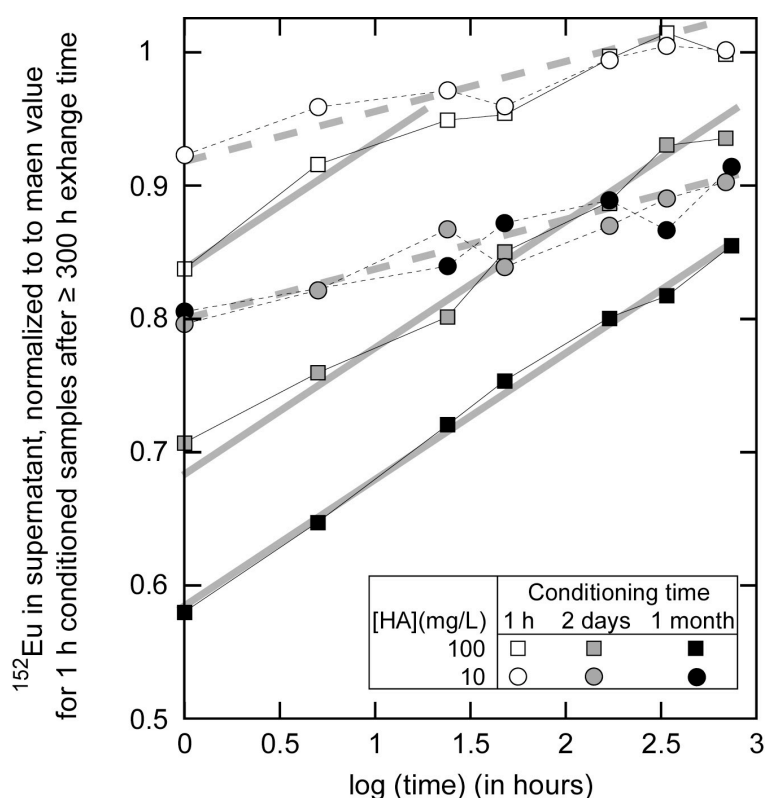


Fig. 2: Results of Eu(III) isotope exchange experiments. See text for details. The gradual increase of ^{152}Eu in the supernatant with time describes the slow exchange between humate bound and non-complexed Eu(III). Gray straight lines indicate initial exchange kinetics for 10 mgHA/L (dashed line) and 100 mgHA/L (continuous line).

TRFLS experiments

In Fig. 3, the fluorescence emission spectra of Cm(III) in humic acid solution are shown after different conditioning times and after 5 hours contact with Chelex resin. The decrease in fluorescence intensity for the Chelex treated sample reflects the decrease in Cm(III) concentration due to humate complex dissociation and removal by the exchanger. Vertical lines show the emission maxima for the aqueous Cm^{3+} ion (594 nm) and the Cm(III) humate complex (600.5 nm) (Kim et al. 1991, Kim et al. 1993). The spectra verify that Cm(III) in solution is basically quantitatively complexed to humate in all samples under the selected conditions. Furthermore,

the spectrum after stripping of fast dissociating Cm(III)-humate has the same maximum as the other spectra. Further analysis, however, shows that this band is narrower, with loss in intensity in the red-shifted range. In Fig. 4, the Cm(III)-humate spectrum after four weeks conditioning time is deconvoluted by a combination of the spectrum from the slow dissociation mode (“slow”) (cf. Fig. 3) and a second spectrum, representing Cm(III) removed from the humic acid solution by binding to the Chelex resin, i.e. dissociated from humic acid after five hours contact with the resin. The second spectrum shows two components, presumably a portion of the “slow” mode that also dissociates in the five hours contact time with Chelex, and a broad peak with a maximum around 602.8 nm associated with a fast dissociation kinetics. These results show that Cm(III)-humate association is rapid, generating a mixture of binding environments, as observed in differences in fluorescence spectra. Furthermore, these different binding environments exhibit different dissociation kinetics.

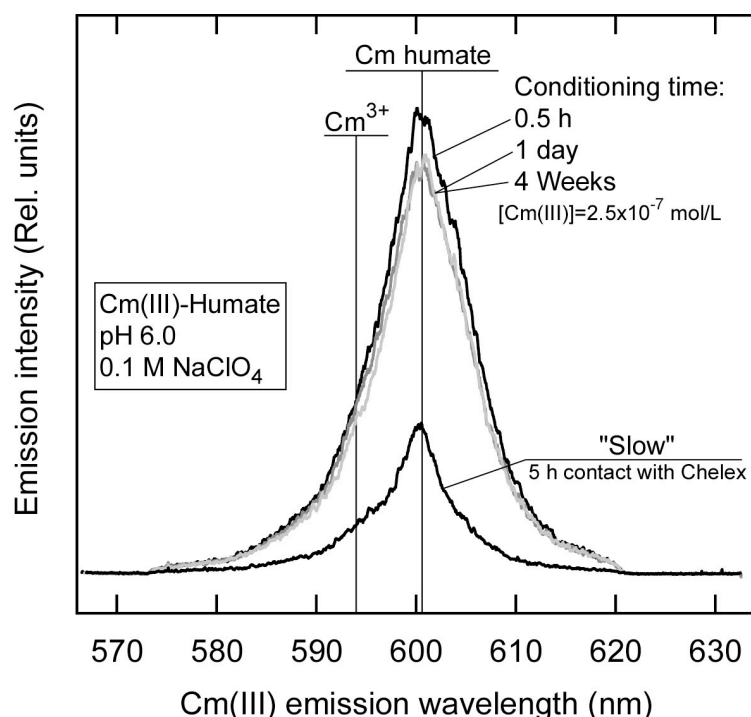


Fig. 3: Fluorescence emission spectra for Cm(III)-humate after different conditioning times and followed by 5 h contact with the cation exchanger Chelex 100 after 4 weeks of conditioning time.

Another source of information from TRLFS is the fluorescence life-time. Different components with different fluorescent life-times can be distinguished by measuring the evolution of their emission bands with fluorescence decay time, i.e., delay time between laser pulse and detector camera gating. Emission spectra after 1 and 256 ns decay time for 4 weeks contact time and the same sample after 5 hours contact with Chelex, are shown in Fig. 5. After 256 ns decay time, the fluorescence intensity has decreased by several orders of magnitude. The normalized spectra in Fig. 5, however, show that there is no significant change in spectral features. Despite differences in the emission bands between the two dissociation modes, no

peak shift with decay time is observed. Evaluation of the life-times yields 72 ± 2 ns for the mixture of fast and slow dissociation modes (602.8 nm peak) and 69 ± 5 ns for the slow dissociation mode (600.5 nm peak), which are essentially the same. Consequently, the life-time of humate complexed Cm(III) does not allow straight forward interpretation of complex coordination differences between the two kinetic modes.

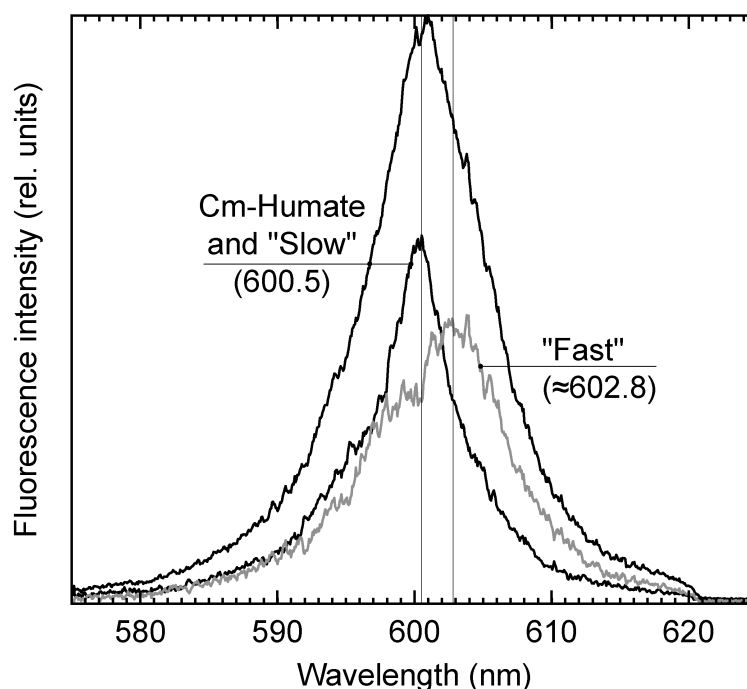


Fig. 4: Separation of the Cm(III)-humate spectrum after four weeks contact time (Cm-Humate) into the spectrum of the slow dissociation mode (“slow”) (cf. Fig. 3) and a the remaining signal representing Cm(III)-humate that has dissociated during five hours and been removed by contact with the Chelex cation exchanger. The latter spectrum is a mixture between fast dissociation mode (“fast”) and a shoulder for the slow mode that also shows partial dissociation within the five hours contact time with Chelex.

In Fig. 6, the Cm(III) fluorescence spectra of the complex with purified humic acid at pH=6.0 are compared to results from the natural groundwater Gohy-532. Also in the case of the natural groundwater, the Cm(III) emission is narrowed after 5 hours contact with the Chelex resin. This natural groundwater has a pH value of 7.5 and contains considerable amounts of carbonate species (Table 1). Under such groundwater conditions, the major reactions with trivalent actinides are likely to be hydrolysis, and complexation with both humic substances and carbonate (Panak et al. 1996, Artinger et al. 1998). In the study of Panak et al., at pH 7.5 and under 1% CO₂, in addition to Cm(III)-humate a considerable amount of the ternary complex Cm(CO₃)HA (peak maximum at 602.7 nm) is observed. In the Gohy-532 humic rich groundwater, Cm(III) spectra are only marginally red-shifted (around 1 nm) compared to the Cm(III) humic acid complex, with a slight broadening on the shoulder towards longer wavelengths (Fig. 6). Removal of fast dissociating Cm(III) complexes by contact with the Chelex resin results in narrowing of the bands in both cases. The results indicate, that the Cm(III)-

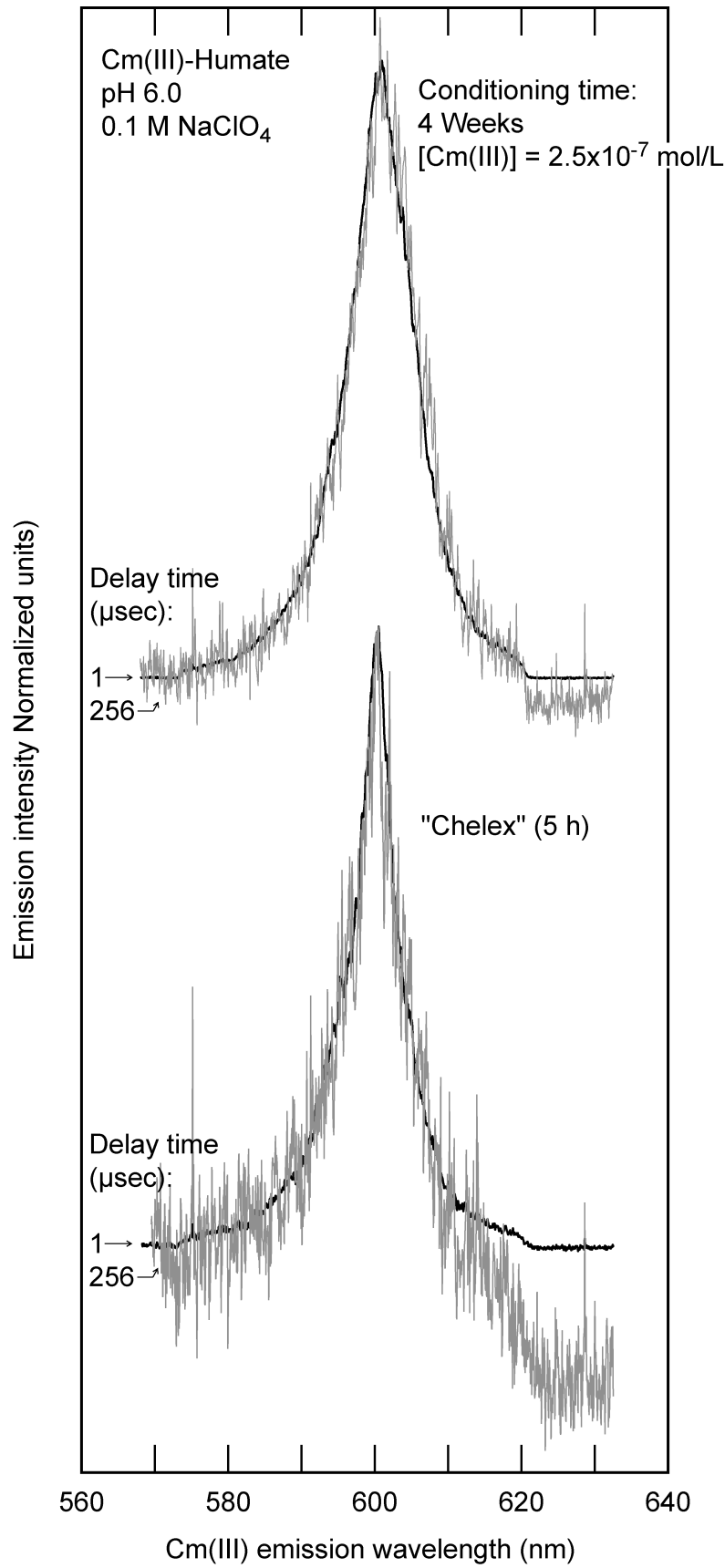


Fig. 5: Normalized fluorescence emission spectra for Cm(III)-humate (for details, see text).

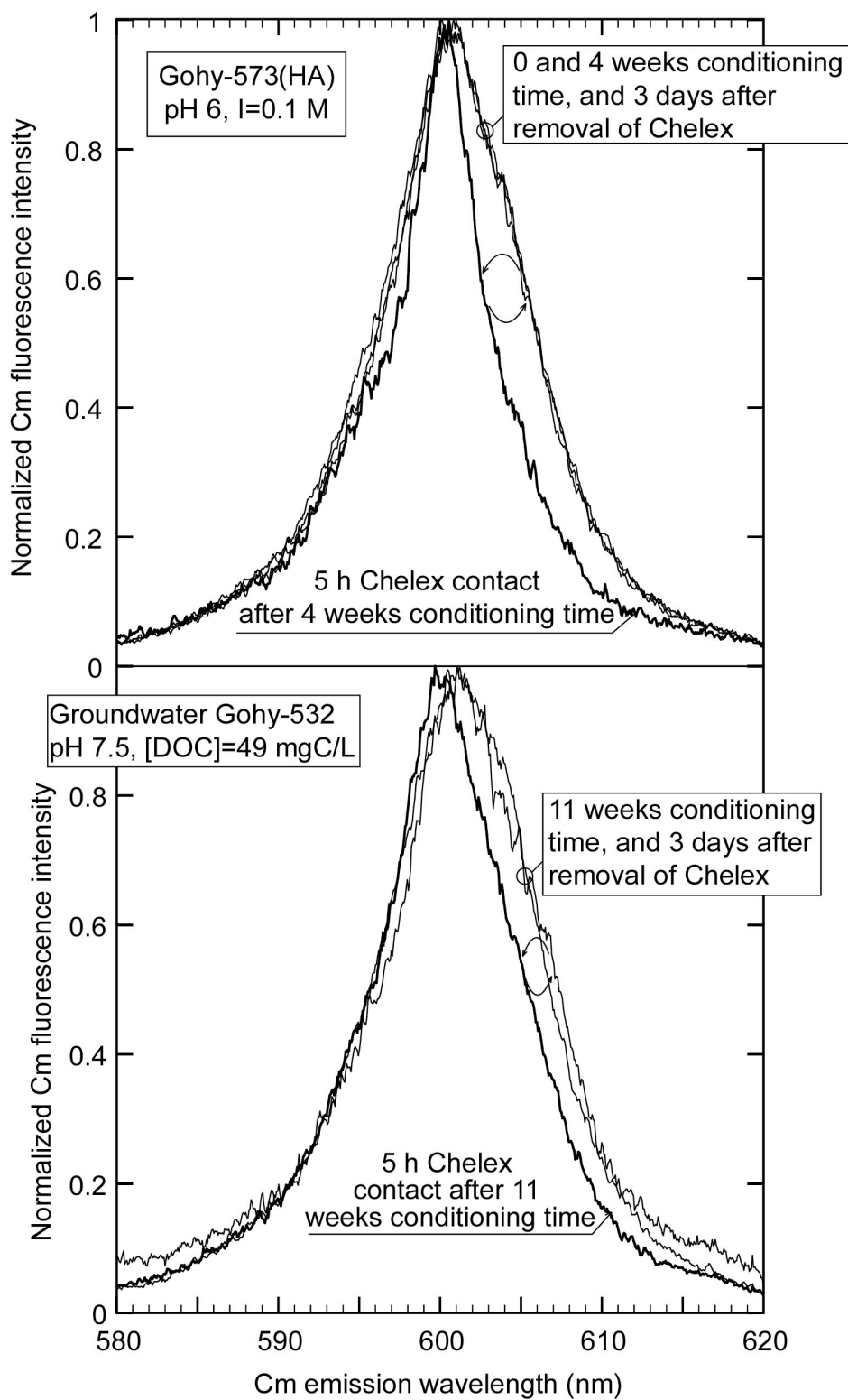


Fig. 6: Normalized fluorescence emission spectra for Cm(III) in purified Gohy-573(HA) humic acid solution in the non-hydrolyzing range (top), and in humic rich natural groundwater Gohy-532 (bottom). Spectra are recorded before and after contact with the cation exchanger Chelex 100, and again 3 days after removal of the cation exchanger. Three days after cation exchanger removal, the original spectra are obtained.

humate complex dominates in this groundwater with a small contribution of the ternary curium carbonate humate complex.

Published data report reversibility between the fast and slow dissociation modes (e.g. Artinger et al. 1998). Comparison of normalized emission spectra of original Cm(III)-humate and after removing the Chelex resin and leaving the samples for three days shows no significant differences (Fig. 6). This result verifies that the reversible exchange between the different dissociation modes reported in the literature applies to both Cm³⁺ ion complexation with purified humic acid in the non-hydrolyzing range (pH=6.0) and in the natural humic rich groundwater, where in addition to Cm-humate, ternary carbonate complexes are also formed.

EXAFS measurements

EXAFS spectra were recorded for Tb(III)-humate at pH 5.0 (I=0.1 M (NaClO₄)) after eight weeks of conditioning and the same sample after five hours treatment with chelex resin. The number of oxygen atoms in the first coordination shell cannot be determined with high precision, however, are found to be comparable (7.5 and 8.0). The average Tb(III) oxygen distance (R) decreases from 2.37 to 2.33 Å with Chelex treatment. The distribution width in average bond distance (σ^2) is also found to decrease (0.007 to 0.006). With comparable coordination numbers for the mixture of “fast” and “slow” modes on one hand, and only the “slow” mode in the second measurement, and about half of the Tb(III) removed by the Chelex treatment, the average Tb(III) oxygen distance in the “fast” mode can be estimated to be around 2.41 Å. These results verify above TRLS findings that the slow and fast dissociation modes are associated with considerable differences in the binding environment of the humate complexed metal ions.

Conclusions

The metal ion-humate interaction is frequently reported to be subject to different kinetic modes. These association/dissociation modes frequently show reversible exchange, whereas part of humate complexed metal ions is bound in a “quasi irreversible” (or, at least, very slow) mode. The present study verifies these findings. An important question is to which extent kinetic modes extracted from experimental data in order to describe the kinetic behavior are separate components representing distinguishable binding environments or represent a minimum number of parameters describing a non-discrete spectrum of binding environments. Trivalent actinide and lanthanide ions conditioned with humic acid under laboratory conditions, for varying time scales, exhibit differences in dissociation kinetics related to considerable differences in the complex coordination or binding environment. The same principle behavior is observed for Cm(III) added under laboratory conditions to a natural humic rich groundwater. This suggests that description the kinetic behavior of humate-metal ion interactions by a restricted number of distinct kinetic modes is appropriate.

References

- Artinger R., Kienzler B., Schuessler W., Kim J.I. (1998) "Effects of humic substances on the ²⁴¹Am migration in a sandy aquifer: Batch and column experiments with Gorleben Groundwater / sediment systems", *J. Contam. Hydrol.*, **35**, 261-275.
- Kim J.I., Buckau G., Li G., H., Duschner H., Psarros N. (1990) "Characterization of humic and fulvic acids from Gorleben groundwater", *Fresenius, J. Anal. Chem.*, **338**, 245.
- Kim J.I., Klenze R., Wimmer H. (1991) "Fluorescence Spectroscopy of Curium(III) and Application", *Eur. J. Solid State Inorg. Chem.*, **28**, 347.
- Kim J. I., Rhee D. S., Wimmer H., Buckau G., Klenze R. (1993) "Complexation of Trivalent Actinides Ions (Am³⁺, Cm³⁺) with Humic Acid: A Comparison of Different Experimental Methods", *Radiochim. Acta*, **62**, 35-43.
- Panak P., Klenze R., Kim J.I. (1996) "A study of ternary complexes of Cm(III) with humic acid and hydroxide or carbonate in neutral pH range by time-resolved laser fluorescence spectroscopy", *Radiochim. Acta*, **74**: 141-146.

Annex 2

**Origin and Mobility of Aquatic Humic Substances from Wetland Recharge in the
Gorleben Aquifer System**

G. Buckau, M. Wolf, S. Geyer, R. Artinger and J.I. Kim

Forschungszentrum Karlsruhe, Institut für Nukleare Entsorgung (FZK/INE)

Origin and Mobility of Aquatic Humic Substances from Wetland Recharge in the Gorleben Aquifer System.

G. Buckau¹⁾, M. Wolf²⁾, S. Geyer³⁾, R. Artinger¹⁾ and J.I. Kim¹⁾

¹⁾ Forschungszentrum Karlsruhe, Institut für Nukleare Entsorgungstechnik, D-76021 Karlsruhe, Germany

²⁾ GSF-Institute of Hydrology, D-85764 Neuherberg, Germany

³⁾ Umweltforschungszentrum Leipzig-Halle GmbH, D-04301 Leipzig, Germany

Abstract

Chemical, isotopic and noble gas temperature data are analyzed from groundwater of the Gorleben aquifer system, south, south-east and east of the Gorleben salt dome. Part of the deep groundwater originates from previous wetland recharge. These deep groundwaters are identified by the ^{18}O and ^2H content, as well as an enhanced ^{14}C source term. Furthermore, there is an indication that noble gas temperature is affected by change in recharge from previous wetland to present drained conditions. In the south-east of the investigation area, a wetland was drained around 290-250 years ago. At present, below this previous wetland, groundwater shows no sign of surface evaporation down to a depth of about 65 meters. It may be assumed that the deeper groundwater from wetland recharge originates from the previous wetland. Transport of groundwater from another present or former distant source affected by surface evaporation, however, cannot be entirely excluded. The existence of this groundwater affected by surface evaporation in the lower part of the aquifer is a key parameter for hydrological modeling. The aquatic humic substances in the deep groundwater from previous wetland recharge are shown to originate from microbiological turnover of young (via ^{14}C content) organic matter. Furthermore, these aquatic humic substances show no indication for retention or decomposition for times well beyond 250 years. This verifies the key statement for the purpose of predicting the influence of humic mediated radionuclide transport under natural groundwater conditions, namely that aquatic humic substances need to be treated like ideal tracers.

Introduction

Drainage of wetland leads to changes in groundwater recharge with respect to the amounts, and chemical and isotopic composition. Groundwater originates from infiltration of precipitated water. Stable isotopes (^2H and ^{18}O) of precipitation show a linear relationship between each other. Depending on distance from the sea, elevation and climatic conditions, the isotope values fall on the so called global meteoric water line (GMWL) (Craig 1961). Consequently, groundwater also falls on, or is slightly displaced from, the GMWL. One exception is groundwater that has experienced considerable surface evaporation prior to recharge. This is the case for wetlands where water is in direct contact with the atmosphere, as well as in arid regions (Gat 1980). Through surface evaporation, heavy water isotopes become enriched. Thereby, the relative enrichment of ^{18}O is higher than that of ^2H . In a wetland, turnover of organic matter is higher compared to the situation after drainage. For this reason, in such recharge the concentration of dissolved inorganic carbon (DIC) of biogenic origin with a high ^{14}C content is elevated relative to the situation after drainage. Consequently groundwater from wetland recharge conditions and after surface drainage can be distinguished from each other both by the stable isotope composition (^{18}O and ^2H) and the DIC ^{14}C inventory.

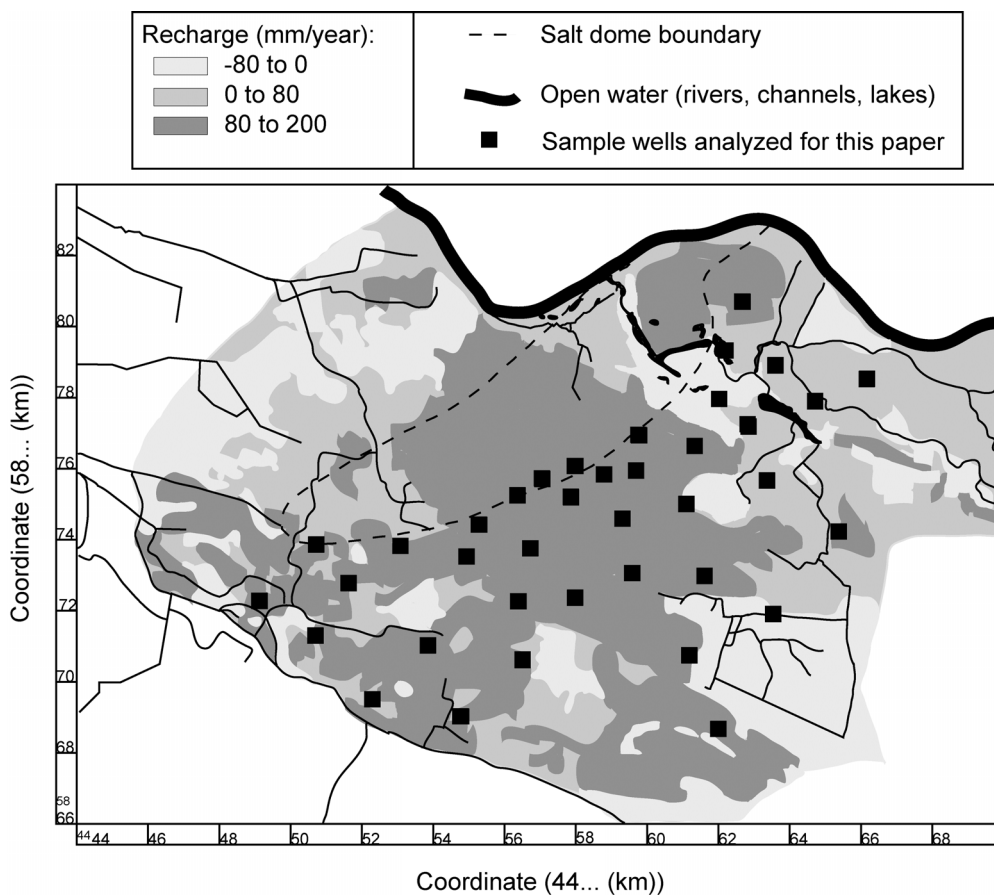


Fig. 1: Gorleben site with position of sampling wells analyzed for the present study.

The aquifer system studied is situated above and around an underlying salt dome in the area of Gorleben, Lower Saxony, Germany (Fig. 1). It is a complex aquifer system with no effective barriers for separation of groundwater into distinct layers, and exchange takes place over the entire depth (Buckau (ed.) 2000). Recharge takes place over large parts of the area, including the Hobeck hill close to the river Elbe in the north. Discharge takes place into the river Elbe flowing from east to west in the northern part of the area. The recharge situation has changed in the past due to drainage of wetland, as seen by the large number of drainage channels carrying water into the Elbe. In the south-east part of the area, drainage channels were constructed between around 1710 and 1750. This previous wetland recharge area thus has changed to a relatively dry area with net discharge. Another important feature of the groundwater composition is high concentrations of dissolved organic carbon (DOC), dominated by humic substances. These are introduced from different sources, including in-situ generation by partial mineralization of Miocene brown-coal particles in sandy sediments at depths below around 50 m (Buckau (ed.) 2000).

In this paper, a part of the Gorleben aquifer system situated south, south-east and east of the Gorleben salt dome is investigated (Fig. 1). Chemical and isotopic data are used in combination with historical records. Emphasis is given to changes introduced by drainage of the previous wetland in the southern part around 290-250 years ago. Conclusions focus on the stability and mobility of aquatic humic substances of different origin.

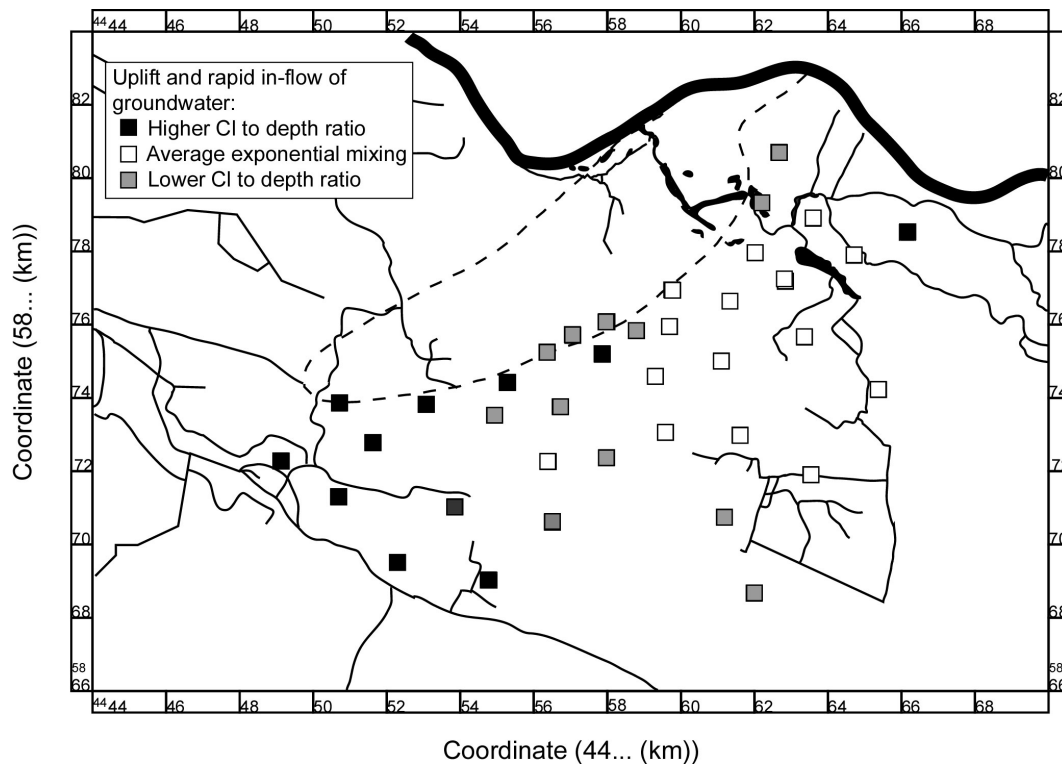


Fig. 2: Mapping of areas where up-lift and rapid inflow of groundwater takes place, relative to average exponential mixing of freshwater and brines, via chloride to depth ratio.

Results and discussion

The concentration of chloride versus depth is used for identification of inflow of recharge freshwater, mixing with salt brines from dissolution of the underlying salt dome and uplift of such brines (Fig. 2). Rapid inflow of freshwater (low chloride to depth ratio) takes place west of the drainage area in the south-east and partly along the salt dome boundary. Along the salt dome boundary also elevated chloride to depth ratios are found, as expected from the salt dome dissolution. Two areas are identified where groundwater up-lift takes place (high chloride to depth ratio). These are close to the Elbe in the north-east and an extended area in the south-west. From this information it can be concluded that in these two areas discharge takes place. The discharge in the south-west area is not only a consequence of drainage channels, but has been the case also prior to their construction. In this part of the investigation area, “iron stone” is found from oxidation of Fe(II) originating from up-lift of reducing groundwater.

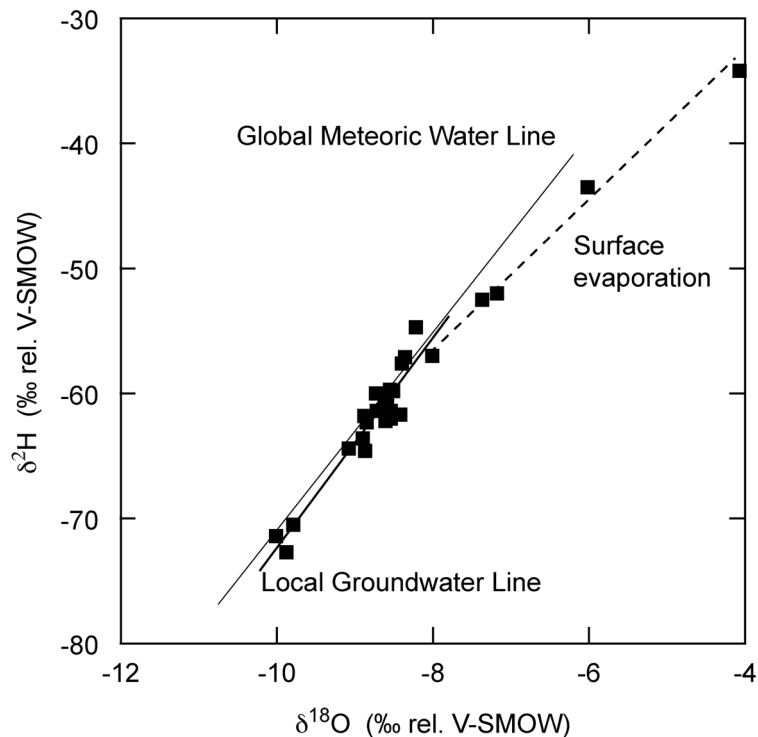


Fig. 3: ^2H and ^{18}O data for the investigated Gorleben groundwaters.

In view of the frequent drainage channels, one may expect that, contrary to the present situation, considerable recharge of water from wetland has taken place in earlier times. In order to identify present and past recharge conditions, the ^2H and ^{18}O isotopic groundwater composition is analyzed. Most of the data fall on a local water line slightly displaced from the GMWL. One group of the data, however, falls on a line with a deviating relationship between the ^2H and ^{18}O contents. These waters show the typical characteristics for isotope fractionation by surface evaporation. There is a limited number of ^2H data for groundwater

from the investigation area. Through surface evaporation, however, ^{18}O isotope data become enriched relative to non-surface evaporation influenced groundwater. Therefore, groundwaters influenced by surface evaporation can be identified by ^{18}O enrichment relative to the typical local distribution.

In Fig. 4, the locations of groundwaters affected by surface evaporation, evaluated by the ^{18}O content, are shown. Three of these waters are located where up-lift is identified by the chloride concentration to depth ratio. This would indicate that these are ancient surface evaporation affected groundwaters. Impact of present local conditions, however, cannot be excluded. More important is that nine such groundwaters cluster in the region east of the salt dome at depth between approximately 65 and 180 meters. Exceptions are groundwaters below the local recharge of the Hohbeck hill in the north-east. Above the cluster of surface evaporation affected groundwaters, non-affected groundwater is found. This implies that the groundwaters at depths greater than 65 m, influenced from surface evaporation, have been recharged before drainage had taken place about 290-250 years ago, whereas in the upper 65 m groundwater from non-wetland recharge is found. An alternative explanation would be that the groundwater in the lower aquifer in this part of the investigation area originates from more distant present of former sources of surface evaporated groundwater recharge. This cannot be entirely excluded from the present data. Given the high concentration of ^{14}C containing dissolved inorganic carbon (DIC) and DOC, dominated by humic and fulvic acids (cf. below), such a source would also presumably be a former or present wetland.

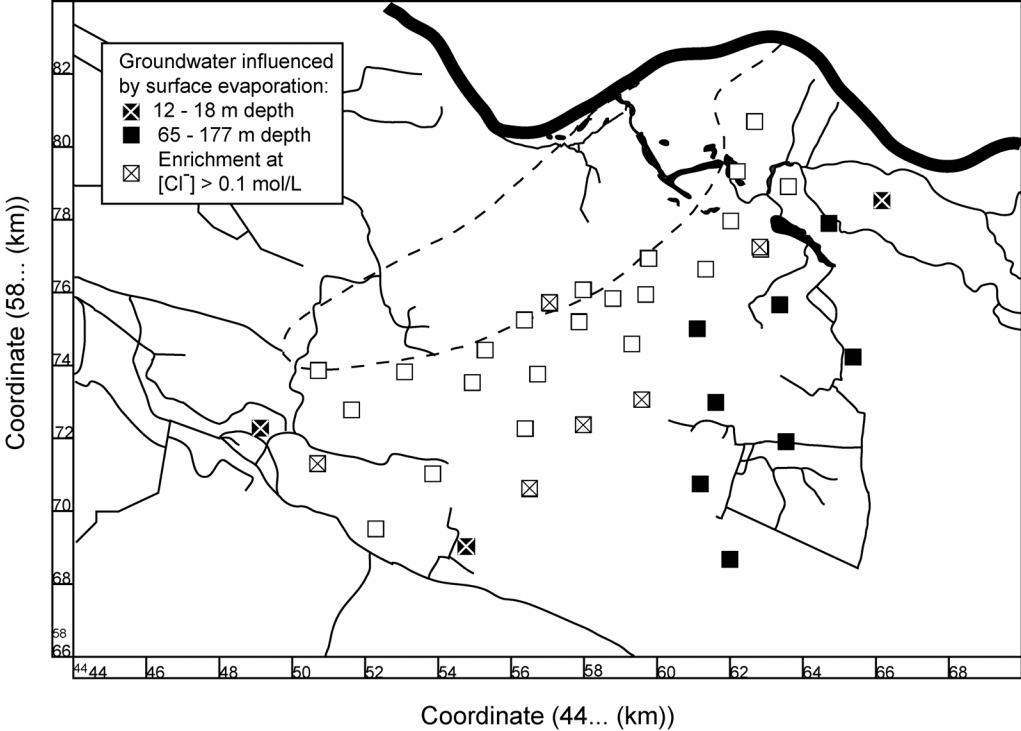


Fig. 4: Position of groundwater affected by surface evaporation prior to recharge.

The concentration of ^{14}C DIC in different types of groundwater from the investigation area is shown in Fig. 5. The ^{14}C concentrations are given as the concentration of DIC with a ^{14}C content of 100 pmc (percent modern carbon, i.e. the typical ^{14}C content of carbon in the atmosphere and thus the concentration in young organic material generated by such uptake). The present conifer forest recharge, deep groundwater of various origin and brines show similar amounts of ^{14}C DIC. The slightly elevated values for the present recharge reflect impact of nuclear atmospheric testing (Buckau et al. 2000). Surface near groundwater under agricultural activities shows elevated values due to the high turnover of organic matter. These values scatter considerable depending on local conditions (Kalblitz et al. 2000, Kalblitz and Geyer 2002) and the relative contribution from different agricultural activities and adjacent land. The values for deep groundwater from previous wetland also show enhanced ^{14}C DIC values that scatter considerably due to various contributions from wetland recharge and mixing with adjacent groundwater.

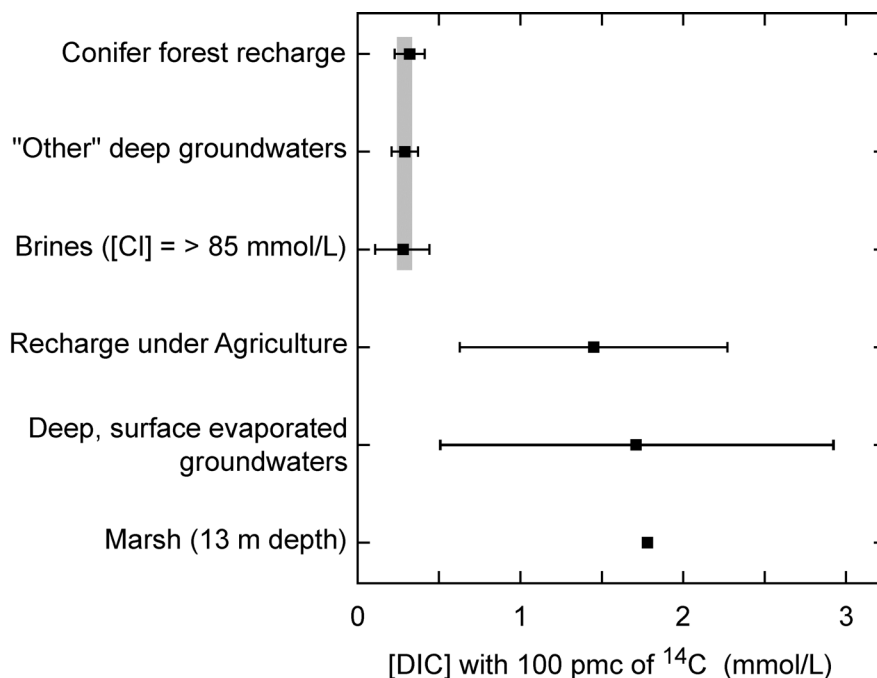


Fig. 5: ^{14}C DIC source term in different types of groundwater from the investigation area (expressed as the calculated concentration of DIC with a ^{14}C concentration of 100 pmc).

The value from a near surface marsh west of the salt dome is in the range of the elevated values for near surface recharge under agricultural land and deep groundwater from previous wetland recharge. These values show that the source term for deep groundwater, including the brines but excluding previous wetland recharge, is comparable to present conifer forest and that there is a considerable groundwater mixing over the entire depth with no significant ^{14}C decay even at around 250 m depth. Furthermore, old deep groundwater from previous wetland can be identified not only by the ^{18}O and ^2H data, but also via the high ^{14}C DIC source term.

This coupling between surface evaporation conditions in wetland (decrease in ^{18}O depletion) and the accompanying enhanced ^{14}C source term is demonstrated in Fig. 6.

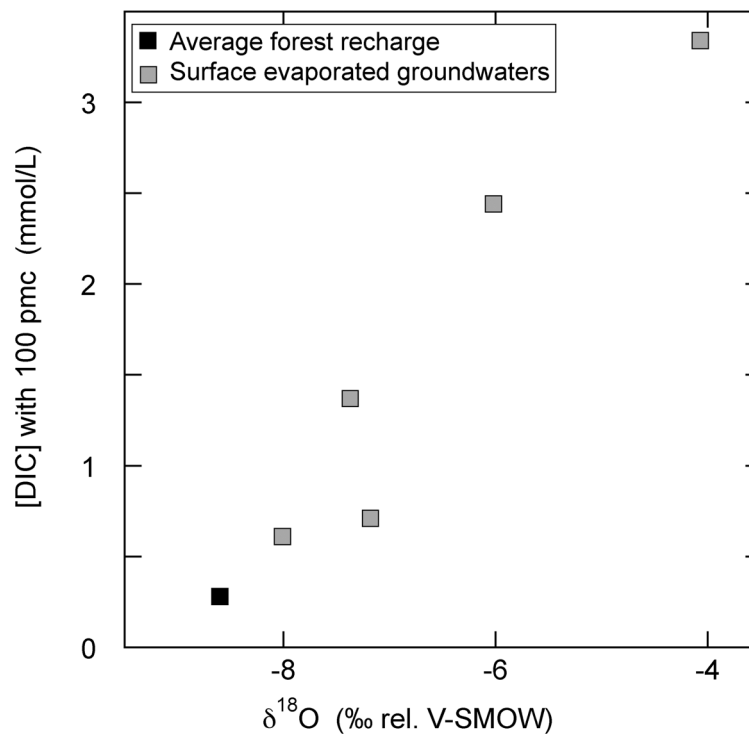


Fig. 6: Calculated concentration of DIC with 100 pmc versus ^{18}O of groundwater matrix.

An additional support for the above findings can be found in the analysis of noble gas temperatures (NGT). NGT of groundwater is based on the different temperature dependency in the solubility of different non-reactive gases in water (Mazor 1972). Precipitation can be expected to be in equilibrium with the different gases at relative concentrations reflecting the temperature of the air. If the water is percolating through an extended unsaturated zone, re-equilibration will take place reflecting the temperature in the unsaturated zone. The result of such a process is that the NGT will be smoothed relative to the variation in the air temperature (Stute and Schlosser 1993). Groundwater standing on the surface will be subject to warming through absorption of sunlight. This water with the corresponding concentrations of dissolved inert gases will then enter into the ground. Consequently, the NGT will be enhanced relative to recharge water under non-wetland conditions, the latter reflecting the average temperature in the unsaturated zone. As a result, an increase in NGT can be expected for groundwater from wetland, compared to the situation after drainage.

In Fig. 7, the noble gas temperature (from Suckow 1993) of Gorleben groundwater is plotted against the ^{18}O values. The values show a trend towards increasing noble gas temperature with increasing surface evaporation (i.e. enrichment in ^{18}O). Despite the low number of values

this is an additional indicator for the deep groundwater with ^{18}O enrichment and enhanced ^{14}C source term to originate from previous wetland recharge.

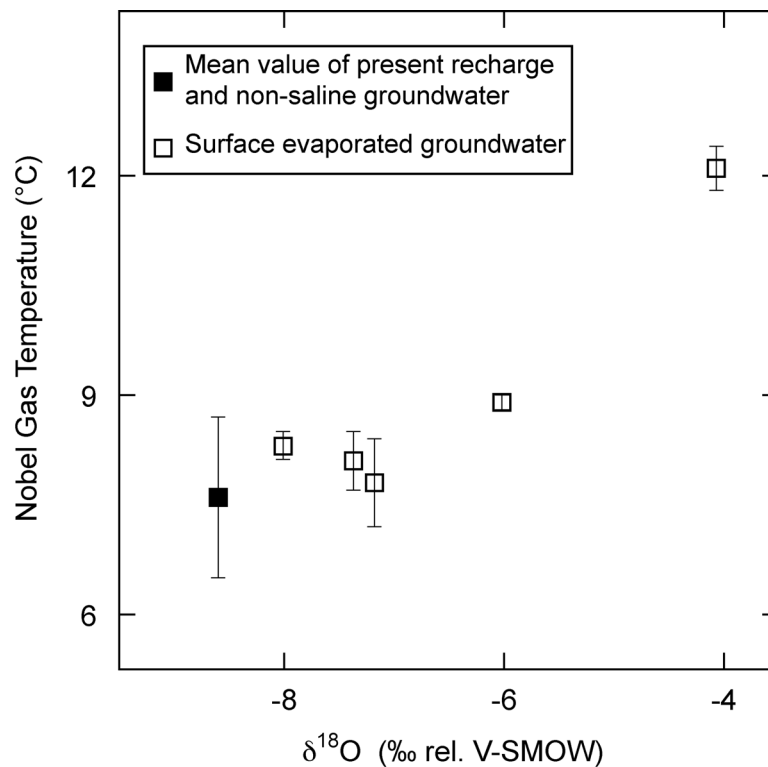


Fig. 7: Nobel gas temperature plotted against ^{18}O of surface evaporated groundwater recharged from previous wetland and average of groundwater from present recharge conditions.

The sum of humic and fulvic acids can be estimated from the concentration of DOC (dissolved organic carbon) and the known fractions of humic and fulvic acid of DOC from different aquifer systems. The concentration of DIC of biogenic origin can be calculated from the total concentration via ^{13}C data. In Fig. 8, the sum of aquatic humic and fulvic acids is plotted against the concentration of DIC of biogenic origin. This figure shows a narrow correlation for groundwater of different origin. This has several consequences. First, the origin of humic and fulvic acid in groundwater of different origin is microbiological turnover of organic matter, resulting in cogeneration of aquatic humic substances and DIC of biogenic origin. Furthermore, retention or decomposition of aquatic humic substances would result in data points below the gray shaded correlation in Fig. 8. Loss or retention of DIC would result in data points above this line. Therefore, aquatic humic and fulvic acids (and DIC) in the different types of Gorleben groundwater show no sign of significant retention or decomposition, but migrate like ideal tracers. This has previously been shown for aquatic humic substances from deep groundwater in-situ generation (Buckau (ed.) 2000). In this work the validity is extended to aquatic humic substances from wetland and non-wetland recharge and thus is also valid for the upper sediment zone.

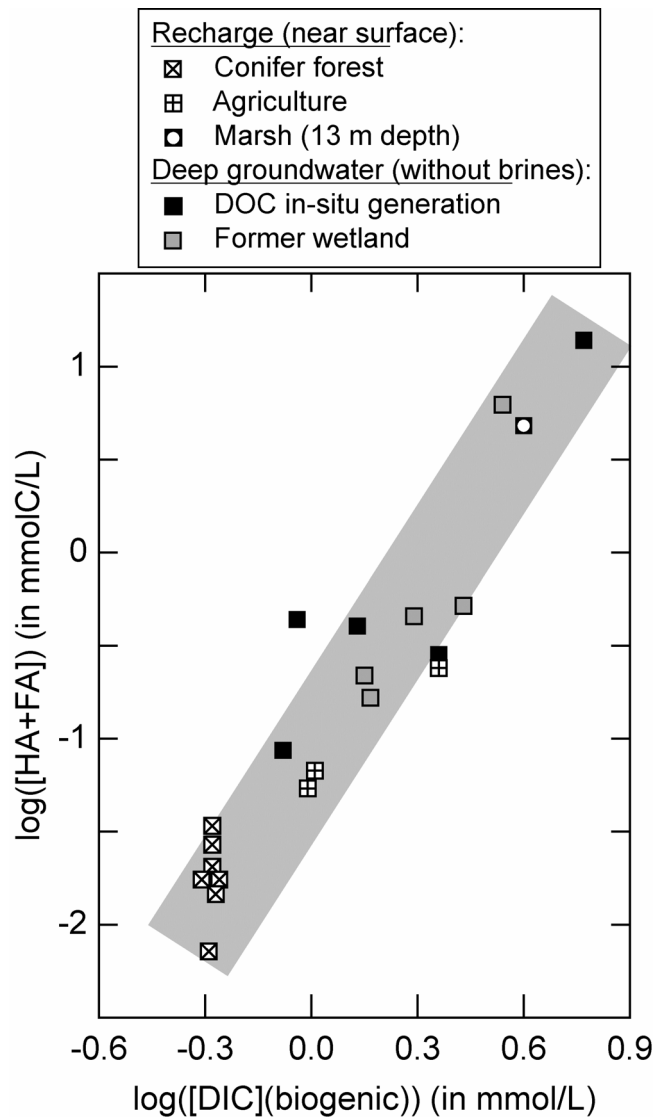


Fig. 8: The sum of aquatic humic and fulvic acids plotted against the concentration of DIC of biogenic origin for Gorleben groundwater of different origin.

Summary and conclusions

It is shown that aquatic humic acid fulvic acids are generated by microbiological turnover of organic matter. The source term for groundwater humic substances is sensitive to the land use and climatic conditions. These humic and fulvic acids remain stable over long transport distances and time spans. This includes transport from previous wetland surface to the depth. Consequently, for the purpose of predicting the influence of humic mediated radionuclide transport under natural groundwater conditions, aquatic humic substances need to be treated like ideal tracers.

Acknowledgement

BfS (“Bundesamt für Strahlenschutz”) is greatly acknowledged for providing the “Gorleben geochemistry database and different non-public reports on hydrology and geology of the Gorleben site from BGR (“Bundesamt für Geowissenschaften und Rohstoffe”). Many thanks to Graf Bernsdorf, the land owner of largest part of the investigation site, for providing information about the historical development with respect to land-use, especially the history of draining large parts of the area. A special thank to Mr. Fährmann, from DBE (“Deutsche Gesellschaft zum Bau und Betrieb von Endlagern für Abfallstoffe mbH”) for providing key information to the understanding of several hydrological features and past variation in vegetation and land-use.

References

- Buckau G. (Editor) (2000) "Effects of Humic Substances on the Migration of Radionuclides: Complexation and Transport of Actinides (Final Report)", Report EUR 19610 EN, 2000.
- Buckau G., Artinger R., Geyer S., Wolf M., Kim J.I., Fritz P. (2000) "¹⁴C Dating of Gorleben Groundwater", *Applied Geochemistry*, 15/5, 583-97.
- Craig H. (1961) "Isotopic Variations in Meteoric Waters", *Science*, **133**, 1702-3.
- Gat J.R. (1980) "The Isotopes of Hydrogen and Oxygen in Precipitation", in: Handbook of environmental isotope geochemistry, Vol. 1, The Terrestrial Environment, A, Eds.: P. Fritz and J. Ch. Fontes, Elsevier, pp. 21-47.
- Kalbitz K., Geyer S., Gehre M. (2000) "Land Use Impacts on the Isotopic Signature (¹³C, ¹⁴C, ¹⁵N) of Dissolved Humic Substances in a German Fen Area", *Soil Science*, 165, 728-36.
- Kalbitz K., Geyer S. (2002) "Different Effects of Peat Degradation on Dissolved Organic Carbon and Nitrogen", *Organic Geochemistry*, 33/3, 319-26.
- Mazor E. (1972) "Paleotemperatures and other Hydrological Parameters Deduced from Noble Gases Dissolved in Groundwaters, Jordan Rift Valley, Israel", *Geochim. Cosmochim. Stute M., P. Schlosser (1993) "Principles and Applications of the Noble Gas Paleothermometer"*, in *Climate Changes in Continental Isotopic Records. Geophysical Monograph*, 78, Eds.: P.K. Swart, K.C. Lohmann, J. McKenzie, and S. Savin, AGU, Washington DC, 89-100.
- Stute M., P. Schlosser (1993) "Principles and Applications of the Noble Gas Paleothermometer", in *Climate Changes in Continental Isotopic Records. Geophysical Monograph*, 78, Eds.: P.K. Swart, K.C. Lohmann, J. McKenzie, and S. Savin, AGU, Washington DC, 89-100.
- Suckow A. (1993) "Isotopenhydrologische und Edelgaspaleotemperatur-Untersuchungen im Deckgebirge über dem Salzstock Gorleben", Thesis, Universität Heidelberg.

Annex 3

**Synthetic Humic Acid Model Substances with Specific Functional Properties for the Use
in Complexation and Sorption Experiments with Actinides**

S. Sachs, K.H. Heise and G. Bernhard

**Forschungszentrum Rossendorf e.V., Institute of Radiochemistry, P.O. Box 510119
01314 Dresden, Germany
(FZR-IfR)**

Abstract

In order to improve the knowledge about the interaction processes between humic acids (HA) and metal ions, e.g., actinide ions, various HA model substances with different functional properties were developed at FZR-IfR. These include synthetic HA with different functional group contents and various structural elements, chemically modified HA with blocked phenolic OH groups as well as ^{14}C -labeled HA. Since start of the project, synthetic HA with distinct redox functionalities were developed.

The report gives an overview about the synthesis, characterization and application of HA with various functional properties. It describes the synthesis and characterization of the melanoidin-based HA type M1 and M42, which are characterized by different carboxyl group contents. In addition, the synthesis and characterization of modified HA with blocked phenolic OH groups as well as of HA with distinct redox functionalities are discussed.

1. Introduction

Due to their strongly pronounced complexation and redox properties, humic acids (HA) can significantly influence the speciation of toxic and radiotoxic metal ions, e.g., actinide ions, in natural aquifer systems and therefore their migration in the environment. Consequently, the study of the interaction processes between HA and metal ions is important for a reliable long-term risk assessment, for instance, for potential nuclear waste repositories or for the remediation of contaminated areas and facilities of the former uranium mining in Germany. However, depending on their origin, HA are characterized by a high structural and functional heterogeneity. Thus, there are a lot of difficulties in the thermodynamic description of the interaction processes between HA and metal ions in the environment. To obtain a more basic knowledge about the interaction processes between HA and metal ions, model investigations with well-defined HA model substances are necessary (Jensen et al., 1996). Such model substances, e.g., synthetic HA, should be characterized by chemical and operational properties which are comparable to natural HA. However, they should show a higher structural homogeneity, a well-defined functionality and a smaller amount of inorganic constituents than their natural analogues. The synthesis of HA model substances should offer the possibility for well-defined variations of the HA functionality and for a defined isotopic labeling (e.g., ^{13}C , ^{14}C) of the HA structure in order to study the impact of specific functional properties of HA on their interaction with metal ions and to determine the fate of HA in sorption experiments, respectively.

In our institute different synthetic HA model substances with various defined functional and structural properties as well as with a stable carbon-14 labeling of the molecular structure were developed based on the melanoidin concept (Pompe 1997, Bubner et al., 1998). These HA are applied for the study of the interaction behavior of HA with actinide ions in complexation and sorption experiments. In addition, a method for the synthesis of chemically modified HA with blocked phenolic OH groups was developed and spectroscopically verified (Pompe et al., 2000, Sachs et al., 2002). Such modified HA are very useful to study the influence of phenolic OH groups on the metal ion complexation by HA in order to improve existing complexation models for HA. For the detailed investigation of the redox behavior of HA

as well as of the redox stability of metal humate complexes, synthetic HA with pronounced redox properties are developed.

The present work describes the synthesis and characterization of HA with specific functional properties and points to applications of these HA model substances.

2. Synthesis and characterization of humic acids with specific functional properties

2.1 Melanoidin-based synthetic humic acids and their C-14 labeling

Melanoidins are formed by condensation of reducing sugars and α -amino acids, peptides or proteins (Angrick and Rewicki, 1980). Their formation is considered as one possible way for the formation of humic substances in the environment (Stevenson, 1994). Comparable to the natural humification process, a mixture of different macromolecular products is formed during the melanoidin synthesis. Due to their various solubilities at different pH values melanoidins can be operationally divided into a humin-like, a humic acid-like and a fulvic acid-like fraction. In previous studies (Pompe, 1997, Pompe et al., 1996 and 1998) we demonstrated that humic acid-like melanoidin fractions show functional, structural and chemical properties that are comparable to those of natural HA. However, compared to their natural analogues the synthetic products show a higher homogeneity in their charge-to-size ratios pointing to a higher homogeneity in their molecular mass distributions. Humic acid-like melanoidin fractions with different structural and functional properties can be synthesized by varying the precursor substances and the experimental conditions during the synthesis (Pompe, 1997). This offers the possibility to synthesize model substances for HA with specific properties, e.g., with different amounts of carboxyl groups or aliphatic and aromatic structural elements, in order to study the influence of these HA properties on the interaction between HA and metal ions. Furthermore, the synthesis of humic acid-like melanoidins starting from isotopically labeled, e.g., C-14 labeled, precursor substances enables us the possibility to synthesize HA that are stable labeled in their molecular structure (Bubner et al., 1998). These HA can be applied in sorption experiments.

In the present HUPA project two melanoidin-based synthetic HA, HA type M1 (Pompe et al., 1996) and type M42 (Pompe et al., 1998), which differ particularly in their carboxyl group contents are applied for comparative studies of the project partners.

2.1.1 Synthesis of humic acid type M1, M42 and [¹⁴C]M42

Generally, the synthesis of HA model substances starts from reducing sugars and α -amino acids in water. The reaction mixture is heated at defined conditions (reaction time and temperature) under reflux and nitrogen. Synthetic HA type M1 is synthesized from a mixture of 34 g xylose, 10 g phenylalanine, 5 g glycine, and 80 mL water which is refluxed for 10 hours. HA type M42 is prepared from 33 g xylose, 22 g glutamic acid monohydrate, and 60 mL water that are heated for 92 hours at 80 ± 2 °C.

After expiration of the reaction time and cooling of the reaction mixture the formed solid melanoidin fractions are separated from the liquid fractions, washed, and ground with ethanol and ether. Similar to the isolation of natural HA (e.g., Stevenson, 1994), the humic acid-like

melanoidin fractions are extracted from the solid product under nitrogen by 2 M NaOH solution. After that, the synthetic HA are precipitated from the alkaline extract with 2 M HCl, isolated by centrifugation, dialyzed against purified water (MWCO < 1000), and lyophilized. Carbon-14 labeled synthetic HA are synthesized according to the unlabeled HA, however, applying ¹⁴C-labeled amino acids as starting materials. We synthesized a ¹⁴C-labeled synthetic HA type M42 [¹⁴C]M42 with a specific activity of 2.38 MBq/g by adding [U-¹⁴C]glutamic acid (111 MBq) to the precursor substances.

2.1.2 Characterization of synthetic humic acids type M1, M42 and [¹⁴C]M42

Tab. 1 summarizes the elemental compositions and the functional group contents of HA type M1, M42 and [¹⁴C]M42 in comparison to the data of commercial available natural HA from Aldrich (AHA) and natural HA from the literature.

Tab. 1: Characterization of humic acid type M1, M42 and [¹⁴C]M42 in comparison to natural humic acids

Humic Acid	Elemental composition						
	C (%)	H ^a (%)	N (%)	S (%)	O ^b (%)	Ash (%)	Moisture (%)
Type M1	64.2 ± 0.9	4.8 ± 0.5	5.1 ± 0.1	-	19.0 ± 1.4	0.08	6.8
Type M42	56.1 ± 0.3	4.1 ± 0.1	4.4 ± 0.1	-	26.8 ± 0.3	0.11	8.4
AHA	58.6 ± 0.1	3.0 ± 0.1	0.8 ± 0.1	3.8 ± 0.1	23.5 ± 0.1	2.39	7.9
Literature (Stevenson, 1982)	50 - 60	4 - 6	2 - 6	0 - 2	30 - 35		
	Functional groups						
	COOH ^c (meq/g)	PEC ^d (meq/g)	Phenolic/acidic OH ^e (meq/g)				
Type M1	1.34 ± 0.05	1.69 ± 0.10	2.4 ± 0.1				
Type M42	3.76 ± 0.09	3.51 ± 0.07	2.0 ± 0.2				
Type [¹⁴ C]M42	3.63 ± 0.03	3.55 ± 0.05	not measured				
AHA	4.49 ± 0.14	4.60 ± 0.08	3.1 ± 0.1				
Literature (Stevenson, 1994)	1.5 - 5.7		2.1 - 5.7				

^a Corrected for the water content of the HA. ^b The oxygen content was calculated from the difference to 100 % in consideration of the ash and moisture content of the HA. ^c Determined by calcium acetate exchange (Schnitzer and Khan, 1972). ^d PEC: Proton exchange capacity. Determined by direct titration. ^e Radiometrically determined (Bubner and Heise, 1994).

Both synthetic HA show elemental compositions that are similar to those of AHA and other natural HA. They contain no sulfur due to the use of sulfur-free precursor substances. Comparing the ash contents of the synthetic HA with that of AHA it becomes obvious that the synthetic HA show only small amounts of inorganic impurities. Using high-purity starting materials and a Teflon equipment for the synthesis it becomes possible to synthesize ultra pure HA.

The carboxyl group content and the proton exchange capacity (PEC) of HA type M1 are low in comparison to natural HA, whereas synthetic HA type M42 has a higher carboxyl group content and PEC which are comparable to natural HA. Both HA show phenolic/acidic OH

group contents which are similar to that of natural HA. The significant differences in the carboxyl group contents and PEC of HA type M1 and M42 demonstrate that it is possible to vary the functional group contents of synthetic HA by changing their precursor substances. The functional group contents of the unlabeled and ^{14}C -labeled HA type M42 agree very well. This fact points to a good reproducibility of the HA synthesis with regard to the HA functional group content.

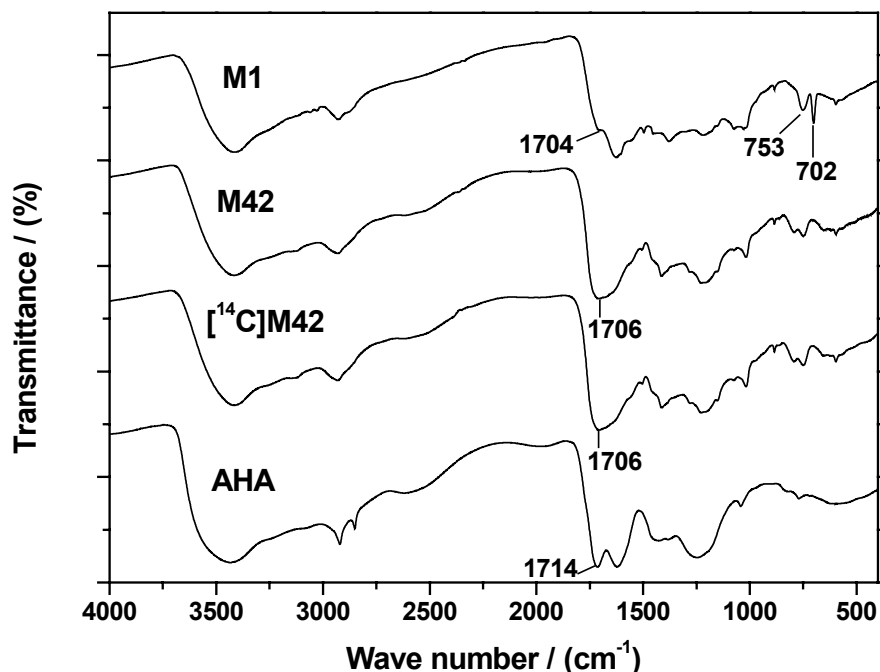


Fig. 1: FTIR spectra of synthetic humic acids in comparison to natural humic acid AHA.

In Fig. 1 the FTIR spectra of HA type M1, M42 and ^{14}C M42 are depicted in comparison to natural HA AHA. In general, synthetic HA type M1 and M42 show IR absorption bands which are similar to those observed for natural HA. The FTIR spectra confirm the results from the functional group analysis. At 1706 cm^{-1} (C=O stretching of COOH groups) synthetic HA type M42 shows an absorption band whose intensity is comparable to that of AHA and more intensive than that of synthetic HA type M1. This result verifies the higher carboxyl group content of HA type M42 compared to HA type M1. Synthetic HA type M1 shows characteristic IR absorption bands at 702 cm^{-1} and 753 cm^{-1} . These bands, which do not occur in the spectra of HA type M42 and AHA, indicate the presence of mono-substituted aromatic carbon structures in the HA molecules which are due to the use of phenylalanine as precursor substance for HA type M1. The differences in the FTIR spectra of synthetic HA type M1 and M42 show the possibility to change the structure of a synthetic HA by varying the precursor substances. The comparison of the FTIR spectra of HA type M42 and ^{14}C M42 in terms of the position of the IR absorption bands and the band intensities shows that both spectra are nearly identical. Thus, it can be concluded that both HA show a comparable structure, which points to a good reproducibility of the synthesis concerning the HA structure.

Synthetic HA type M1 and M42 were already used to study the interaction between HA and uranium(VI) (e.g., Pompe et al., 1996 and 1998, Denecke et al., 1997, Schmeide et al., 2003),

neptunium(IV)/(V) and plutonium(III) (Schmeide et al., 2003a). The actinide complexes of the synthetic HA show structural parameters and complexation constants that are comparable to those of natural HA. The similarities in the actinide ion interaction behavior of melanoidin-based synthetic HA and of natural HA offers us the possibility for the further application of these model substances to improve the knowledge about the interaction between HA and actinide ions.

Carbon-14 labeled synthetic HA were already successfully applied to study the neptunium(V) sorption onto granite and its mineral constituents in the presence of HA (Schmeide et al., 2002) as well as for kinetic studies on the uranium(VI) sorption onto phyllite, ferrihydrite and muscovite in the presence of HA (Schmeide et al., 2000).

2.2 Chemically modified humic acids with blocked phenolic OH groups

It is often assumed that only carboxyl groups act as metal ion complex forming functional groups of HA at pH values lower than pH 9. However, phenolic, enolic and alcoholic OH groups as well as amino groups, may also be involved in the complexation process, for instance, via the formation of chelate rings together with carboxylate groups (Stevenson, 1994). In order to study the influence of phenolic OH groups on the metal ion complexation by HA, we developed a method to modify HA phenolic OH groups by methylation (Pompe et al., 2000).

2.2.1 Synthesis of chemically modified humic acids with blocked phenolic OH groups

We synthesized chemically modified HA with blocked phenolic OH groups starting from original synthetic HA type M1, M42 and natural HA AHA. The chemical modification process, which is described in detail in (Pompe et al., 2000), comprises two steps (Fig. 2).

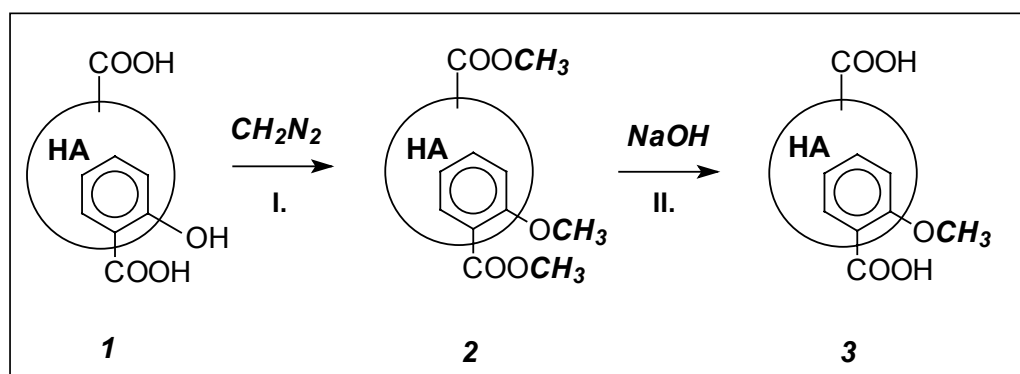


Fig. 2: Reaction scheme for the synthesis of chemically modified HA with blocked phenolic OH groups (Pompe et al., 2000), 1-original HA, 2-methylated HA (HA type HA-B), 3-HA with blocked phenolic OH groups (HA type HA-PB).

In the first modification step the original HA are methylated for three hours at -5 to 5 °C with diazomethane. This methylation results in the formation of methyl esters of carboxyl groups and methyl ethers of phenolic/acidic OH groups. The methylation is repeated several times until the incorporation of diazomethane into the HA molecule is completed, which can be identified on the yellow color of the non-reacted excess of diazomethane. In the second

modification step the methylated HA are treated with alkaline solution (2 M NaOH) under inert gas, whereby methyl esters of carboxyl groups that were formed by methylation with diazomethane are hydrolyzed. However, methyl ethers of phenolic OH groups remain blocked because these cannot be decomposed by alkaline hydrolysis. After hydrolysis, the modified HA are precipitated from the alkaline solution with 2 M HCl, separated by centrifugation, dialyzed (MWCO < 1000), and lyophilized.

It should be noted that in addition to phenolic OH groups also other acidic OH groups, i.e., enolic OH groups can be methylated by diazomethane, which also results in the formation of nonhydrolyzable methyl ether groups.

The applied modification process for the synthesis of HA with blocked phenolic OH groups was validated by ¹³C-CP/MAS-NMR spectroscopy (Sachs et al., 2002). By studying ¹³C-labeled and unlabeled synthetic and natural HA it was verified, that the derivatization causes only the intended structural changes of carboxyl and phenolic OH groups. It was shown that carboxyl groups have a higher affinity for methylation than phenolic OH groups. No significant side reactions, such as carbon and nitrogen methylations, were observed during the modification process. However, the methylation of some enolic OH groups cannot be excluded. The NMR results indicate that the overall structure of the HA is not significantly changed by the modification.

2.2.2 Characterization of HA type M1, M42 and AHA after modification with diazomethane

Tab. 2 summarizes the functional group contents of the unmodified and modified HA type M1, M42 and AHA.

Tab. 2: Characterization of unmodified and modified (HA-PB) HA type M1, M42 and AHA

Humic Acid	COOH ^a (meq/g)	Phenolic/acidic OH ^b (meq/g)	Ratio phenolic/acidic OH : COOH
M1	1.34 ± 0.05	2.4 ± 0.1	1.79
M1-PB	1.16 ± 0.03	0.9 ± 0.3	0.78
M42	3.76 ± 0.09	2.0 ± 0.2	0.53
M42-PB	3.12 ± 0.07	0.51	0.16
AHA	4.49 ± 0.14	3.1 ± 0.1	0.69
AHA-PB	2.67 ± 0.01	0.52	0.20

^a Determined by calcium acetate exchange (Schnitzer and Khan, 1972). ^b Radiometrically determined (Bubner and Heise, 1994).

Due to the chemical modification all HA show significant lower phenolic/acidic OH group contents. However, the results show that a complete methylation of all phenolic/acidic OH groups is not possible. Phenolic/acidic OH groups were still determined after modification. It has not yet been confirmed whether these functional groups are unmodified original phenolic and/or other H-acidic groups of the HA or acidic OH groups that were produced during the derivatization process by uncovering formerly sterically hindered functional groups. Nevertheless, the modified HA with blocked phenolic/acidic OH groups have 62 – 83 % less

phenolic/acidic OH groups than the original HA. A comparison of the carboxyl group contents of the corresponding HA shows that the modified HA have less carboxyl groups than the unmodified HA. An incomplete hydrolysis of methyl ester groups that were formed during the methylation could be one possible reason for that observation, which is supported by our NMR spectroscopic results (Sachs et al., 2002). Nevertheless, for all HA the molar ratio of phenolic/acidic OH to carboxyl groups becomes smaller due to the modification. This enables us to use these chemically modified HA to study the impact of phenolic/acidic OH groups on the interaction between HA and actinide ions.

Chemical modified HA with blocked phenolic/acidic OH groups were already successfully applied to study the influence of HA phenolic/acidic OH groups on the uranium(VI) (Pompe et al., 2000, Schmeide et al., 2003) and neptunium(V) complexation (Schmeide et al., 2003a) by HA. By comparing the complexation results (e.g., stability constants, metal ion loading capacities and structural parameters) of unmodified and modified HA conclusions can be drawn about the contribution of phenolic/acidic OH groups to the HA metal ion interaction process.

2.3 Synthetic humic acids with distinct redox properties

The migration behavior of toxic and radiotoxic metal ions, e.g., actinides, depends also on their oxidation state that can be influenced by HA (Choppin, 1999). Therefore, the detailed description of the influence of HA on the mobility of actinides in the environment requires, besides the knowledge about the actinide ion complexation by HA, the understanding of the effects of HA on the oxidation states of actinides. In order to study the redox properties of HA and the redox stability of actinide humate complexes in more detail, we developed synthetic HA model substances with pronounced redox functionalities.

The redox activity of humic substances can be ascribed to the redox system hydroquinone-quinone and to the oxidation of phenols. Therefore, our aim was to synthesize HA with high amounts of phenolic OH groups in order to get synthetic HA with distinct redox functionalities.

2.3.1 Synthesis of humic acids with distinct redox functionalities

The syntheses are based on the oxidation of hydroquinone in alkaline solution in the presence or absence of amino acids. Potassium peroxodisulfate is used as oxidizing agent (Eller and Koch, 1920, Adhikari et al., 1985). We synthesized HA type R9 by oxidation of 1.25 g hydroquinone in the absence of amino acids and HA type R17 and R18 by oxidation of 2.5 g hydroquinone in the presence of 1.7 g glycine or 1.9 g glutamic acid monohydrate, respectively. For syntheses, the starting materials are dissolved in 0.1 M NaOH at room temperature (pH of the reaction mixture: pH 12). Within 1 hour potassium peroxodisulfate (6.25 g for HA type R9 and 12.5 g for HA type R17 and R18) is charged to the reaction mixture at room temperature (HA type R9) or at 60 °C (HA type R17, R19). After that, the reaction mixtures are cooled down, the humic acid-like fractions of the oxidation products are precipitated with HCl (pH 1.5), separated by centrifugation, purified by dialysis against purified water (MWCO < 1000), and lyophilized.

2.3.2 Characterization of hydroquinone-based synthetic humic acids

The humic acid-like oxidation products of hydroquinone were characterized in terms of their elemental composition, functional group content and structure. In order to characterize the redox properties of these synthetic products we determined the redox capacities of the HA, which represent the charge equivalents per mass unit HA that can be transferred to Fe(III). According to (Mack et al., 2000) we determined the Fe(III) redox capacities of the hydroquinone oxidation products in comparison to HA type M42 and AHA at pH 3. Suspensions of FeCl₃ and HA were shaken under nitrogen and exclusion of light ([Fe³⁺]₀: 8.4-8.8 mmol/L, [HA]: 0.12 g/L, pH 3, I: 0.1 M KCl). The Fe(II) ions that were formed by the reduction process were quantified by UV-vis spectroscopy in form of the 1,10-phenanthroline complex after separation of the HA and masking of Fe(III) (Standard Methods, 1992). Furthermore, we determined the ferricyanide ([Fe(CN)₆]³⁻) redox capacities of the HA at pH 9.2 according to (Matthiessen, 1995). For this we prepared solutions of K₃[Fe(CN)₆] and HA under nitrogen and exclusion of light ([K₃[Fe(CN)₆]]: 0.5 mmol/L, [HA]: 5 mg/L, I: 0.1 M KCl, borate buffer pH 9.2). The time-dependent consumption of K₃[Fe(CN)₆] due to the reduction process was followed by UV-vis spectroscopy.

All humic acid-like oxidation products from hydroquinone show elemental compositions (not shown) that are comparable to natural HA. Depending on the molar ratio of the precursor substances HA type R17 and R18 have different nitrogen contents (4.9 % and 1.8 % for HA type R17 and R18, respectively). Tab. 3 summarizes some functional characteristics of HA type R9, R17 and R18 compared with HA type M42 and AHA. All humic acid-like oxidation products of hydroquinone show larger amounts of phenolic/acidic OH groups than HA type M42 and AHA. As expected, HA type R9 has the highest phenolic/acidic OH group content but a low amount of carboxyl groups. In contrast, HA type R17 and R18 synthesized in the presence of amino acids show higher carboxyl group contents and PEC that are similar to those of HA type M42 and AHA.

Tab. 3: Functional group contents of hydroquinone-based synthetic humic acids in comparison to HA type M42 and AHA

Humic Acid	COOH ^a (meq/g)	PEC ^b (meq/g)	Phenolic/acidic OH ^c (meq/g)
Type R9	1.92 ± 0.05	2.68 ± 0.01	7.2 ± 0.1
Type R17	4.38 ± 0.11	4.53 ± 0.08	6.0 ± 0.3
Type R18	4.21 ± 0.11	3.94 ± 0.26	5.4 ± 0.4
Type M42	3.76 ± 0.09	3.51 ± 0.07	2.0 ± 0.2
AHA	4.49 ± 0.14	4.60 ± 0.08	3.1 ± 0.1

^a Determined by calcium acetate exchange (Schnitzer and Khan, 1972). ^b Determined by direct titration. ^c Radiometrically determined (Bubner and Heise, 1994).

Fig. 3 shows the redox capacities of the humic acid-like hydroquinone oxidation products at pH 3 and pH 9.2 as a function of time compared with HA type M42 and AHA.

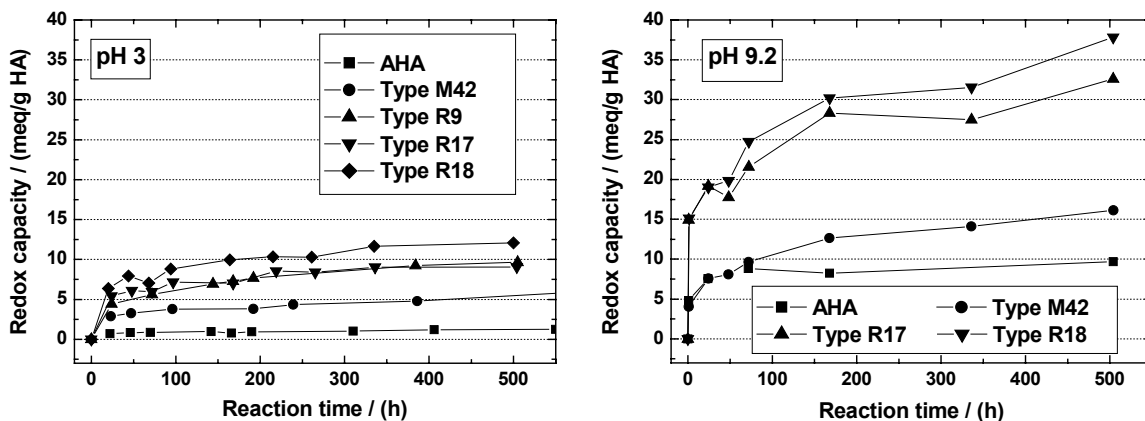


Fig. 3: Redox capacities of different humic acids at pH 3 and pH 9.2.

Both at pH 3 and pH 9.2, all synthetic HA show higher redox capacities than HA AHA. The highest redox capacities show the synthetic products that are based on hydroquinone. Referring the redox capacities of the HA to their phenolic/acidic OH group content, it becomes possible to draw conclusions concerning the kind of the redox active, i.e. electron-transferring, functional groups under the applied experimental conditions. In Fig. 4 the redox capacities of the studied HA after about 3 weeks reaction time are compared to their phenolic/acidic OH group contents.

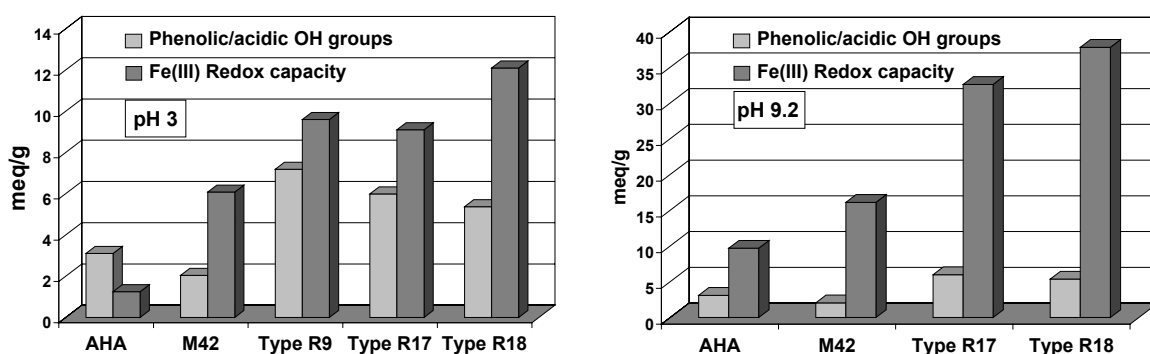


Fig. 4: Redox capacities of different humic acids after 3 weeks in comparison to their phenolic/acidic OH group contents.

In contrast to HA AHA, all synthetic HA show redox capacities at pH 3 that are higher than their phenolic/acidic OH group contents. This result indicates that there are additional HA functional groups or other redox processes than the simple oxidation of phenols contributing to the reduction of Fe(III). At pH 9.2 for all HA ferricyanide redox capacities were determined that are higher than their phenolic/acidic OH group contents.

To characterize the role of HA phenolic/acidic OH groups in the ferricyanide reduction by HA at pH 9.2, we synthesized a modified HA type R18 with blocked phenolic/acidic OH groups by methylation with diazomethane (cf. 2.2). The resulting modified HA type R18-PB has a residual amount of phenolic/acidic OH groups of 1.38 meq/g. We determined the redox

capacity of the modified product at pH 9.2 and compared it with those of the unmodified HA which is shown in Fig. 5.

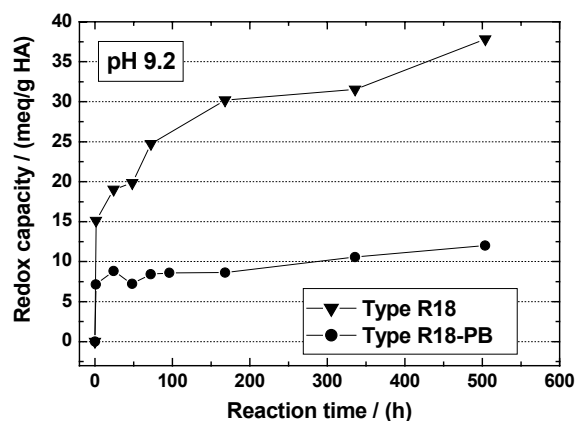


Fig. 5: Redox capacities of the unmodified and modified humic acid type R18 with blocked phenolic/acidic OH groups at pH 9.2.

From Fig. 5 it becomes obvious, that modified HA type R18 with blocked phenolic/acidic OH groups shows a significant lower redox capacity at pH 9.2 than the unmodified HA, where all phenolic/acidic OH groups of the HA are available for the reduction of $[\text{Fe}(\text{CN})_6]^{3-}$. Due to the modification the phenolic/acidic OH group content and the redox capacity of the HA decreased for 76 % and 64 %, respectively. This result indicates that phenolic/acidic OH groups of HA R18 play a major role in the redox behavior of HA type R18. However, also for HA type R18-PB, a redox capacity was determined which is higher than the phenolic/acidic OH group content (1.38 meq/g) of these HA. This result supports the assumption that there are other processes than the simple oxidation of phenolic OH groups contributing to the reduction of $[\text{Fe}(\text{CN})_6]^{3-}$ by this HA. The oxidation of phenols by $[\text{Fe}(\text{CN})_6]^{3-}$ proceeds via intermediate radicals and results in various, often complex products, e.g., complex phenolic compounds (Stewart, 1964). Subsequently, these phenolic compounds can be additionally capable for the reduction of $[\text{Fe}(\text{CN})_6]^{3-}$, resulting in redox capacities that are higher than those which are expected under consideration of the phenolic/acidic OH group content of the original starting compound. Due to the heterogeneous and complex structure of HA, such secondary reactions could occur during the reduction of $[\text{Fe}(\text{CN})_6]^{3-}$ by HA. Thus, this results in the observed redox capacities that are higher than the phenolic/acidic OH group content of the investigated HA.

We conclude that it is possible to synthesize humic acid-like substances with distinct redox capacities based on the oxidation of hydroquinone. These HA can be used to improve the understanding of the redox properties of HA, as exemplary shown for HA type R18 and R18-PB. In future we will apply HA with pronounced redox properties to study the redox stability of actinide humate complexes.

Acknowledgments

This study was supported by the EC Commission under contract No. FIKW-CT-2001-00128 and by the Bundesministerium für Wirtschaft und Arbeit under contract No. 02 E 9299. The authors thank R. Ruske and M. Meyer for their help in humic acid preparation and characterization.

References

- Adhikari, M., Sen, P., Krishnendu, D.: Studies on Synthesis of Humic Substances in Laboratory under Different Conditions. *Proc. Indian Natn. Sci. Acad.* **51A**, 876 (1985).
- Angrick, M., Rewicki, D.: Die Maillard-Reaktion. *Chemie in unserer Zeit* **14**, 149 (1985).
- Bubner, M., Heise, K.H.: Characterization of Humic Acids. II. Characterization by Radioreagent-Derivatization with [¹⁴C]Diazomethane. In: *FZR-43, Annual Report 1993* (Nitsche, H., Bernhard, G., eds.), Forschungszentrum Rossendorf, Institute of Radiochemistry, Rossendorf, Germany, 1994, p. 22.
- Bubner, M., Pompe, S., Meyer, M., Heise, K.H., Nitsche, H.: Isotopically Labelled Humic Acids for Heavy Metal Complexation. *J. Labelled Cpd. Radiopharm.* **XLI**, 1057 (1998).
- Choppin, G.R.: The Role of Humics in Actinide Behavior in Ecosystems. In: *Chemical Separation Technologies and Related Methods of Nuclear Waste Management* (Choppin, G.R., Khankhasayev, M.Kh., eds.), Kluwer Academic Publishers, 1999, p. 247.
- Denecke, M.A., Pompe, S., Reich, T., Moll, H., Bubner, M., Heise, K.H., Nicolai, R., Nitsche, H.: Measurements of the Structural Parameters for the Interaction of Uranium(VI) with Natural and Synthetic Humic Acids using EXAFS. *Radiochim. Acta* **79**, 151 (1997).
- Eller, W., Koch, K.: Synthetische Darstellung von Huminsäuren. *Berichte Dt. Chem. Gesellschaft* **53**, 1469 (1920).
- Jensen, B.S., Halken, T., Jestin, I., Jorgensen, D.: The Role of Colloids in the Migration of Radioelements. Final Report, EUR 16763 EN, 1996, p. 36.
- Mack, B., Baraniak, L., Heise, K.H., Bernhard, G., Nitsche, H.: Reduction of Iron(III) by Natural and Synthetic Melanoidine-Type Humic Acids. In: *FZR-285, Annual Report 1999* (Bernhard, G., ed.), Forschungszentrum Rossendorf, Institute of Radiochemistry, Rossendorf, Germany, 2000, p. 40.
- Matthiessen, A.: Determining the Redox Capacity of Humic Substances as a Function of pH. *Vom Wasser* **84**, 229 (1995).
- Pompe, S.: Entwicklung huminsäureähnlicher Melanoidine als Funktionalitätsmodelle für Huminsäuren und ihr Vergleich mit Fluka-Huminsäure hinsichtlich ihres Komplexbildungsverhaltens gegenüber Uran(VI). Dissertation, TU Dresden, Dresden, 1997.
- Pompe, S., Bubner, M., Denecke, M.A., Reich, T., Brachmann, A., Geipel, G., Nicolai, R., Heise, K.H., Nitsche, H.: A Comparison of Natural Humic Acids with Synthetic Humic Acid Model Substances: Characterization and Interaction with Uranium(VI). *Radiochim. Acta* **74**, 135 (1996).
- Pompe, S., Brachmann, A., Bubner, M., Geipel, G., Heise, K.H., Bernhard, G., Nitsche, H.: Determination and Comparison of Uranyl Complexation Constants with Natural and Model Humic Acids. *Radiochim. Acta* **82**, 89 (1998).

- Pompe, S., Schmeide, K., Bubner, M., Geipel, G., Heise, K.H., Bernhard, G., Nitsche, H.: Investigation of Humic Acid Complexation Behavior with Uranyl Ions Using Modified Synthetic and Natural Humic Acids. *Radiochim. Acta* **88**, 553 (2000).
- Sachs, S., Bubner, M., Schmeide, K., Choppin, G.R., Heise, K.H., Bernhard, G.: Carbon-13 NMR Spectroscopic Studies on Chemically Modified and Unmodified Natural and Synthetic Humic Acids. *Talanta* **57**, 999 (2002).
- Schmeide, K., Brendler, V., Pompe, S., Bubner, M., Heise, K.H., Bernhard, G.: Kinetic Studies of the Uranium(VI) and Humic Acid Sorption onto Phyllite, Ferrihydrite and Muscovite. In: *FZKA 6524, Wissenschaftliche Berichte* (Buckau, G., ed.). Forschungszentrum Karlsruhe, Karlsruhe, Germany, 2000, p. 149-170.
- Schmeide, K., Heise, K.H., Bernhard, G.: Neptunium(V) Sorption onto Granite and its Mineral Constituents in the Absence and Presence of Humic Acid. In: *FZR-343, Annual Report 2001* (Fanghänel, Th., ed.), Forschungszentrum Rossendorf, Institute of Radiochemistry, Rossendorf, Germany, 2002, p. 22.
- Schmeide, K., Sachs, S., Bubner, M., Reich, T., Heise, K.H., Bernhard, G.: Interaction of Uranium(VI) with Various Modified and Unmodified Natural and Synthetic Humic Substances Studied by EXAFS and FTIR Spectroscopy. *Inorg. Chim. Acta*, in press (2003).
- Schmeide, K., Sachs, S., Reich, T., Heise, K.H., Bernhard, G.: Determination of Structural Parameters for Plutonium(III), Thorium(IV), Neptunium(IV) and Neptunium(V) Humate Complexes by Means of XAFS Spectroscopy. This Report (2003a).
- Schnitzer, M., Khan, S.U.: *Humic Substances in the Environment* (McLaren, A.D., ed.), Marcel Dekker, Inc., New York, 1972.
- Standard Methods: *Standard Methods for the Examination of Water and Wastewater* (Greenberg, A.E., Clesceri, L.S., Eaton, A.D., eds.), American Public Health Association, 18th ed., Washington, DC, 1992.
- Stevenson, F.J.: *Humus Chemistry*. 1st ed., John Wiley&Sons, New York, 1982.
- Stevenson, F.J.: *Humus Chemistry*. 2nd ed., John Wiley&Sons, New York, 1994.
- Stewart, R.: *Oxidation Mechanisms. Applications to Organic Chemistry*. W.A. Benjamin, Inc., New York, 1964, p. 84.

Annex 4

**Determination of Structural Parameters for Th(IV), Np(IV), Np(V) and
Pu(III) Humate Complexes by Means of XAFS Spectroscopy**

K. Schmeide, S. Sachs, T. Reich, K.H. Heise and G. Bernhard

**Forschungszentrum Rossendorf e.V., Institute of Radiochemistry, P.O. Box 510119
01314 Dresden, Germany
(FZR-IfR)**

Abstract

Structural parameters for the near-neighbor surrounding of Pu(III), Th(IV), Np(IV) and Np(V) in complexes with various natural and synthetic humic and fulvic acids were determined by means of X-ray absorption fine structure (XAFS) spectroscopy. Furthermore, the interaction of the actinides with Bio-Rex70, a cation exchange resin having solely carboxylic groups as metal binding functional groups, was studied to determine structural parameters for the interaction of the respective actinide ions with carboxylic groups. Applying chemically modified humic acids with blocked phenolic/acidic OH groups, the influence of phenolic/acidic OH groups on the complexation of Np(V) by humic acids was studied in the neutral pH range. The structural parameters determined for actinide humate complexes were further compared with structural parameters of aqueous ions of the actinides and of solid actinide carboxylates given in the literature. The results indicate that the interaction between the actinide ions and humic acid is dominated by humic acid carboxylate groups. These carboxylate groups act predominantly as monodentate ligands. A contribution of phenolic/acidic OH groups to the complexation of Np(V) by humic acids at pH 7 cannot completely be excluded by EXAFS analysis.

1. Introduction

Humic substances (humic acids and fulvic acids) are known for their strong complexing ability towards radionuclides thereby influencing their migration behavior in the environment. Therefore, to understand and predict the mobility of actinides in natural aquifer systems, amongst others, information on the coordination chemistry of the actinides in humate and fulvate complexes is necessary.

In the present paper, we studied the coordination environment of Pu(III), Th(IV), Np(IV) and Np(V) in complexes with humic and fulvic acids by means of XAFS spectroscopy. This includes the X-ray absorption near-edge structure (XANES) spectroscopy and the extended X-ray absorption fine structure (EXAFS) spectroscopy. The XANES spectroscopy provides information on the electronic structure and the molecular symmetry of the absorbing atom and the EXAFS spectroscopy contains information on coordination numbers and bond lengths to neighbor atoms (Koningsberger and Prins, 1988).

Bio-Rex70 was used as reference substance to study the nature of metal complexation sites in humic substances further. Bio-Rex70 is a cation exchange resin that, in contrast to humic substances, has no phenolic OH groups but exclusively carboxylic groups as functional groups capable of binding metal ions. Thus, Th(IV), Np(IV) and Np(V) sorbates onto Bio-Rex70 were studied to determine structural parameters for the interaction of the respective actinide ion with carboxylic groups.

In case of Np(V), the influence of humic acid phenolic/acidic OH groups on the interaction between Np(V) and humic acid was studied at pH 7 applying modified humic acids with blocked phenolic/acidic OH groups in addition to the respective unmodified humic acids.

The structural parameters determined for the actinide humate complexes are further compared with structural parameters of the respective aqueous actinide ions and of solid actinide carboxylate complexes given in the literature.

2. Experimental

2.1 Sorbents

Both natural and synthetic humic substances were applied for the study. The natural humic substances were Kranichsee fulvic acid (KFA) that was isolated from surface water of the mountain bog 'Kleiner Kranichsee' (Johanngeorgenstadt, Saxony, Germany) (Schmeide et al., 1998) as well as the commercially available Aldrich humic acid (AHA; Aldrich, Steinheim, Germany). AHA was purified prior to use according to the literature (Kim and Buckau, 1988). The synthetic humic acid model substances were the humic acids type M1 (Pompe et al., 1996) and type M42 (Pompe et al., 1998). Furthermore, from AHA, M1 and M42 also the modified humic acids with blocked phenolic/acidic OH groups (AHA-PB, M1-PB, M42-PB) (Pompe et al., 2000) were applied which show phenolic/acidic OH group contents that are 62-75 % lower than those of the original humic acids. Bio-Rex70 (Bio-Rad, München, Germany) was used as reference substance.

2.2 Sample preparation

Th(IV) samples

$^{232}\text{Th(IV)}$ samples were prepared from AHA and from Bio-Rex70 at pH 1 (0.1 M HClO_4). The Th loading of the resulting wet pastes was 40.8 mg Th/g AHA and 1.9 mg Th/g Bio-Rex70 which corresponds to a Th loading of 14.7 % and 0.3 % of the proton exchange capacity (PEC) of the sorbents.

Np(IV) samples

A $^{237}\text{Np(IV)}$ stock solution was prepared by electrochemical reduction of a Np(V) solution to Np(III) followed by air oxidation to Np(IV). The tetravalent oxidation state of Np was verified by NIR absorption spectroscopy. Np(IV) samples were prepared from AHA, KFA, M42 and from Bio-Rex70 at pH 1 (0.1 M HClO_4) under inert gas conditions. The Np loading of the resulting wet pastes was between 4 and 41 mg Np/g sorbent (0.7 % to 15 % of the PEC of the sorbents).

Np(V) samples

$^{237}\text{Np(V)}$ complexes were prepared from the unmodified humic acids AHA, M1 and M42 and from the modified humic acids AHA-PB, M1-PB and M42-PB with blocked phenolic/acidic OH groups as well as from Bio-Rex70. The Np(V) humate solutions were prepared at pH 7 under inert gas conditions with Np and humic acid concentrations of 0.88-1.04 mmol/L and of 8.1-27.5 g/L, respectively (ionic strength: 0.1 M NaClO_4). The Np loading was between 2.3 and 2.8 % of the PEC of the sorbents. The Np(V)-Bio-Rex70 sorbate was prepared at pH 7 in 0.1 M NaClO_4 . The Np loading of the resulting wet paste was 121.3 mg Np/g Bio-Rex70 (5.1 % PEC).

Pu(III) samples

^{242}Pu was purified in the tetravalent oxidation state by anion exchange chromatography using TEVA resinTM. Purified Pu(IV) was electrochemically reduced to Pu(III). The trivalent oxidation state of Pu was verified by NIR absorption spectroscopy. Pu(III) samples were

prepared from KFA and from M42 at pH 1 (0.1 M HClO₄) under inert gas conditions. The Pu loading of the resulting wet pastes of KFA and M42 was 11.6 and 3.9 mg Pu per g sorbent, respectively.

The experimental conditions are described in more detail in Schmeide et al. (2003b,c) and Sachs et al. (2003).

2.3 XAFS measurements and data analysis

The XAFS measurements were carried out at the Rossendorf Beamline (ROBL) (Reich et al., 2000a) at the European Synchrotron Radiation Facility (ESRF) in Grenoble, France. The actinide L_{III}-edge X-ray absorption spectra were collected in fluorescence mode (Th(IV) samples, Pu(III) samples, Np(V) humates) and transmission mode (Np(IV) samples, Np(V)-Bio-Rex70), respectively, at room temperature. A Si(111) double-crystal monochromator was used in fixed-exit mode. Several EXAFS scans were collected from each sample and averaged.

Data analysis was performed according to standard procedures (Koningsberger and Prins, 1988) using the EXAFSPAK software (George and Pickering, 1995). The program FEFF6 (Rehr et al., 1992) was used to calculate theoretical scattering amplitudes and phase-shift functions.

The EXAFS oscillations were fitted to the EXAFS equation using one coordination shell with oxygen as backscatterer in case of Th(IV), Np(IV) and Pu(III). In case of Np(V), a two-shell fit with axial and equatorial oxygen atoms (O_{ax}, O_{eq}) as backscatterers was used. The multiple scattering along the neptunyl unit (O_{ax}-Np-O_{ax}) was also included in the fit.

3. Results and discussion

3.1 Th(IV) humate and Bio-Rex70 complexes

The raw Th L_{III}-edge k³-weighted EXAFS spectra and the corresponding Fourier transforms (FTs) of the Th(IV) complexes with AHA and Bio-Rex70 are shown in Fig. 1. Both the EXAFS spectra and the FTs of the samples are comparable. The FTs are dominated by a peak at about 1.8 Å representing oxygen atoms coordinated to Th(IV).

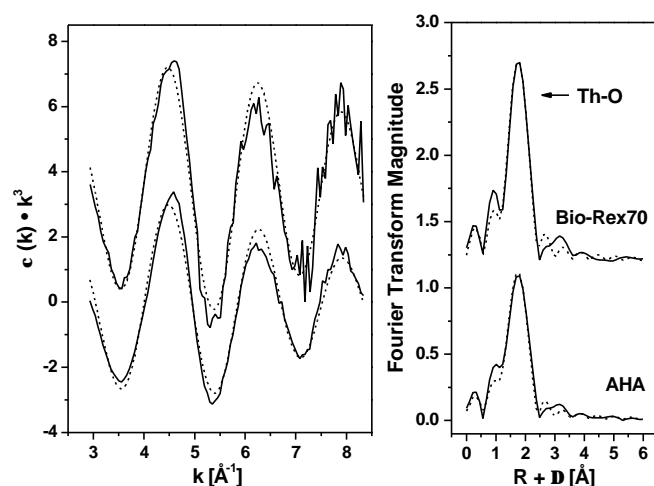


Fig. 1: Th L_{III}-edge k³-weighted EXAFS spectra and corresponding Fourier transforms of Th(IV) samples. Solid lines: experiment, dashed lines: fit.

In Table 1 the structural parameters determined for the Th(IV) complexes are summarized such as coordination number (N), bond length (R) and Debye-Waller factor (σ^2) obtained from fits to the EXAFS equation. The coordination numbers and Th-O bond lengths of Th(IV)-AHA and Th(IV)-Bio-Rex70 are comparable. In both samples, Th(IV) is surrounded by 11 oxygen atoms at a distance of 2.44 Å. Since Bio-Rex70 has no phenolic OH groups but exclusively carboxylic groups as functional groups capable of binding metal ions, it can be concluded that the interaction between AHA and Th(IV) is dominated by humic acid carboxylic groups under the experimental conditions applied. This result was expected since at pH 1 the phenolic OH groups of the humic substances are fully protonated. The larger EXAFS Debye-Waller factor determined for the oxygen coordination shell of Th(IV)-AHA in comparison to those of Th(IV)-Bio-Rex70 and the aqueous Th(IV) ion points to a broader distribution of Th-O bond lengths in the Th(IV) humate complex.

Tab. 1: EXAFS structural parameters of Th(IV) complexes in comparison to literature data of Th(IV) samples

Sample	Th-O			ΔE_0 [eV]	Ref.
	N	R [Å]	σ^2 [Å ²]		
Th(IV)-AHA	10.6 ± 1.5	2.44 ± 0.01	0.013	-17.3	
Th(IV)-Bio-Rex70	11.0 ± 2.1	2.45 ± 0.02	0.009	-17.3	
Th(IV)-AHA	10.1	2.43	0.013	1.0	Denecke, 1999
Th(IV)-Bio-Rex70	9.4	2.44	0.012	1.0	Denecke, 1999
Th(H ₂ O) _x ⁴⁺	10.8 ± 0.5	2.45 ± 0.01	0.007	4.0	Moll, 1999

The 95 % confidence limits are given for N and R as estimated by EXAFSPAK.

Within the experimental error, the structural parameters determined for the Th(IV) humate and Bio-Rex70 complexes agree with those determined by Denecke et al. (1999). Furthermore, the data of Th(IV)-AHA are comparable to those of the aqueous Th(IV) ion (Moll et al., 1999). This shows that the interaction between Th(IV) and humic acid carboxylic groups induces no shortening of the Th-O bond length. Furthermore, since no carbon atoms of the binding humic acid carboxylate groups can be detected, it is not possible to determine separate coordination numbers for carboxylate groups and water molecules coordinated to Th(IV) by EXAFS analysis.

To identify the binding mode (monodentate, bidentate or bridging) of humic acid carboxylate groups to Th(IV), the Th-O bond length of Th(IV) humate is compared with those of Th(IV) model compounds which contain carboxylic groups. The average Th-O bond length observed for monodentate coordinated carboxylate groups in various Th(IV) malonates (Zhang et al., 2000) as well as in Th(IV) oxalate (Akhtar and Smith, 1975) is 2.42 ± 0.04 Å. This bond length is comparable to the bond length obtained for Th(IV)-AHA (2.44 ± 0.02 Å). This points to a predominant monodentate coordination of humic acid carboxylate groups to Th(IV).

3.2 Np(IV) humate and Bio-Rex70 complexes

The tetravalent oxidation state of Np and its stability in the humate and Bio-Rex70 complexes within the time of our experiment was verified by means of NIR absorption spectroscopy (Schmeide et al., 2003b) and XANES spectroscopy. In Fig. 2, the XANES spectrum of Np(IV)-AHA is shown in comparison to that of the corresponding Np(V) sample. The spectrum of Np(IV) humate shows the characteristic near-edge features of Np(IV) compounds: A more intense ‘white line’ peak, but no additional shoulder on the high energy side of the ‘white line’ as generally observed for Np(V) samples. Identical spectral features were obtained for the Np(IV) complexes of KFA, M42 and Bio-Rex70.

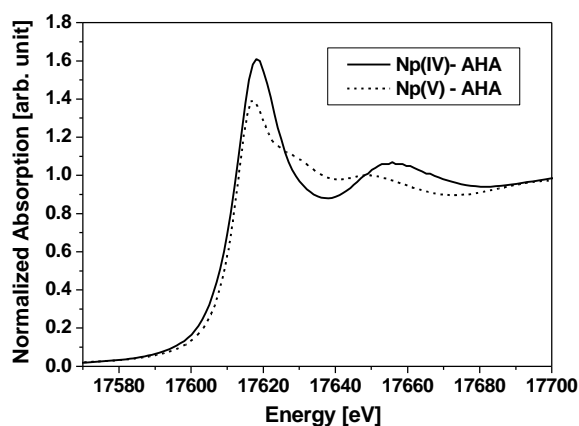


Fig. 2: Normalized Np L_{III} -edge XANES spectra.

The raw Np L_{III} -edge k^3 -weighted EXAFS spectra and the corresponding FTs of the Np(IV) samples are shown in Fig. 3. Both the EXAFS oscillations and the FTs of all Np(IV) complexes are similar. The FTs are dominated by one peak at about 1.7 Å representing one coordination shell with oxygen as backscatterer. No Np-Np contributions were observed in the spectra, i.e., polynuclear Np species did not form.

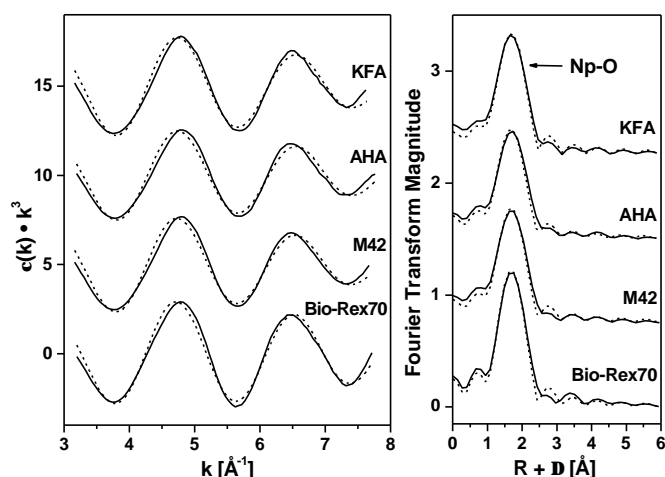


Fig. 3: Np L_{III} -edge k^3 -weighted EXAFS spectra and corresponding Fourier transforms of Np(IV) samples. Solid lines: experiment, dashed lines: fit.

The EXAFS structural parameters determined for the Np(IV) complexes are compiled in Tab. 2 and compared to literature data of Np(IV) samples.

In the Np(IV) humate complexes, the Np(IV) ion is surrounded by about 11 oxygen atoms at a distance of 2.36 Å. Comparable parameters are determined for the Np(IV) complex with

Bio-Rex70. This again verifies the dominance of carboxylic groups for the complexation of actinide ions by humic substances at pH 1 (cf. paragraph 3.1).

Tab. 2: EXAFS structural parameters of Np(IV) complexes in comparison to literature data of Np(IV) samples

Sample	Shell	N	R [Å]	σ^2 [Å ²]	ΔE_0 [eV]	Ref.
Np(IV)-KFA	Np-O	11.3 ± 1.7	2.36 ± 0.01	0.0162	-11.1	
Np(IV)-AHA	Np-O	10.1 ± 1.7	2.36 ± 0.01	0.0159	-11.1	
Np(IV)-M42	Np-O	11.0 ± 1.7	2.36 ± 0.01	0.0166	-11.1	
Np(IV)-Bio-Rex70	Np-O	10.2 ± 1.3	2.37 ± 0.01	0.0127	-11.1	
Np(H ₂ O) _x ⁴⁺ in 1 M HClO ₄	Np-O	9 ± 1	2.37 ± 0.02	0.007		Antonio, 2001
Np(H ₂ O) _x ⁴⁺ in 1 M HCl	Np-O	11.2 ± 1.1	2.40 ± 0.012	0.0075		Allen, 1997
Np(H ₂ O) _x ⁴⁺ in 2 M H ₂ SO ₄	Np-O	11 ± 1	2.39 ± 0.01	0.0118		Reich, 2000a
	Np-S	2.2 ± 0.9	3.07 ± 0.02	0.0070		

The 95 % confidence limits are given for N and R as estimated by EXAFSPAK.

Compared to the aqueous Np(IV) ion in hydrochloric or sulfuric medium (Allen et al., 1997; Reich et al., 2000a), the coordination number of the humates is similar, only the Np-O bond length is shortened by about 0.04 Å due to humate complexation. A similar shortening of the bond length has been previously observed for U(VI) humate complexes ($R_{U-O_{eq}} = 2.37-2.39$ Å) (Denecke et al., 1997, 1998; Schmeide et al., 2003a) compared to $UO_2(H_2O)_5^{2+}$ ($R_{U-O_{eq}} = 2.41$ Å) (Allen et al., 1997) and can be interpreted as further evidence of actinide humate complex formation. However, as found for Th(IV), a differentiation between humic acid carboxylate groups and water molecules coordinated to the Np(IV) ion is not possible by means of EXAFS spectroscopy.

The comparison of the bond length determined for the Np(IV) humates with those of Np(IV) model compounds containing carboxylic groups shows that the bond length of the Np(IV) humates is smaller than found for bridging and chelate forming carboxylate groups in Np(IV) oxalate ($R = 2.39$ Å and 2.51 Å with an average of 2.45 Å) (Grigoriev et al., 1997) or for bidentate binding carboxylate groups in Np(IV) formate ($R = 2.50$ Å) (Hauck, 1976). From this we conclude that the humic acid carboxylate groups are predominantly monodentate bound to Np(IV) ions.

The comparison of the structural parameters of Np(IV) humate and Bio-Rex70 complexes with those of the corresponding Th(IV) complexes (cf. paragraph 3.1) shows that both tetravalent actinides are surrounded by 11 oxygen atoms. However, the Np-O bond length (2.36 ± 0.02 Å) is about 0.08 Å shorter than the Th-O bond length (2.44 ± 0.02 Å). This difference approximates the difference of the effective ionic radii of Np^{4+} (1.02 ± 0.02 Å, (Neck and Kim, 2000)) and Th^{4+} (1.08 ± 0.02 Å, (Neck and Kim, 2000)) in aqueous solution which is 0.06 ± 0.02 Å.

3.3 Np(V) humate and Bio-Rex70 complexes

For all Np(V) humates the complexation of NpO_2^+ by humic acid was verified by means of NIR absorption spectroscopy (Sachs et al., 2003).

The raw Np L_{III}-edge k^3 -weighted EXAFS spectra and the corresponding FTs of the Np(V) complexes are shown in Fig. 4. The FTs show two Np-O coordination shells (Np-O_{ax}, Np-O_{eq}). The structural parameters determined for the Np(V) complexes are summarized in Tab. 3 and compared to literature data of the aqueous Np(V) ion.

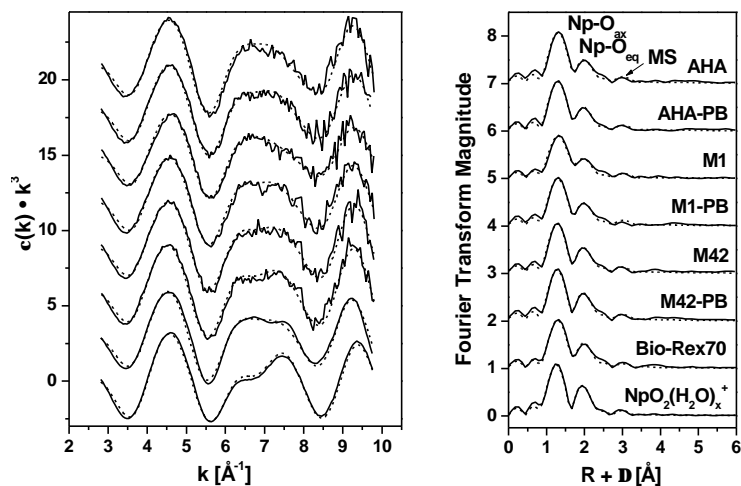


Fig. 4: Np L_{III}-edge k^3 -weighted EXAFS spectra and corresponding Fourier transforms of Np(V) samples. Solid lines: experiment, dashed lines: fit, MS: multiple scattering along the neptunyl unit.

Tab. 3: EXAFS structural parameters of Np(V) complexes in comparison to literature data of the aqueous Np(V) ion

Sample	Np-O _{ax}			Np-O _{eq}			ΔE_0 [eV]	Ref.
	N	R [Å]	σ^2 [Å ²]	N	R [Å]	σ^2 [Å ²]		
Np(V)-AHA	2	1.85 ± 0.01	0.0023	2.6 ± 0.8	2.49 ± 0.01	0.0040	-8.1	
Np(V)-AHA-PB	2	1.85 ± 0.01	0.0030	2.7 ± 0.8	2.49 ± 0.01	0.0048	-8.1	
Np(V)-M1	2	1.85 ± 0.01	0.0044	2.4 ± 0.8	2.49 ± 0.01	0.0050	-6.8	
Np(V)-M1-PB	2	1.85 ± 0.01	0.0033	2.5 ± 0.8	2.50 ± 0.01	0.0040	-7.8	
Np(V)-M42	2	1.84 ± 0.01	0.0029	2.4 ± 0.7	2.49 ± 0.01	0.0023	-9.2	
Np(V)-M42-PB	2	1.84 ± 0.01	0.0026	2.7 ± 0.7	2.50 ± 0.01	0.0030	-9.6	
Np(V)-Bio-Rex70	2	1.85 ± 0.01	0.0032	2.8 ± 0.5	2.50 ± 0.01	0.0044	-8.2	
NpO ₂ (H ₂ O) _x ⁺	2	1.81 ± 0.01	0.0034	3.3 ± 0.4	2.49 ± 0.01	0.0051	-9.7	Reich, 2000a

N_{ax} was held constant during fit.

The 95 % confidence limits are given for N and R as estimated by EXAFSPAK.

Within the experimental error, identical structural parameters were determined for Np(V) humates prepared from original humic acids and from modified humic acids with blocked phenolic/acidic OH groups. From this it can be concluded that the blocking of the phenolic/acidic OH groups of the humic acids has no influence on the local structure around the Np(V) ion in the Np(V) humates. Furthermore, the structural data of the Np(V) humates are also comparable to those of Np(V)-Bio-Rex70. This indicates that carboxylate groups dominate the interaction between Np(V) and humic acid at pH 7. However, a contribution of humic acid phenolic/acidic OH groups to the complexation of Np(V) ions cannot completely be excluded by EXAFS analysis, since the EXAFS results represent average values over all interactions between Np(V) and humic acid functional groups. There is the possibility that

phenolic OH groups interacting with Np(V) show equatorial bond lengths that are similar to those of carboxylate groups.

The coordination number determined for the equatorial shell of Np(V) humate and Np(V)-Bio-Rex70 complexes as well as for the equatorial shell of the aqueous ion of Np(V) is smaller than the theoretically expected value of 5. Up to now, this cannot be explained.

The equatorial Np-O bond lengths of the humates are comparable to the equatorial Np-O bond lengths of monodentate and/or bridging coordinated carboxylate groups in a Np(V) malonate complex (2.47 Å) (Grigoriev et al., 1993). Moreover, the equatorial Np-O bond lengths of the humates are also comparable to the equatorial Np-O bond length of the aqueous Np(V) ion (Reich et al., 2000a). Thus, a differentiation between monodentate and/or bridging carboxylate groups and water molecules is not possible. However, a predominant bidentate coordination of humic acid carboxylate groups to Np(V) can be excluded, since bidentate coordinated carboxylate groups in a Np(V) formate complex (Grigoriev et al., 1994) show equatorial Np-O bond lengths of 2.60 ± 0.04 Å.

3.4 Pu(III) humate complexes

The trivalent oxidation state of Pu and its stability in the complexes with humic substances within the time of the experiment was verified by means of XANES spectroscopy. In Fig. 5, the XANES spectra of Pu(III)-KFA and Pu(III)-M42 are shown in comparison to that of the aqueous ion of Pu(III) (Reich et al., 2000b). The energy scale of the spectra was calibrated with a Zr metal foil (Zr K edge at 17998 eV). The edge energy, determined as the inflection point of the edge, of the three spectra is identical (aqueous Pu(III) ion: 18059.0 eV, Pu(III) humates: 18059.2 eV). This confirms that the humate complexes contain exclusively Pu(III).

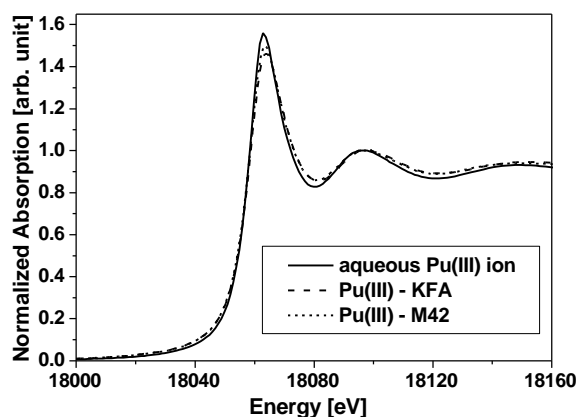


Fig. 5: Normalized Pu L_{III}-edge XANES spectra.

The raw Pu L_{III}-edge k^3 -weighted EXAFS spectra and the corresponding FTs of the Pu(III) humates are shown in Fig. 6. The FTs indicate a single coordination shell (Pu-O) arising from the ligands.

The structural parameters determined for the Pu(III) complexes are summarized in Tab. 4 and compared to literature data of aqueous ions of Pu(III) and Pu(IV). In the Pu(III) humate complexes the Pu(III) ion is surrounded by about 7 oxygen atoms at a distance of 2.45 Å. The Pu-O bond length in the Pu(III) humate complexes is significantly longer than that of the aqueous Pu(IV) ion. Furthermore, no evidence for the formation of polynuclear Pu(IV)

species was found in the EXAFS spectra. That means, the EXAFS structural parameters confirm the conclusion drawn from the XANES spectra namely that the humate complexes contain exclusively Pu(III).

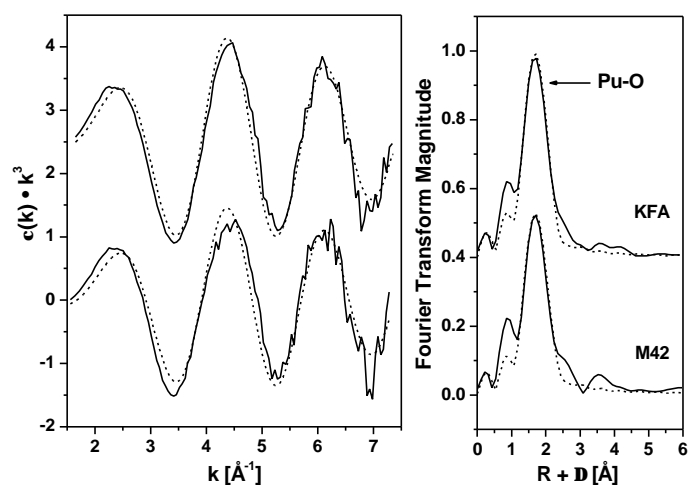


Fig. 6: Pu L_{III}-edge k^3 -weighted EXAFS spectra and corresponding Fourier transforms of Pu(III) samples. Solid lines: experiment, dashed lines: fit.

Tab. 4: EXAFS structural parameters of Pu(III) complexes in comparison to literature data of aqueous ions of Pu(III) and Pu(IV)

Sample	Shell	N	R [Å]	σ^2 [Å ²]	E ₀ [eV]	Ref.
Pu(III)-KFA	Pu-O	7.3 ± 1.2	2.45 ± 0.02	0.0150	-17.3	
Pu(III)-M42	Pu-O	6.1 ± 1.4	2.45 ± 0.02	0.0137	-17.0	
Pu(H ₂ O) _x ³⁺	Pu-O	7.6 ± 0.6	2.48 ± 0.01	0.0102	-16.8	Reich, 2000b
Pu(H ₂ O) _x ⁴⁺	Pu-O	8	2.39	0.0118		Ankudinov, 1998

The 95 % confidence limits are given for N and R as estimated by EXAFSPAK.

Within the experimental error, the coordination numbers determined for the Pu-O shell of the humate complexes agree well with the value reported for the aqueous Pu(III) ion in 1 M HClO₄ (Reich et al., 2000b). The bond length determined for the Pu(III) humate complexes is 0.03 Å shorter than that determined for the aqueous Pu(III) ion. This shortening of the bond length is similar to that observed for U(VI) and Np(IV) humates (cf. paragraph 3.2) upon complexation of these actinides with the functional groups of the humic substances.

Acknowledgments

This study was supported by the EC Commission under contract No. FIKW-CT-2001-00128 and by the Bundesministerium für Wirtschaft und Arbeit under contract No. 02 E 9299. The authors thank G. Geipel for his help in sample preparation, C. Hennig, A. Roßberg and H. Funke for their support during the XAFS measurements and V. Brendler for speciation calculations.

References

- Akhtar, M.N., Smith, A.J.: The Crystal Structure of Tetrapotassium Tetraoxalatothorium(IV) Tetrahydrate, $K_4Th(C_2O_4)_4 \cdot 4H_2O$. *Acta Crystallogr.* **B31**, 1361 (1975).
- Allen, P.G., Bucher, J.J., Shuh, D.K., Edelstein, N.M., Reich, T.: Investigation of Aquo and Chloro Complexes of UO_2^{2+} , NpO_2^+ , Np^{4+} , and Pu^{3+} by X-ray Absorption Fine Structure Spectroscopy. *Inorg. Chem.* **36**, 4676 (1997).
- Ankudinov, A.L., Conradson, S.D., Mustre de Leon, J., Rehr, J.J.: Relativistic XANES Calculations of Pu Hydrates. *Phys. Rev.* **B57**, 7518 (1998).
- Antonio, M.R., Soderholm, L., Williams, C.W., Blaudeau, J.-P., Bursten, B.E.: Neptunium Redox Speciation. *Radiochim. Acta* **89**, 17 (2001).
- Denecke, M.A., Pompe, S., Reich, T., Moll, H., Bubner, M., Heise, K.H., Nicolai, R., Nitsche, H.: Measurements of the Structural Parameters for the Interaction of Uranium(VI) with Natural and Synthetic Humic Acids using EXAFS. *Radiochim. Acta* **79**, 151 (1997).
- Denecke, M.A., Reich, T., Pompe, S., Bubner, M., Heise, K.H., Nitsche, H., Allen, P.G., Bucher, J.J., Edelstein, N.M., Shuh, D.K., Czerwinski, K.R.: EXAFS Investigations on the Interaction of Humic Acids and Model Compounds with Uranyl Cations in Solid Complexes. *Radiochim. Acta* **82**, 103 (1998).
- Denecke, M.A., Bubnitz, D., Kim, J.I., Moll, H., Farkes, I.: EXAFS Investigation of the Interaction of Hafnium and Thorium with Humic Acid and Bio-Rex70. *J. Synchrotron Rad.* **6**, 394 (1999).
- George, G.N., Pickering, I.J.: *EXAFSPAK: A Suite of Computer Programs for Analysis of X-Ray Absorption Spectra*. Stanford Synchrotron Radiation Laboratory, Stanford, USA, 1995.
- Grigoriev, M.S., Charushnikova, I.A., Krot, N.N., Yanovskii, A.I., Struchkov, Yu.T.: Crystal and Molecular Structure of Neptunyl Malonate Tetrahydrate $(NpO_2)_2C_3H_2O_4 \cdot 4H_2O$. *Radiokhim.* **4**, 24 (1993).
- Grigoriev, M.S., Charushnikova, I.A., Krot, N.N., Yanovskii, A.I., Struchkov, Yu.T.: Crystal Structure of the Neptunyl Formate Complex $(NH_4)NpO_2(OOCH)_2$. *J. Neorgan. Chim.* **39**, 1328 (1994).
- Grigoriev, M.S., Charushnikova, I.A., Krot, N.N., Yanovskii, A.I., Struchkov, Yu.T.: Crystal Structure of Neptunium(IV) Oxalate Hexahydrate $Np(C_2O_4)_2 \cdot 6H_2O$. *Radiokhim.* **39**, 419 (1997).
- Hauck, J.: The Crystal Structure of $Me(HCOO)_4$, Me = Th, Pa, U, Np. *Inorg. Nucl. Chem. Lett.* **12**, 617 (1976).
- Kim, J.I., Buckau, G.: *Characterization of Reference and Site Specific Humic Acids*. RCM-Report 02188, TU München, Institute of Radiochemistry, München, Germany, 1988.
- Koningsberger, D.C., Prins, R. (eds.): *X-ray Absorption: Principles, Applications, Techniques of EXAFS, SEXAFS and XANES*. Wiley, New York, USA, 1988.
- Moll, H., Denecke, M.A., Jalilehvand, F., Sandström, M., Grenthe, I.: Structure of the Aqua Ions and Fluoride Complexes of Uranium(IV) and Thorium(IV) in Aqueous Solution an EXAFS Study. *Inorg. Chem.* **38**, 1795 (1999).
- Neck, V., Kim, J.I.: An Electrostatic Approach for the Prediction of Actinide Complexation Constants with Inorganic Ligands-Application to Carbonate Complexes. *Radiochim. Acta* **88**, 815 (2000).
- Pompe, S., Bubner, M., Denecke, M.A., Reich, T., Brachmann, A., Geipel, G., Nicolai, R., Heise, K.H., Nitsche, H.: A Comparison of Natural Humic Acids with Synthetic Humic Acid Model Substances: Characterization and Interaction with Uranium(VI). *Radiochim. Acta* **74**, 135 (1996).
- Pompe, S., Brachmann, A., Bubner, M., Geipel, G., Heise, K.H., Bernhard, G., Nitsche, H.: Determination and Comparison of Uranyl Complexation Constants with Natural and Model Humic Acids. *Radiochim. Acta* **82**, 89 (1998).

- Pompe, S., Schmeide, K., Bubner, M., Geipel, G., Heise, K.H., Bernhard, G., Nitsche, H.: Investigation of Humic Acid Complexation Behavior with Uranyl Ions Using Modified Synthetic and Natural Humic Acids. *Radiochim. Acta* **88**, 553 (2000).
- Rehr, J.J., Albers, R.C., Zabinsky, S.I.: High-Order Multiple-Scattering Calculations of X-Ray Absorption Fine Structure. *Phys. Rev. Lett.* **69**, 3397 (1992).
- Reich, T., Bernhard, G., Geipel, G., Funke, H., Hennig, C., Roßberg, A., Matz, W., Schell, N., Nitsche, H.: The Rossendorf Beam Line ROBL – A Dedicated Experimental Station for XAFS Measurements of Actinides. *Radiochim. Acta* **88**, 633 (2000a).
- Reich, T., Geipel, G., Funke, H., Hennig, C., Roßberg, A., Bernhard, G.: First XANES and EXAFS Measurements of Plutonium Solutions at ROBL. In: *FZR-285, Annual Report 1999* (Bernhard, G., ed.). Forschungszentrum Rossendorf, Institute of Radiochemistry, Rossendorf, Germany, 2000b, p. 72.
- Sachs, S., Schmeide, K., Reich, T., Brendler, V., Heise, K.H., Bernhard, G.: EXAFS Study on the Neptunium(V) Complexation by Various Humic Acids under Neutral Conditions. *Radiochim. Acta*, submitted (2003).
- Schmeide, K., Zänker, H., Heise, K.H., Nitsche, H.: Isolation and Characterization of Aquatic Humic Substances from the Bog 'Kleiner Kranichsee'. In: *FZKA 6124, Wissenschaftliche Berichte* (Buckau, G., ed.). Forschungszentrum Karlsruhe, Karlsruhe, Germany, 1998, p. 161-195.
- Schmeide, K., Sachs, S., Bubner, M., Reich, T., Heise, K.H., Bernhard, G.: Interaction of Uranium(VI) with Various Modified and Unmodified Natural and Synthetic Humic Substances Studied by EXAFS and FTIR Spectroscopy. *Inorg. Chim. Acta*, in press (2003a).
- Schmeide, K., Sachs, S., Reich, T., Brendler, V., Heise, K.H., Bernhard, G.: Neptunium(IV) Complexation by Humic Substances Studied by X-ray Absorption Fine Structure Spectroscopy. *Radiochim. Acta*, submitted (2003b).
- Schmeide, K., Sachs, S., Reich, T., Heise, K.H., Bernhard, G.: Plutonium(III) Complexation by Humic Substances Studied by X-ray Absorption Fine Structure Spectroscopy. *Inorg. Chim. Acta*, submitted (2003c).
- Zhang, Y.-J., Collison, D., Livens, F.R., Powell, A.K., Wocadlo, S., Eccles, H.: Synthesis, Spectroscopic, and X-ray Crystallographic Characterization of Thorium(IV) and Uranium(IV) Malonate and Substituted Malonate Compounds. *Polyhedron* **19**, 1757 (2000).

Annex 5

**Uranium Mining Waste Rock Pile No. 250 in the Region
Schlema/Alberoda (Saxony, Germany)**

K. Schmeide, G. Geipel, K.H. Heise and G. Bernhard

**Forschungszentrum Rossendorf e.V., Institute of Radiochemistry, P.O. Box 510119
01314 Dresden, Germany
(FZR-Ifr)**

Abstract

The overall objective of the EC project “Humic Substances in Performance Assessment of Nuclear Waste Disposal: Actinide and Iodine Migration in the Far-Field” is the determination of the effect of humic substances on the actinide migration in natural systems to assess their impact on the long-term safety of radioactive waste repository sites and abandoned uranium mines. This task includes also the implementation of the present knowledge to real existing natural systems thereby verifying the correlation between important parameters, evaluating their environmental impact and finally, uncovering issues not addressed so far.

Uranium mining waste rock piles in the southern parts of the former East Germany represent a significant long-term environmental concern and liability. Although the uranium mines were decommissioned with the end of the uranium ore production in 1990, the legacy of forty-five years of uranium mining, such as abandoned mines, huge waste rock piles and mill tailings, represents a permanent reservoir and source of radioactive and non-radioactive contaminants. The discharge of radionuclides from the waste rock piles and contamination of the surrounding geosphere has to be minimized.

For the case study presented in this paper, the uranium mining waste rock pile no. 250 in Schlema/Alberoda (Saxony, Germany) was chosen. In many respects, this pile resembles other rock piles of this region. The site is characterized comprehensively with regard to composition and activity inventory of rock material and seepage water, uranium species occurring in the seepage water, TOC content and much more. Some important data of other uranium mining waste rock piles that were located in the vicinity of the rock pile no. 250 are also included in this study, especially the fulvic and humic acid content in the seepage water of rock piles and their loading with uranium. The data presented in this natural system study constitute the basis of performance assessment modeling.

1. Introduction

The uranium ore production in the southern parts of the former East Germany (Saxony, Thuringia) was accomplished by intensive underground and open-pit mining by the SDAG WISMUT. 220,000 tons of uranium were mined from 1945 to 1990 (BMWi, 1995). The mines have a total shaft length of some 1400 km and reach a depth of up to 1800 m. Considerable amounts of rock material were transported to the surface and thus, many rock piles were generated above ground in the mining areas. Traditionally, the waste rock was stockpiled as near as possible to the mine and thus, to residential areas. Altogether, the rock piles, containing environmentally harmful elements, had a total volume of about 290 million m³ covering an area of about 1100 ha (Gatzweiler and Marski, 1996). After decommissioning of the mines, backfilling the rock material into the mine shafts is mostly not possible. Therefore, these waste rock piles represent a special kind of final repositories with radioactive contamination.

The mining district of Schlema/Alberoda was the largest uranium vein ore deposit of the world. About 80,830 tons uranium were extracted. The deepest mine shafts of Europe are located in this area. The depth of the mine shaft no. 371 was up to 1800 m related to the level of the river ‘Zwickauer Mulde’. About 45 million m³ rock material were moved and deposited

in this mining region covering an area of about 3 km² (Meyer, 1995). A geological map of the mining region Schlema/Alberoda, depicted in Fig. 1, shows the abundance of mining shafts and waste rock piles in this area. In 1995 there were still 37 waste rock piles, among them 9 piles with volumes > 1 million m³, that together represent 90 % of the total volume (Meyer, 1995). The rock piles are up to 50 m high.

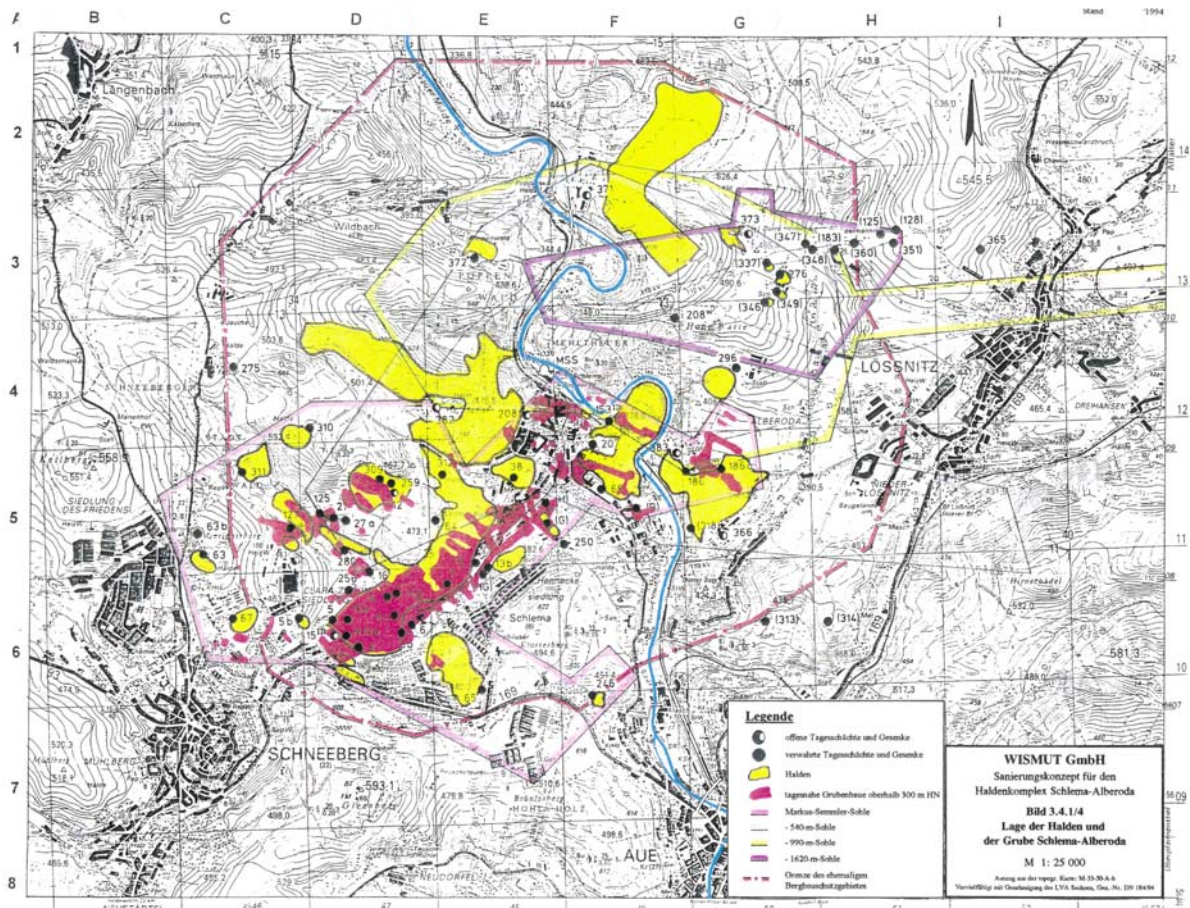


Figure 1: Geological map of the mining region Schlema/Alberoda: Location of waste rock piles (light gray areas) and mining shafts (black spots) (Köhler and Wolf, 1995)

For the case study, the rock pile no. 250, located in the mining area Schlema/Alberoda, exactly in Niederschlema, was chosen. This rock pile is especially suitable for such a study for several reasons. First, this waste rock pile was investigated in detail by the Institute of Radiochemistry of the Forschungszentrum Rossendorf. Second, with regard to its most important features such as, for instance, its mineral content, radioactive inventory and composition of the seepage water, the rock pile is considered as representative of other piles in the region Schlema/Alberoda.

2. Sources of contamination caused by a uranium mining waste rock pile

A rock pile resulting from uranium mining consists of rock waste that still contains radioactive contaminants. Furthermore, metals that were not industrially used or solid wastes,

which contain elevated levels of radioactivity, such as building wastes, mine timber, non-salvageable containment equipment, were sometimes deposited on the pile as well. Additionally, the rock piles were used as open interim store for low grade uranium ore. From these materials, further radioactive contaminants, heavy metals and other constituents could be introduced into the water path of the pile by weathering.

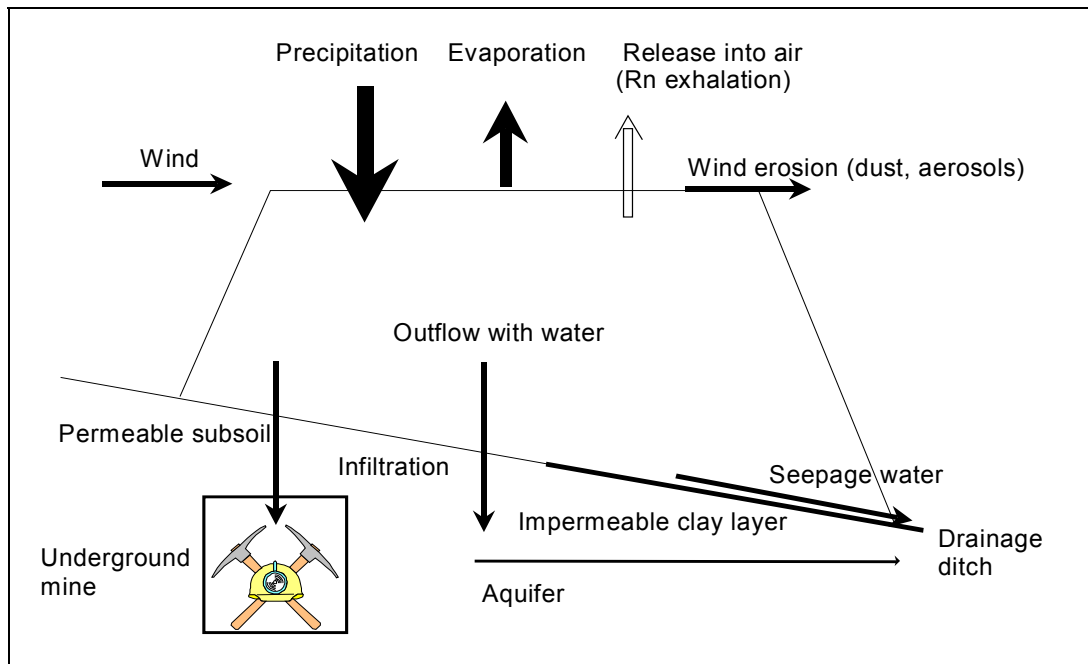


Figure 2: Sources of contamination caused by a waste rock pile of uranium mining (Geipel et al., 1994a)

In Fig. 2 a profile through a waste rock pile is shown together with several possibilities for release of contaminants from the pile leading partly to uncontrolled spreading of contaminants. The rock material is continuously exposed to weathering processes. The precipitation, lessened by evaporation, penetrates the waste rock pile. Simultaneously, the water becomes contaminated. The loadings of radionuclides and metals released from the waste rock piles can be further enhanced by acid generation due to chemical reactions inside the pile, for instance, oxidation of the rock material such as pyrite as well as by acidic rain. The water, containing dissolved or colloidal contaminants, flows out of the pile either as seepage water finally reaching a drainage ditch or infiltrates the permeable subsoil reaching the underground mine or the aquifer. Furthermore, gaseous products are released from the pile into the air. Especially the exhalation of radon and consequently, polonium, as a decay product of the uranium decay chain, has to be taken into account. This radon exhalation can only be decreased by sealing the waste rock pile. Due to wind erosion dust and aerosols are generated. This can be minimized by covering the pile with various layers of clay and humus soil or with engineered multi barrier systems (Kistinger et al., 2002; Schneider et al., 2002). Consequently, waste rock piles as well as mines represent a permanent reservoir and source of radioactive and non-radioactive contaminants. Primary sources of external contamination are the groundwater that has flooded the mine shafts and seepage waters coming from the piles.

Uranium, its decay products and arsenic are the main potential hazards to the biosphere (BfS, 1992).

3. Uranium mining waste rock pile no. 250 in Schlema/Alberoda

All data given for the uranium mining waste rock pile no. 250 in Schlema/Alberoda are compiled from the following literature unless otherwise stated: Bernhard et al., 1996; Geipel et al., 1994a; Geipel et al., 1994b; Geipel and Thieme, 1994c; Geipel et al., 1996.

The uranium mining waste rock pile no. 250 was generated between 1949 and 1954. It was 30 m high, its total volume was about 1 million m³ and it covered an area of about 30,000 m².

The rock pile was finally leveled in 1990/91 by the WISMUT GmbH. This was necessary because it was located in a densely populated area and it was not possible to remediate the waste rock pile in place. The rock pile was completely relocated and used to fill up a depression 2 km to the north-west of the former location. There, the rock material was covered with different layers of clay (2 m) and humus soil (0.5 m).

During the leveling period (about 1 year) the rock pile was comprehensively investigated by the Institute of Radiochemistry of the Forschungszentrum Rossendorf. That means, about 120 rock samples were taken systematically from controlling points on different levels of the pile (between 3 to 30 m from the top of the rock pile), together with 12 seepage water samples from one sampling point. The samples were taken at seven different dates. The objective of the study was to investigate a typical uranium mining waste rock pile of the mining district Schlema/Alberoda to determine the inventory of radioactive contaminants, their distribution and their transport with seepage water.

3.1 Rock material

The uranium ore deposit is located at the border line between bright metamorphites and a diabase-chlorite formation. Thus, most of the mine shafts are located in both zones.

The main components of the deposited rock materials of the rock pile no. 250 are given in Tab. 1. It is obvious that bright metamorphites such as fruit schists and phyllite dominate.

Table 1: Rocks and minerals of the Schlema/Alberoda area

Rocks	Content	Examples
bright metamorphites	55 %	fruit schist, phyllites
dark metamorphites	25 %	silicic schist, C-containing phyllites
eruptive metamorphites	15 %	diabase, wollastonite
vein rock	<5 %	chlorite, granite
hydrothermal minerals	<2 %	sulfides, carbonates, quartz

Mineralogical investigations have further shown that the rock material is a densely cross-linked conglomerate of the various rock and mineral components.

The elemental composition of two samples of the rock material (no. 14/1 and 14/2) is given in Tab. 2. This is a selection of major elements and elements that are important for the saxonian uranium mining.

Table 2: Elemental composition of rock material (XFA) (in mg/kg)

Element	Pile 250, no. 14/1 (14.05.1991)	Pile 250, no. 14/2 (14.05.1991)
Iron	80,000	57,500
Potassium	29,000	24,000
Calcium	18,000	20,000
Barium	9,500	3,900
Titanium	8,300	7,900
Magnesium	3,300	2,100
Arsenic	1,060	220
Copper	440	280
Zinc	410	195
Zirconium	170	130
Lead	125	27
Uranium	63	37
Thorium	19	12
Bismuth	9	0.4

Furthermore, a sieve analysis was performed to determine the grain distribution of the rock material. Especially the fine-grain fractions are most important for contaminant migration studies because most contaminants will be released from fine-grain fractions of the rock material. Moreover, due to the higher specific surface areas and the greater amount of reactive sites dissolved contaminants can be sorbed on their surfaces or can be transported together with finest particles or colloids of the seepage water. Tab. 3 gives the results of sieve analysis (mean values of 15 determinations) and BET-determination of the rock material.

Table 3: Results of sieve analysis and BET-determination of rock material

Particle size (in μm)	Content (in %)	Relative error (in %)	Specific surface area (BET) (in m^2/g)	Error (in m^2/g)
> 2,500	63.6	7.7		
1,000 - 2,500	14.0	3.4		
500 - 1,000	6.1	1.8		
250 - 500	4.7	1.2		
125 - 250	3.7	0.8	13.5	2.8
63 - 125	4.0	0.8	16.6	2.8
< 63	4.6	1.2	20.6	3.5

The results show that the fine-grain fractions ($< 500 \mu\text{m}$) exist approximately in equal parts in the rock material. The specific surface areas increase with decreasing particle sizes.

The cavity (void space) of the rock pile no. 250 amounted to about 35 % of the total rock pile volume.

3.2 Activity inventory

A complete separation of the uranium ore from the uranium bearing vein rock material during the mining process is usually not possible. Therefore, uranium and its natural decay products were introduced into the rock pile. Due to weathering of the rock material these radionuclides can be mobilized and transported through the pile.

The distribution pattern for the nuclide U-238 (measured as Th-234) is shown in Fig. 3, which is a rough section drawing of the rock pile taken in the course of progressive leveling. Little change in U-238 concentration with depth was found. Activity concentrations of 500 - 600 Bq/kg were generally measured, corresponding to 40 - 50 mg U/kg of the dark metamorphites. In contrast, the light metamorphites stored in the northwestern part of the rock pile contained less than 200 Bq/kg. Generally, it can be concluded that similar activity concentrations are found for rock material of the same type.

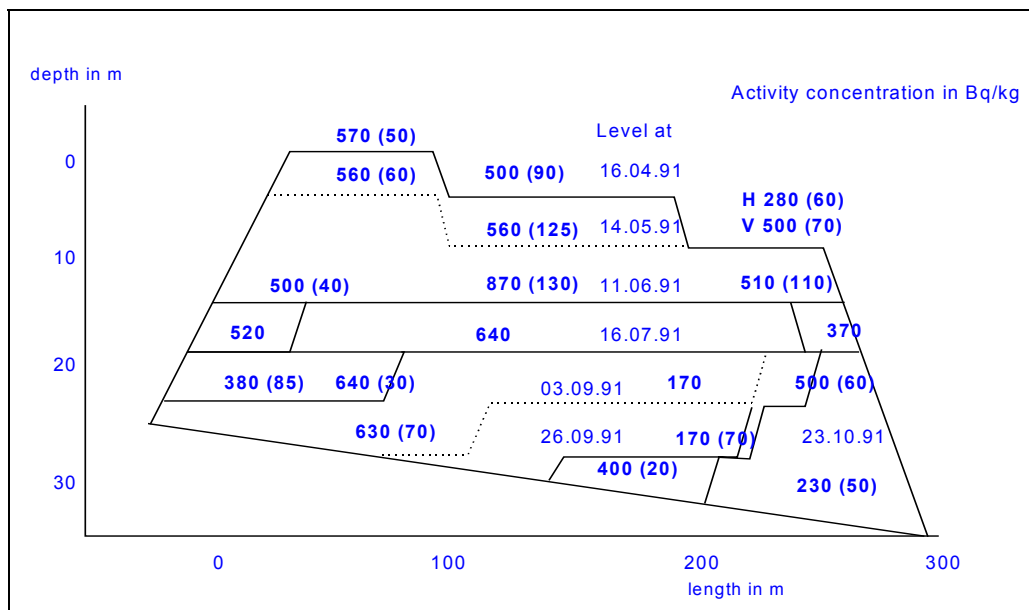


Figure 3: Activity concentration for U-238 (measured as Th-234) in Bq/kg in the rock pile no. 250 (mean errors in brackets). The inserted lines present the dates of sampling.

The depth distributions of Th-230 and Ra-226 in the rock pile were similar, but there were differences to the U-238 depth distribution. This can be shown clearly by comparing the activity ratios of the respective nuclides with U-238. As an example, the Ra-226/U-238 activity ratio is given in Fig. 4. At the top of the rock pile, where sampling started, a Ra-226/U-238 ratio of 1.0 ± 0.1 was found. With increasing depth, an increase of the Ra-226/U-238 activity ratio was found. At a depth of 30 m a maximum ratio of 1.4 ± 0.1 was measured. Altogether, a radionuclide enrichment with depth was found for the nuclides Th-230 and Ra-226 in comparison to U-238, and Th-227 in relation to U-235. This can be explained by

different migration rates of the individual radionuclides. The possible reasons for the different movement of the radionuclides through the rock pile are discussed in detail by Geipel et al. (1994b).

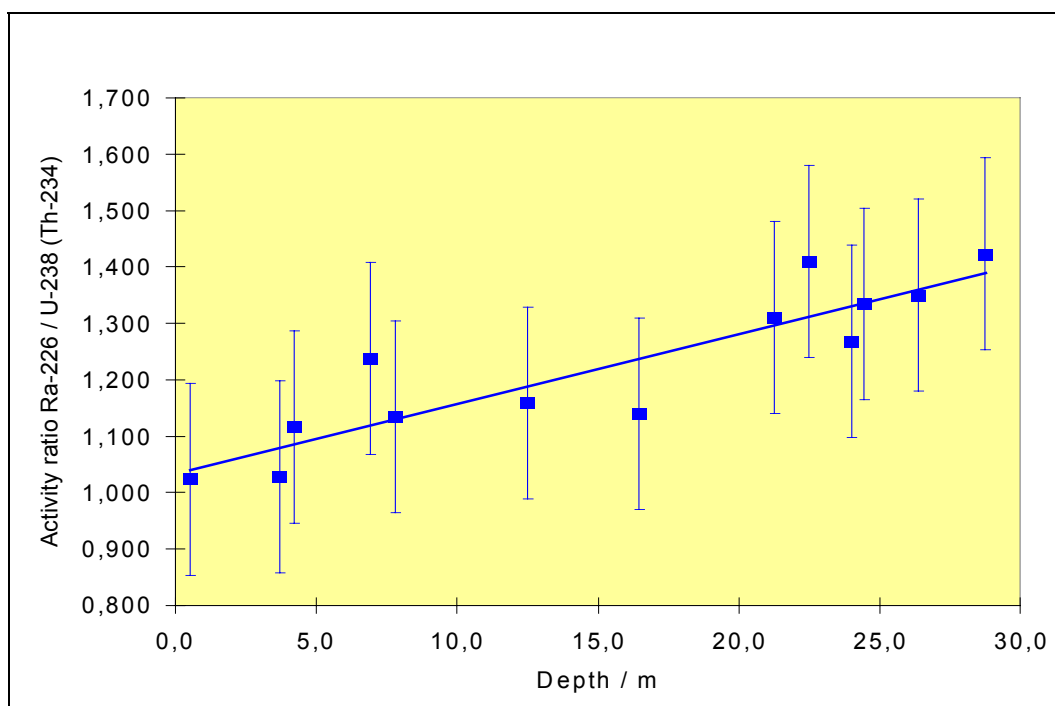


Figure 4: Activity ratio Ra-226/U-238 (Th-234) as function of depth for the waste rock pile no. 250

From these results the total activity inventory of the waste rock pile was estimated. Tab. 4 shows the estimated amounts of selected radionuclides for the waste rock pile no. 250 compared to the total activity inventory of all waste rock piles in Schlema/Alberoda.

Table 4: Activity inventory of the waste rock pile no. 250 compared to the total activity inventory of all waste rock piles in Schlema/Alberoda

Radionuclide	Mass (in kg) (distributed in the pile no. 250)	Mass (in kg) (total inventory of all waste rock piles in Schlema/Alberoda)
U-238 series: U-238	100,000	4,000,000
U-234	5	200
Th-230	2	80
Ra-226	0.033	1.32
U-235 series: U-235	700	28,000
Pa-231	0.032	1.28

The rock pile no. 250 had an uranium inventory of about 100 tons. A mean activity concentration of 600 Bq/kg was determined. From this an average uranium concentration of

50 mg/kg follows. The activity inventory of the main part of the waste rock pile exceeds the geological basic level (which is about 150 Bq/kg for U-238) by a factor of 3 - 4.

The calculation of the total activity inventory for all waste rock piles in Schlema/Alberoda with the data obtained for the rock pile no. 250 is only a rough estimation. For more exact calculations a monitoring of all waste rock piles of this region would be necessary.

For the fine-grain fraction of the rock material the activity concentration was determined separately. The results are shown in Tab. 5.

Table 5: Activity concentration of fine-grain fractions (in Bq/kg)

Particle size (in mm)	U-238 (U-235)	Th-234	Th-230	Ra-226	Pb-/Bi- Isotopes
2.2	630	330	550	600	470
1.3	720	360	530	800	570
0.75	870	410	830	1220	820
0.25	1210	500	1140	1710	1200
0.05	1560	760	1790	2810	1910

Generally, the activity concentration increases with decreasing particle sizes. This becomes especially evident for Ra-226. The activity of the smallest particle size fraction is more than four times higher than the activity of the larger particle size fractions. This activity enhancement can be attributed to the higher specific surface area of the smaller particles resulting in a high sorption capacity of mineral surfaces. Furthermore, the fine-grain fractions are mostly weathering products of the rock material. These substances contain the main part of the montmorillonite as a natural ion exchanger with an exchange capacity up to 1.3 mval/g. These fine-grain fractions necessarily have to be taken into account because they can easily adsorb radionuclides from the water penetrating the pile and transport them. Thus, there is the possibility that adsorption products can break through with the seepage water.

3.3 Seepage water

The water penetrating the rock pile no. 250 flows out on the base of the pile as seepage water. Only a small part of the seepage water (which finally can be neglected) is able to infiltrate the bedrock beneath the rock pile, because the waste rock was stockpiled on an at least 1 m thick clay layer with an extremely low permeability.

The composition and the pH of seepage waters depend on the chemical reactions inside the rock pile. They are determined both by the type of the stored rock material and by its weathering. The weathering process can be strengthened by a high acidity of the rain together with a large amount of rainfall. The mean annual precipitation in the Schlema/Alberoda area is 800-850 mm (mainly summer semester, pH \approx 4.3, approximately 8 mg sulfate per liter). The mean annual temperature is 7.5 °C, with seasonal variations from -15 °C to +35 °C.

Characteristic parameters of the seepage water coming from the rock pile no. 250 are given in Tab. 6.

Table 6: Characterization of the seepage water of the rock pile no. 250, Schlema/Alberoda

Parameter		
pH		7.5 - 7.9
Specific conductivity	mS/cm	3.3 - 3.7
Ionic strength	mol/L	0.1
Oxygen concentration	μmol/L	500 - 600
Total inorganic carbon	μmol/L	(2 - 3) · 10 ³
<u>Anion concentration</u>		
Sulfate	μmol/L	(19 - 30) · 10 ³
Nitrate	μmol/L	80 - 320
Chloride	μmol/L	170 - 410
<u>Metal ion concentration</u>		
Uranium	μmol/L	5 - 8
Mass ratio U-234/U-238		(6.0 - 6.3) · 10 ⁻⁵
Iron	μmol/L	0.7 - 46.5
Zinc	μmol/L	0.1 - 1.9
Arsenic	μmol/L	0.3 - 62.5
Alkali ions	μmol/L	≈ 1.3 · 10 ³
Alkaline earth ions	μmol/L	≈ 3 · 10 ⁴

The seepage water samples were always clear and homogeneous. The absence of particulate material indicates a high filtration effect of the rock pile.

The high contents of sulfate, carbonate, and alkaline earth ions such as calcium and magnesium ions indicate an ongoing weathering process. The concentration of arsenic in the seepage water is also high and reaches toxic concentrations. The ionic strength of the seepage water is about 0.1 M.

The high oxygen content of the seepage water, which is near the saturation limit, shows that the porosity of the rock pile surface is sufficient to allow the diffusion of ample oxygen, which is necessary for oxidation processes, into the rock pile.

The high sulfate content cannot only be explained by the acidic rain but is mainly attributed to the oxidation of sulfidic minerals, for instance pyrite, inside the pile. This was shown by measurements of the distribution of sulfur isotopes. Due to the oxidation, sulfate and ferrous ions are released. If the seepage water comes into contact with the atmosphere, the ferrous ions are oxidized and immediately hydrolyzed. The precipitation of the ferric hydroxide causes co-precipitation of the remaining thorium and radium ions, so that they are not present in the seepage water. Consequently, uranium has the highest concentration of all radionuclides present in the seepage water. The uranium content in the seepage water is additionally increased by oxidation of insoluble U(IV) by microbial produced Fe(III) (Glombitza et al., 1992; Seidel et al., 1995).

Seepage waters from other waste rock piles in the region Schlema/Alberoda contain more uranium than the seepage water of the pile no. 250. For instance, total uranium concentrations

up to 30 $\mu\text{mol/L}$ and 15 $\mu\text{mol/L}$ have been reported for pile no. 38 neu and pile no. 66, respectively.

The U-234/U-238 mass ratio in the seepage water of the rock pile no. 250 was found to be $(6.0 - 6.3) \cdot 10^{-5}$. The radioactive equilibrium would correspond to a value of $5.1 \cdot 10^{-5}$. This corresponds to an activity ratio of 1.22 ± 0.08 . The slightly increased concentration of U-234 is attributed to an enhanced solubility of U-234 compared to U-238 in natural rock material and thus, to an increased migration of $^{234}\text{U(VI)}$. Comparisons of the uranium content of the rock material and of the seepage water of different rock piles in the mining area Schlema/Alberoda showed that the uranium content in the seepage water is closely linked to the uranium content of the rock material.

The sulfuric acid, primarily formed by pyrite oxidation and the infiltration of acidic rain, does not lead to an acidification of the seepage water. Chemical reactions inside the rock pile cause the change of the pH value from 4.3 of the rain to nearly 8 in the seepage water. Due to the buffering ability of the rock material the pH of the rain water increases up to pH 7 - 8.8 already after penetrating the first 2 m of the rock material starting from the surface of the pile (weathering zone) (GLU, 1995). Mainly alkaline earth carbonates (calcite, dolomite), silicates and clay minerals (e.g., montmorillonite) act as buffering materials. The reaction of the sulfuric acid with alkaline earth carbonates results in high carbonate contents in the seepage waters thereby forming readily soluble uranyl carbonate complexes (cf. speciation calculations).

The mean residence time of the seepage water inside the rock pile is assumed to be less than one year (Geipel et al., 1994a). In contrast to this, a mean residence time of 12 to 18 years was found for the seepage water of the pile no. 309 in Schlema/Alberoda and is generally assumed as more than 10 years by Kupsch (1998a).

Furthermore, it is estimated that only 10 % of the precipitation meeting the pile is able to penetrate the pile and finally to flow out from the pile as seepage water (Geipel et al., 1994a). One reason is that the rock pile was only sparsely vegetated resulting in high temperatures on the rock pile surface, e.g., between 40 to 50 $^{\circ}\text{C}$ during the summer semester. Therefore, a large amount of the precipitation evaporates, mainly from the pile surface but also from inside the pile. Furthermore, especially the rock material on the surface of the pile was strongly weathered. The thereby formed clayey layers hinder the penetration of the precipitation into the rock pile. That means, that another part of the precipitation meeting the pile runs off directly from the pile surface.

The average amount of seepage water coming from waste rock piles is given with 1 - 20 m^3/h in dependence on volume and shape of the pile and in dependence on the existence of a protective cover (base, surface) as well (Gatzweiler, 1997).

3.4 Speciation calculations

According to the quantitative composition of the seepage water, the distribution of U(VI) species was calculated as a function of pH with the speciation modeling software EQ3/6 (Wolery, 1992) using the NEA data base (Grenthe et al., 1992). The results are shown in Fig. 5.

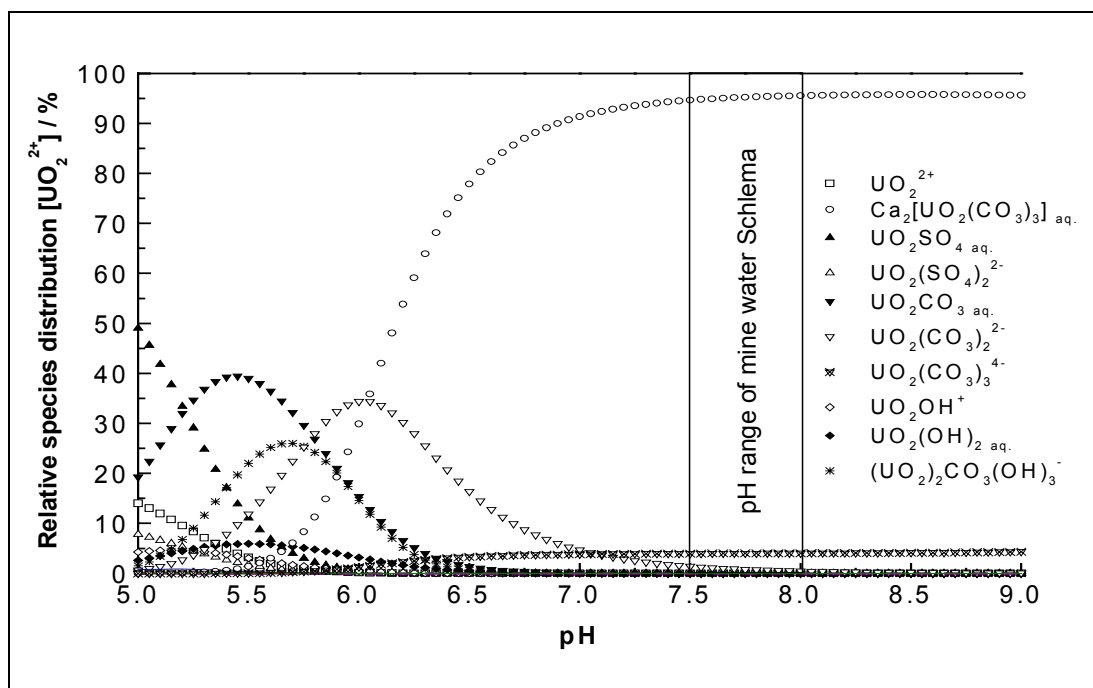


Figure 5: Distribution of U(VI) species, calculated according to the quantitative composition of the seepage water.

The speciation calculations indicate the following results:

- (i) The seepage water (pH = 7.5 - 7.9) is not supersaturated with respect to the minerals dolomite ($\text{CaCO}_3 \cdot \text{MgCO}_3$) and soddyite ($(\text{UO}_2)_2\text{SiO}_4 \cdot 2\text{H}_2\text{O}$). The reason is that the uranium speciation in this seepage water is predominated by a soluble aquo-complex of di-calcium uranyl carbonate ($\text{Ca}_2[\text{UO}_2(\text{CO}_3)_3]_{\text{aq}}$: 95 - 96 %) which was identified by time-resolved laser-induced fluorescence spectroscopy (Bernhard et al., 1996). The complex formation constant for this complex was determined to be $\log \beta_{213}^0 = 30.55 \pm 0.25$ (Bernhard et al., 2001). According to the speciation calculation the water only contains about 3 - 4 % of the $\text{UO}_2(\text{CO}_3)_3^{4-}$ complex. At lower pH values (pH = 6.5 - 6), the $\text{UO}_2(\text{CO}_3)_2^{2-}$ complex would be present with more than 15 %.
- (ii) The solution has a large buffering capacity. There is only a very low likelihood that the pH of the seepage water reaches values higher than 9.

3.5 TOC content

The TOC (Total Organic Carbon) content of the seepage water coming from the waste rock pile no. 250 was not determined. However, TOC measurements were performed on seepage water coming from waste rock piles that are located in immediate vicinity of the waste rock pile no. 250. For the seepage waters of the rock pile no. 66 and of the rock pile no. 38 a TOC content of 1 mg/L and 3 mg/L, respectively, was determined.

An average TOC content of ≤ 5 mg/L is given by the WISMUT GmbH for seepage waters of uranium mining waste rock piles (Trommler and Kuchler, 1997).

However, despite of the present relatively low organic carbon content of the seepage waters it is anticipated that the amount of organic carbon and thus, the concentration of humic material

as degradation product of biomass will increase in the future due to the presence of different suppliers of organic carbon on and inside a waste rock pile.

Potential suppliers of organic carbon are:

- Protective covers, used for remediation of waste rock piles, for instance, humus soil. From the layers of humus soil readily soluble reactive fulvic acids are released (Kupsch et al., 1998b).
- Natural revegetation, which forms a natural cover and finally, results in humic topsoil layers: beginning vegetation such as grass, shrubbery, growth of trees (mainly birches); shed leaves. Beginning natural revegetation of a waste rock pile in Schlema/Alberoda is depicted in Fig. 6.
- Direct reforestation.
For instance, the rock pile no. 38 neu in Schlema/Alberoda was reforested with pines, larches and deciduous trees, e.g., alders. In 1995 there was a densely natural cover on horizontal surfaces that was 5 to 6 m high and a thin cover on the slopes of the pile that was only 1 to 2 m high (Daenecke, 1995). Only some birches were found on steeply inclined strata of the rock pile.
The reforestation of the waste rock pile H382 with pines and alders has led within 40 years to the formation of a several cm thick organic layer (Dienemann et al., 2002).
- Large amounts of mine timber, used during the mining process and then deposited on the waste rock piles.
- Release of organic carbon due to weathering of carbon containing rock material, for instance, alum schist, metamorphic diabase and dark phyllites.



Figure 6: Waste rock pile in the mining area Schlema/Alberoda (Runge and Böttcher, 1994)

Finally, it should be noted that in case of some rock piles, organic garbage such as sludge fertilizer, liquid manure, timber, lignitic coal and other wastes have been approved for codisposal either inside the rock piles or on their surfaces (GLU, 1995).

The influence of such suppliers of organic carbon on the DOC (Dissolved Organic Carbon) content of three waste rock piles (no. 296, 309, 371) of the region Schlemma/Alberoda was investigated by Kupsch et al. (1998a, 1998b) and Franke et al. (2000). By comparative measurements of DOC concentrations in the input and output flow of the piles it was shown that DOC is produced and/or supplied within the waste rock piles. For instance, the seepage water of the rock pile no. 296 had strongly increased DOC contents (≥ 15 mg/L) caused by deposited liquid manure and domestic garbage. In Tab. 7 mean values are given for seepage water flow rates (Q in m³/h), DOC contents and uranium concentrations determined in the seepage waters (in mg/L) and estimated values for the total DOC and uranium outlets per year (in kg/a).

Table 7: Characteristic data of seepage waters coming from three different rock piles with regard to flow rate (Q), DOC and uranium loading of the seepage water and the percentage of uranium bound to humic and fulvic acid (U_{FA+HA}) (Kupsch et al., 1998b)

	Q m ³ /h	DOC mg/L	U mg/L	DOC kg/a	U kg/a	U_{FA+HA} %	U_{FA+HA} kg/a
H296 / MP005	1.5	27.6	1.6	358	21	10.5	2.2
H309 / MP160	3.6	1.7	0.8	54	25	0.7	0.2
H371 / MP109c	32.9	2.9	2.0	835	576	2.3	13.2

Fulvic and humic acids were identified in the seepage waters of the three rock piles. It is assumed that fulvic and humic acids were formed from the organic matter during pedogenesis. The humic material was found to be still in an early to middle stage of humification. This very reactive humic material is characterized by a high content of functional groups and low molecular weights. The percentage of uranium bound to humic and fulvic acid (U_{FA+HA}) is given in Tab. 7. For the rock pile no. 296 seasonal variations between 3.5 and 26.6 % were found. Generally, it was concluded that 5 to 20 % of uranium, present in the flow path, exists in form of fulvic and humic acid species in which uranium is permanently bound.

The covering of rock piles with organic layers (e.g., humus soil), as used for remediation of waste rock piles, results in an increased release of reactive fulvic acids into the water path (Kupsch et al., 1998b). There, the fulvic acids interact with radioactive contaminants and thus, contribute to the discharge of radionuclides from the rock piles. The effect of organic layers has to be studied in more detail.

3.6 Leaching and Sorption Behavior of the Rock Material

The chemical transport of contaminants through a uranium mining waste rock pile is strongly influenced by the leaching and sorption behavior of the rock material.

The high uranium content in the fine-grain fractions of the rock material (cf. paragraph 3.2) shows that the weathering of the rock material has two effects. On the one hand, radionuclides are released from the rock material but on the other hand, substances are formed simultaneously that have a high sorption capacity for radionuclides because of their large specific surface areas, e.g. montmorillonite and ferrihydrite. The size of these weathering products is very small. In dependence on the environmental conditions, the small particles that are loaded with contaminants can either migrate as colloids in the seepage water or can be cemented to the surrounding minerals. For phyllite, which is closely associated with uranium ore deposits in East Germany, the formation of ferrihydrite as secondary mineral phase due to the weathering of the rock material and its great importance for the uranium(VI) sorption onto phyllite in the absence and presence of humic acid was shown by Arnold et al. (1998, 2001) and Schmeide et al. (2000).

Thus, processes such as release of contaminants due to weathering of the rock material, sorption of contaminants onto the rock material and its weathering products, and again the release of contaminants from weathering products or the transport of the contaminant loaded weathering products play a decisive role.

Labor-scale column experiments were conducted using original rock material of the pile no. 250 that was leached with water over a period of one year (Geipel, 1994a). By leaching it was possible to distinguish between uranium coming from desorption and from weathering processes. The distribution ratio of uranium between the rock material and the solution showed a maximum at pH ~ 7. Depending on grain size and pH, distribution ratios of uranium up to 10^3 were found. The results showed that 2.8 % of the uranium inventory of the waste rock pile no. 250 are bound to the rock surface and that leaching of this uranium is very easy. The balance of weathering processes in the rock pile showed that about 0.8 mg U/L in the seepage water originated from weathering processes. From this value an annual uranium discharge of 1920 g U/a can be calculated. However, the total uranium discharge via the seepage water (2,400,000 L/a, 1.6 mg U/L) caused by weathering and desorption amounts to about 3840 g U/a which is $3.8 \cdot 10^{-3}$ % of the total uranium inventory of the rock pile (100,000 kg).

That means, there is a difference of about 50 % with regard to the uranium content in the seepage water. One reason for this difference is (beside the fact that the estimations are erroneous) that weathering products (e.g., montmorillonite, ferrihydrite) are present in the rock pile that have a large sorption capacity for radionuclides. Neither the true amount of the weathering products in the pile is exactly known nor their loading with uranium. However, it is important to know that during uranium mining low grade uranium ore was deposited on the pile as well. The amount of uranium and other contaminants that were leached out of this material due to rainfall and introduced into the pile are not known. Although the low grade uranium ore as a primary uranium source was removed from the pile, the pile still delivers uranium that results from this source via the seepage water.

Determination of the uranium discharge from the waste rock pile no. 250:

Summary of calculations made on the basis of column experiments (Geipel et al., 1994a) and the data given in this study.

- Total uranium discharge via the seepage water due to weathering and desorption:

Area covered by the rock pile: 30,000 m²

Precipitation: 24,000,000 L/a

(calculated from the annual precipitation in this region: 800 mm/a)

Evaporation: 90 %

→ Seepage water: 2,400,000 L/a

→ Flow rate: 0.2739 m³/h

Total uranium content of the seepage water: 1.6 mg U/L

⇒ Total uranium discharge via the seepage water

due to weathering and desorption:

3840 g U/a (= 100 %)

(corresponds to $3.8 \cdot 10^{-3}$ % of the total uranium inventory of the rock pile which is 100,000 kg)

- Uranium discharge estimated on the basis of pyrite weathering, sulfate content in the seepage water, neutralization of protons formed etc.:

Total weathering of rock material: 40 tons/a (this is only $1.6 \cdot 10^{-3}$ % of the total mass of the rock material which is 2,500,000 tons)

Mean uranium content of the rock material: 45 mg U/kg

⇒ Uranium discharge per year due to weathering:

1800 g U/a (= 47 %)

⇒ Uranium discharge per year due to desorption of previously sorbed uranium (difference)

2040 g U/a (= 53 %)

- Uranium discharge determined by means of long-term leaching experiments:

Total uranium content of the seepage water: 1.6 mg U/L = 3840 g U/a (= 100 %)

⇒ Uranium content due to weathering processes:
(determined by laboratory experiments)

0.8 mg U/L = 1920 g U/a (= 50 %)

⇒ Uranium content due to desorption of previously sorbed uranium (difference)

0.8 mg U/L = 1920 g U/a (= 50 %)

Easily leachable uranium: 1.27 mg U/kg (= 2.8 % of the mean uranium content of the rock material, which is 45 mg U/kg)

It is assumed that a part of the sorption sites of the rock material that were set free due to desorption of previously sorbed uranium is occupied immediately by uranium just released from the rock material by weathering.

- Leaching rate:

Volume of the rock pile: 1,000,000 m³

Density of rock material: 2.5 g/cm³

Mass of rock material: 2,500,000 tons

⇒ Leaching rate: $1.54 \cdot 10^{-3} \text{ g U}/(\text{tons} \cdot \text{a}) \quad \equiv \quad 1.54 \cdot 10^{-3} \text{ mg U}/(\text{kg} \cdot \text{a})$

3.7 Summary and conclusion

In this natural system study, characteristic data of the uranium mining waste rock pile no. 250 in Schlema/Alberoda were compiled as well as important data of other uranium mining waste rock piles of this area. The overall picture obtained is considered as representative of the piles in this uranium mining region.

With the information given in this study together with further observations on natural systems it should be possible to identify data that are relevant for performance assessment modeling but still missing and to verify the realism of scenarios that will be used for performance assessment modeling.

4. References

- Arnold, T., Zorn, T., Bernhard, G. and Nitsche, H. (1998) Sorption of Uranium(VI) onto Phyllite. *Chemical Geology* 151, 129.
- Arnold, T., Zorn, T., Zänker, H., Bernhard, G. and Nitsche, H. (2001) Sorption Behavior of U(VI) on Phyllite: Experiments and Modeling. *J. of Contaminant Hydrology* 47, 219.
- Bernhard, G., Geipel, G., Brendler, V. and Nitsche, H. (1996) Speciation of Uranium in Seepage Waters of a Mine Tailing Pile Studied by Time-Resolved Laser-Induced Fluorescence Spectroscopy (TRLFS). *Radiochim. Acta* 74, 87.
- Bernhard, G., Geipel, G., Brendler, V., Reich, T., Amayri, S. and Nitsche, H. (2001) Uranyl(VI) carbonate complex formation: Validation of the $\text{Ca}_2\text{UO}_2(\text{CO}_3)_3$ (aq) species. *Radiochim. Acta* 89, 511.
- BfS (1992) Radiologische Erfassung, Untersuchung und Bewertung Bergbaulicher Altlasten, BfS Schriften 8/92 (ISSN 0937-449), Bundesamt für Strahlenschutz, Salzgitter, Germany.
- BMWi (1995) WISMUT – Progress in Decommissioning and Rehabilitation, Doc. No. 370 (ISSN 0342-9288), German Federal Ministry of Economics, Bonn, Germany.
- Daenecke, R. (1995) Erfahrung aus durchgeführten Haldensanierungen bis 1990. In: *Proceedings of the Workshop ‘Sanierung von Bergbauhalden’ 06.11.95-08.11.95*, Chemnitz, Germany.
- Dienemann, H., Brackhage, C., Dannecker, A., Dudel, G. and Rotsche, J. (2002) Soil Formation and Quality on Uranium Mining Dumps Depending on Different Tree Species Under Special Consideration of Selected Radionuclide Contamination. In: *Uranium in the Aquatic Environment*. B.J. Merkel, B. Planer-Friedrich and C. Wolkersdorfer (Eds.), Springer Verlag, Berlin, p. 489.
- Franke, K., Rössler, D., Gottschalch, U. and Kupsch, H. (2000) Mobilization and Retardation of Uranium DOC Species at Three Mine Piles in Schlema/Alberoda, Saxony, Germany. *Isotopes Environ. Health Stud.* 36, 223.

- Gatzweiler, R. and Marski, R. (1996) Haldensanierung - eine interdisziplinäre Herausforderung. *Geowissenschaften* 11, 461.
- Gatzweiler, R. (1997) Einbindung der Wasserbehandlung in die Sanierung des sächsisch-thüringischen Uranerzbergbaus: Technische und wirtschaftliche Aspekte. In: Proceedings of the International Workshop 'Wasserbehandlung und Rückstandsentsorgung - konventionelle und innovative Lösungen' 24.09.97-26.09.97, Chemnitz, Germany.
- Geipel, G., Thieme, M. and Bernhard, G. (1994a) Verhalten radiotoxischer Schadstoffe in Hinterlassenschaften des Uranbergbaus als Grundlage für Sanierungskonzepte. Final Report 1994, Bundesministerium für Forschung und Technologie, Contract No. 02 S 7533.
- Geipel, G., Thieme, M., Bernhard, G. and Nitsche, H. (1994b) Distribution of Uranium and Radionuclides in a Uranium-Mining Rockpile in Schlema, Saxony, Germany. *Radiochim. Acta* 66/67, 309.
- Geipel, G. and Thieme, M. (1994c) Determination of Inorganic Species in Seepage Water of Uranium-Mining Rockpiles and in Related Media. *J. Radioanal. Nucl. Chem.* 183, 139.
- Geipel, G., Bernhard, G., Brendler, V. and Nitsche, H. (1996) Sorption of Uranium(VI) on Rock Material of a Mine Tailing Pile: Solution Speciation by Fluorescence Spectroscopy. *Radiochim. Acta* 74, 235.
- Glombitza, F., Iske, U., Bullmann, M. and Ondruschka, J. (1992) Biotechnology Based Opportunities for Environmental Protection in the Uranium Mining Industry. *Acta Biotechnol.* 12 (2), 79.
- GLU (1995) Geohydrochemische Modellierung des Stofftransportes aus Berghalden im Gebiet Schlema/Alberoda und Pöhla-Tellerhäuser des Sanierungsgebietes Aue. Geologische Landesuntersuchungs-GmbH (GLU), Freiberg 21.03.95.
- Grenthe, I., Fuger, J., Lemire, R.J., Muller, A.B., Nguyen-Trung, C. and Wanner, H. (1992) *Chemical Thermodynamics of Uranium*, 1st ed., Elsevier Science Publishers, Amsterdam, Netherlands.
- Kisting, S., Deissmann, G., Goldsworthy, M. and Stollenwerk, R.H. (2002) Evaluation of the Long-term Durability of Engineered Dry Covers for Mining Wastes, and Consideration of Associated Design Constraints. In: *Uranium in the Aquatic Environment*. B.J. Merkel, B. Planer-Friedrich and C. Wolkersdorfer (Eds.), Springer Verlag, Berlin, p. 155.
- Köhler, M. and Wolf, J. (1995) Untersuchungen zu Abdeckvarianten für Berghalden. In: Proceedings of the Workshop 'Sanierung von Bergbauhalden' 06.11.95-08.11.95, Chemnitz, Germany.
- Kupsch, H. (1998a) Mobilisation and Immobilisation of Uranium-DOC-Species in three Waste Dumps in the District of Schlema/Alberoda. In: *Uranium Mining and Hydrogeology II. Proceedings of the International Conference and Workshop*. Freiberg, Germany, September 1998, B. Merkel, C. Helling and St. Hurst (Eds.), von Loga, Köln, p. 236.
- Kupsch, H., Franke, K., Gottschalch, U., Krüger, A., Richter, M., Rößler, D., Schulze, D., Süß, R. and Delakowitz, B. (1998b) Radioaktive Belastung im Bereich von Altbergbauhalden - Austrag radioaktiver Schadstoffe aus Halden des Erzbergbaus. unpublished work.
- Meyer, J. (1995) Überblick zum Stand der Vorbereitungen und Durchführung des Sanierungsvorhabens Schlema/Alberoda - Standortbeschreibung, Stand der Sanierungsarbeiten, Schwerpunkte der Sanierungsvorbereitung, Haldenkonzept. In: Proceedings of the Workshop 'Sanierung von Bergbauhalden' 06.11.95-08.11.95, Chemnitz, Germany.
- Runge, W. and Böttcher, J. (1994) Informationen zur WISMUT. In: *Prospekt der WISMUT GmbH, Abteilung Öffentlichkeitsarbeit*, Chemnitz, Germany.
- Schmeide, K., Pompe, S., Bubner, M., Heise, K.H., Bernhard, G. and Nitsche, H. (2000) Uranium(VI) Sorption onto Phyllite and Selected Minerals in the Presence of Humic Acid. *Radiochim. Acta* 88, 723.

- Schneider, P., Schaffrath, M. and Nindel, K. (2002) Hydrology of Engineered Covers of Waste Rock Dumps towards Heavy Rainfall Phenomena: A Case Study in Uranium Mill Tailings Mitigation. In: Uranium in the Aquatic Environment. B.J. Merkel, B. Planer-Friedrich and C. Wolkersdorfer (Eds.), Springer Verlag, Berlin, p. 165.
- Seidel, H., Ondruschka, J., Kusch, P. and Stottmeister, U. (1995) Einfluß des Schwefelgehaltes von Sedimenten auf die Mobilisierung von Schwermetallen durch bakterielle Laugung. *Vom Wasser* 84, 419.
- Trommler, K. and Kuchler, A. (1997) Biologische Schwermetallabtrennung aus Sicker- und Grubenwässer der WISMUT GmbH. In: Proceedings of the International Workshop 'Wasserbehandlung und Rückstandsentsorgung - konventionelle und innovative Lösungen' 24.09.97-26.09.97, Chemnitz, Germany.
- Wolery, T.J. (1992) EQ3/6. A Software Package for the Geochemical Modeling of Aqueous Systems. Report UCRL-MA-110662. Part I. Lawrence Livermore National Laboratory, Livermore, USA.

Annex 6

Chemical Data on Iodine-Natural Organic Matter Interaction

P. Reiller and V. Moulin

Commissariat à l'Energie Atomique (CEA)

Chemical Data on Iodine-Natural Organic Matter Interactions

Pascal Reiller*

CE Saclay, Nuclear Energy Division, DPC/SCPA/LCRE, Bâtiment 450 pièce 167, F-91191 Gif sur Yvette Cedex

Valérie Moulin

CEA Saclay, Nuclear Energy Division, DDIN/MR Bâtiment 125, F-91191 Gif sur Yvette Cedex.

ABSTRACT

Iodine radioactive isotope ^{129}I , is an important radionuclide due to its significant impact in geological disposal as shown by the PA exercise: under conditions of natural reducing groundwaters, iodine would essentially be present in the form of highly mobile iodide anion. But in shallow waters the presence of molecular iodine is to be taken into account.

Iodine can be strongly associated to soil organic matter and particularly to humic substances (HS). The reaction leading to this association can be assumed to be an electrophilic substitution of molecular iodine onto phenolic groups contained in HS. But if the halogenation of substituted phenols is now well identified, little is known about the interactions between iodine and more complex organic structures like HS.

For this purpose, the iodination of a purified humic acid has been studied as a function of different physical and chemical parameters such as pH, ionic strength or concentration of HS or diiodine/iodide ratios. The reaction was studied either by ultrafiltration that allows to quantify remaining iodine in solution, or by the decay of the triiodide absorbance (351 nm), that allows to assess the kinetic of the reaction. It comes out that (i) iodide has only weak or no interaction with HS, (ii) iodination kinetic of HS is slower than for substituted phenols, and cannot be linearised, which is in good agreement with the pH dependency.

This study confirms the significance of iodine - organic matter interactions as a governing process for iodine migration in natural environment. More studies are on going to develop predictive models of iodination kinetics.

* pascal.reiller@cea.fr

1. INTRODUCTION

The behaviour of iodine in natural environments is of great importance in case of an accidental release from nuclear installations and in the safety of a geologic repository. The most important radioisotopes of iodine, ^{129}I ($t_{1/2} = 1.6 \times 10^7$ years), and ^{131}I ($t_{1/2} = 8$ days), are produced as a result of the fission process during the normal operation of a nuclear reactor, and represent the most radiologically significant release following a reactor accident. Iodine would be released as CsI but can be radiolytically oxidised to I_2 (Ashmore et al., 1996; Cordfunke and Konings, 1993). Anionic radionuclides, like halogenides ($^{129}\text{I}^-$, $^{36}\text{Cl}^-$), are of primordial importance in, due to their period and potential mobility. Actually, under reducing conditions of a geologic repository, iodine or chlorine are in the (-I) redox state (Bard et al., 1985; Jensen, 1982; Ramette and Sandford, 1965), as it is shown on the predominance diagram of figure 1 in the case of iodine.

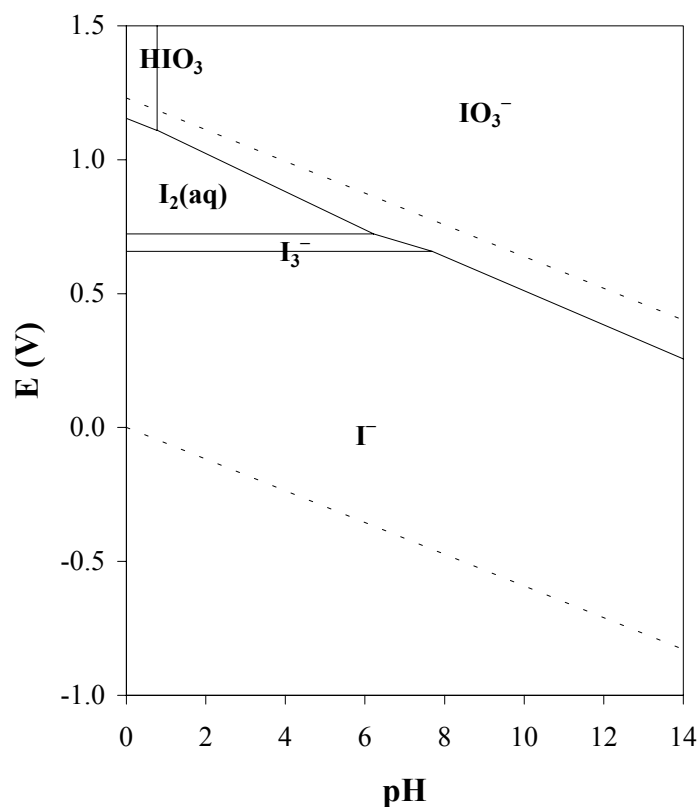


Figure 1: Predominance diagram of the iodine species involving I(V), I(0) and I(-I) (Bard et al., 1985; Ramette and Sandford, 1965); $[\text{I}]_{\text{total}} = 1 \times 10^{-4}$ M

Halogens are known to be associated to natural organic matter in soils (Johanson, 2000; Lee et al., 2001; Sheppard et al., 1989). In natural water disinfection processes, it has been shown that the mechanism of this association is an electrophilic substitution of molecular halogens (X_2), catalysed by hypohalogenous acid (HOX), on phenolic compound (Lee, 1967; Rook, 1974). The interaction of iodide with HS was postulated by Christiansen and Carlsen

(1991) to interpret an apparent reversibility of the association of iodine with humic acids catalysed by peroxydase enzymes.*

The most commonly accepted reaction scheme involving halogens and HS is an electrophilic substitution of aromatic structures. If this mechanism requires the polarisation of the dihalogen molecule (X_2) by a Lewis acid in the case of benzenic moieties, a Brønsted acid, the hypohalogenous acid, is sufficient in the case of phenolic structures to polarise the halogen molecule (Bichsel and von Gunten, 2000a; Gallard and von Gunten, 2002; Rebenne et al., 1996; Warner et al., 2000). The kinetic of this reaction is strongly influenced by the substitution of the phenolic ring (Lee, 1967; Warner et al., 2000). The chlorination of phenolic structures (Gallard and Von Gunten, 2002; Lee, 1967; Rebenne et al., 1996; Warner et al., 2000) and HS (Gallard and von Gunten, 2002; Warner et al., 2000), highly depends on pH through the ionisation of phenolate functions ($pK \approx 8-9$) and of the hypohalogenous acid – $pK_a(\text{HClO}) = 7.87$ (Stumm and Morgan, 1996); $pK_a(\text{HIO}) = 10.4$ (Bichsel and von Gunten, 2000b).

If the reaction mechanism is well known in the case of simple phenolic structures, the case of HS is more complex as it involves more than one step (Rädlinger and Heumann, 2000). Actually, the reaction kinetic in the case of HS is slower than in the case of phenolic compounds due to the presence of carboxylic function on the aromatic ring (Warner et al., 2000) and to the accessibility in the aggregate structure as postulated by Warwick et al. (1993). Thus, the formation of iodo-derivatives of phenolic structures induces the formation of a covalent bonding between carbon and iodine, evidenced in XPS by Mercier et al. (2000) and in ESI-MS by Moulin et al. (2001).

If the kinetic analysis of the iodination reaction of HS has been done by Warner et al. (2000), it relies on a narrow pH range (from 4.75 to 5.75) and on rough approximations about the use of Hammett coefficient (Exner, 1972). The extrapolation to natural conditions can thus be difficult. This study proposes to assess some key points in the reaction between iodine and humic substances:

- Is there a specific reactivity between iodide and HS?
- What is the influence of pH on a large pH scale?
- What is the influence of the composition of the solution?

With this objective, the iodination of HS (Aldrich HA and aquatic FA as in a previous study (2001)) was performed. The analysis were performed either in scintillation counting of ^{125}I after separation by ultrafiltration for the separation of iodide and HS aggregates, or direct spectrophotometric determination of I_3^- complex in solution for the consumption of iodine by HS (Bichsel and von Gunten, 1999).

* Lactoperoxydase and chloroperoxydase

2. EXPERIMENTAL

2.1. Materials

Purified Aldrich HA and aquatic FA (Mol, Belgium) are used in a protonated form. Characteristics of these HS were described elsewhere (Kim et al., 1991; Montjotin, 1996; Plancque et al., 2001). ^{125}I was obtained from Amersham (Amersham Pharmacia Biotech, IMS30).

2.2. Methods

2.2.1. Ultrafiltration

Millipore[®] Ultrafree-4 centrifugation units holding a polyethersulfone membrane of a molecular weight cut-off of 5 kDa were used. The membranes were washed thrice with Millipore[®] water. The filtration was conducted at 5,700 rpm during 30 minutes.

The validation of the Ultrafree-4 units for HA (50 mg/L) and ^{125}I separation were conducted at different ionic strengths (0.1 M, 10^{-2} M and 10^{-3} M) adjusted by NaClO_4 (Merck, Darmstadt, Germany). The pH value is adjusted by freshly prepared NaOH and HClO_4 solutions.

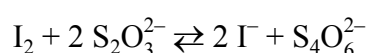
The HA concentrations were determined spectrophotometrically at 254 nm using a Shimadzu UV 2100, neglecting the chromism effect induced by the separation (Gu et al., 1994; Vekshin, 1987; Vekshin, 1999). The retention efficiency is defined as:

$$R = 1 - \frac{[\text{HA}]_{\text{uf}}}{[\text{HA}]^{\circ}}$$

where $[\text{HA}]_{\text{uf}}$ is the HA concentration determined in the ultrafiltrate and $[\text{HA}]^{\circ}$ is the initial HA concentration. The same formalism is applied to iodide.

Initial solutions containing 5×10^{-5} M of NaI (Merck) were spiked with 950 Bq of ^{125}I . After the separation by ultrafiltration, the activity of ^{125}I was measured by liquid scintillation counting: 1 ml-sampled aliquots were added to 4 ml of liquid scintillator (Packard Ultima Gold AB). The counting was performed within an energy range from 6 to 70 keV during 10 minutes

In order to stabilise iodine in its reduce form I^- , sodium thiosulphate ($\text{Na}_2\text{S}_2\text{O}_3$) was added to the solution so that the reaction (Charlot, 1961):



which impede the formation and volatilisation of molecular iodine (Evans et al., 1993).

2.2.2. Spectrophotometric study of the reaction

The consumption of iodine, through the decrease of the triiodide complex absorbance (I_3^- , $\epsilon_{288 \text{ nm}} = 38\,200 \text{ M}^{-1} \text{ cm}^{-1}$, $\epsilon_{351 \text{ nm}} = 25\,700 \text{ M}^{-1} \text{ cm}^{-1}$) (Bichsel and von Gunten, 1999), was

monitored in UV-Visible spectrophotometry using a Cary 500 spectrophotometer – 351 nm band of I_3^- was chosen in order to minimise the HS absorbance overlapping. The stock solution of triiodide complex was composed of a saturated solution of iodine 2.66×10^{-3} M (Ramette and Sandford), and 2.6×10^{-2} M of NaI (Merck) in $NaClO_4$ (Prolabo) as electrolyte. The speciation of iodine in this stock solution can be calculated (table 1) using the data of Ramette and Sandford (1965). In a typical assay, the zero absorbance was set with a 2 ml HS solution and a 200 μ l aliquot of the triiodide complex solution was added at t_0 . In this case the speciation of iodine can also be estimated in table 1.

The kinetic data presented hereafter are the mean of five to six different experiments acquired in the same conditions.

Table 1: Speciation of iodine in the experimental conditions.

Equilibria			
$I_2(c) \rightleftharpoons I_2(aq)$	$\log K_{25^\circ C} = -2,88$		
$I_2(aq) + I^- \rightleftharpoons I_3^-$	$\log K = 2,86$ (Ramette and Sandford, 1965)		
Solution composition	Proportion of species		
	I^-	I_3^-	$I_2(aq)$
Stock solution [NaI] = 2.6×10^{-2} M [$I_2(c)$] = 2.66×10^{-3} M	75%	24%	1%
200 μ l aliquot in 2 ml of HS solution	78%	12%	10%

3. RESULTS AND DISCUSSION

3.1. Interaction of iodide with HA by ultrafiltration

3.1.1. Qualification of the ultrafiltration modules

The size of HS aggregates in solution is around 100-200 nm (Caceci and Moulin, 1991), and HS are known to be efficiently separated from solution by ultrafiltration membrane (Aster et al., 1996; Ephraim and Marinsky, 1990), as are other aggregates like micellar systems (Pramauro et al., 1992; Reiller et al., 1996; Reiller et al., 1994; Scamehorn and Harwell, 1988). In a first step, we have verified that Ultrafree-4 modules with 5kDa MWCO membrane can be used under our conditions, yielding maximum retention of HS and minimal retention of iodide, which is a prerequisite to use ultrafiltration for studying the uptake of iodine with HS.

The results obtained as a function of pH are reported on figure 2 for three different ionic strengths: 0.1, 10^{-2} and 10^{-3} M. The retention of HA, expressed in percentage, by the 5 kDa membrane are close to 90% for low ionic strength of 10^{-2} and 10^{-3} M, and fairly constant in the pH range. Mean values of $R_{0.01\text{ M}} = (89.4 \pm 2.3)\%$ and $R_{0.001\text{ M}} = (93.4 \pm 1.7)\%$ can be calculated with 95% confidence interval. On the other hand, the retention at ionic strength of 0.1 M is too scattered and insufficient to be used in the rest of this study.*

* $R_{0.1\text{ M}} = 66,0 \pm 11.3$

The evolution observed in term of retention efficiency is in conformity with the general properties of HS. When the ionic strength decreases, the Debye length increases and the electrostatic interactions increase as well as the hydrodynamic volume and the apparent molecular mass (Cornel et al., 1986; Vermeer, 1996).

In the following, we will use an ionic strength of 10^{-3} M in order to maximise the retention of HA.

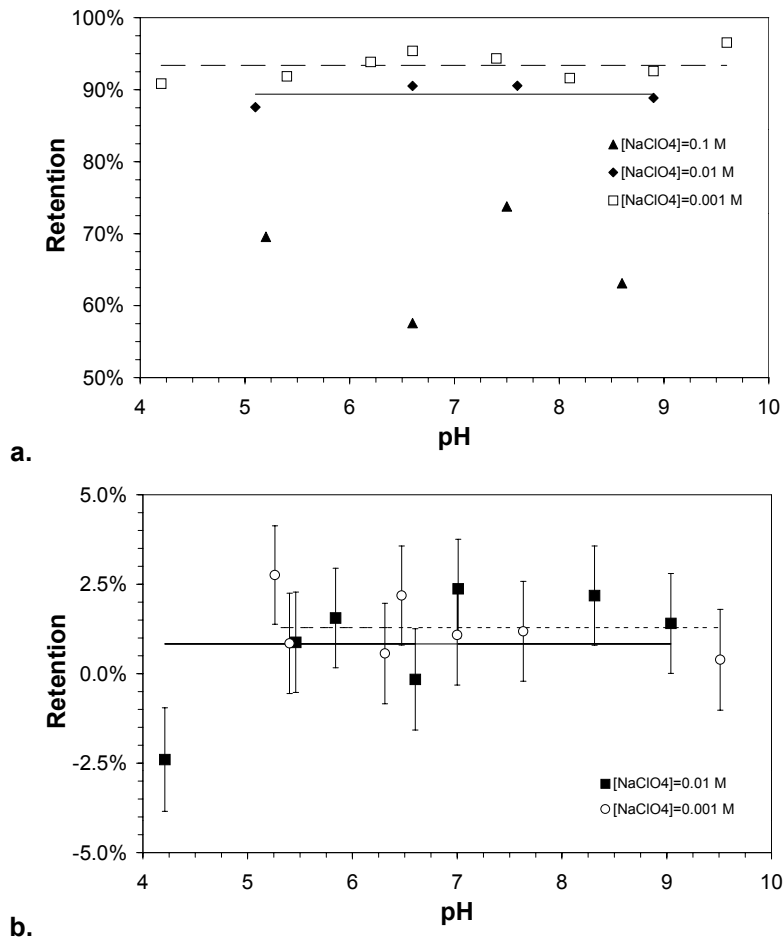


Figure 2: Retention of (a.) HA and (b.) iodide vs. pH on Ultrafree-4 5 kDa modules for different ionic strength; a. [HA] = 50 mg/L., b. [I⁻] = 5×10^{-5} M

The retention of iodide by the UF membrane vs. pH in Ultrafree-4 modules with 5 kDa MWCO membrane is reported on figure 2b. These results show that the retention of iodide can be considered as negligible as $R_{0.01\text{ M}} = (0.8 \pm 1.5)\%$, and $R_{0.001\text{ M}} = (1.3 \pm 0.8)\%$. These two values cannot be considered as statistically different.

3.1.2. Interaction of iodide with HA

A solution containing 50 mg/L of HA, 5×10^{-5} M of NaI and 6×10^{-6} M of $\text{Na}_2\text{S}_2\text{O}_3$ at an ionic strength of 10^{-3} M (NaClO_4) at pH = 6 was spiked with ^{125}I . The concentration of $\text{Na}_2\text{S}_2\text{O}_3$ can be considered as sufficiently high regarding the slow spontaneous formation of

I₂ from iodide (Wong, 1991).^{*} The solution was constantly agitated in a polythene flask at room temperature (t ≈ 22°C) during 17 days. Filtrations were performed and the filtrate activities were measured. The retention efficiency vs. time is reported on figure 3.

Within the 17 days period, no significant increase in the retention of iodide could be observed, as no values are statistically different from one another. The maximum retention percentage of iodide was 0.8 % and the mean value was (0.01 ± 0.30) %. The same experience was realised adding 2 mg/L of lactoperoxydase enzyme (EC 1.11.1.7, 61328 Biochemika, Fluka) that catalyses the reaction in the presence of H₂O₂ (Morrison, 1970), and no enhancement of the iodide retention was achieved. Hence, the hypothesis of a possible reaction of iodide with this type of humic acid can be postponed when reducing condition occur.

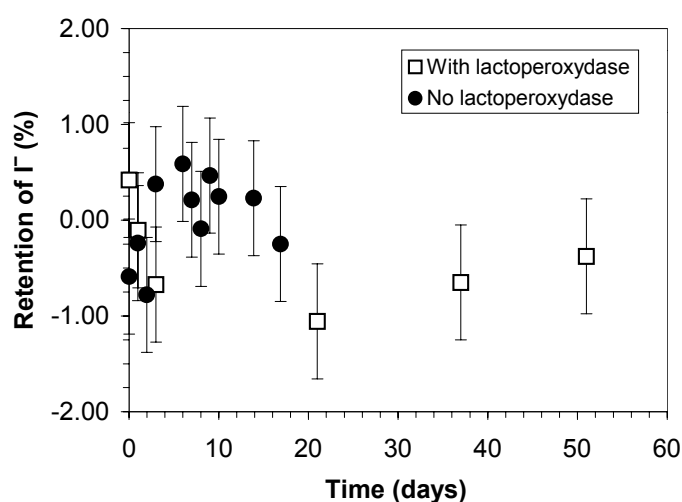


Figure 3: Retention of iodide by ultrafree-4 modules with 5 kDa MWCO membrane, in the presence of HA; [HA] = 50 mg/l, [I⁻] = 5 × 10⁻⁵ M, [Na₂S₂O₃] = 6 × 10⁻⁶ M, [NaClO₄] = 10⁻³ M, pH = 6.

3.2. Kinetic study

On figure 4 the decrease in triiodide complex for different pH values, reflecting the consumption of I₂(aq) in solution by HA (20 mg/L), is reported. As it has been observed for the iodination and chlorination of phenolic derivatives, the reaction depends upon the pH value (Bichsel and von Gunten, 2000a; Gallard and Von Gunten, 2002; Lee, 1967; Rebenne et al., 1996; Warner et al., 2000). A negative order relative to [H⁺] is expected. This evolution depends directly upon the ionisation of phenolate and hypohalogenous acid (Bichsel and von Gunten, 2000a; Lee, 1967). This evolution has also been observed on different HS by Warner et al. (2000), but only on a narrow range of pH. As it has also been observed by Warner et al. (2000), the kinetics cannot be linearised either in first or second order.

^{*} $v = 1.3 \times 10^{-11} \mu\text{M}\cdot\text{day}^{-1}$

Actually, as it has been clearly evidenced in ESI-MS in a previous study (Moulin et al., 2001), HS can be considered as a mixture of a great variety of different phenolic compounds. The various substituents (carboxylic acids, alkyl chains...) directly influence the iodination reaction depending on their inductive or mesomeric effect and position on the phenolic ring (Exner, 1972). In the case of substituted phenols, the observation of first order kinetics is the consequence of mechanisms that do not involve mixture of molecules. Thus, in the case of HS the great variety of molecules sharing a “common core” may possibly not induce simple reaction orders.

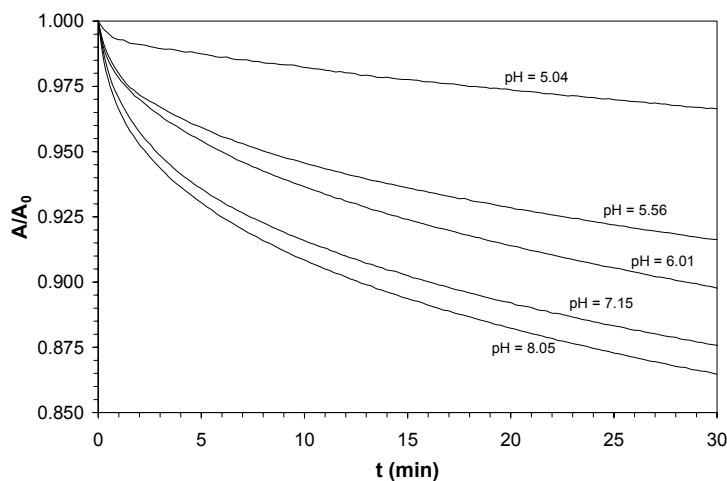


Figure 4: Influence of pH on the consumption of iodine by HA; [HA] = 20 mg/L, [NaClO₄] = 0.1 M, [I₂] = 1.3 × 10⁻⁴ M, [I⁻] = 1.2 × 10⁻³ M, speciation in table 1.

On figure 5 is reported the consumption of iodine with time for different concentration of Aldrich HA (figure 5a) and Mol FA (figure 5b) from 5 to 150 mg/L (pH = 6, [NaClO₄] = 0.1 M, [I₂] = 1.3 × 10⁻⁴ M, [I⁻] = 1.2 × 10⁻³ M). The evolution suggests that the reaction order is positive respective to HS concentration but, like in the case of the influence of pH, the kinetics cannot be linearised. The consumption of iodine by aquatic FA appears to be slightly slower than in the case of Aldrich HA. This result agrees well with the observation of Warner et al. (2000) who normalised their kinetic data to the number of phenolic function in their humic and fulvic acids and seemed to show that the kinetics of soil HA and FA are within the same order of magnitude. The authors also showed that the reaction with Suwannee River FA was faster than for soil FA and ascribed this difference to the presence of methoxy groups in this FA.

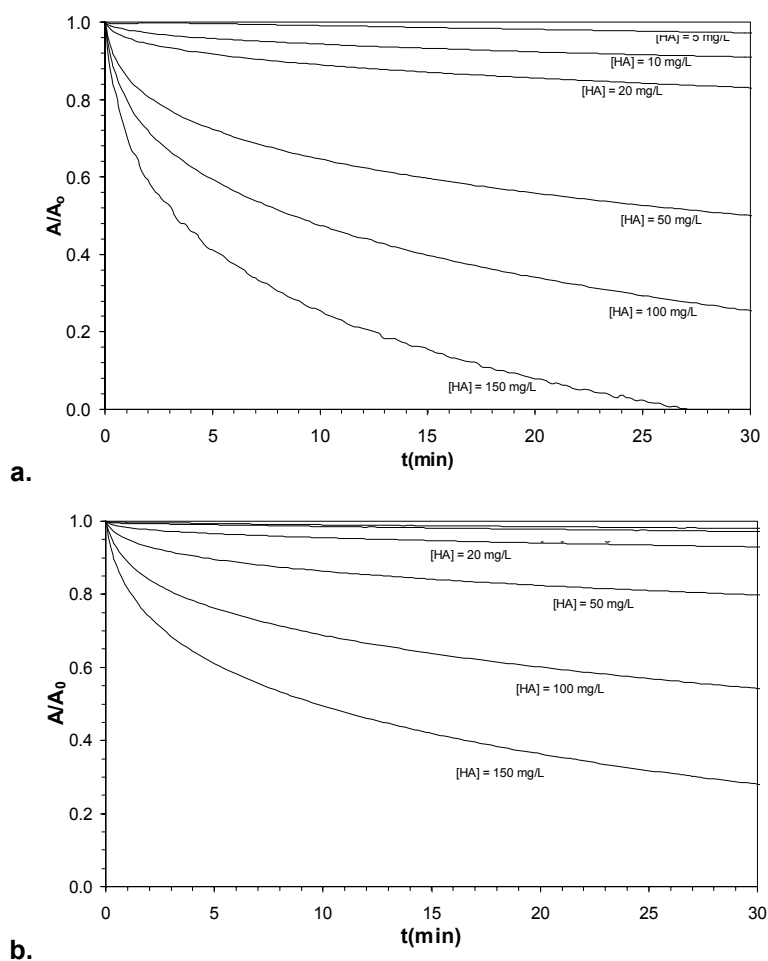


Figure 5: Influence of concentration of HS on the consumption of iodine: a. case of Aldrich HA, b. case of Mol fulvic acid; $[\text{NaClO}_4] = 0.1 \text{ M}$, $[\text{I}_2] = 1.3 \times 10^{-4} \text{ M}$, $[\text{I}^-] = 1.2 \times 10^{-3} \text{ M}$, $\text{pH} = 6$, speciation in table 1.

Humic substances are very sensitive to the variations of the physico-chemical properties of the solution such as ionic strength. These variations induces differences in the sorption properties of HS onto mineral surfaces (Reiller et al., 1999; Reiller et al., 2002). The consumption of iodine by HA for three different ionic strengths, 0.1, 10^{-2} and 10^{-3} M NaClO_4 , is reported on figure 6. The kinetics at 10^{-3} M is significantly slower than those obtained at 10^{-2} and 0.1 M.*

The variation of the reaction rate k with ionic strength can be attempted theoretically (Moore and Pearson, 1981, p. 272). The increase in $\log k$ could be written for an electrolyte XY as:

$$\ln k \approx \ln k_0 + \frac{2 z_X z_Y A \sqrt{I}}{1 + B a \sqrt{I}},$$

where z_X and z_Y are the charge of X and Y respectively, A and B are the parameters of the Debye-Hückel theory (Lyklema, 1995), and a is the mean value for the distance of closest

* Overlapping of confidence interval for 0.1 M and 10^{-2} M

approach. In this case the predicted increase in $\log k$ is greater between 0.1 M and 10^{-2} M ($\Delta \log k_2$) than it is between 10^{-2} M and 10^{-3} M ($\Delta \log k_1$). Finally we see that:

$$\Delta \log k_2 > \Delta \log k_1.$$

The results reported in figure 6 reveal that $\Delta \log k_1 > \Delta \log k_2$. Hence, the observed variation of reaction rate with ionic strength cannot be the only explanation of this dependence.

We have already seen that the variation of the hydrodynamic volume of the HA aggregates is inversely proportional with ionic strength mostly due to the variation of the Debye length. Vermeer showed that the decrease in ionic strength is related to the decrease of the surface potential of humic substances moieties that induces the repulsion of negative charges (Vermeer, 1996). Under our conditions, the speciation of iodine in solution is governed by anionic species (Ramette and Sandford, 1965).^{*} The accessibility of I_3^- to the vicinity of the humic aggregates is then hindered by the increase of the electrostatic field.

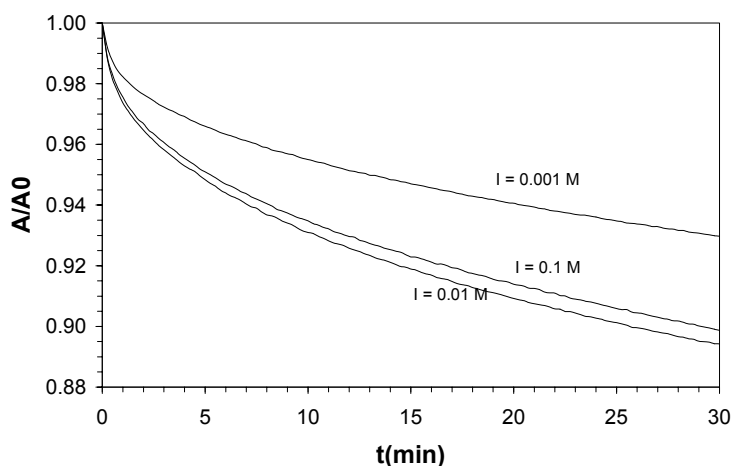


Figure 6: Influence of ionic strength (NaClO_4); $[\text{HA}] = 20 \text{ mg/L}$, $[\text{I}_2] = 1.3 \times 10^{-4} \text{ M}$, $[\text{I}^-] = 1.2 \times 10^{-3} \text{ M}$, $\text{pH} = 6$, speciation in table 1.

This hypothesis is supported by the variation of the kinetics with the iodide concentration in solution. These types of kinetics are reported on figure 7, where the proportion of iodide in solution is increased from $2.2 \times 10^{-4} \text{ M}$ to $8.3 \times 10^{-4} \text{ M}$ and the total concentration of $\text{I}_2(\text{aq})$ is fairly stable. These results are in agreement with those of Warner et al. (2000). This increase in iodide concentration induces an increase in the proportion of I_3^- complex illustrated by the increase of initial absorbance on figure 7a (56.4%, 61.5% and 68.6% of total I_2 using the data from Ramette and Sandford, 1965) that is repelled by the negative surface of the humic aggregate.

^{*} 78% I^- , 12% I_3^- , 10% $\text{I}_2(\text{aq})$

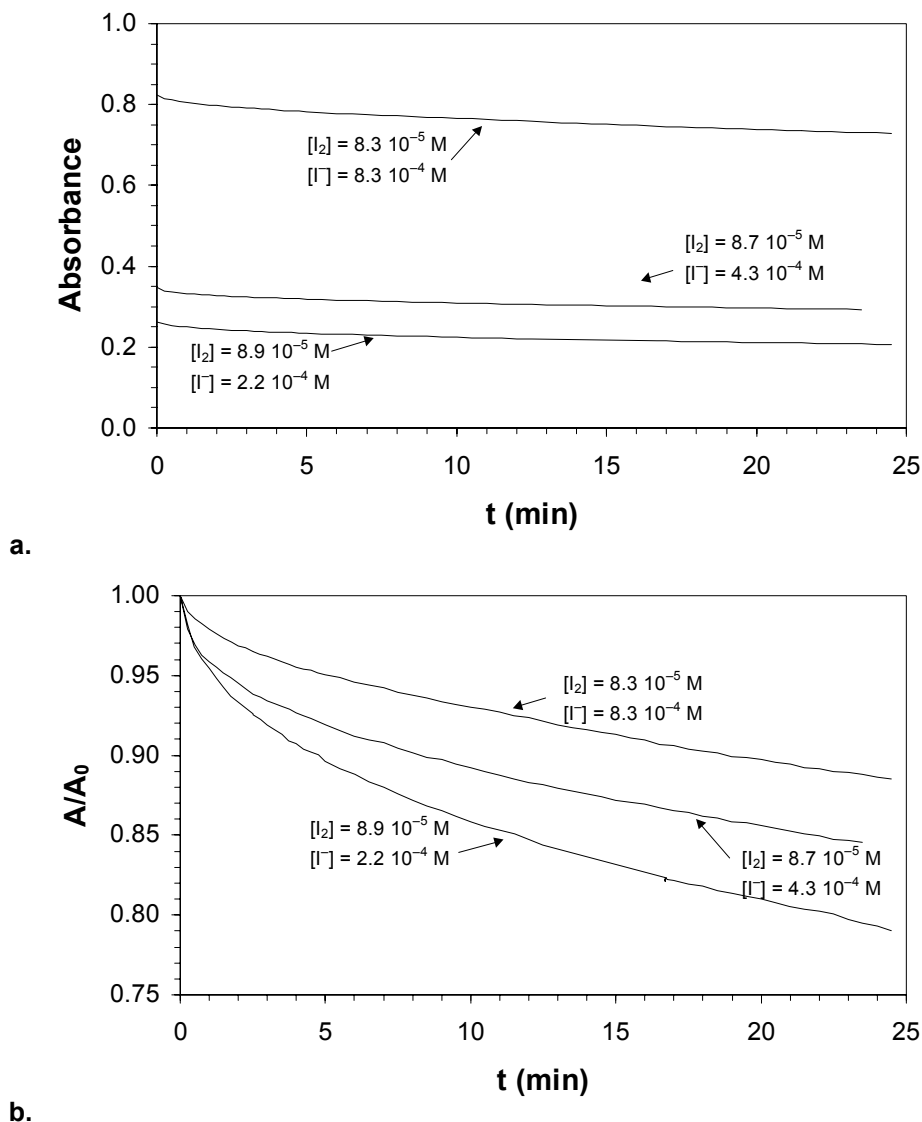


Figure 7: Influence of iodide concentration on the consumption of iodine by HA.

4. CONCLUSION

The iodination reaction of HS does not rely on univocal mechanisms, as it is the case for substituted phenols. The supra molecular structure of HS, and the phenolic “common core” of the building blocks, might be responsible of the fact that impossibility the kinetics cannot be linearised in simple reaction order. Therefore, recent developments on the theoretical description of supra molecular aggregates (Lefrancois et al., 1999), or the description of distribution of reaction sites, as it has already been done for the humic complexation of metal ions (Milne et al., 2001), would improve the comprehension and modelling of these systems.

ACKNOWLEDGEMENT

The authors would like to thank Marie-Hélène Fauré (†), for her compilation work on iodine chemistry in CEA, and Florence Casanova, Arnaud Spicq and Benoit Arduino for their help in the experimental work.

5. REFERENCES

- Ashmore C. B., Gwyther J. R., and Sims H. E. (1996). Some effects of pH on inorganic iodine volatility in containment. *Nuclear Engineering and Design* **166** (3), 347-355.
- Aster B., Burba P., and Broekaert J. A. C. (1996). Analytical fractionation of aquatic humic substances and their metal species by means of multistage ultrafiltration. *Fresenius Journal of Analytical Chemistry* **354** (5-6), 722-728.
- Bard A. J., Parsons R., and Jordan J. (1985). Standard potentials in aqueous solution, pp. 834. IUPAC, Marcel Dekker.
- Bichsel Y. and von Gunten U. (1999). Determination of iodide and iodate by ion chromatography with postcolumn reaction and UV/visible detection. *Analytical Chemistry* **71** (1), 34-38.
- Bichsel Y. and von Gunten U. (2000a). Formation of iodo-trihalomethanes during disinfection and oxidation of iodide-containing waters. *Environmental Science and Technology* **34**, 2784-2791.
- Bichsel Y. and von Gunten U. (2000b). Hypoiodous acid: kinetics of the buffer-catalyzed disproportionation. *Water Research* **34** (12), 3197-3203.
- Caceci M. and Moulin V. (1991). Investigation of humic acid samples of different sources by photon correlation spectroscopy. In *Lecture Notes in Earth Sciences, Humic substances in the Aquatic and Terrestrial Environment*, Vol. 33 (ed. B. Allard, H. Boren, and A. Grimvall), pp. 97-104.
- Charlot G. (1961). *Analyse quantitative minérale*. Masson, Paris.
- Christiansen J. and Carlsen L. (1991). Enzymatically controlled iodination reactions in the terrestrial environment. *Radiochimica Acta* **52/53**, 327-333.
- Cordfunke E. H. P. and Konings R. J. M. (1993). The release of fission products from degraded UO₂ fuel: thermochemical aspects. *Journal of Nuclear Materials* **201**, 57-69.
- Cornel P. R., Summers R. S., and Roberts P. V. (1986). Diffusion of humic acid in dilute aqueous solutions. *Journal of Colloid and Interface Science* **110**, 149.
- Ephraim J. H. and Marinsky J. A. (1990). Ultrafiltration as a technique for studying metal-humate interactions: studies with iron and copper. *Analytica Chimica Acta* **232**, 171-180.
- Evans G. J., Mirbod S. M., and Jervis R. E. (1993). The volatilization of iodine species over dilute iodide solutions. *Canadian Journal of Chemical Engineering* **71** (5), 761-765.
- Exner O. (1972). The Hammett equation - The present position. In *Advances in Linear Free Energy Relationships* (ed. N. B. Chapman and J. Shorter), pp. 1-69. Plenum Press.
- Gallard H. and von Gunten U. (2002). Chlorination of natural organic matter: kinetics of chlorination and of THM formation. *Water Research* **36** (1), 65-74.
- Gallard H. and Von Gunten U. (2002). Chlorination of phenols: Kinetics and formation of chloroform. *Environmental Science and Technology* **36** (5), 884-890.
- Gu B., Schmitt J., Chem Z., Liang L., and McCarthy J. F. (1994). Adsorption and desorption of natural organic matter on iron oxide: mechanisms and models. *Environmental Science and Technology* **28**, 38-46.

- Jensen B. S. (1982). Migration phenomena of radionuclides into the geosphere. In *Radioactive Waste Management*. Harwood.
- Johanson K. J. (2000). Iodine in soil, pp. 45. SKB.
- Kim J. I., Buckau G., Klenze R., Rhee D. S., and Wimmer H. (1991). Characterisation and complexation of humic acids. CCE.
- Lee C. F. (1967). Kinetics of reactions between chlorine and phenolic compounds. Principles and Applications of water chemistry proceedings (ed. S. D. Faust and J. V. Hunter), pp. 54-74. Wiley.
- Lee R. T., Shaw G., Wadey P., and Wang X. (2001). Specific association of ^{36}Cl with low molecular weight humic substances in soils. *Chemosphere* **43**, 1063-1070.
- Lefrancois L., Belnet F., Noel D., and Tondre C. (1999). An attempt to theoretically predict third-phase formation in the dimethyldibutyltetradecylmalonamide (DMDBTDMA)/Dodecane/Water/Nitric acid extraction system. *Separation Science and Technology* **34** (5), 755-770.
- Lyklema J. (1995). *Fundamentals of colloid and interface science*. Academic Press Ltd.
- Mercier F., Moulin V., Guittet M. J., Barré N., Toulhoat N., Gautier-Soyer M., and Toulhoat P. (2000). Applications of NAA, PIXE and XPS for the quantification and characterization of the humic substances/iodine associations. *Radiochimica Acta* **88**, 779-785.
- Milne C. J., Kinniburgh D. G., and Tipping E. (2001). Generic NICA-Donnan model parameters for proton binding by humic substances. *Environmental Science and Technology* **35** (10), 2049-2059.
- Montjotin C. (1996). Isolation, caractérisation et mesures des teneurs en ^{14}C de substances humiques aquatiques : application à la datation des eaux souterraines, Université d'Orsay, Paris Sud.
- Moore J. W. and Pearson R. G. (1981). *Kinetics and mechanism, third edition*. John Wiley & Sons.
- Morrison M. (1970). Iodination of tyrosine: Isolation of lactoperoxidase (Bovine). In *Methods in Enzymology*, Vol. XVIIIA (ed. H. Tabor and C. Tabor), pp. 653. Academic Press.
- Moulin V., Reiller P., Amekraz B., and Moulin C. (2001). Direct characterization of iodine covalently bound to fulvic acids by electrospray mass spectrometry. *Rapid Communication in Mass Spectrometry* **15**, 2488-2496.
- Plancque G., Amekraz B., Moulin V., Toulhoat P., and Moulin C. (2001). Molecular structure of fulvic acids by electrospray with quadrupole time-of-flight mass spectrometry. *Rapid Communication in Mass Spectrometry* **15** (10), 827-835.
- Pramauro E., Prevot A. B., Pelizzetti E., Marchelli R., Dossena A., and Biancardi A. (1992). Quantitative Removal of Uranyl Ions from Aqueous Solutions Using Micellar-Enhanced Ultrafiltration. *Analytica Chimica Acta* **264**, 303-310.
- Rädlinger G. and Heumann K. G. (2000). Transformation of iodide in natural and wastewater systems by fixation on humic substances. *Environmental Science and Technology* **34**, 3932-3936.
- Ramette R. W. and Sandford R. W. (1965). Thermodynamics of iodine solubility and triiodide ion formation in water and in deuterium oxide. *Journal of the American Chemical Society* **87**, 5001-5005.
- Rebenne L. M., Gonzalez A. C., and Olson T. M. (1996). Aqueous chlorination kinetics and mechanism of substituted dihydroxybenzenes. *Environmental Science and Technology* **30** (7), 2235-2242.

- Reiller P., Lemordant D., Hafiane A., Moulin C., and Beaucaire C. (1996). Extraction and release of metal ions by micellar-enhanced ultrafiltration: Influence of complexation and pH. *Journal of Colloid and Interface Science* **177** (2), 519-527.
- Reiller P., Moulin C., Beaucaire C., and Lemordant D. (1994). Dual use of micellar enhanced ultrafiltration and time-resolved laser-induced spectrofluorometry for the study of uranyl exchange at the surface of alkylsulfate micelles. *Journal of Colloid and Interface Science* **163** (1), 81-86.
- Reiller P., Moulin V., and Casanova F. (1999). Sorption behaviour of humic substances towards iron oxides. In Buckau G. Ed. 2nd Technical Report EC Project "Effects of humic substances on the migration of radionuclides: complexation and transport of actinides", pp. 119-136. Institut für Nukleare Entsorgungstechnik.
- Reiller P., Moulin V., Casanova F., and Dautel C. (2002). Retention behaviour of humic substances onto mineral surfaces and consequences upon thorium (IV) mobility: case of iron oxides. *Applied Geochemistry* **17** (12), 1551-1562.
- Rook J. J. (1974). Formation of haloforms during chlorination of natural waters. *Water Treatment Exam* **23** (2), 234-243.
- Scamehorn J. F. and Harwell J. H. (1988). *Surfactant based separation processes*. Marcel Dekker.
- Sheppard M., Thibault D., and Smith P. (1989). Iodine dispersion and effects on groundwater chemistry following a release to a peat bog, Manitoba, Canada. *Applied Geochemistry* **4**, 423-432.
- Stumm W. and Morgan J. J. (1996). *Aquatic Chemistry, chemical equilibria and rates in natural waters, Third Edition*. Wiley.
- Vekshin N. L. (1987). Screening hypochromism in chromophore stacks. *Optics and Spectroscopy* **63**, 517-519.
- Vekshin N. L. (1999). Screening hypochromism of chromophores in macromolecular biostructures. *Biophysics* **44** (1), 41-51.
- Vermeer A. W. P. (1996). Interaction between humic acid and hematite and their effects upon metal speciation, Landbouwniversiteit Wageningen.
- Warner J. A., Casey W. H., and Dahlgren R. A. (2000). Interaction kinetics of I₂(aq) with substituted phenols and humic substances. *Environmental Science and Technology* **34** (15), 3180-3185.
- Warwick P., Zhao J., Higgs J., Smith B., and Williams G. (1993). The mobility and stability of iodine-humic and iodine-fulvic complexes through sand. *The Science of the Total Environment* **130/131**, 459-165.
- Wong G. T. F. (1991). The marine geochemistry of iodine. *Reviews in Aquatic Sciences* **4** (1), 45-73.

Annex 7

Characterization of Humic Wafers by AFM, TOF-SIMS, ATR-FTIR Development of New Synthesis Routes

**Cécile Barbot, Jacques Pieri, Jean-Pierre Durand, Françoise Goudard¹
Markus Plaschke, Gunnar Buckau, Jae-II Kim²
Wilfried Szymczak, Manfred Wolf³
Othman Bouloussa⁴**

- 1. GERMETRAD Laboratory, U-Nantes, Faculté des Sciences et des Techniques, 2, Rue de la Houssinière BP 92208 44322 Nantes cedex 03, France**
- 2. Forschungszentrum Karlsruhe, Institut für Nukleare Entsorgungstechnik, P.O. Box 3640, 76021 Karlsruhe, Germany**
- 3. GSF-Institute of Hydrology, D-85764 Neuherberg, Germany**
- 4. Institut Curie, 11, Rue Pierre et Marie Curie 75005 Paris, France**

Abstract

The surface grafting of organic chains on hydrophilic substrates is of great importance in surface science and industry. Organosilanes are commonly used for surface functionalization (amino, vinyl, epoxy, chlorosilanes...) in order to modify its chemical or physical properties. Generally, silica is the most appropriated substrate for covalent binding due to its chromatographic applications.

In the precedent contract HUMICS, humic gel was synthesized from Sorbsil silica via a silanization and a subsequent nucleophilic reaction between phenolic groups of humic acids and epoxy grafted. Characterization of the phases have continued (FTIR, elementary analysis, potentiometric titrations). To improve the quantification of epoxy groups, new potentiometric titrations were developed to ascertain that a certain amount of epoxy groups grafted is intact and has not been destroyed during the process.

Moreover, in the framework of this contract, humic acid immobilization on silicon wafers has been undertaken. Modifications of silicon wafers are widespread for many applications: adhesion in composites, biomedical applications (silicon-chip-based DNA microarray), wettability of surfaces...

The activation has been performed by immersion of the wafers into a water-free solution of 3-glycidoxypropyltrimethoxysilane (GPTMS) in toluene, in reflux conditions, under continuous stirring (solvent method) followed by a nucleophilic reaction with humic acids.

Many advantages can be useful for applications of modified silicon wafers:

-they have less surface roughness and allow to have better uniformity of silane deposition.

-grafted surfaces allow surface analyses to give information about organic molecule grafted.

The research has been devoted to characterization of the phases synthesized by AFM, TOF-SIMS, ATR-FTIR...The results obtained by these methods have shown that polymerization occurs during the silane grafting due to the short chain of the GPTMS, complicating the detection of the humic layer.

Consequently, new syntheses routes have been tested: grafting of a long chain silane and further immobilization of humic acids. The wafers obtained were analyzed, considering the hydrophilicity/hydrophobicity (contact angle), ATR-FTIR, and detection of carboxylic groups was made by a UV method and europium complexation.

-When these phases will be well-characterized, they will permit also surface analyses after contacting with radionuclides to better understand their speciation form (sorption isotherms, EXAFS..).

I. Introduction

Organosilanes are extensively used as adhesion promoters (adhesion between polymers and metals) (Plueddeman, 1991), corrosion protectors in the aerospace (Digby and Shaw, 1998), automotive and construction industry. In the research area, silanisation has numerous applications to immobilize molecules of biological interest such as proteins (Prime and Whitesides, 1991), DNA molecules (Lenigk et al., 2001), enzymes (Bustamante et al., 1997) and antibodies (Delamarche et al., 1996), and also inorganic catalysts, chromophores, to modify electrodes and chromatographic phases.

These coupling agents acts at the interface between an inorganic substrate (glass, metal, mineral) and an organic substrate (organic polymer, coating or adhesives).

General formula of organosilanes is $\text{RSi}(\text{OR}')_3$ (Mittal, 1992) with R an organofunctional group (vinyl, amino, epoxy, mercapto) and R'an hydrolyzable group (halide, acyloxy, alkoxide). An important literature exists on the grafting of organosilanes on a substrate,

generally a porous or non porous oxide matrix. Nevertheless, covalent binding of organosilanes on porous (for instance silica) and non porous (ex. silicon wafers) are not comparable: steric hindrance influences orientation of molecules and accessibility to reactional sites in the porous network (3D system) or at the surface (2D system).

A few chemical reactions are possible at an oxide surface: modifications by an aminosilane, vinylsilane, epoxysilane, chlorosilanes. From this synthesized phases, it is possible, by nucleophilic attack of the groups present at the surface, to immobilize a wide variety of molecules of interest to obtain the physical and chemical properties required. γ -glycidoxypropyltrimethoxysilane has been used by the authors in order to activate silica gels (Barbot et al., 2002). γ -glycidoxypropyltrimethoxysilane interaction with iron oxide was investigated by Gettings and Kinloch (1977) and Davis and Watts (1996) using XPS and TOF-SIMS. They concluded that there was formation of a covalent bond (Fe-O-Si) between the oxide of steel or iron and the GPTMS molecule. In the case of aluminium, various researchers brought evidence of the formation of a similar covalent bond between aluminium oxide and organosilanes (Al-O-Si) (Leung et al., 1993 ; Fang et al., 1997 ; Leung et al., 1992 ; Abel et al., 2000).

Many parameters influence the formation of self-assembled monolayers and many researchers have studied the influence of a wide variety of experimental conditions. The most important parameter is the solvent used in anhydrous (Tsukruk et al., 1999 ; Wasserman et al., 1989) or hydrous conditions (Abel et al., 2000). Drying and curing temperature effect was studied by Abel et al. (2000). Brzoska et al. (1990) showed how temperature controls the formation of grafted alkylsilane monolayers on hydrophilic substrates and Silberzan et al. (1991) demonstrate that room temperature favors grafting.

Mc Govern et al. (1994) study a cleaning process to obtain non-contaminated and reproducible surfaces whereas Duchet et al. (1997) study the advantages of two experimental procedures: solvent and vapor phase deposition.

This work has been devoted to the humic acid immobilization on a silica matrix, already undertaken during the HUMICS project (Barbot et al., 2002). In this report additional characterizations are given, such as quantification of epoxy groups grafted on epoxy silica determined by two different potentiometric methods (Porsch, 1993 ; Mingalyov and Fadeev, 1996 ; Jay, 1964).

In the framework of HUPA, covalent binding of humic acids on silicon wafers has been undertaken. Silanization was performed by the solvent method (in toluene medium) in anhydrous conditions. Characterizations of the phases were done by FT-IRRAS, AFM and TOF-SIMS methods.

Atomic force microscopy (AFM) is a scanning probe technique. It probes the surface with a sharp tip. Tips are made from Si_3N_4 and are located at the free end of a cantilever 100 to 200 μm long. Van der Waals forces between the surface sample and the tip cause the cantilever to bend or deflect. A detector measures the tip deflection as the sample is scanned under the tip and the surface topographical data are obtained. Therefore, this technique allows to obtain, by the image structures, informations about small colloids, colloid aggregation, adsorption onto surfaces.

AFM characterization has been employed by several authors to study the structural organization of organosilanes (Navarre et al., 2001 ; Bierbaum, 1995). Recent work has been performed by several authors to understand the aggregation of humic substances layers adsorbed on muscovite (Plaschke et al., 1999) and mica (Liu et al., 2000) and the influence of Eu on the formation of agglomerates in aqueous solutions containing the trivalent ion (Plaschke et al., 2002).

Time-of-flight secondary ion mass spectrometry (TOF-SIMS) is a powerful tool for obtaining chemical informations on surfaces (molecular and structural, and in some cases quantitative

information). TOF-SIMS uses a pulsed primary ion beam to desorb and ionize species from the pure or covered silicon from the wafer. The outgoing secondary ions (positively or negatively charged ions) are accelerated into a field free region of a TOF-mass analyzer (flight tube) in which they are separated according to their mass-dependent time-flight from the surface to the detector. Molecular parent ions and fragmentation patterns are characteristic of the surface molecules as well as of the silicon surface itself or crystalline structure of the surface.

TOF-SIMS has been a method of choice to prove that the silane is well-grafted at the surface. Quinton and Dastoor (2000) used it to study the chemical sorption of aminopropylsilane on an iron oxide surface. Other authors used TOF-SIMS to characterize organosilane at the surface of aluminium oxide (Houssiau and Bertrand, 2001 ; Rattana et al., 2002) and on glass surfaces (Wang and Jones, 1993) and particularly of γ -GPTMS (Abel et al., 2000).

In our study, humic acids will be grafted chemically on humic wafers. Several authors are interested in the organic matter characterization by electrospray mass spectrometry (Plancque et al., 2001 ; Kujawinski et al., 2002). These investigations should help to interpret results obtained in case of humic acids bound to silicon wafers.

Improvements to the grafting procedure are also given in view of obtaining self-assembled monolayers substrates after humic acid immobilisation.

II. Experimental

Informations about the immobilisation of humic acids on silica can be found in the work done by Barbot et al., 2002 [1]

Humic acids immobilization on silica

II. 1. Quantification of epoxy groups grafted on epoxy silica.

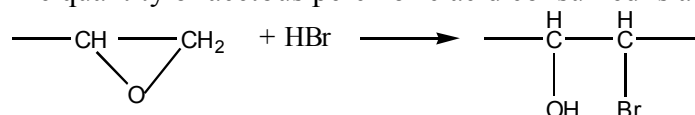
Epoxy groups were quantified by two different methods, based on direct potentiometric pH titrations elaborated with a DL50 Mettler Toledo titrator.

II. 1. 1. First method.

Principle:

The sample is dissolved in a mixture of acetic acid and an excess of a quaternary ammonium halide. The solution is then titrated with acetous perchloric acid, and hydrogen bromide generated in situ by the addition of perchloric acid to the quaternary ammonium halide rapidly opens the oxiran ring with the subsequent formation of an halohydrin.

The quantity of acetous perchloric acid consumed is a measure of the epoxy group content.



Reagent preparation :

Standardisation of acetous perchloric acid with potassium hydrogenophthalate, initially dried below 130°C.

0.3594 g of potassium hydrogenophthalate are dissolved in a 50 mL-glacial acetic acid solution and titrated at a rate of 0.1 mL/20 s with acetous perchloric acid (near 0.1 N).

The blank is realised, with the same manner, without potassium hydrogenophthalate.

Finally, the concentration of acetous perchloric acid is deduced from :

$$c = \frac{m \times 10^3}{(V_1 - V_2) \times M}$$

m : potassium hydrogenophthalate (0.3594 g)

V_1 : acetous perchloric acid volume used for the titration of potassium hydrogenophthalate (18 mL)

V_2 : acetous perchloric acid volume used for the titration of the blank (0.1 mL)

Molar concentration of acetous perchloric acid is then $0.09831 \text{ mol l}^{-1}$.

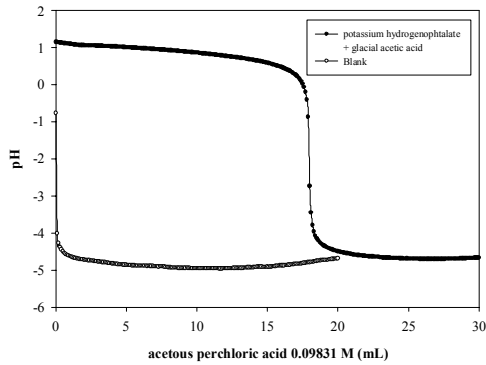


Fig. 1. : Standardization of acetous perchloric acid

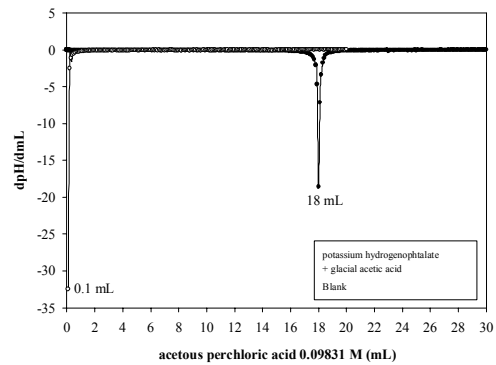


Fig. 2. : First derivative for standardization

Epoxy group titration on silica epoxy :

-3.0021 g of epoxy silica in a 50 mL-glacial acetic acid are mixed with 2.0647 g of tetraethylammonium bromide.

-The blank is done with silica instead of epoxy silica. In that case, 3.0165 g of silica in a 50 mL-glacial acetic acid are mixed to 2.0545 g of tetraethylammonium bromide.

Titration are done with the standard acetous perchloric acid at a rate of 0.1 mL/30 s.

The amount of epoxy groups is then deduced from the titrations.

$$\text{epoxy groups (mmol / kg) in epoxy silica} = \frac{V_3 \times c \times 10^3}{3.0021}$$

$$\text{blank (mmol / kg)} = \frac{V_4 \times c \times 10^3}{3.0165}$$

V_3 : acetous perchloric acid volume used for the titration of epoxy silica HUMICS (4.4 mL)

V_4 : acetous perchloric acid volume used for the titration of the blank (0.4 mL)

V_5 : acetous perchloric acid volume used for the titration of epoxy silica HUPA (6.6 mL)

The amount of Sorbsil epoxy synthesized for the HUMICS contract is **131.05 $\mu\text{mol/g}$** .

The amount of Sorbsil epoxy synthesized for this HUPA contract (20 g) is **202.30 $\mu\text{mol/g}$** .

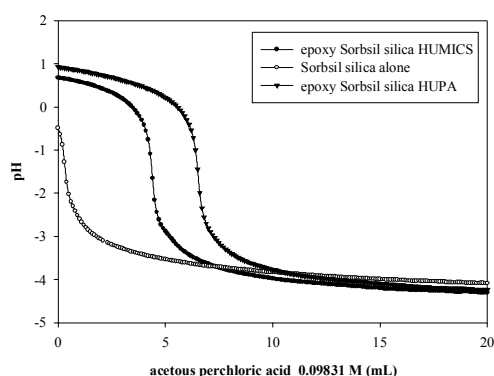


Fig. 3. : Quantification of epoxy groups

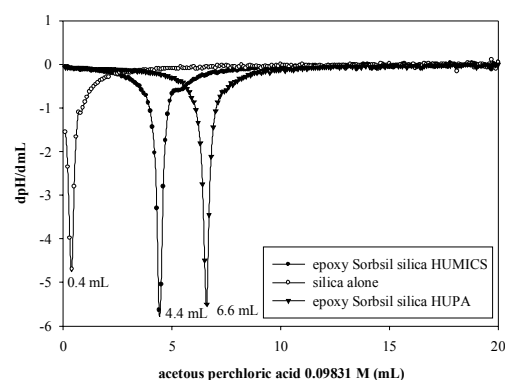


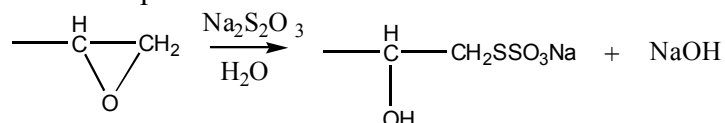
Fig. 4. : First derivative of the titration of the substrate in tetraethylammonium bromide and glacial acetic acid by acetous perchloric acid

II. 1. 2. Second method

Principle :

The amount of epoxy silica is determined by this method :

Epoxy silica is put in contact with a saturated aqueous solution of sodium thiosulfate. Attached epoxides react as follows :



The resulting NaOH is titrated with standard 0.1 N HCl and finally the amount of attached epoxides is equal to the amount of HCl needed for titration.

Epoxy groups titration on the epoxy silica :

Four titrations were undertaken to do the determination of epoxy groups. In each set, all the solutions were degased and incubated 3 hours in a nitrogen atmosphere. Titrations were undertaken at a rate of 0.1 mL/2s.

Two titrations were done in water to know the difference of OH⁻ present in solution due to equilibration of silica or epoxy silica. These titrations will allow to estimate the error done on the epoxy evaluation.

m₁ epoxy silica = 1.0036 g and V_{eq1} = 0.24 mL

m₂ silica = 1.002 g and V_{eq2} = 0.16 mL

Consequently, the error is 7.95 μmol g⁻¹.

The two other titrations were done in presence of an excess of thiosulfate for epoxy silica and for silica (blank).

m₃ epoxy silica = 1.005 g and V_{eq3} = 1.38 mL

m₄ silica = 1.0076 g and V_{eq4} = 0.22 mL

Consequently, the epoxy amount represents : **115.5 ± 7.95 μmol g⁻¹**

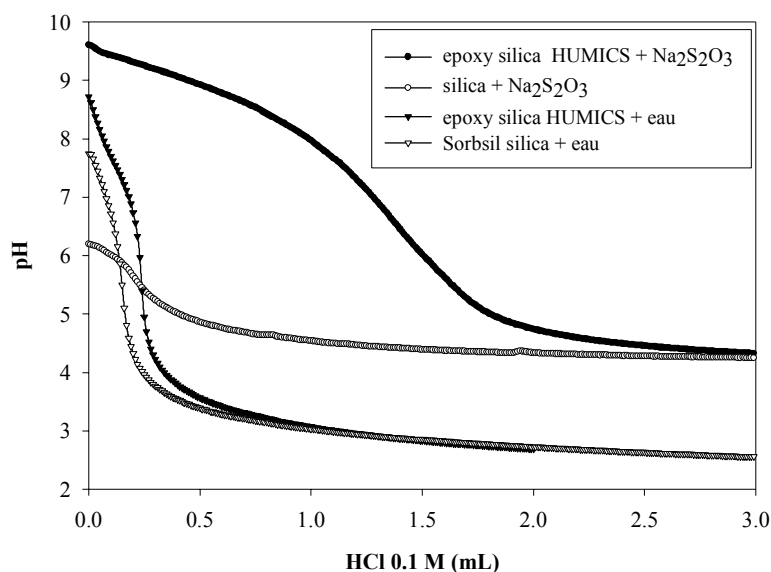


Fig. 5. : Titration of the NaOH produced during the reaction by HCl 0.1 M.

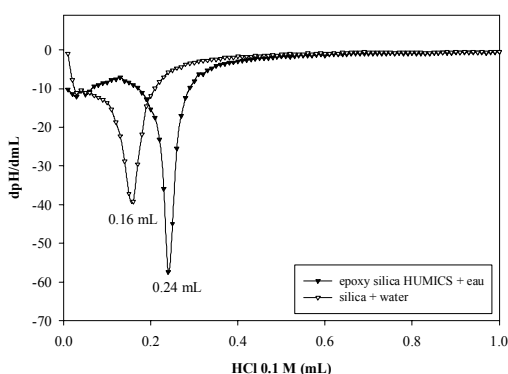


Fig. 6. : First derivative for the substrate in water

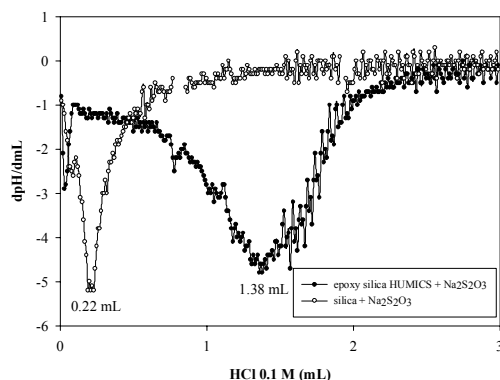


Fig. 7. : First derivative for the substrate in presence of Na₂S₂O₃.

II. 1. 3. Comparison of the two methods.

The first method will be preferred to the second for several reasons:

-very sharp visual end-points are obtained.

-titrations are done at a pH extremely low and prevent carbonate contaminations.

In conclusion, in all the subsequent determinations, we will choose the first method.

II. 1. 4. Elementary analysis

Elementary analysis allows to obtain the percentage of C present in the sample and in consequence the amount of silane grafted to the difference of the titration methods which give the sample epoxy content. Generally, even if there is one epoxy for one silane molecule grafted, some epoxy groups can be deteriorated in the grafting or opened and there is no more one epoxy for one silane molecule. The rate between the two represents the rate of efficiency. The amount of silane grafted can be calculated by the formula:

$$c(\text{groups} / \text{nm}^2) = \frac{6.10^5 P_c}{[(1200n_c - WP_c)S]}$$

c : linked groups concentrations.

P_c : % C in the sample

n_c : number of C atoms in the linked group.

W : corrected mass of the modifier.

S : specific surface area.

	% C	Epoxide ($\mu\text{mol/g}$) titration	Ligand ($\mu\text{mol/g}$) elemental analysis	% intact epoxide
epoxy silica HUMICS	2.05	131.05	227.82	57.52
epoxy silica HUPA	2.27	202.3	252.28	80.19

Table 1 : Quantification of epoxy groups and ligand immobilized on humic gels

Humic acids immobilization on humic wafers

II. 2. Grafting synthesis on the silicon wafer by 3-GPTMS

II. 2. 1. Washing of the wafer before grafting.

-Organic contaminant layer was removed from the wafer with a mixture of acetone/methanol in a ultrasonic bath during 15 min (degreasing).

-They were immersed in milli Q water in a ultrasonic bath for 15 min.

-then in H₂O₂ (30 %)/ NH₃ (25 %)/H₂O for 25 min at 80°C.

-washed with milli Q water.

-washed in concentrated HCl/H₂O₂ (30 %)/H₂O for 35 min at 80°C to render the surface hydrophilic.

-washed with milli Q water thoroughly and finally with acetone and dried at 130°C for the subsequent activation.

II. 2. 2. Activation of the wafers with 3-glycidoxypropyltrimethoxysilane.

All the glassware and the wafers were washed with acetone and dried during 2 days before doing the activation, at 120°C.

The grafting was done by the method as follows:

1 mL of GPTMS was added to a solution of pure toluene (stored under a septum, immersion with an optimized epoxysilane volume concentration of 1 % (Tsukruk et al., 1999) after the experimental setup has been put into argon atmosphere. The wafers were put into the silane solution and heated at 120°C for 22 h.

II. 2. 3. Washing of the wafers after activation.

The wafers were washed with toluene, dichloromethane, acetone and ether.

They were subsequently dried in an oven at 40°C.

II. 2. 4. Humic acids grafting on the wafer.

The procedure used for grafting of humic acids on silica was used for the wafer (Barbot et al., 2002).

0.1 g of purified humic acids were added to KCl, dioxane and pH adjusted to 9.5 with Tris 2 M. They were incubated 2 days.

II. 2. 5. Wafer washing.

Wafers were thoroughly washed with 0.1 M Tris to remove humic acids that were only physisorbed and subsequently with MilliQ water.

II. 3. Characterizations

II. 3. 1. FT-IRRAS characterization

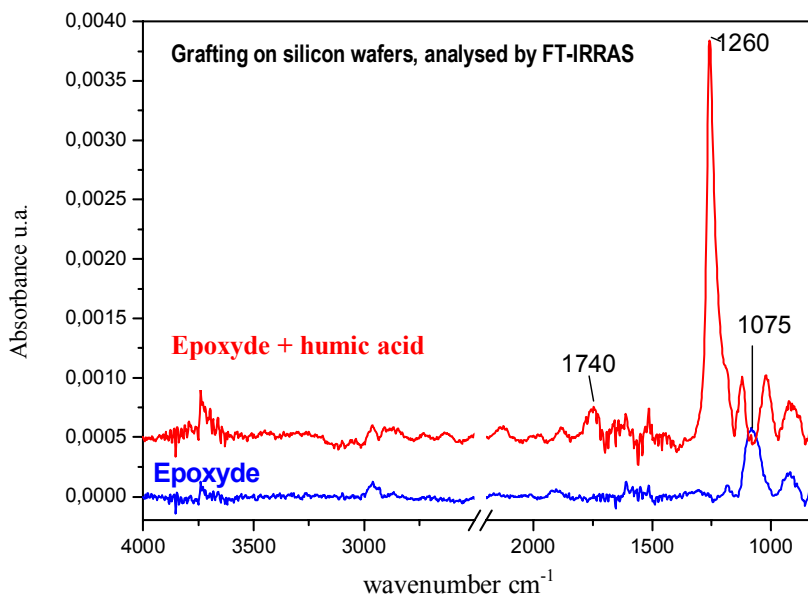


Fig. 8.: FT-IRRAS spectrum for epoxy wafer and humic acid wafer

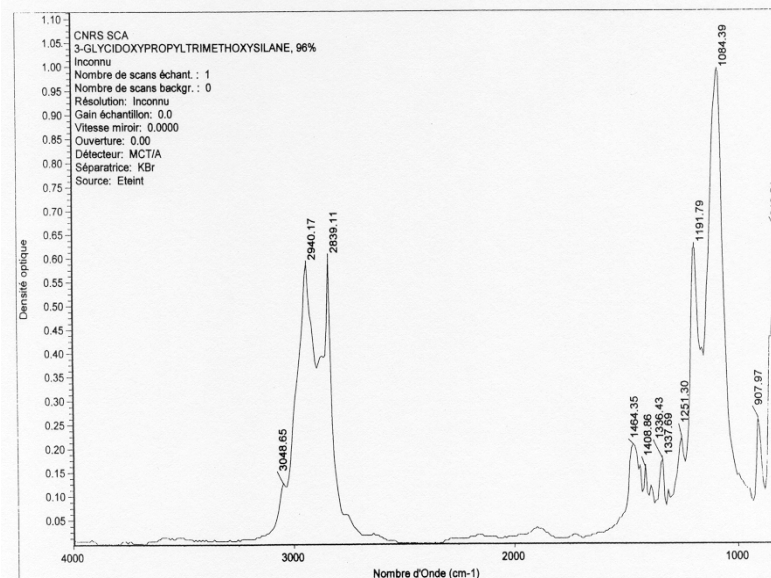


Fig. 9. Comparison with the spectrum from 3-glycidoxypropyltrimethoxysilane

FT-IRRAS spectra were recorded on a Nicolet Magna 550 spectrometer equipped with mirrors optimized for reflection at grazing incidence. A wide band HgCdTe detector, cooled with liquid nitrogen, was used to collect the data at 4 cm^{-1} resolution. The FTIR beam was focused onto the sample at an incidence angle of 70° . The entire experimental setup was purged to eliminate water and CO_2 absorption contributions. A reference spectrum was taken on a clean silicon wafer sample which has been washed a second time with a piranha solution and rinsed with MilliQ water just before the recording. For all spectra 600 scans were collected.

Spectra are represented below (epoxy only, humic acid + epoxy Fig.8.). Comparison with 3-glycidoxypropyltrimethoxysilane is done on Fig. 9.

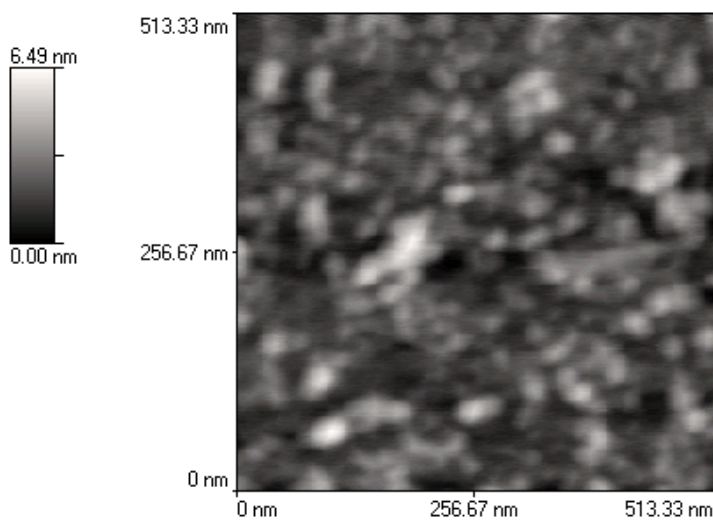
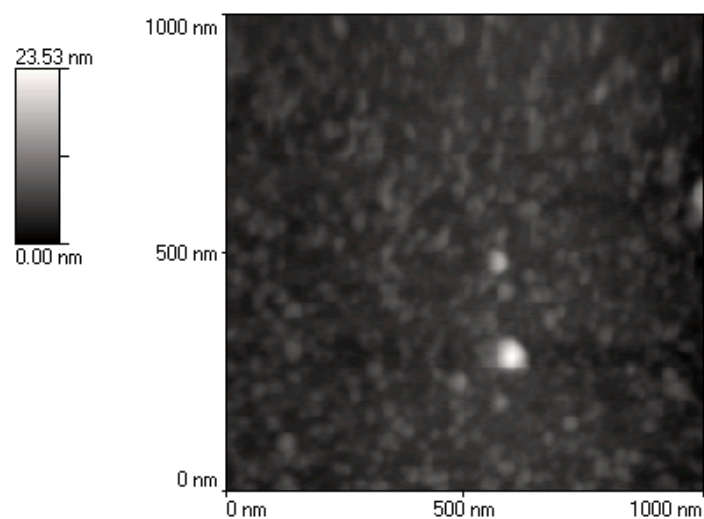
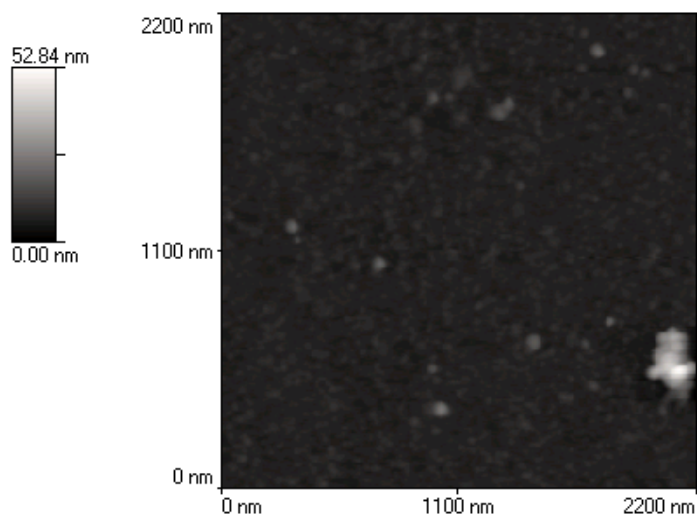
II. 3. 2. AFM characterizations

Non-contact mode AFM imaging was performed with a Topometrix TMX 2000 Explorer, which is equipped with cantilever oscillating hardware, with Markus Plaschke at INE (Karlsruhe). Two kinds of experiments have been conducted - on dried and liquid samples.

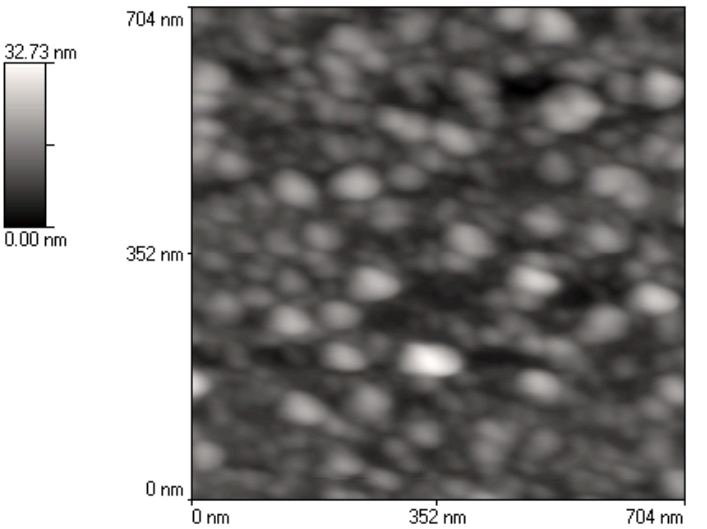
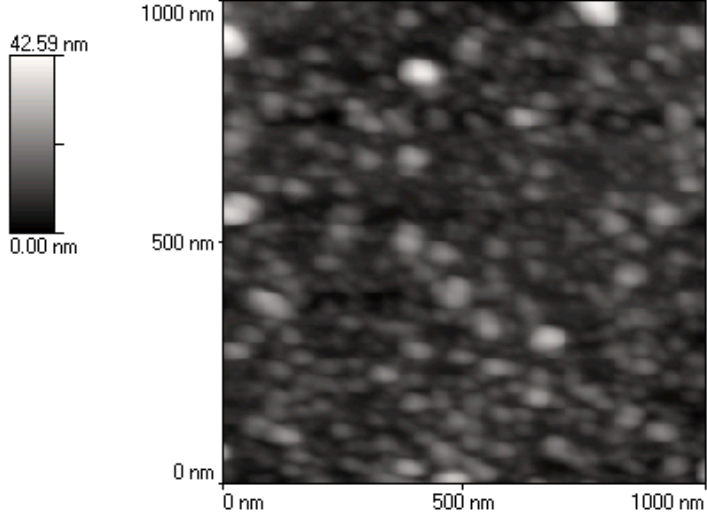
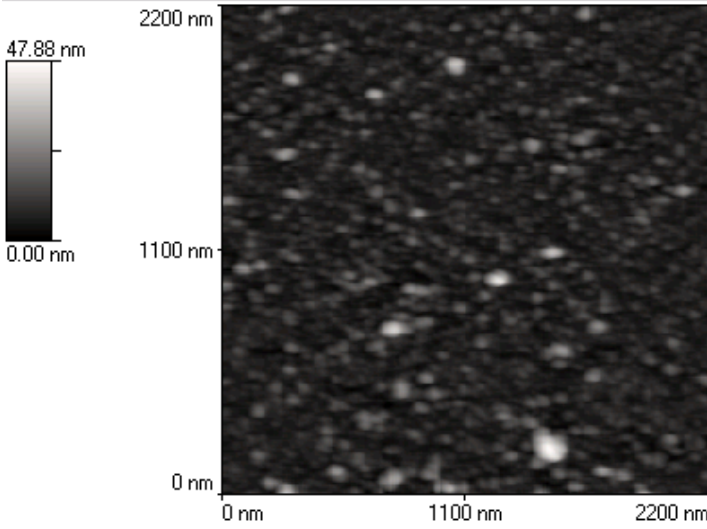
For measurements on dried samples silicon tips are used (nominal radius of curvature $<10\text{ nm}$; nominal spring constant 48 N/m ; nominal resonance frequency 190 kHz). Triangular probes with silicon nitride tips (radius $< 50\text{ nm}$, nominal resonance frequency 17 kHz , cantilever spring constant about 0.06 N m^{-1}) are used for measurements in water. Piezo scanners with a maximum range of about $2\text{ }\mu\text{m}$ in the x-y direction and 900 nm in the z-direction are mounted. For liquid measurements, all the samples have been put in water during 24h and are then investigated using a liquid cell. About five measurements in different points on each wafer were undertaken.

**AFM investigation of silicon wafers coated with purified Aldrich humic acid
Dried conditions**

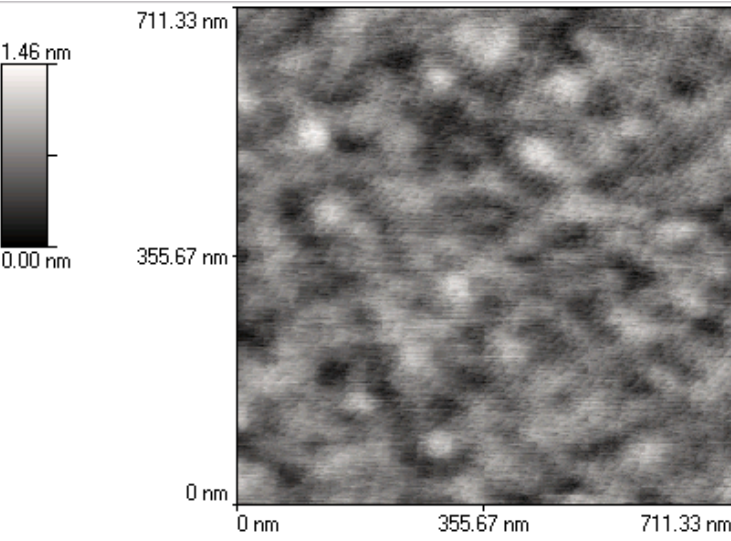
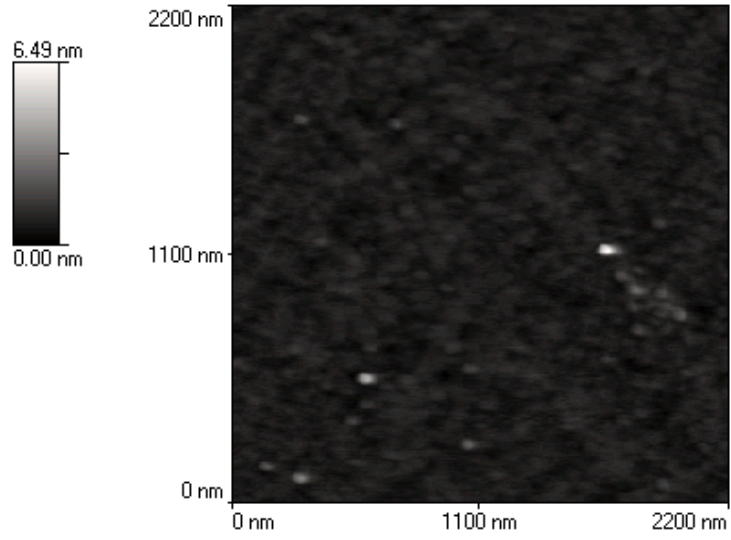
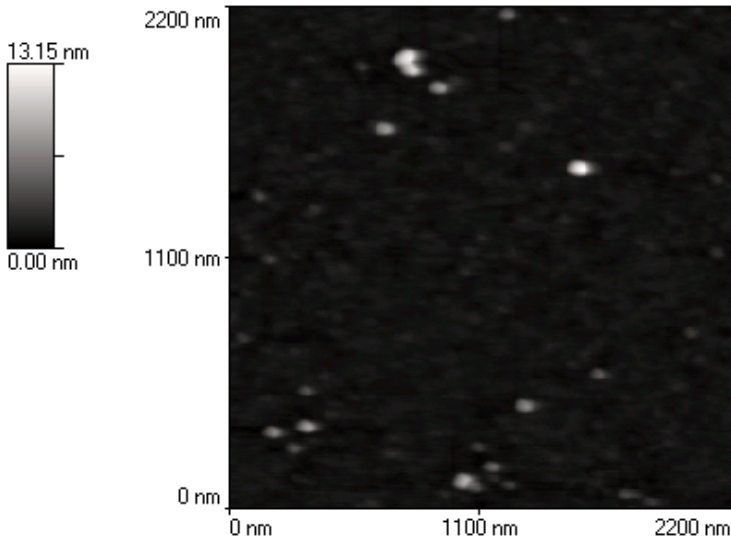
A) Wafer with Aldrich HA (Fig. 10)



B) Wafer exposed to epoxy silane (Fig. 11)



C) Bare silicon wafer (Fig.12)



II. 3. 3. TOF-SIMS characterizations

The SIMS measurements were performed using a time-of-flight (TOF) instrument developed at the GSF. In this study the bombarding parameters were as follows: primary ions SF_5^+ , ion source terminal voltage 30 kV, target bias 6 kV (ion impact energy 36 keV for negative secondary ions, 24 keV for positive secondary ions), stationary beam current 1–2 nA, bunched pulse width about 3 ns, repetition rate 19 kHz, 2×10^7 pulses per spectrum. The angle between the primary ion beam line and the surface normal of the sample is 60° and the area of ion bombardment $0.3 \times 0.4 \text{ mm}^2$, the beam was deflected strongly in the electric field between the sample and the acceleration electrode. Under these conditions the actual angle of beam incidence is estimated to 75.5° in the case of positive target bias, resp. 52° with a negative target bias.

The beam was realigned by electric means to hit the sample on axis of the TOF analyser. Sample position were changed by moving the sample under the beam.

Neutrals generated along the first half of the drift tube were removed by tilting the second half of the drift tube by 3° . The secondary ions were directed to the detector electrostatically.

With a target bias of 6 kV the mass resolution in the low mass range ($u \leq 100$) is about 600. Applying deconvolution techniques in the low mass region improves the mass resolution to 3000. Mass calibration is based on the same selected peaks on each spectrum.

TOF-SIMS has been conducted on different samples in positive and negative mode:

- bare silicon wafer,
- epoxy silicon wafer,
- purified humic acids on silicon wafer,
- epoxy + Eu wafer exposed to $3.8 \times 10^{-4} \text{ mol L}^{-1}$ at pH 5.2 and washed with milliQ water,
- humic acid + Eu, " " "
- non purified Aldrich humic acid deposited by jet-spray deposition from a 0.2 mg/mL solution on a bare silicon wafer,
- purified humic acids deposited by jet-spray deposition from a 0.2 mg/mL solution on a bare silicon wafer.
- purified humic acids deposited by jet-spray deposition from a 0.2 mg/mL solution on an epoxy wafer.

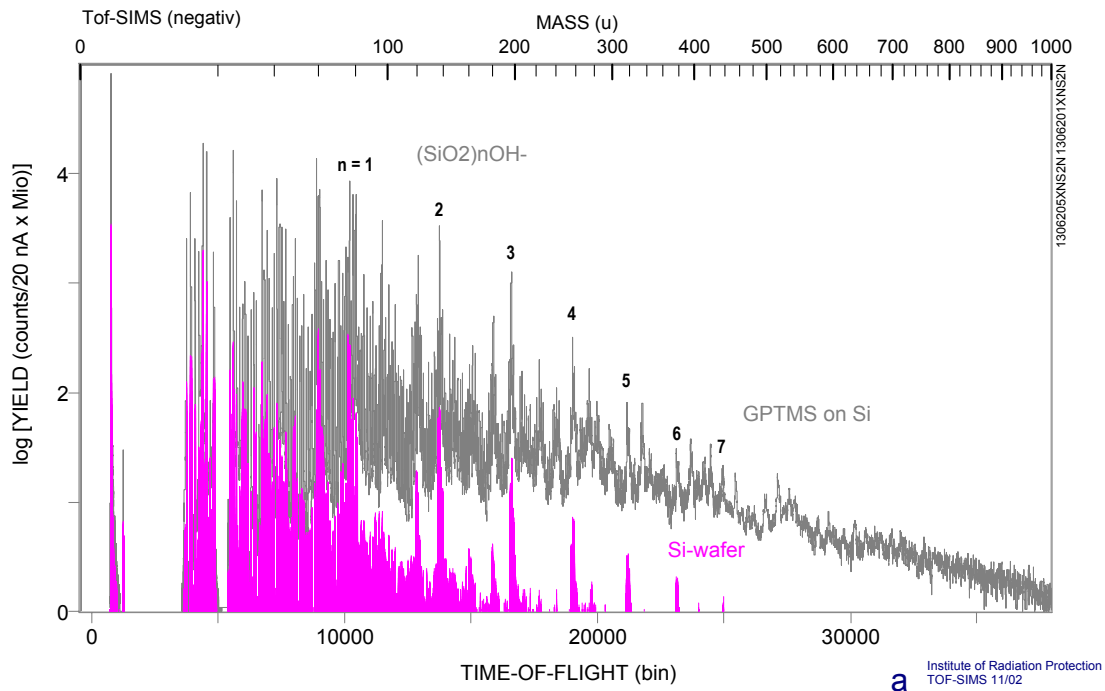


Fig. 13. Comparison between GPTMS covalently grafted on pure silicon wafer and pure silicon wafer (negative spectra)

Fig.14. See annexes

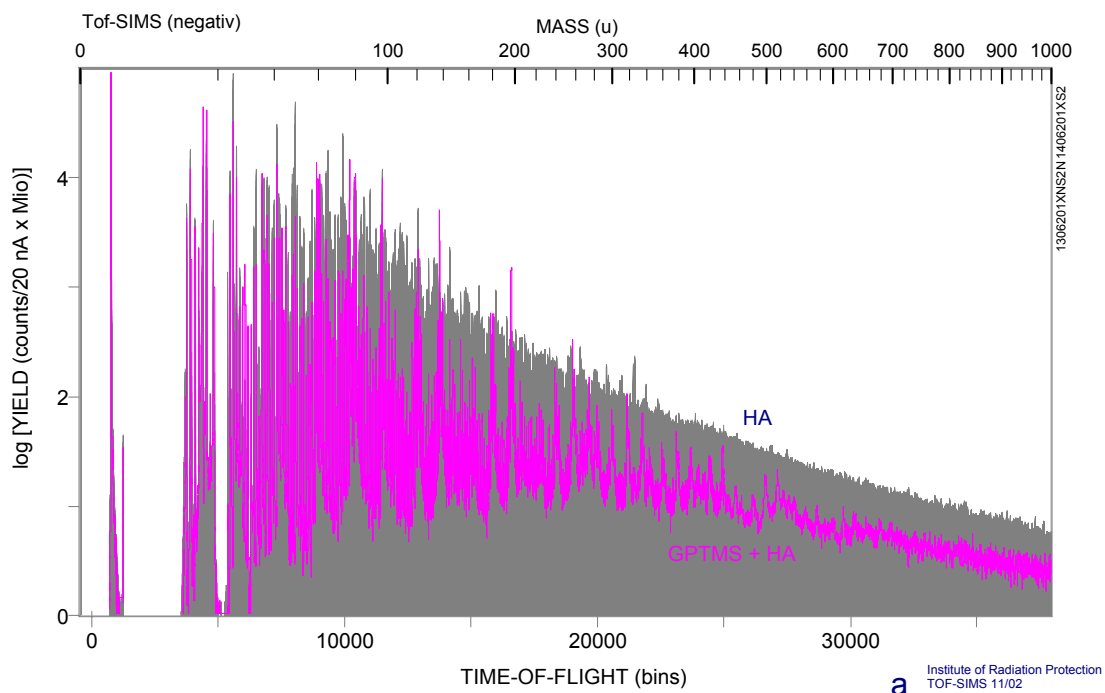


Fig. 15. Comparison between HA sprayed on pure silicon wafer and HA grafted on GPTMS (negative spectra).

II. 4. Grafting synthesis on the silicon wafer by a long chain trichlorosilane

II. 4. 1. Washing of the wafers before grafting

Wafers have been washed with a piranha solution ($\text{H}_2\text{SO}_4 + \text{H}_2\text{O}_2$) at 80°C and thoroughly rinsed with Milli-Q water. Then, they have been dried with a nitrogen stream. Contact angle has been evaluated to check the hydrophilicity of the surface obtained.

II. 4. 2. Activation of the wafers by a long chain trichlorosilane

Wafers have been immersed in a solution containing hexane and the trichlorosilane: 9-(trichlorosilyl)nonylchloroacetate (synthesized and distilled in a Kugelrohr distillator at Curie Institute). They have been incubated 90 min and finally washed with chloroform four times in an ultrasonic bath. After the washing, wafers have been cured in an oven at $100\text{--}120^\circ\text{C}$ during 30 min.

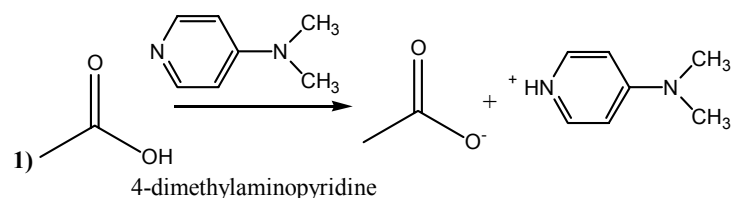
Contact angle has been evaluated to check that the wafers were not too hydrophilic and not too hydrophobic.

II. 4. 3. Humic acids grafting on the wafer

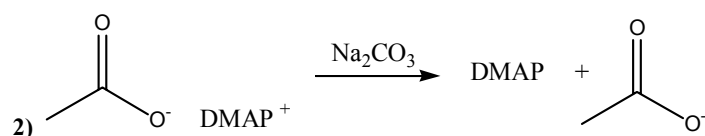
Humic acid from Aldrich on the sodium form have been dissolved in DMSO and water in presence of NaI and incubated three days at $40\text{--}50^\circ\text{C}$. Washing has been performed with DMSO and ethanol and dried with a nitrogen stream. Contact angle has been evaluated to check that the wafers were hydrophilic.

II. 4. 4. Checking of the grafting by surface UV

4-dimethylaminopyridine ($\lambda=260\text{ nm}$, $\epsilon = 17\ 114\ \text{cm}^{-1}$) was used to quantify the number of COOH present on the wafer. The first step implies the formation of a ionic complex between DMAP and carboxylic groups from humic acids as follows:



The second step implies the displacement of DMAP present on the wafer by a solution of Na_2CO_3 .



Quantification of DMAP released in the solution at 260 nm, permit to determine the amount of COOH (mole to mole reaction).

II. 4. 5. Checking of the grafting by europium complexation

Europium complexation was used to check that humic acids were present at the surface of the wafer. Wafers were put into contact with $1.5 \cdot 10^{-4}$ mol of Eu in presence of 0.1 M NaClO_4 at pH 6, during one night. A blank was done with a wafer bringing the silane. Differences between blank and wafer bringing humic acids would be observed in case humic acids are immobilized.

III. Results and discussion

III. 1. FT-IRRAS

Results obtained from FT-IRRAS on epoxy wafer (Fig. 8) and humic wafer are a proof of the epoxy and humic acids grafting. Spectra are similar to FTIR spectra collected in reflectance mode for epoxy and humic gel (Barbot et al., 2002).

The presence of epoxy on silica is highlighted by the presence of 1075 cm^{-1} vibration due to C-O-C stretching in epoxy group (1084.39 cm^{-1} in the 3-glycidoxypropyltrimethoxysilane (Fig. 9).

1191 cm^{-1} is a feature of CH_2 wagging, 1251 cm^{-1} of oxirane ring breathing, 1464 cm^{-1} of CH_2 bending.

At $2900\text{-}2950\text{ cm}^{-1}$, are also present methyl and methylene stretching.

The presence of humic acids on the wafers is characterized by an additional band at 1740 cm^{-1} due to C=O stretching vibrations from carboxylic and ketonic groups (Chen et al., 2002 ; Jerzykiewicz et al., 2002 ; Kim et al., 1990, 1997) and the 1260 cm^{-1} band due to C-O stretching and O-H bending deformation of COOH groups. It arises also from phenyl-oxygen stretching due to complex in-plane ring mode (Nyquist, 2001, p 128) This band doesn't belong to epoxy groups that were subtracted during data treatment. Furthermore, when are present in the same sample epoxy groups and phenyl-oxygen, the strong absorption band from phenyl-oxygen appears to mask the epoxy ring breathing vibrations (Nyquist, 2001, p 4).

The shoulder before 1260 cm^{-1} can be assigned to the in-plane OH bending from phenyl-oxygen.

Moreover the band at 1075 cm^{-1} has disappeared due to the aperture of epoxy group, in case of humic wafers.

III. 2. AFM

Dried conditions

i) AFM performed on bare silicon wafer (Fig. 10)

Bare silicon wafer showed that washing was appropriated to eliminate organic impurities and particles at the surface and proved that there was less than 10% of contamination. Consequently, the washing procedure, before grafting, will be pursued in this way.

Silicon oxides can be put in evidence with a layer of 1.46 nm height maximum (scan 711.33 nm by 711.33 nm)

ii) Wafers exposed to epoxy silane (Fig. 11)

Wafers show epoxysilane aggregation at the surface with holes in the network and agglomerates of on average 33 nm for the maximum heights. Consequently, it is necessary to think how it is possible to obtain a more homogeneous layer.

iii) Wafers with purified Aldrich humic acids (Fig. 12)

Wafers show always aggregation on the wafer due to polymerization at the surface with a maximum height of 6.49 nm. It is difficult to compare epoxy wafers and Aldrich humic acid wafer because batches were different between the two steps. Due to polymerization at the surface, it is impossible to conclude that humic acids are grafted at the surface.

Liquid conditions

- i) Analyses were not performed because it is less interest in solution for bare silicon wafer.
- ii) Concerning epoxy wafers in water, there are some differences between dried and liquid samples. Liquid samples show aggregation of several particles but it is difficult to conclude to an extension of the network because the radius of the cantilever tip used for liquid measurements is larger than for dried samples. Therefore, the tip artifact typical for AFM is different for liquid and dry measurements.
- ii) For humic acid wafers, aggregation of particles are also greater. Dried samples present aggregates of several nm whereas in water aggregates measure 20-28 nm.
Several hypotheses:
 - polymerization of silane groups at the surface occurred.
 - humic acids extend in the solution forming higher aggregates.

III. 3. TOF-SIMS

It is to note that TOF-SIMS is a powerful tool for obtaining molecular and structural information owing to its unique sensitivity to the chemical surface.

- i) Cleaned silicon wafers show a low contamination of hydrocarbons $C_x H_y^+$ and an intense Si^+ mass line. The negative TOF-SIMS spectrum exhibits in the mass range ≥ 60 only a $(SiO_2)_nH^-$ and $(SiO_2)_nOH^-$ pattern (Fig. 13) which is a characteristic of a clean oxidized silicon surface.
In the positive TOF-SIMS spectrum masslines 44 (SiO^+) and 45 $SiOH^+$ have a relative higher yield compared to otherwise cleaned silicon wafers.

- ii) Epoxy wafers show grafting of GPTMS on the wafers.

-Differences between pure silicon wafer and GPTMS wafer occur (Fig.13). The GPTMS spectrum shows a higher intensity than the spectrum of the pure silicon oxide, on the overall spectrum. The high mass range shows the presence of high-molecular fragments that are not present on the pure silicon oxide. Consequently, GPTMS has been well-grafted on the silicon wafers.

-Total secondary ion yield varies strongly over the sample, e.g. near the center of the disk only 10 % of the yield 2.5 mm apart from the center which reveals an heterogeneous coverage.

- $(SiO_2)_nH^-$ and $(SiO_2)_nOH^-$ still constitute a dominant pattern (Fig.13): surface is not fully covered.

-there is the presence of high-yield cyclic and linear fragments (Fig. 14). Is it a polymerization or a cross-linking? The question remains open.

-GPTMS fragment are present with a low yield (Fig. 14). It is the signification that GPTMS has polymerized.

Table 2 summarises identified characteristic peaks in the positive TOF-SIMS spectrum, Table 3 in the negative spectrum.

- iii) GPTMS + HA: In the positive TOF-SIMS spectrum the yield of cyclic and linear fragments is strongly reduced, but most of the spectral features is present with GPTMS alone.

The negative spectrum still exhibits strong silicon dioxide based cluster signals. GPTMS covered area are HA-covered, whereas the bare silicon surface is not fully covered with HA.

iv) Epoxy wafer + Eu ($3.8 \cdot 10^{-4} \text{ mol L}^{-1}$ at pH 5.2 and washed with Milli-Q water): presence of EuOH^+ at masslines 168 and 170.

HA wafer + Eu: the same Eu-induced spectral features as the epoxy wafer + Eu.

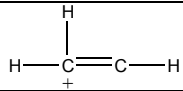
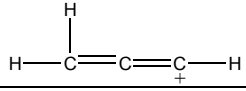
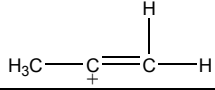
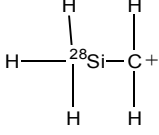
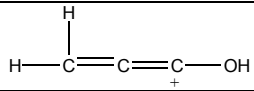
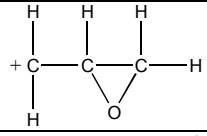
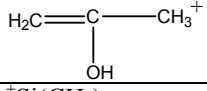
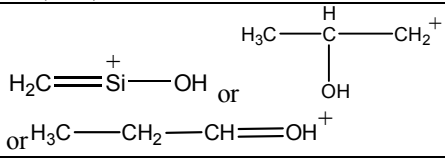
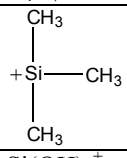
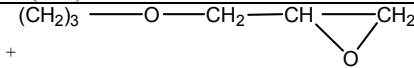
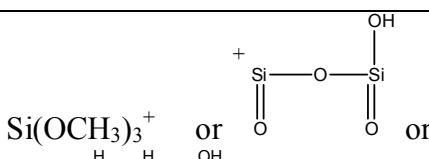
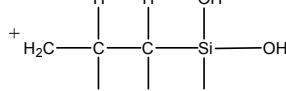
v) Jet-spray experiments (Fig.15):

-Purified humic acids deposited by jet-spray deposition ($55 \mu\text{g}/\text{cm}^2$) from a 0.2 mg/mL solution on a bare silicon wafer.

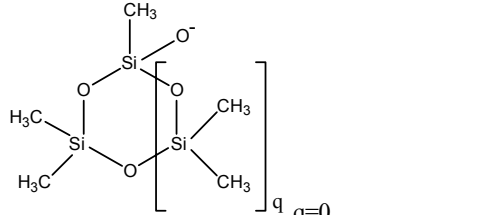
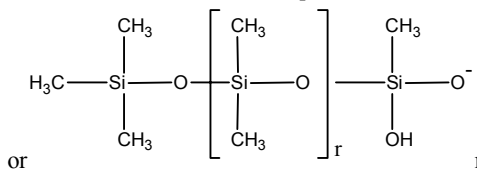
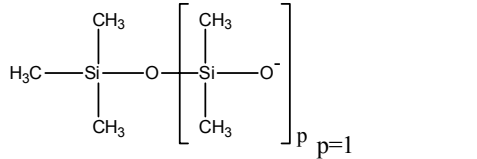
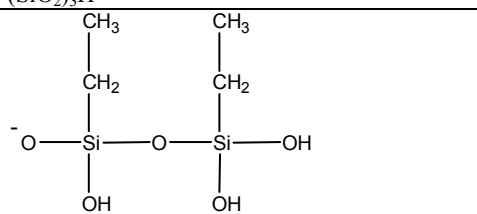
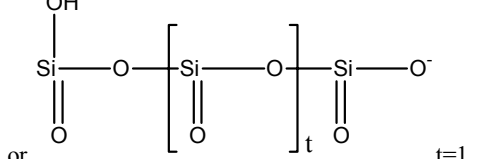
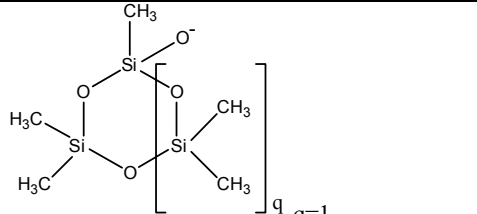
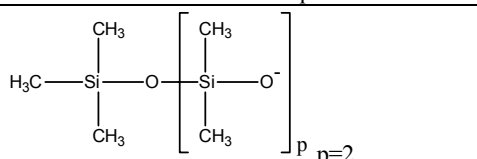
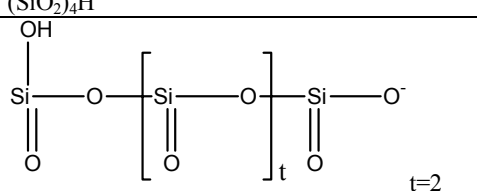
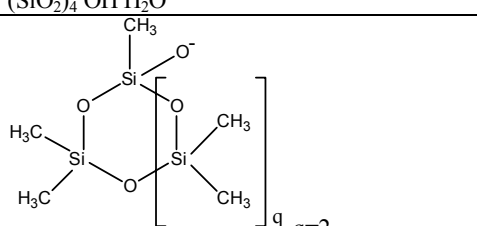
-Purified humic acids deposited by jet-spray deposition ($10\mu\text{g}/\text{cm}^2$), from a 0.2 mg/mL solution on an epoxy wafer.

The jet-sprayed sample shows the characteristic broad mass distribution of a saturated ($55\mu\text{g}/\text{cm}^2$), but not closed HA layer on Si. The feature-rich spectrum of GPTMS + HA clearly reflects a lower amount of HA on GPTMS.

Table 2: GPTMS Positive spectrum-characteristic peaks

Peak Code	Ion	calc. mass	mass of ToF-SIMS-peak-maximum	Comment
A	Na ⁺	22.99	22.99	
		27.00		
B	Si ⁺	27.98	27.93	
C	CH ₂ OH ⁺	31.02	31.01	
		39.00		
		41.00		
D	⁺ SiCH ₃	43.00	43.00	
	Si-O ⁺	44.00		
E	 SiOH ⁺ or	44.98	44.95	
		55.00		
		57.00		GPTMS
		58.00		GPTMS
F	⁺ Si(CH ₃) ₂	58.02	58.03	
		59.00		GPTMS
	C ₅ H ₃ ⁺ ou SiH(OH) ₂ ⁺	63.00		
	H ₂ C=CH-Si=O ⁺ or C ₅ H ₁₁ ⁺ or C ₄ H ₇ O ⁺ or C ₃ H ₂ O ₂ ⁺	71.00		
G		73.05	73.03	m (H ₂ C-O-CH-CH ₂) = 73.03 or linear fragment
	Si(OH) ₃ ⁺	79.00		
H		115.08	114.94	GPTMS
		121.00		
				

	$\begin{array}{c} \text{CH}_3 \quad \text{CH}_3 \\ \quad \\ \text{CH}_2 \quad \text{CH}_2 \\ \quad \\ \text{H}-\text{Si}^+-\text{O}-\text{Si}-\text{H} \\ \quad \\ \text{H} \quad \text{H} \end{array}$ <p style="text-align: center;">or</p> $\left[\begin{array}{c} \text{CH}_3 \\ \\ \text{Si}^+ \\ / \quad \backslash \\ \text{O} \quad \text{O} \\ \quad \\ \text{H}_3\text{C}-\text{Si} \quad \text{Si}-\text{CH}_3 \\ / \quad \backslash \quad / \quad \backslash \\ \text{H}_3\text{C} \quad \text{O} \quad \text{O} \quad \text{CH}_3 \end{array} \right]_m \quad m=0$	133.00		Cyclic fragment
I	$\left[\begin{array}{c} \text{CH}_3 \\ \\ \text{H}_3\text{C}-\text{Si} \\ \\ \text{CH}_3 \end{array} \right]_n \left[\begin{array}{c} \text{CH}_3 \\ \\ \text{O}-\text{Si}^+ \\ \\ \text{CH}_3 \end{array} \right]_{n=1}$	147.07	147.01	Linear fragment
	$\begin{array}{c} \text{OH} \quad \text{OH} \\ \quad \\ \text{Si}^+-\text{O}-\text{Si}-\text{O}-\text{Si} \\ \quad \quad \\ \text{O} \quad \text{O} \quad \text{O} \end{array}$	181.00		Partial crosslinking with three silane molecules?
	$\begin{array}{c} \text{OCH}_3 \\ \\ \text{Si}^+-\text{O}-\text{Si}-\text{O}-\text{Si} \\ \quad \quad \\ \text{OH} \quad \text{OH} \quad \text{OH} \end{array}$	191.00		GPTMS
J	$\begin{array}{c} \text{OH} \\ \\ \text{O}^+-\text{Si}^+-\text{O}-\text{Si}-\text{O}-\text{Si} \\ \quad \quad \\ \text{OH} \quad \text{OH} \quad \text{OH} \end{array}$	193.05	192.87	GPTMS
	$\begin{array}{c} \text{OCH}_3 \\ \\ \text{Si}^+-\text{O}-\text{Si}-\text{O}-\text{Si} \\ \quad \quad \\ \text{OCH}_3 \quad \text{OCH}_3 \quad \text{OCH}_3 \end{array}$	205.00		GPTMS
K	$\left[\begin{array}{c} \text{CH}_3 \\ \\ \text{Si}^+ \\ / \quad \backslash \\ \text{O} \quad \text{O} \\ \quad \\ \text{H}_3\text{C}-\text{Si} \quad \text{Si}-\text{CH}_3 \\ / \quad \backslash \quad / \quad \backslash \\ \text{H}_3\text{C} \quad \text{O} \quad \text{O} \quad \text{CH}_3 \end{array} \right]_m \quad m=1$	207.03	206.88	Cyclic fragment
L	$\left[\begin{array}{c} \text{CH}_3 \\ \\ \text{H}_3\text{C}-\text{Si} \\ \\ \text{CH}_3 \end{array} \right]_n \left[\begin{array}{c} \text{CH}_3 \\ \\ \text{O}-\text{Si}^+ \\ \\ \text{CH}_3 \end{array} \right]_{n=2}$	221.08	221.04	Linear fragment
M	$\left[\begin{array}{c} \text{CH}_3 \\ \\ \text{Si}^+ \\ / \quad \backslash \\ \text{O} \quad \text{O} \\ \quad \\ \text{H}_3\text{C}-\text{Si} \quad \text{Si}-\text{CH}_3 \\ / \quad \backslash \quad / \quad \backslash \\ \text{H}_3\text{C} \quad \text{O} \quad \text{O} \quad \text{CH}_3 \end{array} \right]_m \quad m=2$	281.05	280.99	Double peak at (1) 280.88 and 280.99 (2) Cyclic fragment

 <p>or</p> 	149.00		Linear or cyclic fragment
	163.00		Linear fragment
(SiO ₂) ₃ H	181.00	*	
 <p>or</p> 	197.00	*	
	223.00		Cyclic fragment
	237.00		Linear fragment
(SiO ₂) ₄ H	241.00	*	
	257.00	*	
(SiO ₂) ₄ OH H ₂ O	274.88		
	297.00		Cyclic fragment
(SiO ₂) ₅ OH H ₂ O	334.81		

III. 4. Analyse of the wafers grafted with the long chain alkyle silane

-Silane choice

It was a necessity to use hydrocarbon with long chains for two important reasons:

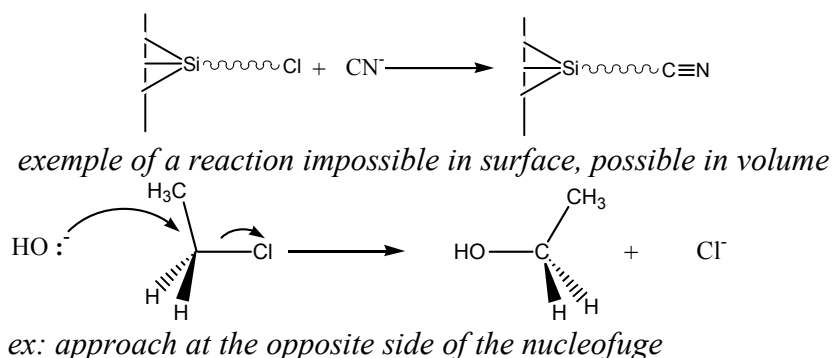
-they give monolayers well-defined on contrary to short chains.

-IR spectra present bands corresponding to the vibration modes of CH₂ groups, whose intensity is proportional to the number of CH₂ groups.

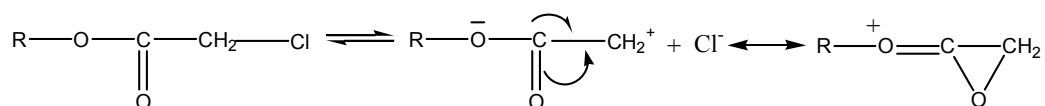
In the case of nucleophilic substitution, humic acid constitutes the nucleophilic entity, in basic medium. Cl acts as a good nucleofuge group and it must be chosen to be the most labil possible to obtain the substitution reaction.

Moreover, it is necessary to consider that there are differences between reaction in surface (wafer) and in volume (silica gel):

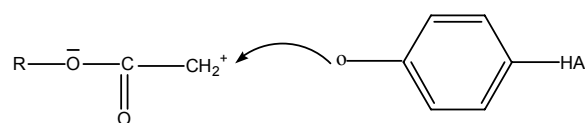
For instance, the reaction below, occurs in volume (rapid and quantitative) but is impossible in surface because there is an impossibility for the nucleophilic group to approach at the opposed side of the nucleofuge due to compacity of 2D system and nucleophilic substitution is prevented.



9-(trichlorosilyl)nonylchloroacetate was used to give a stabilised cation by mesomer effect.



Then a subsequent frontal attack of phenate ion occurs on the carbocation formed:



-ATR-FTIR on 9-(trichlorosilyl)nonylchloroacetate immobilized on silicon ATR crystal

ATR-FTIR reveals the presence of vas (CH₂) at 2923 cm⁻¹ and vs (CH₂) at 2853 cm⁻¹.

v (C=O) from ester is visible at 1758.30 and 1741.54 cm⁻¹. Consequently, the trichlorosilane has been well grafted on the silicon wafer.

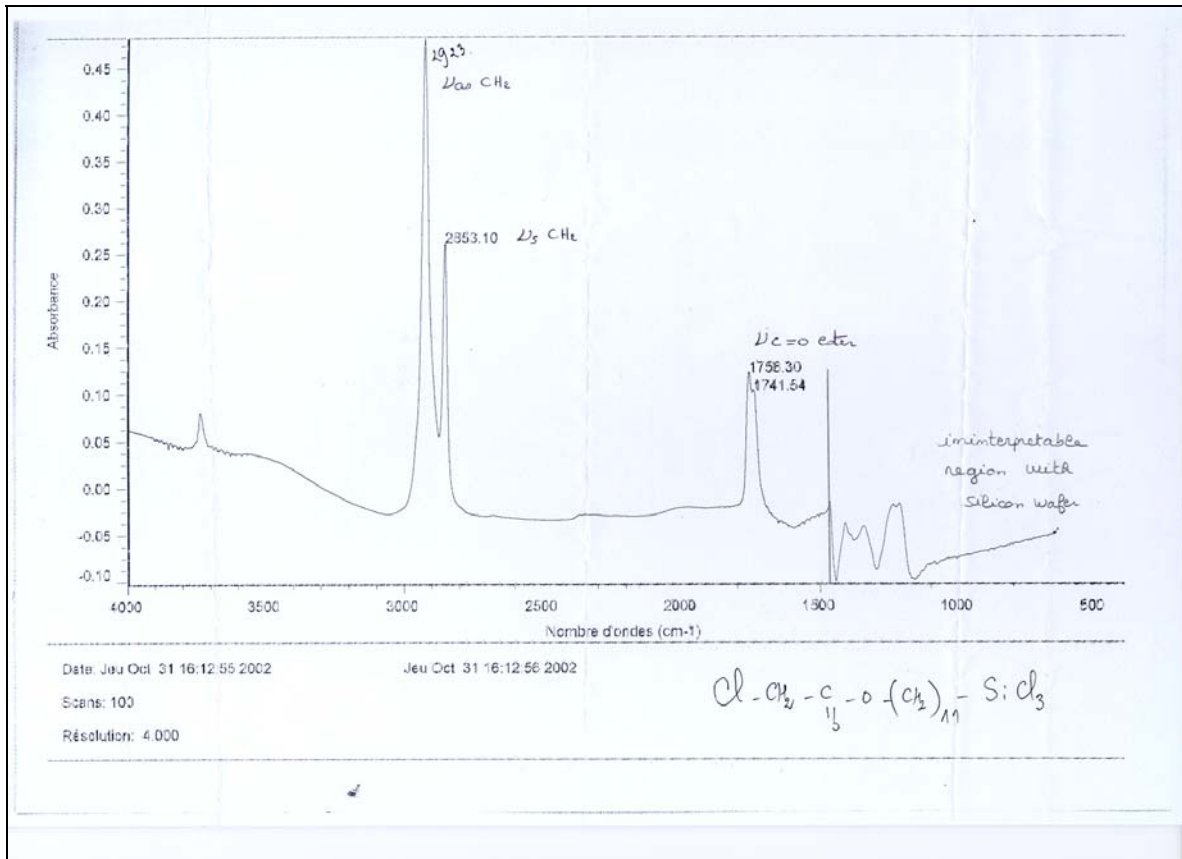


Fig. 10: ATR-FTIR on 9-(trichlorosilyl)nonylchloroacetate immobilized on silicon ATR crystal

-Evaluation of the number of COOH present on the wafers has been done by a surface UV method. DMAP released during the experiment gives directly the number of COOH/nm².

DO after 2 h	0,0085	Considered as a blank
DO after the night	0,0157	
DMAP ΔDO	0,0072	
concentration (mol/L)	6,13288E-08	
V=10 mL (mol)	6,13288E-10	

Table 4: Evaluation of the number of COOH groups immobilized by DMAP method

From the above table $6.132 \cdot 10^{-10}$ mol of DMAP are released by this method which is equivalent to $6.132 \cdot 10^{-10}$ mol of COOH and consequently 5.16 COOH/nm^2 .

-Evaluation of the europium amount complexed to humic acids give the following results: $1.143 \cdot 10^{-10}$ mol Eu bound to humic acids on the wafer which corresponds to 0.1404 Eu/nm^2 .

Some physic parameters influence the kinetic of fixation of Eu on functionalized wafers:

- ionic strength,
- viscosity,
- dielectric constant...

They are important to evaluate the variations of diffusion coefficient of this element and its efficacy to reach the surface.

Consequently, it will be very important to compare different techniques for humic acids immobilization. The binding reaction will be done between a spacer with an azo function and humic acid, by the way of an electrophilic reaction (less prevented than SN₂ reaction), in conditions of surface chemistry, for comparison.

	before incubation (cpm)	after incubation (cpm)	bound (cpm)	bound (mol) E-10	% d'Eu fixé
Blank wafer silane (9mL)	91368,0	84924,90	6443,10	1,297 E-10	7,05
wafer HA (9 mL)	92097,0	79922,70	12174,30	2,45 E-10	13,22
Without HA (9 mL) -7.05%			6494,50	1,307 E-10	
Due to HA (9 mL)			5679,79	1,143 E-10	

Table 5: Evaluation of the amount of Eu complexed by the silane wafer (blank) and the humic wafer.

IV. Experiments to perform-Perspectives

-Activation:

To obtain an homogeneous layer, it will be necessary to do the covalent binding of long chain silane with a reactive functional group, at the end of the chain. In that case, and only in that case, silane can orient themselves producing a monolayer at the wafer surface instead of making uncontrolled polymerization at the surface.

-Characterizations at each step of the grafting

(bare wafer, epoxy wafer, hydrolyzed wafer, humic wafer, hydrolyzed humic wafer)

-ellipsometry

-C size mapping

-AFM

-Fluorescence in reflexion mode

-XPS/UPS

-ATR-FTIR measurements-Total reflectance infra-red spectroscopy.

-Soft X-ray in reflectance

-TOF-SIMS

-S-NEXAFS: project submitted in october at LURE with Philippe Parent.

-Sorption isotherms with europium.

V. Conclusion

Experiments performed allow to better understand the different steps of the grafting and to think about a new protocole in view of obtaining a surface monolayer coverage.

A successful grafting has been done via a nucleophilic substitution between a trichlorosilane and phenate ions. The reaction must be optimized, testing the effect of different parameters (solvent, solvent/water rate, temperature, silane choice...) Electrophilic reaction will be undertaken, by diazotation procedure, to immobilize humic acids and the different techniques used will be compared to obtain maximum humic acids immobilized.

It is also necessary to find out which techniques will be better to characterize the wafers and to gather all the informations they are able to bring.

References

ABEL M.-L., DIGBY R.P., FLETCHER I., WATT J.F. Evidence of specific interaction between γ -glycidoxypropyltrimethoxysilane and oxidized aluminium using high-mass resolution TOF-SIMS. Surface and interface analysis (2000) 29, 115-125.

ABEL M.-L., RATTANA A., WATTS J.F. The interaction of γ -glycidoxypropyltrimethoxysilane with oxidised aluminium substrates : the effect of drying temperature. Journal of adhesion (2000) 73, 313-340.

BARBOT C., CZERWINSKI K., BUCKAU G., KIM J.I., MOULIN V., VIAL M., PIERI J., DURAND J.-P., GOUDARD F. Characterization of a humic gel synthesized from an activated epoxy silica gel. Radiochimica Acta (2002) 90, 211-218.

BIERBAUM K., GRUNZE M. BASKI A.A., CHI L.F., SHREPP W., FUCHS H., Growth of self-assembled n-alkyltrichlorosilane films on Si(100) investigated by atomic force microscopy. Langmuir (1995) 11, 2143-2150.

BRZOSKA J.B., BEN AZOUZ I. and RONDELEZ F. Silanization of solid substrates: a step toward reproducibility. Langmuir (1990) 10, 4367-4373.

BUSTAMANTE C., RIVETTI C., AND KELLER D. Scanning force microscopy under aqueous solutions. Current Opinion in Structural Biology, (1997) 7, 709-716.

CHEN J., GU B., LEBOEUF E.J., PAN H., DAI S. Spectroscopic characterization of the structural and functional properties of natural organic matter fractions. Chemosphere (2002) 48, 59-68.

DAVIS S.J. and WATTS J.F. Organization of methoxysilane on iron. International journal of adhesion and adhesives (1996) 16, 5-15.

DELAMARCHE E., SUNDARABABU G., BIEBUYCK H., MICHEL B., GERBER Ch., SIGRIST H., WOLF H., RINGSDORF H., XANTHOPOULOS N., MATHIEU H.J. Immobilization of antibodies on a photoactive self-assembled monolayer on gold. Langmuir (1996) 12, 1997-2006.

DIGBY R.P. and SHAW S.J. The international collaborative programme on organosilane coupling agents: an introduction. International Journal of Adhesion and Adhesives (1998) 18, 261-264.

DUCHET J., CHABERT B., CHAPEL J.P., GERARD J.F., CHOVELON J.M., JAFFREZIC-RENAULT. Influence of the deposition process on the structure of grafted alkylsilane layers. Langmuir (1997) 13, 2271-2278.

FANG J., FLINN B.J., LEUNG Y.L., WONG P.C., MITCHELL K.A.R., FOSTER T. A characterization of the γ -glycidoxypropyltrimethoxysilane and aluminium interface by SIMS and XPS. Journal of materials science letters (1997) 16, 1675-1676

- GETTINGS M. and KINLOCH A.J. *Journal of materials science* (1977) 12, 2511.
- HOUSSIAU L., BERTRAND P. TOF-SIMS study of organosilane self-assembly on aluminum surfaces. *Applied surface science* 175-176, 351-356 (2001)
- JAY R.R. Direct titration of epoxy compounds and aziridines. *Analytical chemistry* (1964) 36, 667-668.
- JERZYKIEWICZ M., JEZERSKI A., CZECHOWSKI F., DRODZ J. Influence of metal ions binding on free radical concentration in humic acids. A quantitative electron paramagnetic resonance study. *Organic geochemistry* (2002) 33, 265-268.
- KIM J.I., BUCKAU G., LI G.H., DUSCHNER H. and PSARROS N. Characterization of humic and fulvic acids from Gorleben groundwater. *Fresenius Journal of Analytical Chemistry* (1990) 338, 245-252.
- KIM J.I., RHEE D.S., BUCKAU G., MORGENSTERN A. Americium(III)-humate interaction in natural groundwater: influence of purification on complexation properties. *Radiochimica acta* (1997) 79, 173-181.
- KUJAWINSKI E.B., FREITAS M.A., ZANG X., HATCHER P.G., GREEN-CHURCH K.B., JONES R.B. The application of electrospray ionization mass spectrometry (ESI MS) to the structural characterization of natural organic matter. *Organic geochemistry* (2002) 33, 171-180.
- LENIGK R., CARLES M., IP N.Y., SUCHER N.J. Surface characterization of a silicon-chip-based DNA microarray. *Langmuir* (2001) 17, 2497-2501.
- LEUNG Y.L., YANG Y.P., WONG P.C., MITCHELL K.A.R. J., FOSTER T. X-ray photoelectron spectroscopic studies with a bias-potential method for studying silane-aluminium interfaces. *Journal of materials science letters* (1993) 12, 844-846.
- LEUNG Y.L., ZHOU M.Y., WONG P.C., MITCHELL K.A.R. XPS studies of interfaces between gamma-glycidyloxypropyltrimethoxysilane and aluminum surfaces. *Applied surface science* (1992) 59, 23-29.
- LIU A., WU C.H., ESCHENAZI E., PAPADOPOULOS K. AFM on humic acid adsorption on mica. *Colloids and surfaces A: Physicochemical and engineering aspects* (2000) 174, 245-252.
- McGOVERN M.E., KALLURY K.M.R., THOMPSON M. Role of solvent on the silanization of glass with octadecyltrichlorosilane. *Langmuir* (1994) 10, 3607-3614.
- MINGALYOV P.G., FADEEV A.Y. Activated silica supports for preparation of chromatographic sorbents. A comparative study of silicas containing attached epoxy, tosyloxy and halogen groups. *Journal of Chromatography A* (1996) 719, 291-297.
- MITTAL K.L. ED. (VSP, Utrecht, 1992). *Silane and other coupling agents*,
- NAVARRE S., CHOPLIN F., BOUSBAA J., BENNETAU B., NONY L., AIME J.-P. Structural characterization of self-assembled monolayers of organosilanes chemically bonded onto silica wafers by dynamical force microscopy. *Langmuir* (2001) 17, 4844-4850.
- NYQUIST Richard Allen. *Interpreting infrared, Raman and nuclear magnetic resonance spectra*. Academic press 2001.
- PLANCQUE G., AMEKRAZ B., MOULIN V., TOULHOAT P., MOULIN C. Molecular structure of fulvic acids by electrospray with quadrupole time-of-flight mass spectrometry. *Rapid communications in mass spectrometry* (2001) 15, 827-835
- PLASCHKE M., RÖMER J., KLENZE R., KIM J.I. In situ AFM study of sorbed humic acid colloids at different pH. *Colloids and surfaces A: Physicochemical and engineering aspects* (1999) 160, 269-279

PLASCHKE M., ROTHE J., SCHÄFER Th., DENECKE M., DARDENNE K., POMPE S., HEISE K.-H. Combined AFM and STXM in situ study of the influence of Eu(III) on the agglomeration of humic acid. *Colloids and surfaces A: Physicochemical and engineering aspects* (2002) 197, 245-256.

PLUEDDEMAN E.P. *Silane coupling agents* (Plenum Press, New-York, 1991).

PORSCH B. Epoxy- and diol-modified silica: optimization of surface bonding reaction. *Journal of Chromatography A* (1993) 653, 1-7.

PRIME K.L., WHITESIDES G.M. Self-assembled organic monolayers: model systems for studying adsorption of proteins at surfaces. *Science* (1991) 252, 1164-1167.

QUINTON J.S. and DASTOOR P.C. Conformational dynamics of γ -APS on the iron oxide surface: an adsorption kinetic study using XPS and TOF-SIMS. *Surface and interface analysis* (2000) 30, 21-24.

RATTANA A., HERMES J.D., ABEL M.L., WATTS J.F. The interaction of a commercial dry film adhesive with aluminium and organosilane treated aluminium surfaces: a study by XPS and TOF-SIMS. *International Journal of Adhesion and Adhesives* 22, 205-218 (2002)

SILBERZAN P., LEGER L., AUSSERRE D., BENATTAR J.J. Silanation of silica surfaces. A new method of constructing pure or mixed monolayers. *Langmuir* (1991) 7, 1647-1651.

TSUKRUK V.V., LUZINOV I., JULTHONGPIPUT D. Sticky molecular surfaces: epoxysilane self-assembled monolayers. *Langmuir* (1999) 15, 3029-3032.

WANG D., JONES F.R.

TOF-SIMS and XPS studies of the interaction of silanes and matrix resins with glass surfaces. *Surface and interface analysis* 20 (1993) 457-467.

WASSERMAN S.R., TAO Y.-T., WHITESIDES G.M. Structure and reactivity of alkylsiloxane monolayers formed by reaction of alkyltrichlorosilanes on silicon substrates. *Langmuir* (1989) 5, 1074-1087.

Annex 8

An Experimental and Modeling Study of Metal Ion/Humate Non-Exchangeable Binding

N.D. Bryan, D.M. Jones, R. Keepax, P. Warwick, S. Stephens and J.J.W. Higgs

University of Manchester (U-Manch)

An Experimental and Modelling Study of Metal Ion/Humate Non-Exchangeable Binding.

N.D. Bryan¹⁾, D.M. Jones¹⁾, R. Keepax¹⁾
P. Warwick²⁾, S. Stephens²⁾, J.J.W. Higgs³⁾

¹ Centre for Radiochemistry Research, Department of Chemistry, University of Manchester, Oxford Road, Manchester, UK, M13 9PL.

² Department of Chemistry, Loughborough University, Loughborough, Leicestershire, UK.

³ British Geological Survey, Keyworth, Nottinghamshire, UK.

Abstract

Pulsed column experiments using Co, fulvic acid and porous sediment packing, along with up/down-flooding experiments using Eu, humic acid and intact sandstone blocks were performed as part of the previous E.C.-HUMICS project. The elution of metal and humic and their distribution along the sandstone columns were measured. A mixed equilibrium and kinetic model, k1-D, has been used to simulate the results. In both cases, one exchangeable and one non-exchangeable component have been used to simulate the interaction of metal and humic substance. For the pulsed experiments, a simple equilibrium approach was used to model humic sorption, while a two component, kinetic model was required for the sandstone columns.

A sample of humic acid containing relatively high specific activities of isotopes of Am and Pu has been isolated from a site in the Esk estuary, Cumbria, U.K. The desorption kinetics of the Am and Pu from the sample have been measured using an ion exchange technique. ²⁴¹Am and ¹⁵²Eu have been added to the same samples in the lab, and their desorption kinetics determined also. The preliminary results suggest that all of the isotopes desorb with similar rates (of the order of 10^{-8} s^{-1}), regardless of origin. However, the relative amounts in the non-exchangeable fraction are lower for the isotopes added in the lab.

A mechanistic modelling study has been performed to investigate the possible mechanisms responsible for the non-exchangeable binding of metal ions by humic substances. In this initial phase of the work, the possibility that the association/disassociation of humate monomer units is responsible has been assessed. Electrophoretic mobility distributions have been determined for a number of humic samples, for which the molecular weight mass distributions have been measured by ultracentrifugation. These data have been combined to provide estimates of size and charge distributions. A Poisson-Boltzmann model, which treats the humic species as penetrable gels, has been used to estimate the potentials at the humic/diffuse layer boundary for the members of the estimated charge and size distributions. These potentials have been used in a simple model to calculate interaction potential energies and hence theoretical aggregation rates. The preliminary results predict that, although aggregation of smaller units to produce much larger species will take place, the magnitudes of the rates and their dependency on solution conditions suggest that this self association is not responsible for the non-exchangeable behaviour.

1 Introduction

Humic substances have a high affinity for most cations, and have long been suspected as possible vectors for the movement of heavy metals and radionuclides in the environment (Jones and Bryan 1998). It has become clear that, although the initial uptake of metals is rapid, not all of the metal loading may be removed instantaneously. Rather, a fraction of the metal becomes 'non-exchangeably' bound, the size of the fraction depending upon the contact time (Choppin and Clark 1991). Metals bound in the exchangeable mode are bound very strongly, but nevertheless may still be removed instantaneously by a ligand or surface with a sufficiently high affinity (Warwick et al 2000). The non-exchangeably bound metal may be desorbed: however, the process is slow, and the rate is independent of the strength or concentration of the competing sink (Warwick et al 2000).

There have been a number of studies that have examined this kinetic effect (Choppin 1988, Choppin and Clark 1991, Chakrabati et al 1994, Cacheris and Choppin 1998, Schussler et al 1998, King et al 2001, Schussler et al 1999, Warwick et al 2000). There are in fact a number of these non-exchangeable components, and a number of first-order rate constants are required to describe the data. Choppin et al (Choppin 1988, Choppin and Clark 1991, Cacheris and Choppin 1998) have used a 'kinetic spectrum' approach, which defines a number of these components. Other studies (Schussler 1998, King et al 2001, Schussler et al 1999, Warwick et al 2000) have acknowledged the existence of the faster fractions, but have concentrated upon the longest lived fraction, since this is expected to be the most significant for transport in the environment (Warwick et al 2000). In fact, there is a continuum of desorption rates ranging from virtually instantaneous to this slowest fraction. The most surprising result is that this slow fraction is found for all humic samples. Even more surprising is that, outside of some small variation, the rate is the same for most metals, regardless of metal ion chemistry (Keepax et al 2002). This behaviour is in contrast to that for exchangeable binding, where the binding strength depends very much upon the identity of the metal ion (Tipping and Hurley 1992, Read and Falck 1996).

Three distinct studies have been undertaken: column modelling; mechanistic modelling; study of natural samples contaminated with anthropogenic actinides. The aim of all three studies is to shed light on the nature of the kinetic interactions of humic substances, both the interaction with metal ions and the sorption of humic materials onto surfaces.

2 Column Modelling

2.1 Introduction

The non-exchangeable component is the most likely to be responsible for the humate-mediated movement of metals in the environment (McCarthy et al 1998, Warwick et al 2000), since this metal fraction is less likely to be immobilised by sorption. Transport will depend upon residence time, with breakthrough decreasing with increasing residence time. To address this issue, a coupled chemical transport model, k1D, has been developed during the past few years (Schussler et al 2001, Warwick et al 2000). This model incorporates simple 1-D transport, and allows chemical processes to be described with both equilibrium and rate constants simultaneously. It has been used successfully to model the migration of metals, Eu (Warwick et al 2000) and Am (Schussler et al 2001), through porous columns. However, in both cases, the behaviour of the humic itself was not treated explicitly.

Most transport modelling has naturally focussed upon simulating the behaviour of the metal, rather than the humic substance itself. In some cases, where the solid phase has been pre-equilibrated with the humic, it has been found that there is no significant retardation of metal-humic complexes. For example, Warwick et al (2000) were able to simulate Eu transport, by assuming that the Eu-humate complex moved as a conservative tracer, whilst Schussler et al (2001) found that Am-humate complex moved slightly faster than a conservative tracer, presumably because of exclusion effects. This work concerns the modelling of both metal and humate transport in column experiments.

2.2 Materials and Methods

Two separate sets of column experiments were performed: (1) short, pulsed experiments with cobalt (Co) and using columns packed with porous sediment; (2) up/down-flooding experiments with europium (Eu) and using intact sandstone blocks.

2.2.1 Pulsed column experiments

These experiments involved short columns (6-20cm), packed with sand. The packing was fully equilibrated with groundwater, which contained humic substances, at a low concentration (2.8 ppm). The metal, ^{57}Co , and fulvic acid, isolated from the Broubster site in Scotland, UK, were injected as a pulse of metal-fulvate complex ($[\text{fulvic}] = 32.5\text{ppm}$; $[\text{Co}] = 1.3 \times 10^{-8}\text{M}$) in a stream of groundwater. The metal/fulvate complex was allowed to equilibrate for a known period of time, prior to injection. The porosity and dispersivity were determined at the same time by injection of inert ^{36}Cl . The breakthrough of the ^{57}Co and ^{36}Cl were determined radiometrically, and the humic via U.V./vis. absorption spectroscopy. These experiments were performed at the British Geological Survey, Keyworth, UK.

2.2.2 Up/down-flooding column experiments

These experiments used intact cylindrical columns cut from sandstone blocks. The sides of the columns were coated with impermeable resin, such that solutions could only pass into or out of the column via the ends. Iodinated (^{125}I) humic acid was prepared from Aldrich humic acid, using the method of Lassen et al (1994). Previous work has shown that the behaviour of the humic is unaffected by iodination (Dierckx et al 1998). Prior to the experiments, each sandstone column was equilibrated with the humic acid (non-radiolabelled) and inert electrolyte. All the columns had radii of 2.5cm, and the lengths were either 10, 20 or 30 cm. The flow rates varied from 5 to 15ml/hr.

These experiments had two distinct parts: up-flooding and down-flooding. In the up-flooding section, a known volume of $\text{Eu}/^{125}\text{I}$ -humate complex in 0.3M NaCl, pH 6.5 electrolyte was injected into the column ($[\text{HA}] = 40\text{ppm}$, $[\text{Eu}_{\text{TOTAL}}] = 5 \times 10^{-8} \text{ M}$, $[^{125}\text{I}] = 360 \text{ kBq/dm}^3$, $[^{152}\text{Eu}] = 2.4 \text{ MBq/dm}^3$). During down-flooding, the feed solution was changed to one that contained 40ppm HA (**not** labelled with ^{125}I), but no Eu. The breakthrough of the Eu and ^{125}I -humic were determined radiometrically. At regular intervals, the distribution of the ^{152}Eu and ^{125}I along the column were determined using a collimated detector, which was tracked along the length of the column. The porosities and dispersivities were determined by injection of tritiated water. These experiments were performed at Loughborough University, Loughborough, U.K.

2.3 Modelling

For both types of experiments, regardless of whether the humic colloid was sorbed or in solution, one parameter set was used to describe the interaction of the metal with the humic substance.

The set of equations and parameters for the pulsed column experiments are shown in Table 1. HA_{S} and HA_{FREE} represent humic substance bound to the sediment surface and in solution respectively, and Eq is the humic exchangeable binding site. $\text{Co}_{(\text{aq})}$ and Co_{S} represent free Co and Co bound to the surface, while Co_{Eq} and Co_{FIX} represent Co bound in the humic exchangeable and non-exchangeable fractions respectively. Square brackets ($[*]$) represent concentrations, \leftrightarrow equilibria, \rightleftharpoons kinetic reactions. For mathematical simplicity, a single surface site was used for metal and humic sorption, which was present in vast excess, and hence had a virtually constant concentration ($[\text{S}] = 0.1 \text{ mol dm}^{-3}$). However, this does **not** suggest that the species are actually bound at a single, 'real' common site.

In the case of the sandstone columns, a more complex series of reactions and equations was required (Table 2): two surface bound humic fractions were required, HA_{S1} and HA_{S2} , whose behaviour required a first order kinetic description. The transfer of metal into and out of the humic non-exchangeable fraction was described by a simple first order relationship. For these columns, the model parameters were obtained by fitting the elution profiles, and these parameters were then used 'blind' to predict the distribution profile along the column. The

interaction of the Eu with the sandstone surface was modelled with a kinetic equation, in agreement with previous work (Warwick et al 2000).

Table 1: reaction, equation and parameter set used to model the pulsed, Co columns

Chemical reaction	Mathematical equation	Parameter values
$\text{Co}_{(\text{aq})} + \text{S} \leftrightarrow \text{Co}_{\text{S}}$	$K_{\text{S}} = \frac{[\text{Co}_{\text{S}}]}{[\text{Co}_{(\text{aq})}][\text{S}]}$	$K_{\text{S}}=1.0 \times 10^7 \text{ dm}^3 \text{ mol}^{-1}$
$\text{Co}_{(\text{aq})} + \text{Eq} \leftrightarrow \text{Co}_{\text{Eq}}$	$K_{\text{Eq}} = \frac{[\text{Co}_{\text{Eq}}]}{[\text{Co}_{(\text{aq})}][\text{Eq}]}$	$K_{\text{Eq}}=5.0 \times 10^8 \text{ dm}^3 \text{ mol}^{-1}$
$\text{HA}_{\text{FREE}} + \text{S} \leftrightarrow \text{HA}_{\text{S}}$	$K_{\text{HA}} = \frac{[\text{HA}_{\text{S}}]}{[\text{HA}_{\text{FREE}}][\text{S}]}$	$K_{\text{HA}}=10.0 \text{ dm}^3 \text{ mol}^{-1}$
$\text{Co}_{\text{Eq}} \begin{matrix} \rightarrow \\ \leftarrow \end{matrix} \text{Co}_{\text{FIX}}$	$\frac{d[\text{Co}_{\text{FIX}}]}{dt} = k_{\text{f}}[\text{Co}_{\text{Eq}}] - k_{\text{b}}[\text{Co}_{\text{FIX}}]$	$k_{\text{f}} = 2.9 \times 10^{-7} \text{ s}^{-1}$ $k_{\text{b}} = 1.3 \times 10^{-6} \text{ s}^{-1}$

Table 2: reaction, equation and parameter set used to model the sandstone, Eu columns

Chemical reaction	Mathematical equation	Parameter values
$\text{Eu}_{(\text{aq})} + \text{Eq} \leftrightarrow \text{Eu}_{\text{Eq}}$	$K_{\text{Eq}} = \frac{[\text{Eu}_{\text{Eq}}]}{[\text{Eu}_{(\text{aq})}][\text{Eq}]}$	$K_{\text{Eq}}=2.0 \times 10^5 \text{ dm}^3 \text{ mol}^{-1}$
$\text{Eu}_{\text{Eq}} \begin{matrix} \rightarrow \\ \leftarrow \end{matrix} \text{Eu}_{\text{FIX}}$	$\frac{d[\text{Eu}_{\text{FIX}}]}{dt} = k_{\text{f}}[\text{Eu}_{\text{Eq}}] - k_{\text{b}}[\text{Eu}_{\text{FIX}}]$	$k_{\text{f}} = 2.4 \times 10^{-7} \text{ s}^{-1}$ $k_{\text{b}} = 5.0 \times 10^{-7} \text{ s}^{-1}$
$\text{Eu}_{(\text{aq})} \begin{matrix} \rightarrow \\ \leftarrow \end{matrix} \text{Eu}_{\text{S}}$	$\frac{d[\text{Eu}_{\text{S}}]}{dt} = k_{\text{EuSf}}[\text{Eu}_{(\text{aq})}] - k_{\text{EuSb}}[\text{Eu}_{\text{S}}]$	$k_{\text{EuSf}}=2.0 \times 10^{-4} \text{ s}^{-1}$ $k_{\text{EuSb}}=1.0 \times 10^{-6} \text{ s}^{-1}$
$\text{HA}_{\text{FREE}} \begin{matrix} \rightarrow \\ \leftarrow \end{matrix} \text{HA}_{\text{S1}}$	$\frac{d[\text{HA}_{\text{S1}}]}{dt} = k_{\text{HAS1f}}[\text{HA}_{\text{FREE}}] - k_{\text{HAS1b}}[\text{HA}_{\text{S1}}]$	$k_{\text{HAS1f}}=1.7 \times 10^{-5} \text{ s}^{-1}$ $k_{\text{HAS2f}}=1.5 \times 10^{-5} \text{ s}^{-1}$
$\text{HA}_{\text{FREE}} \begin{matrix} \rightarrow \\ \leftarrow \end{matrix} \text{HA}_{\text{S2}}$	$\frac{d[\text{HA}_{\text{S2}}]}{dt} = k_{\text{HAS2f}}[\text{HA}_{\text{FREE}}] - k_{\text{HAS2b}}[\text{HA}_{\text{S2}}]$	$k_{\text{HAS1f}}=6.0 \times 10^{-6} \text{ s}^{-1}$ $k_{\text{HAS2f}}=1.0 \times 10^{-7} \text{ s}^{-1}$

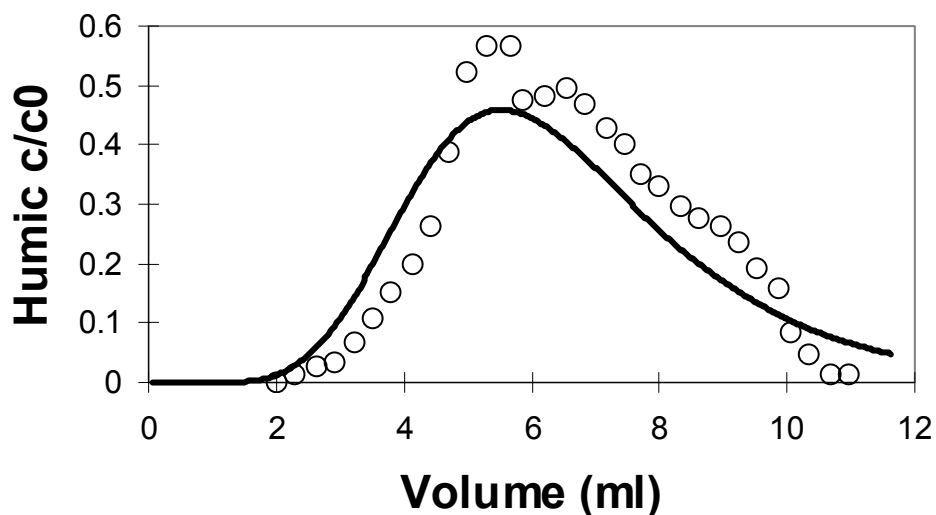


FIGURE 1: experimental humic elution data for 6.4cm pulsed column (flow rate = 0.5 ml/hr, diameter = 1 cm) (o=humic expt.); and model prediction (line).

2.4 Results

All elution data (Figs. 1-4) are displayed as C/C_0 , where C is the concentration of metal or humic eluting, and C_0 is the injected concentration. For the profile data, Figures 5 and 6, the experimental technique provides only relative concentrations of ^{152}Eu and ^{125}I .

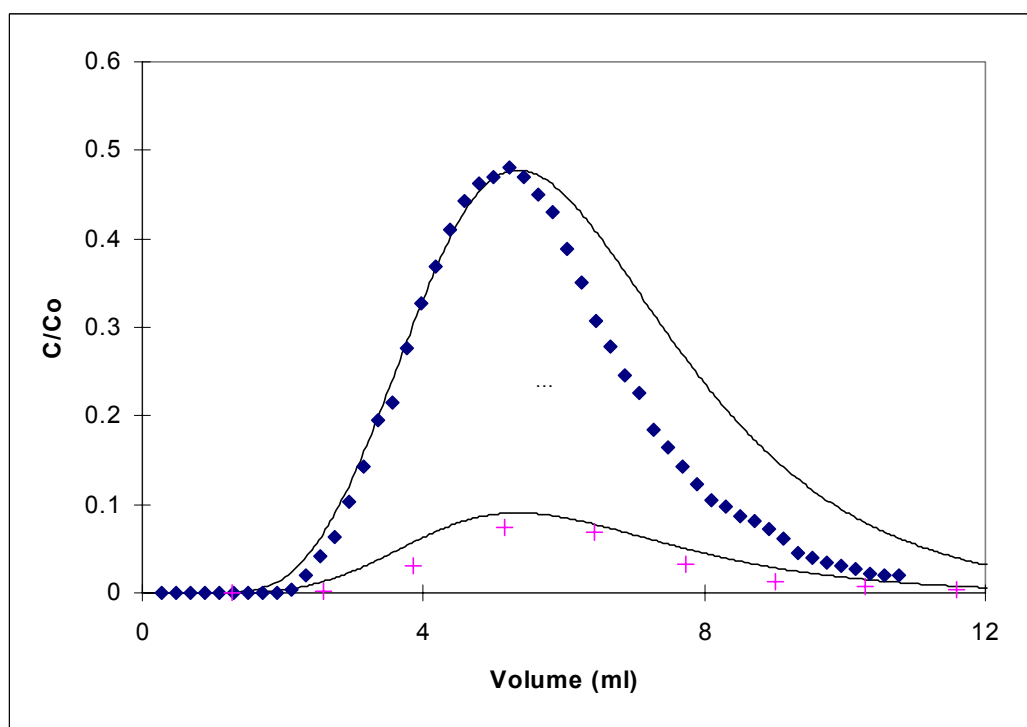


FIGURE 2: experimental elution data for 6cm (flow rate 0.5ml/hr, diameter = 1 cm) pulsed column (◆=humic, +=Eu); and model predictions (lines).

Figures 1 and 2 show typical experimental and modelling results obtained with the pulsed columns. Both species were retarded by the columns, Co to a greater extent than the humic. The interaction of the humic with the packing is relatively weak ($K_{HA} = 10 \text{ dm}^3 \text{ mol}^{-1}$, table 1), whereas the interaction of the Co is very strong. In fact, in the absence of humate, there was no Co breakthrough, and only humate associated Co emerges in the effluent. In all of these experiments, the Co and humic breakthrough maxima always coincide. The model is achieving a fairly reasonable fit to both the humic and Co effluent data. There were similar results for a number of different column experiments. Although it was essential to have a mixed kinetic and equilibrium description of the metal-humate interaction, for the sorption of the humate, it was found that the use of a kinetic approach did not improve the fit.

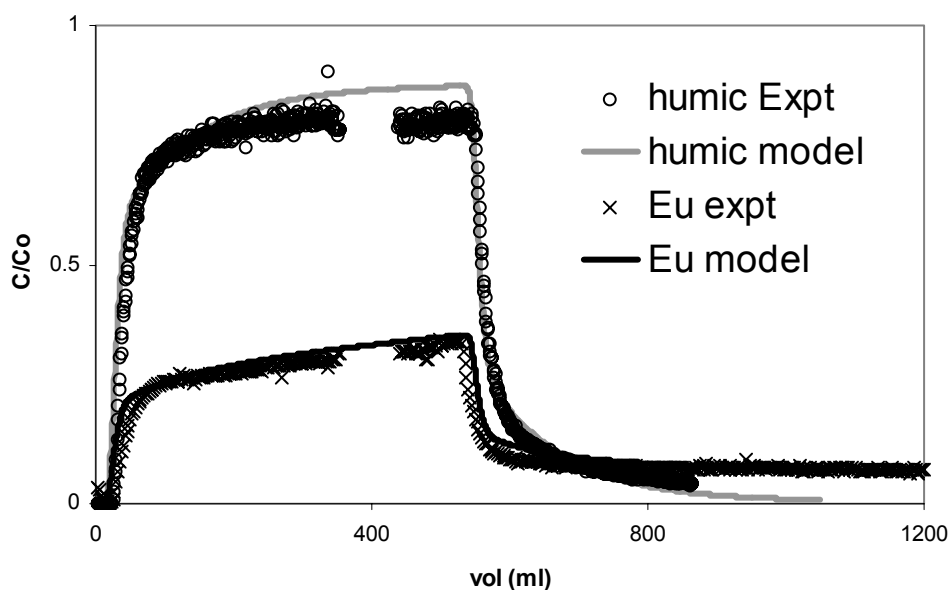


FIGURE 3: experimental elution data for 10cm (flow rate 15ml/hr) sandstone column (x=Eu, o=humic); and model predictions (lines).

Figures 3 and 4 show typical elution profiles and modelling results for the sandstone column experiments. It is significant that, although the relative amount of the humic breaking through is different to that of the Eu, the shape of the elution plot is similar. Again, a kinetic description was required to simulate the behaviour correctly. The shapes and positions of the Eu and humic plots are indicative of a multi-component system. In each case, there is a fairly rapid breakthrough followed by a decrease in gradient to give a relatively steady outflow concentration. Since the steady value (C/Co) is less than 1, there must be at least 2 chemical reactions involved: the exchangeable and non-exchangeable components in the case of the Eu, and the two humic sorption reactions in the case of the humic. Figure 5 shows the distribution of ^{152}Eu and ^{125}I activity along a 30cm column as a function of elution time for 6 equally spaced segments along the length of the column. During the up-flooding stage, Eu activity in all 6 segments increases steadily with time. The maximum for the first segment marks the start of down-flooding. As down-flooding proceeds, the Eu activity at the start (injection end) of the column decreases as the humic acid, pulls the sorbed metal into solution. In the middle

and at the outflow end of the column, the Eu activity actually increases slightly, because Eu released from further up the column is replacing that removed by the humic acid. Eventually, the activities in these segments would also start to decrease. In the case of the humic (Figure 5B), the activity in all 6 segments starts to decrease immediately with the onset of down-flooding, indicative of the weaker interaction between the humic acid and the sandstone. Figure 6 shows Eu column profiles for 10cm columns at two different flow rates. Because of the short length of the columns, experimental data for only a single segment were recorded. Three model predicted profiles have been produced for each column, for the start, middle and outflow end.

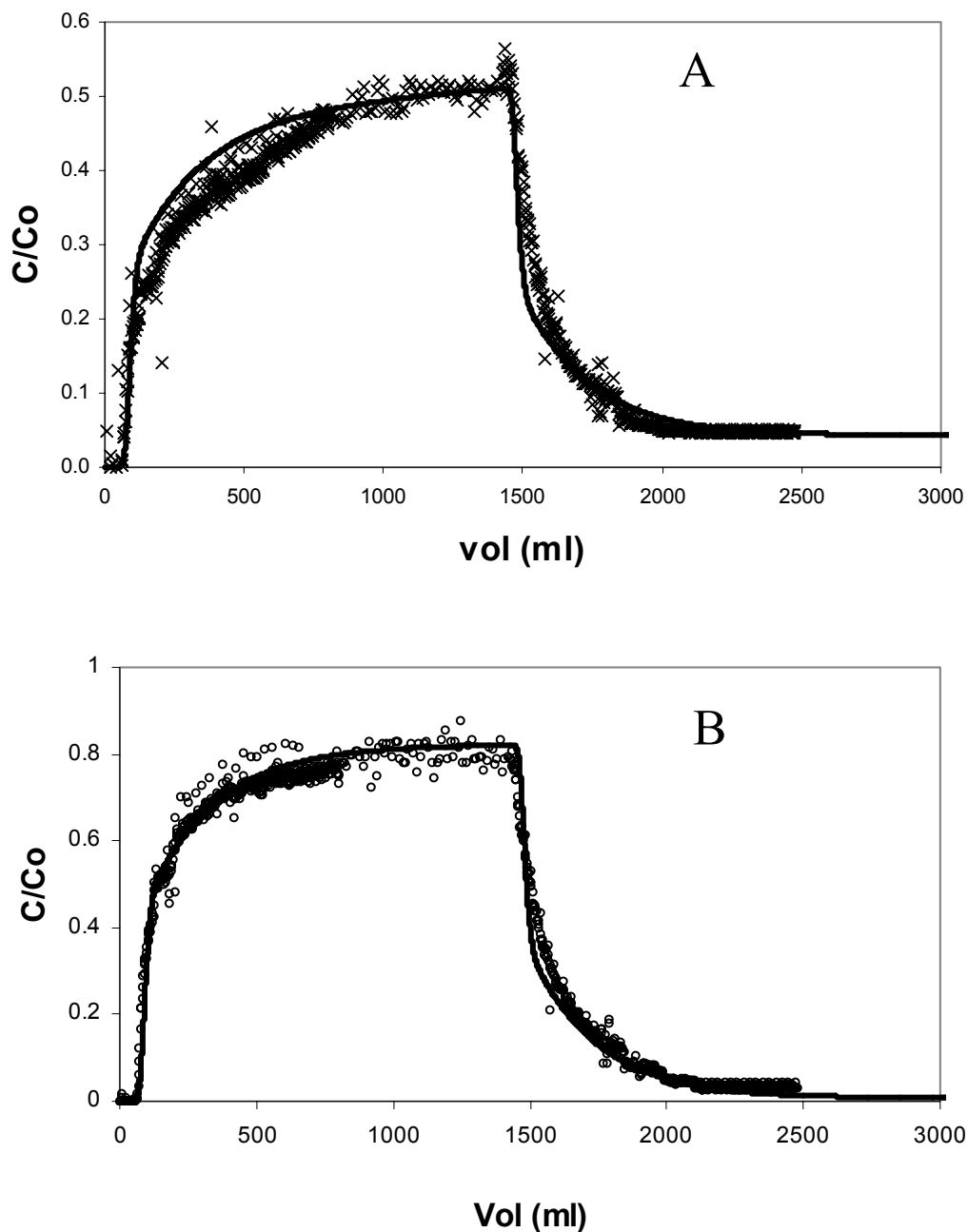


FIGURE 4: experimental elution data for 30cm (flow rate 10ml/hr) sandstone column, A, x=Eu, B, o=humic; and model predictions (lines).

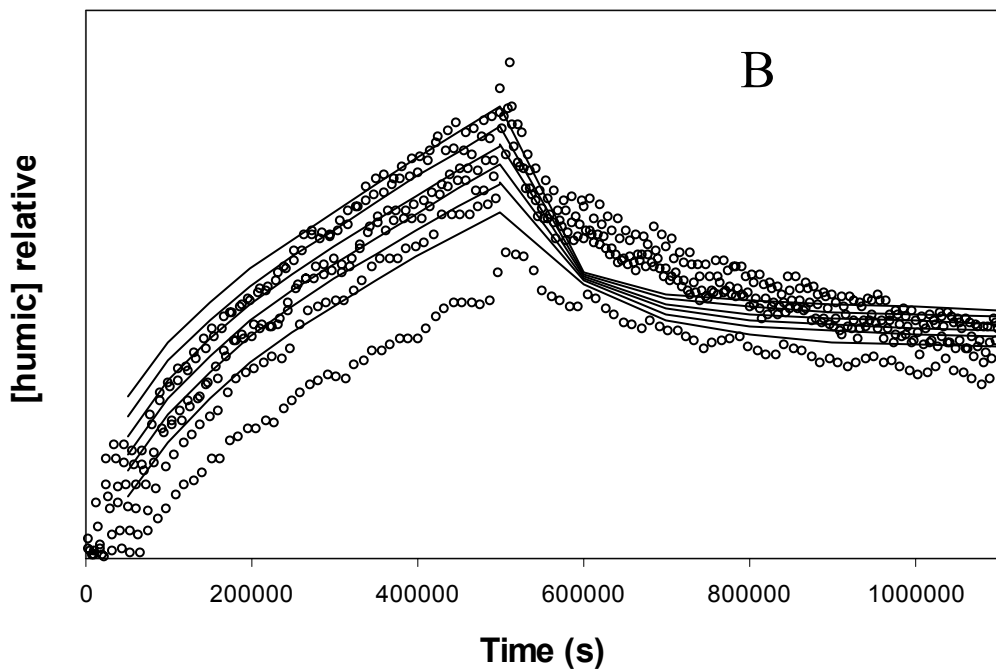
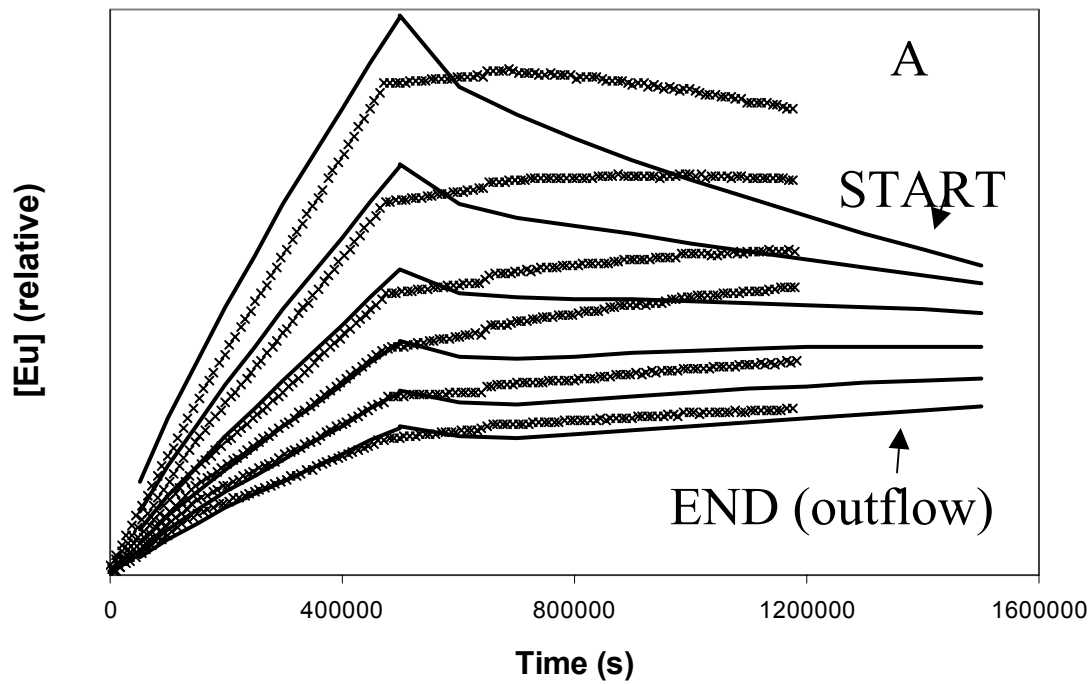


FIGURE 5: (A) experimental Eu profile (x) and model prediction (lines) for 6 segments, plotted as relative concentration vs elution time; (B) corresponding experimental humic profile (o), and model predictions (lines). 30cm column, flowrate=10ml/hr.

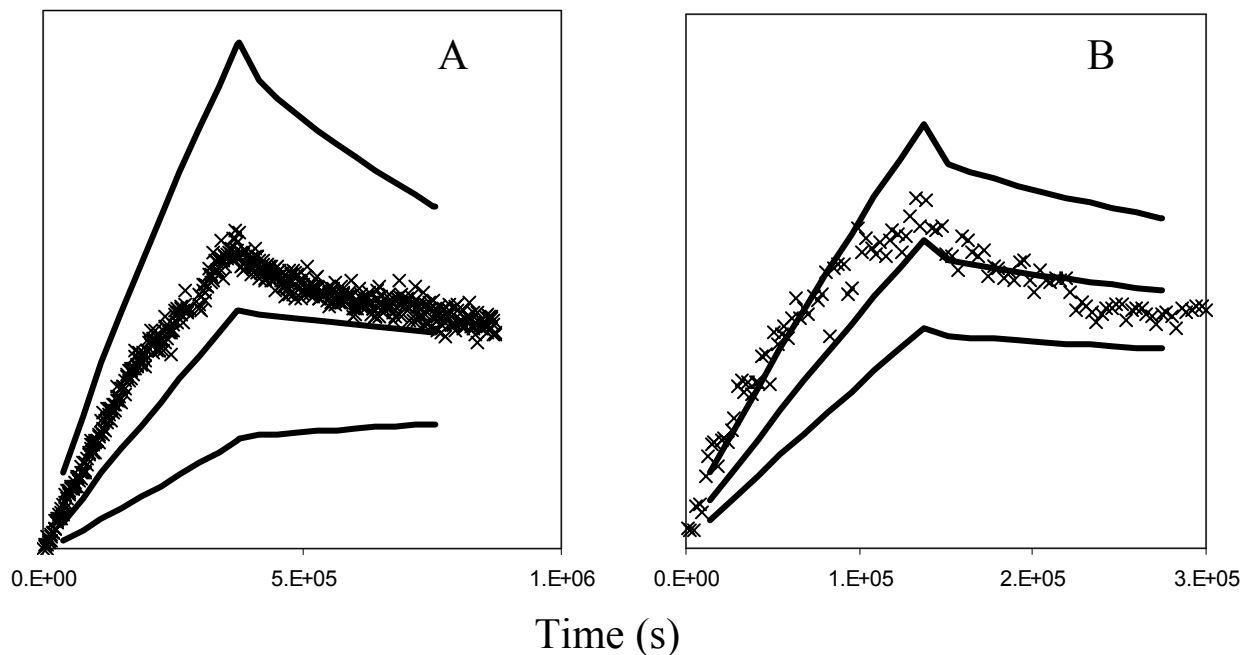


FIGURE 6: Experimental Eu profiles (x) plotted as relative concentration vs elution time for 10cm columns and model predicted profiles for start, middle and ends of the columns: A - flow rate = 5 ml/hr; B - flow rate = 15 ml/hr.

2.5 Discussion

The experimental data demonstrate that metal transport is dominated by humic interactions, since there is a strong correlation between the elution of the metals and the humics. Indeed, for both sets of experiments, metal transport was negligible in the absence of humic material. The correlation between the Co and humic elution plots (Figure 2) demonstrates the role of the humic in promoting transport. This demonstrates the importance of understanding the sorption behaviour of the humic: the Co and humate maxima are coincident, because the only Co emerging from the column is associated with the humic, and so has assumed the sorption characteristics of the humic itself. Any free Co, and indeed any not in the non-exchangeable fraction, does not make it past the very beginning of the column.

Batch kinetic studies have found evidence for the existence of a spectrum of desorption rates, ranging from instantaneously exchangeable to very slow (e.g. Choppin and Clark 1991, King et al 2001). However, amongst the continuum there appears to be a distinct, most slowly desorbing component, which may be described with a single pair of definite rate constants (forward and backward). It is the kinetic parameters for this fraction (determined by batch experiments) that have been used here (k_f and k_b , table 2). It seems that although the spectrum of desorption rates does exist, it is only necessary to consider the distinct, slowest fraction in order to predict metal transport.

The model fit for the sandstone profiles (Figures 5 and 6) is less close than for the elution data (Figures 3 and 4), because these profiles were blind modelled (i.e., profile data were not included in the parameter fitting process). The 30cm humic profile fit (Figure 5B) is closer

than the corresponding Eu profile (Figure 5A): the model occupies the correct region of the plot, but the shape in the down-flooding section is incorrect. For the Eu profile (Figure 5A), the up-flooding section is quite good. During down-flooding the model performs less well, but the fit at the outflow end of the column is much better than at the start. This is not surprising, since the model parameters were determined by analysis of the elution (outflow) data, and hence, the model is bound to be better at predicting the conditions at the outflow end. This result shows the importance of considering elution and profile data. Elution data are more common than profile data; and it is certainly possible to define transport parameters using only these data (e.g. Warwick et al 2000). However, when transport parameters are used to make field scale predictions, it is the predicted profile that is of most interest. This work shows that parameters derived from the elution data of column experiments cannot be relied upon to predict the profile of those **same** columns. Therefore, with humic substances care should be exercised when applying parameters to simulations outside of the scope of the data used to obtain them. The origin of the 30cm Eu profile discrepancy is unclear. Unless the humic associated with Eu behaves significantly differently to the bulk, it seems unlikely that it is an error in the simulation of the behaviour of the Eu-humate complex, because the humic profile does not show the same problems. It seems more likely that the error lies in the description of the interaction of the Eu direct with the sandstone. The fit to the 10cm columns (Figure 6) seems better, although with only one segment, it is harder to make a comparison. Certainly, the shape seems to be roughly correct.

In this study, two different approaches were used to model humic sorption. In the case of the pulsed columns, a simple equilibrium approach was sufficient, whereas for the sandstone columns, an equilibrium approach would not work, and a two component kinetic approach was required. It is unlikely that the difference is due to variations in residence time, which are similar: ≈ 4 hrs, Figure 2; ≈ 9 hrs, Figure 4. However, the total experiment times are very different: ≈ 10 hrs, Figure 2; ≈ 250 hrs, Figure 4. In the case of the pulsed experiment, there is insufficient time for significant desorption. Hence, only the sorption step need be accounted for, and an equilibrium approach works. In the sandstone experiments, there is sufficient time for desorption, and a full kinetic description is required. There are other possible explanations for this difference. The pulsed columns used fulvic acid and a solid phase not equilibrated with the fulvic, while the sandstone experiments used humic acid and fully equilibrated columns. Previous column modelling was able to work without considering sorption of humic material. There may be a number of reasons for this difference. Both previous studies used columns filled with sediment rather than intact sandstone blocks. In one case (Schussler et al 2001), the columns used a pulsed methodology, whilst in the other (Warwick et al 2000), which did use the up/down-flooding method, the packing was acid washed sand, which would be a less effective sorber. Humic sorption has been observed in the sandstone columns, but the modelling has shown that neither desorption nor exchange between sorbed and solution phase humic acid take place instantaneously.

For the metal-humic interaction, it has been found that a single description may describe a wide variety of systems, including fulvic and humic acids (King et al 2001, Schussler et al

2001, Warwick et al 2000). Whatever the reason for the difference, there may not be a single, universally applicable description for the humic-mineral surface interaction.

2.6 Conclusions

It is now clear that a mixed equilibrium and kinetic approach is essential to describe the humate-mediated transport of metal ions. Humic sorption seems as complex as the interaction with metals, and that, although an equilibrium approach may suffice for some systems, a multi-component, kinetic approach is needed for others. The precise definition of the humic sorption model does seem to depend upon the specific properties of the system. No evidence has been found for 'irreversibility' in these experiments.

We now have a more detailed understanding of the transport of humic substances in column experiments **under these particular laboratory conditions**. However, this understanding must be treated with care. Although models and parameters have been developed to describe lab experiments, it would be wrong to assume that they could be applied 'blind' to field-scale problems. The difference in the modelling between the pulsed and sandstone columns illustrates this point: the initial pulsed columns indicated that an equilibrium approach could model humic sorption, but this approach fails to simulate the sandstone columns. Hence, more work is required, perhaps on the field scale itself, before long range predictions may be made with confidence.

3 Mechanistic Modelling

3.1.1 Origin of the kinetic effect

There is now no doubt that humic substances bind metals non-exchangeably. However, the mechanism by which this happens is uncertain. Beyond the kinetic effect itself, there are a few clues. Von Wandruska et al (1997) found that, although solution phase humic colloids are broadly hydrophilic, the addition of metal ions resulted in the formation of hydrophobic zones, with metals of high charge density being the most efficient at producing the effect. In addition, structural changes have been observed that take place on the time-scale of days after initial binding, which is similar to that observed for the development of non-exchangeable binding (Engebretson and Von Wandruszka 1998).

Two conceptual models of humic structure have been proposed. The *Random Coil* approach treats the humic as an essentially contiguous single molecular strand, and that the loose coiling of that strand imparts gel-like properties. Conversely, the *Self Association* approach assumes that the humic species, which exist in solution, are in fact (loose) associations of smaller units, and that this accounts for the penetrability.

3.1.2 The Random Coil Model (Swift, 1999)

Strictly speaking, the Random Coil Model treats the humic as a single contiguous molecular strand, which coils randomly with respect to time and space. This strand carries, along its length, charged and hydrated functional groups. It assumes a conformation, which is roughly spherical in shape and in which the distribution of mass is Gaussian about its centre. The solvent penetrates throughout the structure, and at the periphery exchanges freely with the bulk solvent. The colloid may be tightly or loosely coiled depending upon several factors: the nature of the solvent; the extent of the solvent penetration; the charge of the colloid; the concentration of counterions; the surrounding pH (Hayes and Swift, 1978; 1990). At neutral to alkaline pH, the charged sites will be dissociated, giving rise to electrostatic repulsion within the colloid. In an attempt to reduce its electrostatic free energy, it will expand (and rearrange). Intramolecular expansion and solvation, together with intermolecular repulsion will keep these species in solution. Increasing I will reduce the repulsion and will lead to contraction. Adding specifically bound metal ions will reduce the magnitude of the charge, and hence, will also lead to contraction, as will protonation at lower pH. The colloid will shrink until the point where all the solvent is expelled and the flexible colloid has shrunk to its most collapsed state.

In its strictest sense, the Random Coil approach does treat the humic as a single molecular chain. However, given the complex and chaotic mechanisms of humic formation, it seems unlikely that humic colloids really have a single, contiguous chain. In fact, Schulten and Schnitzer (1993) have found experimental evidence for significant cross-linking. Hence, it might be more realistic to think of the humic as having a sponge like structure, which is cross-

linked, but is still able to expand and contract to allow penetration by the solvent and small ions. The net effect is a penetrable, gel-like structure (Benedetti et al 1996).

3.1.3 The Self Association Model

This hypothesis holds that the humic species observed in solution are actually aggregates of smaller monomers (Wershaw 1986, 1993; Piccolo et al 1996; Piccolo 1997; Conte and Piccolo 1999). The strongest evidence in support of self association has come from mass spectrometric studies. It has been known for some time that large humic species exist in solution, since they have been detected by non-invasive techniques, such as analytical ultracentrifugation and light scattering. However, recent studies using conventional mass-spectrometric techniques, e.g., electrospray mass spectrometry, have found no evidence of these large species (Plancque et al 2001; Moulin et al 2001). If these two sets of results are both correct, then it could be that the large species observed in solution are actually aggregates of the smaller moieties observed by the invasive techniques.

Support for the two conceptual models is fairly polarised. However, the two are not mutually exclusive. There is no reason why the large species in solution cannot behave like flexible, penetrated gels, which are formed by the self association of smaller units.

3.1.4 Possible mechanisms

Thinking in terms of the Self Association and Random Coil/Penetrable Gel models, one can propose mechanisms by which both could induce chemical kinetics. In the case of Self Association, metals could bind at a site on one of the smaller units, which make up the larger aggregates. Initially, that metal would remain exposed to the solution, and available for removal by surfaces or competing ligands. However, rearrangement of the humic aggregate could trap the metal within the structure of the aggregate, hiding it from the solution (Figure 7).

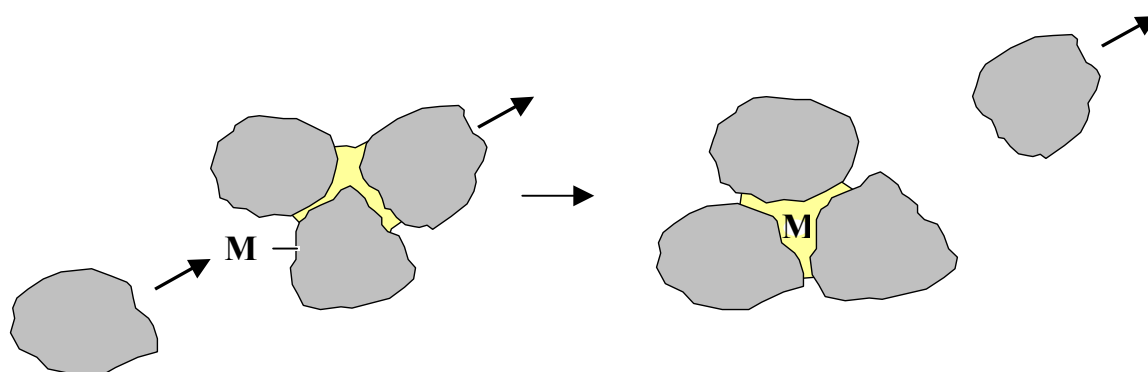


FIGURE 7: Possible 'Self-Association' mechanism for non-exchangeable binding

For the Random Coil/Penetrable Gel Model, dissociation and reassociation cannot trap the metal. However, if the humic has an open structure, which is penetrated by solvent and small ions, then metal ions could migrate into the interior and become hidden. Now, the exact mechanism by which they could become trapped is unclear. Choppin (1988) describes the

metal moving from exchangeable (weaker) to non-exchangeable (stronger) sites, i.e., the metal is required to move from one place on the humic to another. An alternative is illustrated in Figure 8. The metal binds at an exchangeable site within the humic, and initially, is available for further reaction. However, with time, the humic rearranges its structure, completely surrounding the metal ion. The metal is now surrounded by the humic organic skeleton, and a hydrophobic zone has been formed, isolating the metal from aqueous solution phase chemistry, and rendering it non-exchangeable.

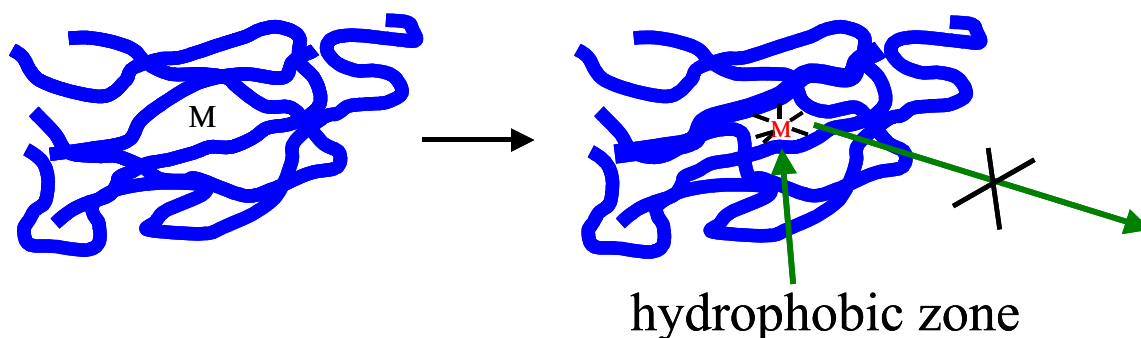


FIGURE 8: Possible 'Random Coil' mechanism for non-exchangeable binding

In the first instance, a series of calculations have been made to examine the 'self-association' mechanism for the origin of non-exchangeable binding.

3.2 Electrophoretic mobilities

A series of on-going experiments have been performed at Manchester to measure the effect of solution conditions (pH, I etc.) on electrophoretic mobility for a number of humic samples.

The electrophoretic mobility of a molecule/colloid (μ) is given by (Hiemenz and Rajagopalan 1997),

$$\mu = \frac{ZeD}{kT} \quad [2.1]$$

where Z is the number of charges on the colloid, D is its diffusion coefficient, e is the electronic charge, k is Boltzmann's constant and T is the absolute temperature. If we assume that the colloid is spherical then the diffusion coefficient will be given by (Hiemenz and Rajagopalan 1997),

$$D = \frac{kT}{6\pi\eta R} \quad [2.2]$$

where η is the solution viscosity and R is the (hydrodynamic) radius of the colloid. Therefore, measurements of electrophoretic mobility have the potential to provide information about colloidal size and charge, and both of these parameters will be crucial in controlling aggregation (and disaggregation) phenomena.

The electrophoretic mobilities were measured via the laser-Doppler technique using a Malvern Instruments zetasizer. In addition, the average charges of each of the humic samples has been determined as a function of pH by potentiometric titration.

The Laser-Doppler technique is particularly useful, since it not only provides average electrophoretic mobilities for a sample under a given set of conditions, but also the distribution of electrophoretic mobilities present within the sample. We expect a distribution, since the individual colloids within the sample will have a range of sizes and charges. For example, Figure 9 shows the effect of ionic strength and pH on the average electrophoretic mobilities for the peat humic acid, WBPFA2, whilst, Figure 10 shows the variation in the distribution of electrophoretic mobilities with solution pH.

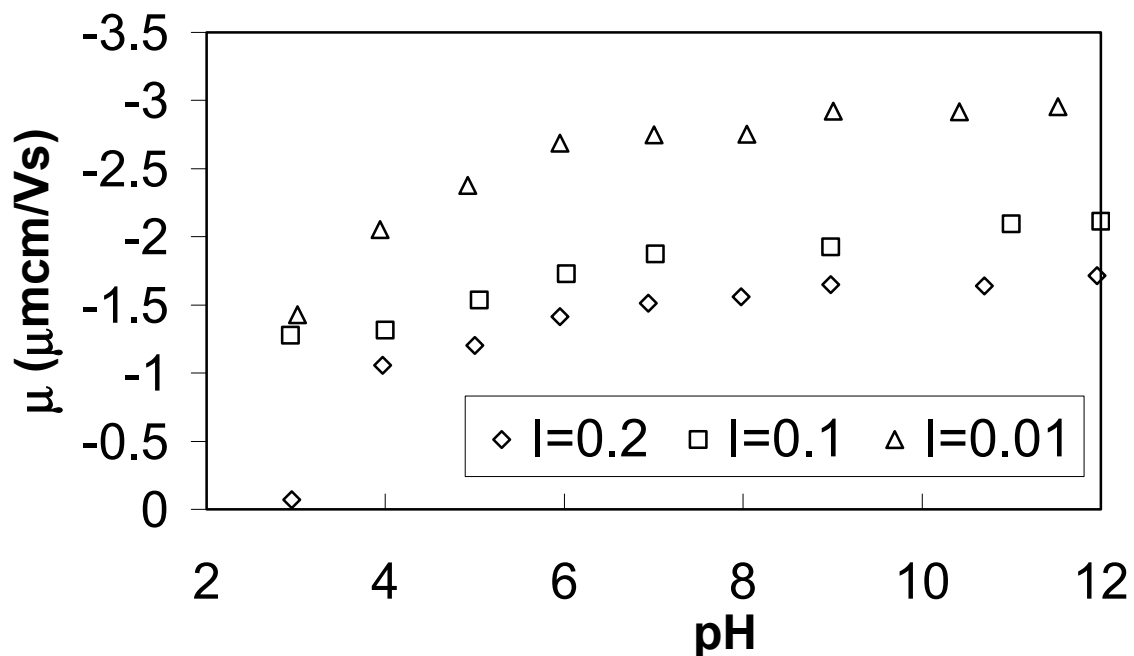


FIGURE 9: variation in average electrophoretic mobility for peat humic, WBPFA2.

Qualitatively, the results are fairly easy to understand: as the pH increases, and the humic charge grows, the electrophoretic mobility increases in magnitude, although the change is much less significant at higher pH for both the average values and the distributions.

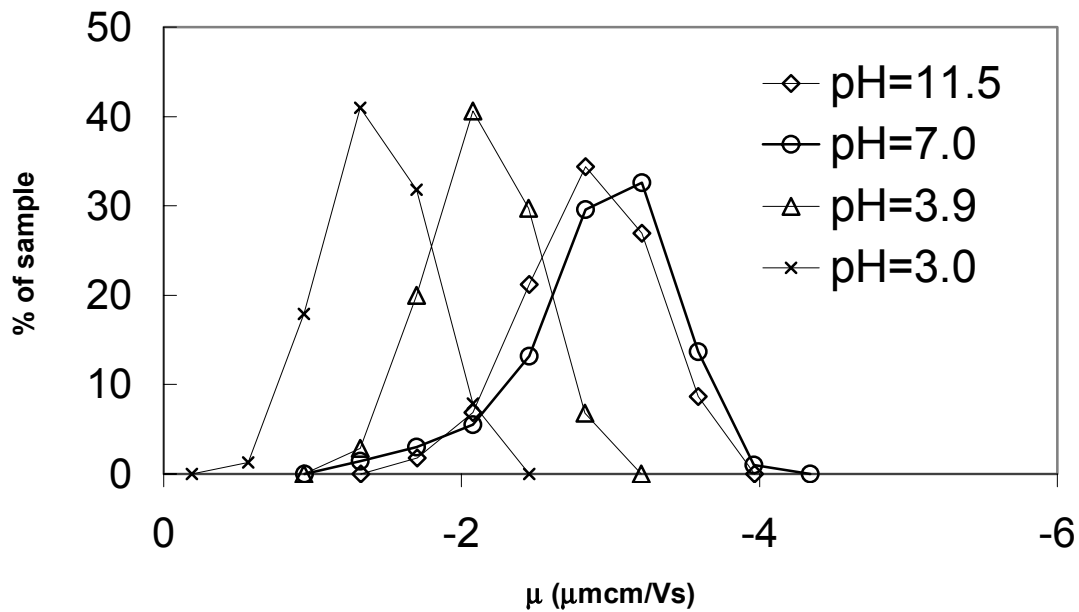


FIGURE 10: variation in the distribution of electrophoretic mobilities for peat humic, WBPHA2, I=0.01.

3.3 Modelling

3.3.1 Average electrophoretic mobilities

The first modelling study addressed the average electrophoretic mobilities, which were interpreted using equations [2.1] and [2.2], which may be combined to give

$$R = \frac{Ze}{6\pi\eta\mu} \quad [2.3]$$

The (average) values of μ are provided directly by the laser-Doppler technique, and hence the only 'unknown' in equation [2.3] is the number of charges on the colloid (Z). Although the average charge of the humic sample is known from potentiometric titration, in order to calculate Z , we must know the mass of the humic (M). This is problematic, since the sample contains a distribution of masses. Unfortunately, the distribution of charge over the mass range cannot be determined by titration. Therefore, calculations were performed for a range of possible colloid masses, and assuming that the charge density (meq/g) was equal across the mass range. Figure 11 shows the variation in charge and electrophoretic mobility for humic WBPHA2 with pH at I=0.01. These data were used in the model calculations. Figure 12 shows the variation in predicted radius with pH for the peat humic sample.

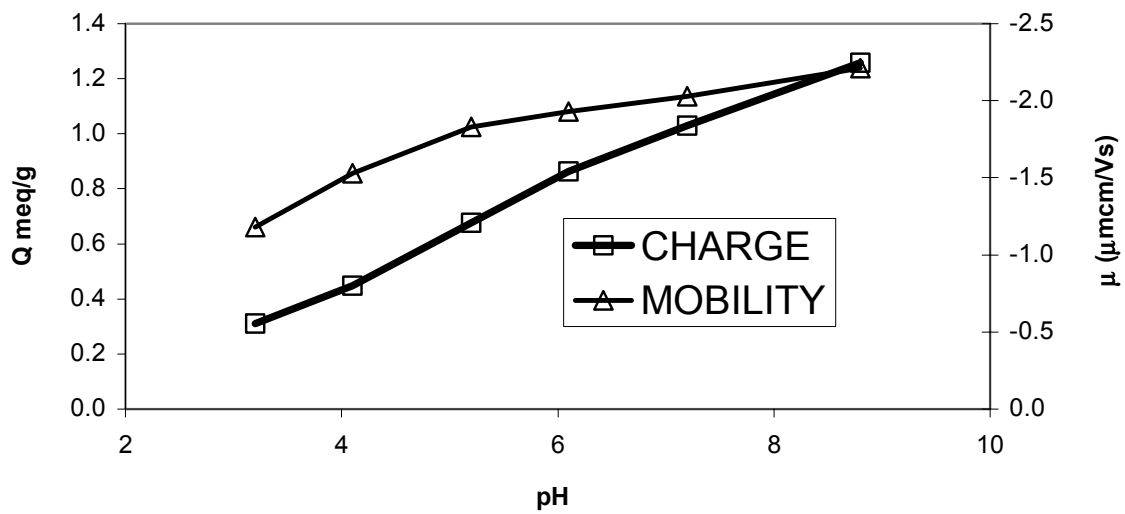


FIGURE 11: variation in average electrophoretic mobility and charge density for sample WBHA2, [HA]=150ppm, I=0.01, data used to produce predictions in Figure 12.

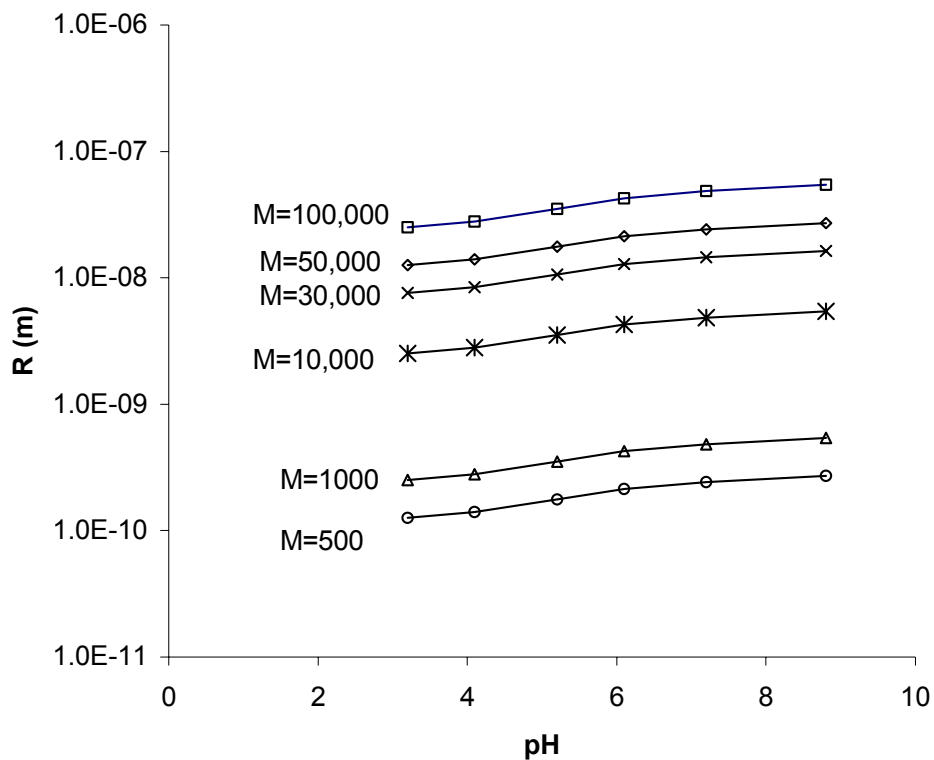


FIGURE 12: predicted variation in humic radius for a range of potential colloid masses for sample WBPHA2 (from data in Figure 11).

Regardless of the colloid mass used in the calculations, the same general pattern is always observed: as pH, and hence humic charge, increase, there is an increase in the effective radius of the humic. This strongly suggests that humic substances, at least those that are large enough to scatter light in the laser-Doppler technique, do indeed exist in solution as flexible structures that are able to expand and contract. It seems that as the humic charge increases, the humic reduces its electrical free energy (Coulombic self repulsion) by expansion, which will move its charges further away from each other, and will also allow increased penetration of shielding counterions, such as Na⁺.

Although the relative changes in the predicted radii do demonstrate the flexibility of the humic structures, there is a problem with some of the absolute values. For the larger humic masses, the values are not realistic. The partial specific volumes of humic acids are known to lie typically in the range 0.5 - 0.6 cm³/g (Jones and Bryan 1998). Using these values, it is possible to estimate the volume associated with the humic organic structure itself. Combining these values with the predicted radii in Figure 12 we may estimate the fraction of the total colloidal volume taken up by the humic itself, and then by difference, the fraction occupied by penetrating solvent and small ions. In the case of the calculations for M=100,000, the largest predicted radius is 54 nm. If this is true, then the humic structure accounts for only 0.01% of the total volume of the colloid, which is clearly unfeasible. The most plausible explanation is that the charge density data refer to the whole of the mass distribution, whereas the laser-Doppler technique is most sensitive to the larger species. Hence, the average charge density is **not** representative of the whole population. More than this, these data indicate that the larger species present in solution must have lower charge densities than the smaller, more numerous species. Hence, the average electrophoretic mobilities and charge densities demonstrate qualitatively that the humics do swell and contract as solution conditions change. However, they cannot provide quantitative colloid charges and sizes. Therefore, the subsequent modelling work has used the electrophoretic mobility distributions.

3.3.2 Electrophoretic mobility distributions

Humic substances lie at the lower end of the colloidal size range (typically <10 nm). Therefore, during the electrokinetic experiments, the scattering of the laser light may be described by Rayleigh theory. Hence, the sensitivity of the technique will depend upon R⁶. Fortunately, the molecular weight distribution of the humic samples, WBPHA2 (peat humic) and WBHA2 (aquatic humic) in aqueous solution have been measured via uv scanning analytical ultracentrifugation (Bryan et al 2001a, 2001b). Therefore, the strength of the signal produced by a colloid (S_M) will be related to its mass, M, radius, R, and particle concentration, N_M (derived from the relative molecular weight number distribution and the total mass concentration of the sample),

$$S_M \propto N_M R^6$$

Colloidal/molecular charges and sizes were estimated by fitting the experimental electrophoretic mobility distributions and using this relationship. However, there is one remaining unknown, the relationship between mass and size, which is one of the principle

uncertainties in humate science. The partial specific volume allows us to calculate the volume taken up by the humic organic structure, V_{struc} . However, the total volume, V_T , will be the sum of the structure volume and the volume of penetrating solvent, V_{solv} , which is unknown,

$$V_T = V_{\text{solv}} + V_{\text{struc}}$$

We define, β , the fraction of the total volume occupied by the solvent,

$$\beta = \frac{V_{\text{solv}}}{V_T} = \frac{V_T - V_{\text{struc}}}{V_T}$$

In fact, the value of β will be a function of mass. This must be the case, since although it is possible for large species to accommodate significant amounts of penetrating solvent, it seems likely that the small species, e.g. $M < 1000$, are too small to behave as penetrated gels, and are best described as 'simple' molecules, with $\beta \rightarrow 0$. Unfortunately, the exact form of the β function is unknown, except that we expect it to tend to zero as mass decreases. This means that for any given electrophoretic mobility distribution, there will be more than one possible set of corresponding distributions of charge and radius with mass. Therefore, for each distribution, a wide range of β functions were defined, and their effect determined. The procedure was:

1. Define the β function, and hence calculate V_T and R for each mass number;
2. For each mass number, the charge was fitted such that a plot of $N_M R^6$ vs μ had the same form as the experimental distribution. The values of μ were calculated using equation [2.3] with the values of R calculated in step 1 and the fitted value of Z . The fitting was performed by a process of trial and error. Figure 13 shows the results of a typical fitting process.

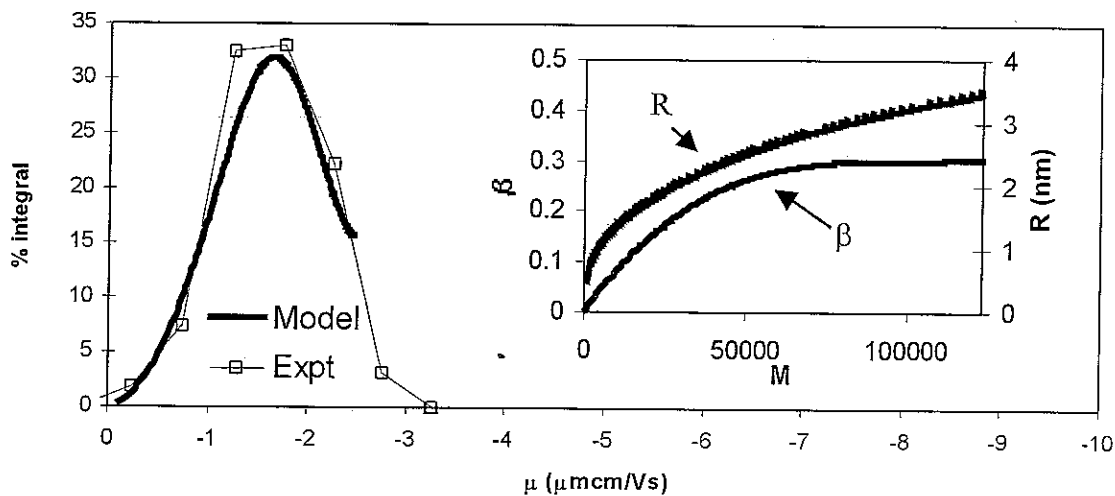


FIGURE 13: experimental electrophoretic mobility distribution and model fit for WBPHA2 peat humic, pH=6, I=0.1, and the values of β and R used in the fitting (inset).

Figure 14 shows an example of the effect of various β functions on the fitted charge density function. It was found that even though a wide range of β functions were used, the effects were relatively small, particularly at moderate and high mass numbers, which might not be expected, because it is in the high and moderate mass range that the β functions have their largest variations, and in fact, they all converge as mass number tends to zero. Nevertheless, the results demonstrate that we may be fairly confident of the calculated charge distributions, at least for $M \geq 10,000$.

Therefore, the fitting of the electrophoretic mobility distributions produces values of R and charge as a function of mass number. These were used as input values to the next stage of the modelling. Clearly, these calculations have assumed that all species of the same mass also share common sizes, penetrabilities and charges, and there is no guarantee that this will always be the case. In other words, at each mass number the model is calculating average properties. However, to allow separate distributions of size and charge at each mass would introduce a vast number of parameters into the calculations, and given the current state of understanding of humic properties, these would be impossible to define. This unavoidable simplification will introduce some uncertainty into the predictions.

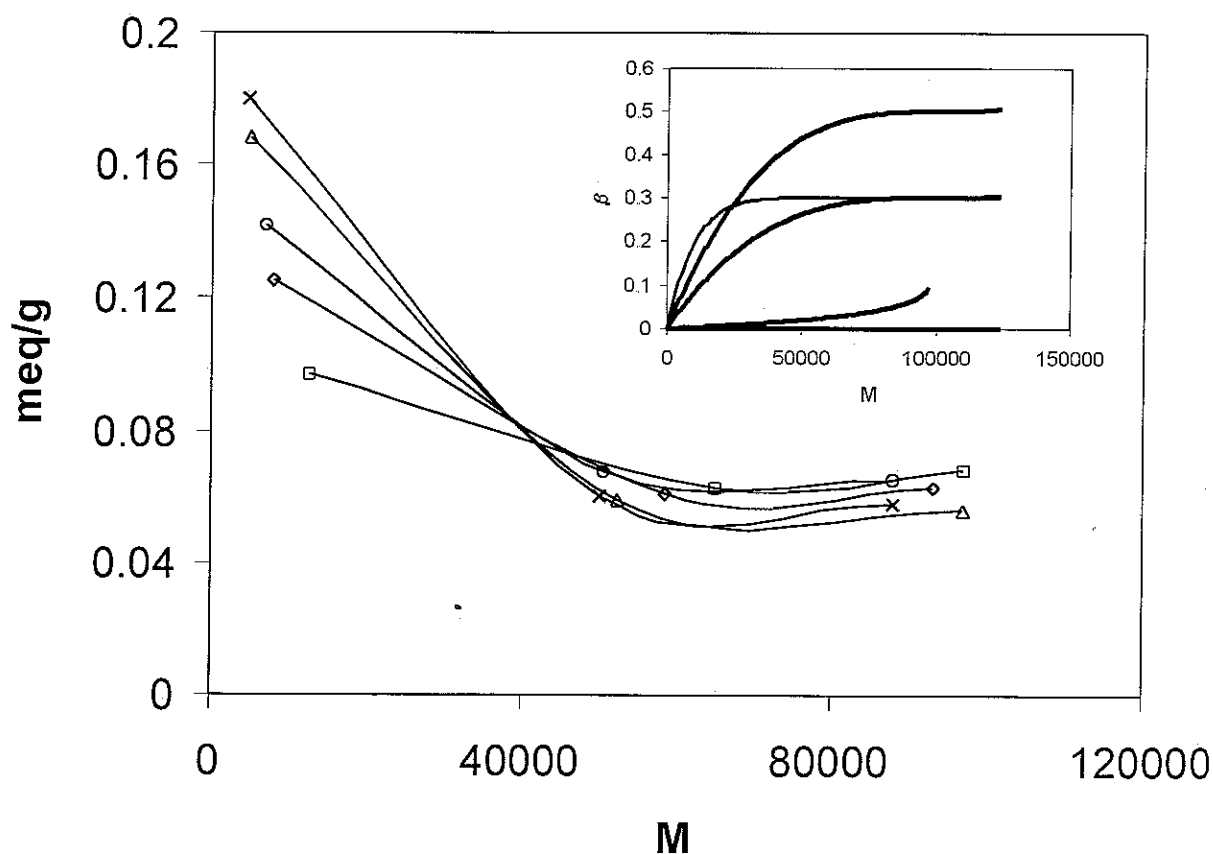


FIGURE 14: effect of β function (inset) on fitted values of charge for WBPFA2 humic acid. pH=3, I=0.01.

3.3.3 Theoretical potential energy curves and aggregation rates

This purpose of this modelling exercise is to examine the Self-Association model, and in particular to examine whether the aggregation/disaggregation processes could be responsible for the non-exchangeable binding of metals.

To estimate the rates of aggregation or disaggregation one must calculate the form of the potential energy curve as the two particles either approach to contact, or separate. There will be two forces acting on the pair of particles:

- (1) the repulsive Coulombic interaction that will tend to retard or prevent aggregation;
- (2) the attractive, Van der Waal's interaction that will promote aggregation.

The first step in calculating the Coulombic interaction is to calculate the potentials at the surfaces of the two particles. The method of Bryan et al (2000) was used.

The potential around a charged colloid particle, ψ , will be governed by Poisson's equation (Tanford 1961):

$$\nabla^2 \psi = \frac{-\rho}{\epsilon} \quad [2.4]$$

where ∇^2 is the Laplacian operator, ρ is the charge density, and ϵ is the permittivity. ρ will vary with distance from the centre of the colloid, and will depend upon both the humic and counterion charges (Bartschat et al 1992). The concentration of any counterion, i , will be governed by a Boltzmann equation (Tanford 1961),

$$[X_i^{z_i^+}]_r = [X_i^{z_i^+}]_{\text{BULK}} e^{-\left(\frac{\psi_r z_i e}{kT}\right)} \quad [2.5]$$

where ψ_r is the potential at a distance r from the centre of the colloid, and $[X_i^{z_i^+}]_r$ and $[X_i^{z_i^+}]_{\text{BULK}}$ are the counterion charges at r and in the bulk solution respectively.

Now, there are two distinct regions that need to be considered: Region I is the colloid itself, and here there will be charge from both the counterions and the humic, and Region II, where only the counterions make a contribution. Combining equations (2.4) and (2.5) gives two 'Poisson-Boltzmann' equations (Bryan et al 2000): one for region II

$$\nabla^2 \psi_{II} = -\frac{NAe}{\epsilon} \left(\sum_{i=1}^{N_{\text{IONS}}} z_i [X_i^{z_i}]_{\text{BULK}} \exp^{-\left(\frac{\psi_r z_i e}{kT}\right)} \right) \quad [2.6]$$

And the other for region I,

$$\nabla^2 \psi_I = -\frac{1}{\epsilon} \left[\rho_{\text{HUMIC}} + \beta NA e \left(\sum_{i=1}^{N_{\text{IONS}}} z_i [X_i^{z_i}]_{\text{BULK}} \exp^{-\left(\frac{\psi_r z_i e}{kT}\right)} \right) \right] \quad [2.7]$$

where ρ_{HUMIC} is the charge density of the humic. The boundary conditions are (Bartschat et al 1992, Bryan et al 2000),

$$\left(\frac{\partial \psi}{\partial r} \right) \Big|_{r=0} = 0$$

and,

$$\psi_r \rightarrow 0 \text{ as } r \rightarrow \infty$$

The magnitude and shape of the potential is dependent upon the humic charge: the potential at any point increases with increasing humic charge, but decreases with increasing ionic strength. In addition, the extent of the double layer is affected, shrinking or compressing as ionic strength increases. Using these equations, the potential generated by the humic charge as a function of distance from the center of each particle was calculated although only the potential at the colloid/diffuse layer boundary, ψ_R , was carried forward.

The methods of Hogg et al (1966) and Wiese and Healy (1970) were used to calculate the Coulombic interaction energy, Φ_{Coul} , as a function of d , the surface-surface separation of the two particles (labelled 1 and 2) (Figure 15)

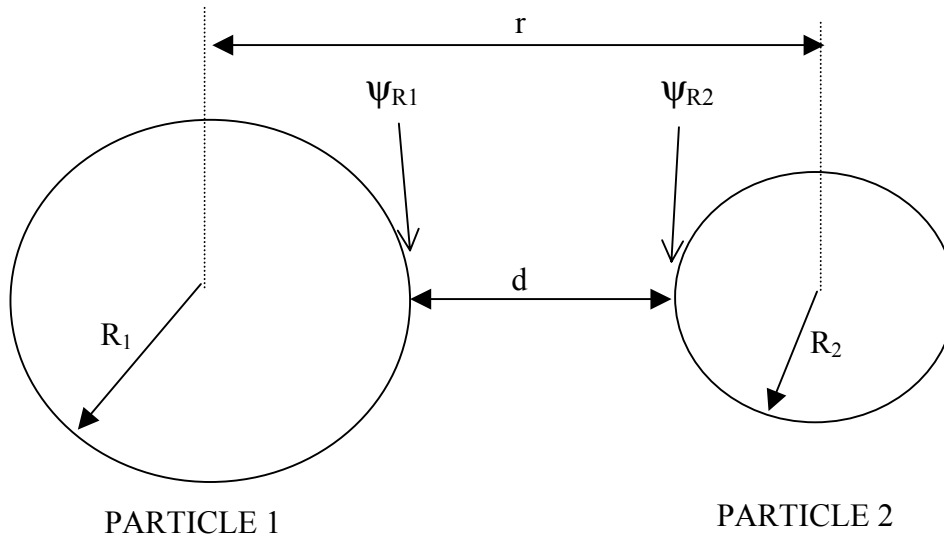


FIGURE 15: parameters used to calculate Φ_{Coul} . Note, the particles may be dissimilar.

If R_1 and R_2 are the radii of particles 1 and 2 respectively, and ψ_{R1} and ψ_{R2} are their surface potentials, then the Coulombic interaction energy will be given by:

$$\Phi_{\text{Coul}} = \pi \epsilon R_1 R_2 \left(\frac{(\psi_{R1})^2 + (\psi_{R2})^2}{R_1 + R_2} \right) \left[\left(\frac{2\psi_{R1} \cdot \psi_{R2}}{(\psi_{R1})^2 + (\psi_{R2})^2} f(d) \right) - \ln(1 - \exp(-2\kappa d)) \right]$$

where the function, $f(d)$, is defined by,

$$f(d) = \ln \left(\frac{1 + \exp(-\kappa d)}{1 - \exp(-\kappa d)} \right)$$

and κ is the ionic strength dependent Debye-Huckel parameter,

$$\kappa = \sqrt{\frac{2e^2 N_A I}{\epsilon k T}}$$

The attractive, Van der Waals interaction energy, Φ_{ATT} , will be given by (Hiemenz and Rajagopalan 1997)

$$\Phi_{ATT} = -\frac{A}{6} \left[\frac{2R_1 R_2}{d^2 + 2R_1 d + 2R_2 d} + \frac{2R_1 R_2}{d^2 + 2R_1 d + 2R_2 d + 4R_1 R_2} + \ln \left(\frac{d^2 + 2R_1 d + 2R_2 d}{d^2 + 2R_1 d + 2R_2 d + 4R_1 R_2} \right) \right]$$

Combining the repulsive, Coulombic and attractive, Van der Waals energies provides the total interaction energy, Φ_T ,

$$\Phi_T = \Phi_{Coul} + \Phi_{ATT}$$

Figure 16 shows examples of total interaction energy plots along with the corresponding Coulombic and Van der Waals contributions. There are 3 general shapes of interaction profile. In the case where the Coulombic term dominates over the Van der Waals for all values of d , for example where the particles have high surface potentials, then the total interaction energy becomes increasingly positive (repulsive) as the particles approach (Figure 16A). Under these conditions, it is not possible for a stable doublet to form when the two particles come into contact. Alternatively, in the case of low surface potentials, where the Van der Waals interaction dominates, then the interaction becomes steadily more negative (attractive) as the separation decreases (Figure 16B). In this case, a stable doublet will form and the process will be diffusion limited (fast). Finally, when the Coulombic and Van der Waals contributions are more evenly balanced, then the characteristic shape shown in Figure 16C is obtained. The Coulombic interaction is a longer range effect than the Van der Waals, and therefore, initially the total interaction energy increases as the particles get closer, but at very short separations, the attractive contribution dominates, and the total becomes more negative. The result is that a potential well forms at small d , which is preceded by a 'Coulomb barrier'. In these cases, the particles may form a doublet when they come into contact, the stability of which will depend upon the depth of the potential well. However, the particles first must overcome the Coulomb barrier. The effect is that the aggregation process will be slow, and the rate will depend directly upon the height of the barrier.

For a system containing two distinct particle populations, 1 and 2, with particle concentrations (particles/m³) of N_1 and N_2 respectively. The rate of loss of particle type 1, via aggregation will be given by,

$$\frac{dN_1}{dt} = -\alpha N_1 N_2 \quad (\approx -k' N_1)$$

where the definition of α depends upon the form of the total interaction energy profile. While the particle concentrations do not change significantly, α and N_2 can be combined to produce a pseudo first order rate constant, k' .

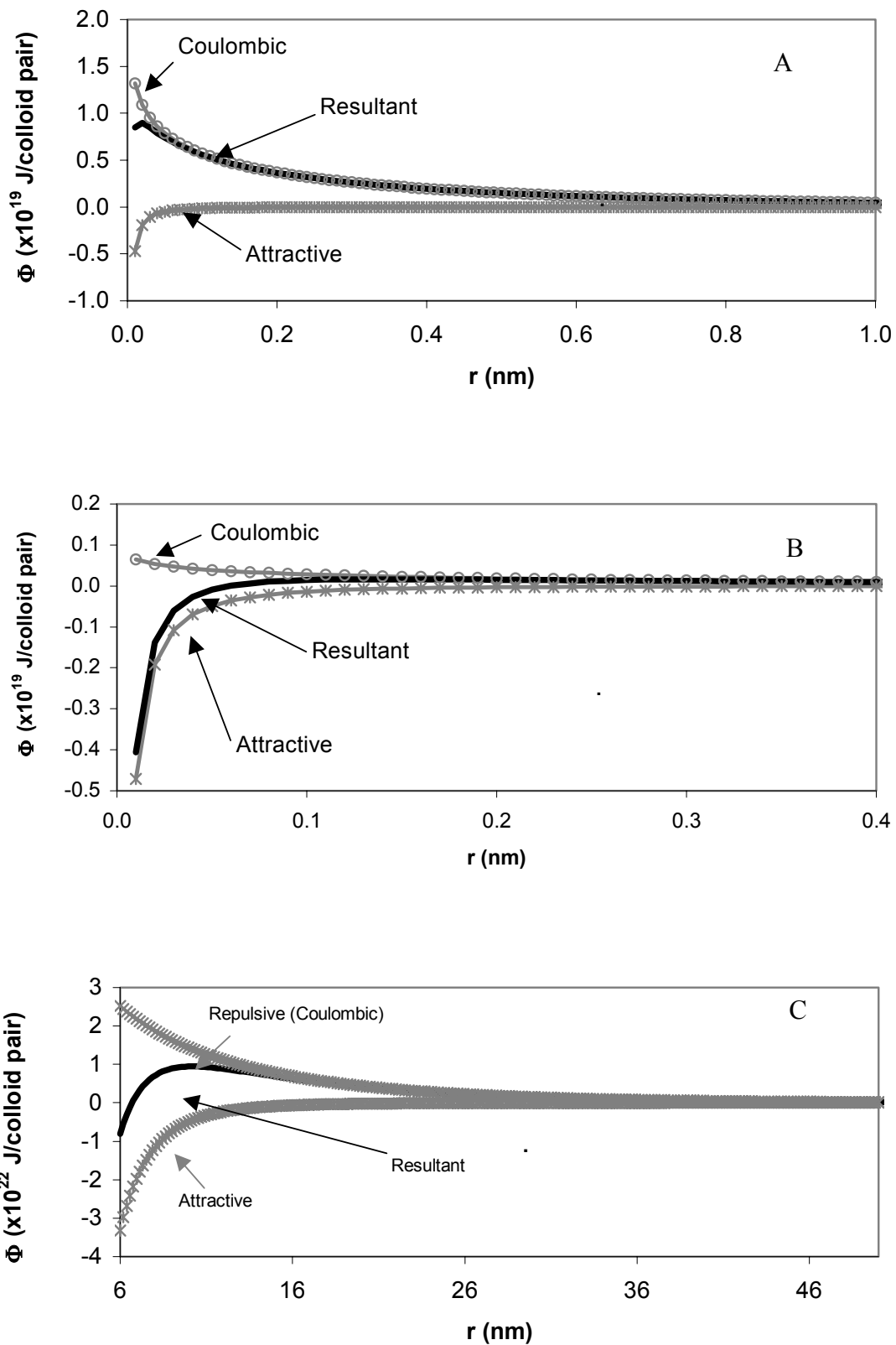


FIGURE 16: the three types of potential energy profile: A - Coulomb dominated; B - Van der Waals dominated; C - balanced, giving a Coulomb barrier and a potential well.

Fast aggregation (diffusion limited)

In the case of a profile of the type shown in Figure 16B (attractive interaction dominated), the rate of aggregation will be diffusion limited. In this case, α_f , will be given by (Hiemenz and Rajagopalan 1997),

$$\alpha_f = 4\pi(R_1 + R_2) \cdot \left(\frac{kT}{6\pi\eta R_1} + \frac{kT}{6\pi\eta R_2} \right)$$

where the subscript, f, denotes that this result is for fast aggregation.

Slow aggregation (Coulomb barrier limited)

In the case of a significant Coulomb barrier, α_s , is given by (Hiemenz and Rajagopalan 1997),

$$\alpha_s = \frac{4\pi \left(\frac{kT}{6\pi\eta R_1} + \frac{kT}{6\pi\eta R_2} \right)}{\int_0^{\infty} \frac{\exp\left(\frac{\Phi_{\text{Coul}}(r) + \Phi_{\text{ATT}}(r)}{kT}\right)}{r^2} dr}$$

where the subscript, s, denotes the fact that this result is for slow aggregation, r is the separation of the particle centres (Figure 15, note $r \neq d$), and $\Phi_{\text{Coul}}(r) + \Phi_{\text{ATT}}(r)$ are the Coulomb and Van der Waals interaction energies at r respectively.

3.3.4 Humic aggregation rate distributions

All real humic samples are highly polydisperse, and therefore, it is not possible to define a single value of α that describes all the aggregation reactions that might take place. Rather, there will be a unique value of α for each possible combination of particle types.

Figure 17 shows the variation in α for the WBPFA2 peat humic acid at pH 6 and I=0.1. As for all of the following distributions of rates, values were calculated using the size and charge distributions calculated from the electrophoretic mobility data (as described above). In order to calculate a particular value of alpha it is necessary to define the two particle types, 1 and 2. The procedure adopted here was to define particle 1 (M_1) first and then in series define each of the species in the distribution as particle 2 (M_2). The figure shows the results of two such series of calculations, the first for a particle 1 mass (M_1) of 500, and the second for $M_1 = 123,000$. It is clear that the identity of particle 1 does have an impact upon the distribution of α values. The α profiles in Figure 17 are examples of the two general types. For $M_1 = 500$, the values increase with increasing particle 2 masses, because the small particles have very low surface potentials, and hence lower Coulomb terms. As the mass of particle 2 increases, the attractive, Van der Waals, term increases more rapidly than the Coulomb, and hence, α and the rate of aggregation increases. When $M_1 = 123,000$, however, because of the higher surface potential, the Coulomb term increases more rapidly than the Van der Waals, and α generally decreases. That said, there is a slight increase in α for very large values of M_2 , because, although there is an increase in surface potential with mass, the rate of increase is much lower at high mass, which is due to the reduction in particle charge density (e.g. Figure 14). Therefore, the Van der Waals term becomes more significant.

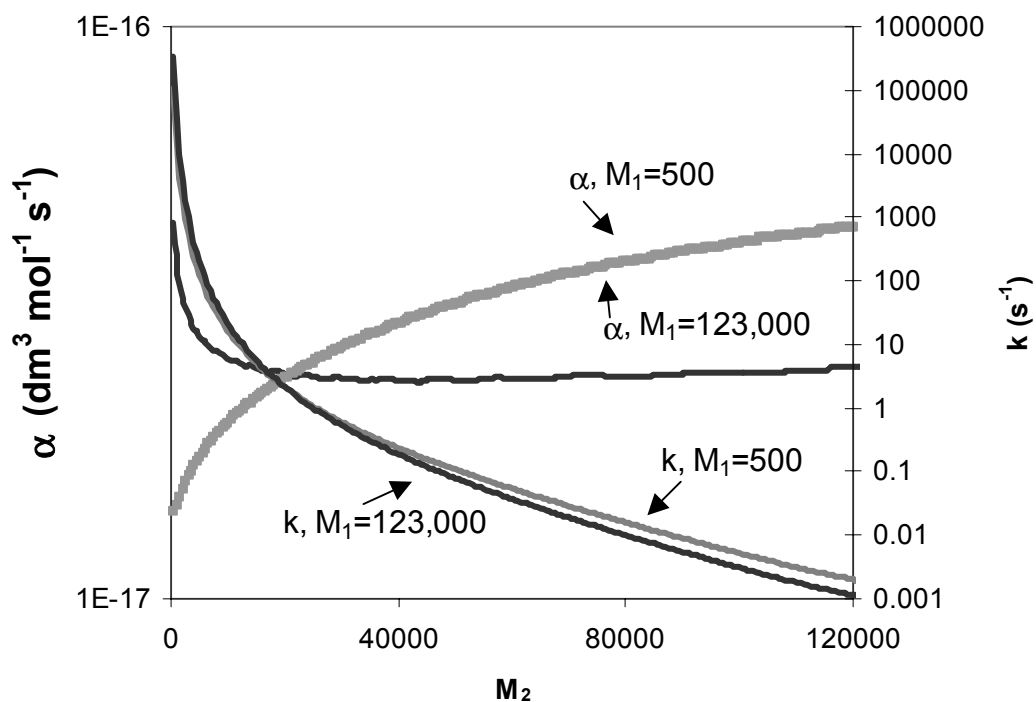


FIGURE 17: calculated α and k' distributions for two particle 1 masses, 500 (grey) and 123,000 (black) for WBPHA2, [HA]=10ppm, pH=6, I=0.1.

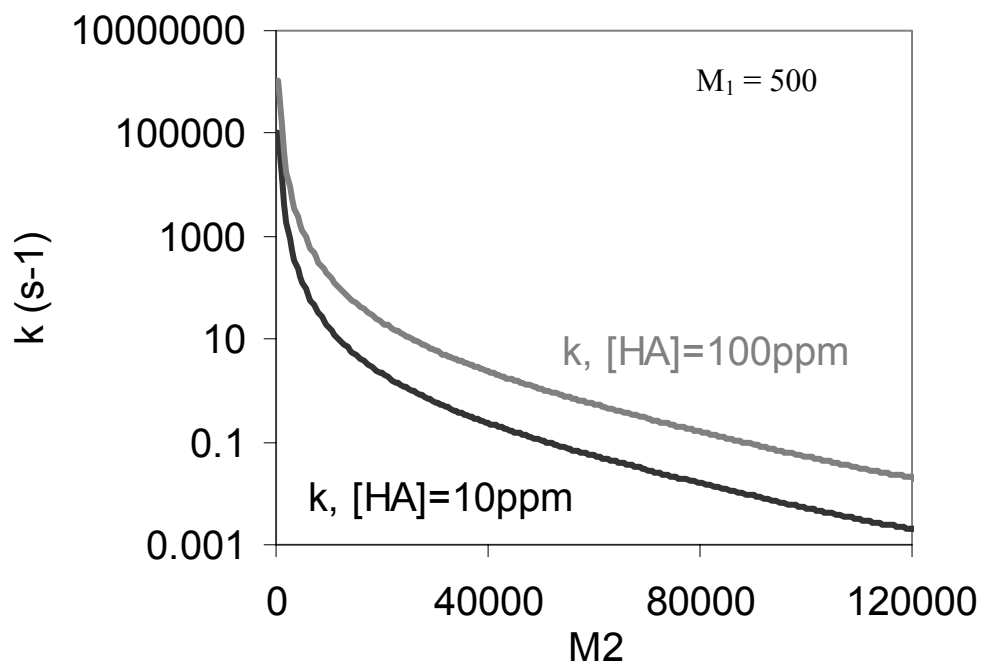


FIGURE 18: calculated k' distributions for two humic concentrations ([HA]), 100ppm (grey) and 10ppm (black), for WBPHA2, $M_1=500$, pH=6, I=0.1.

Figure 17 also shows the corresponding distribution of pseudo first order rate constants, k' ($k'=N_2\alpha$). These values have been calculated using the particle mass distributions measured

by ultracentrifugation. Although the α distributions are radically different, there appears to be much less difference for k' . The particle concentrations (N_2) decrease very significantly with particle mass, in the case of WBPFA2 by a factor of 10^4 between $M=2000$ and $123,000$. Hence, this variation, which will be the same for both series, dominates over the much more modest changes in α .

Figure 18 shows calculated distributions of k' for two humic acid concentrations (10 and 100ppm) for the WBPFA2 sample at $\text{pH}=6$ and $I=0.1$. In both cases, the mass of particle 1 is 500. For all masses of particle 2, the first order rate is higher for the higher humic concentration. This is to be expected, since k' is the product of α (concentration independent) and the concentration of particle type 2.

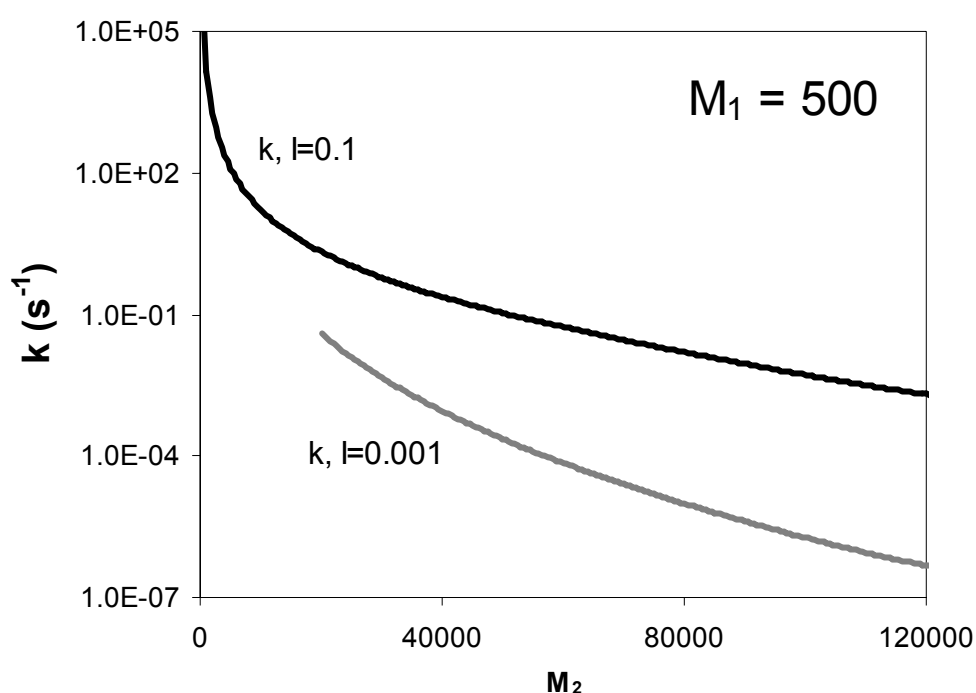


FIGURE 19: calculated k' distributions for two ionic strengths, 0.001 (grey) and 0.1 (black), for WBPFA2, $M_1=500$, $[\text{HA}]=10\text{ppm}$, $\text{pH}=6$.

The effect of ionic strength on pseudo first order rate distributions is demonstrated in Figure 19. There is a significant reduction in the predicted rates for $I=0.001$ for all particle 2 masses. The Coulomb term is highly sensitive to ionic strength: at lower ionic strengths, the humic charge is less shielded, and the surface potentials are higher, which leads to increased repulsion, and hence lower rates. The ionic strength effect is larger than the effect of humic concentration, and for the larger particle 2 masses, the rates are starting to approach those rates observed for metal ions in batch experiments, which are typically of the order of 10^{-7} s^{-1} (King et al 2001).

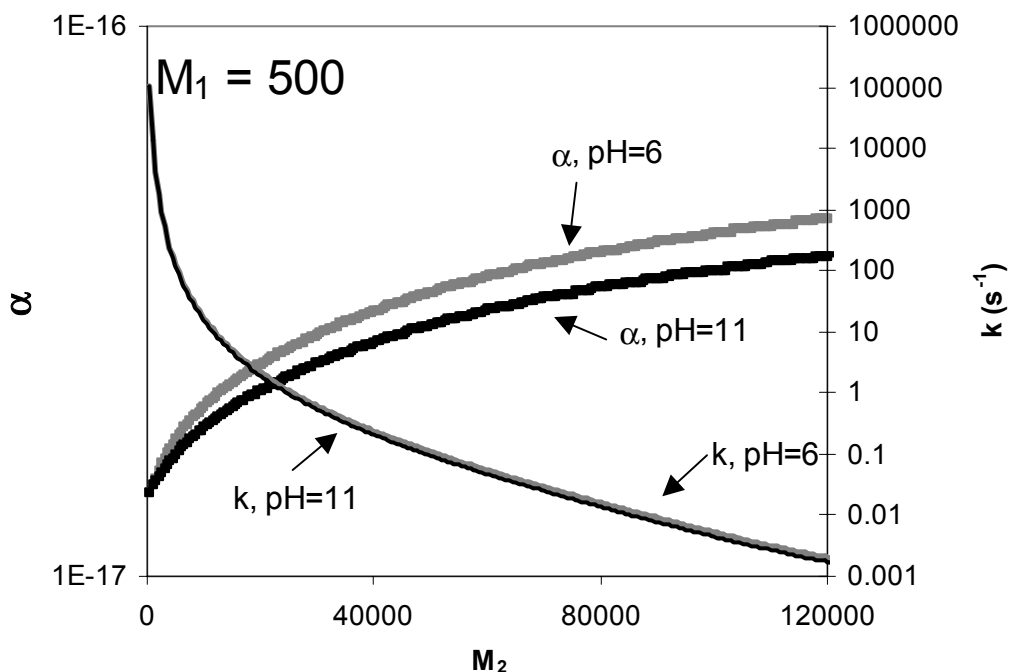


FIGURE 20: calculated α and k' distributions for two values of pH, pH=6 (grey) and pH=11 (black) for WBPFA2, $M_1=500$, $[HA]=10\text{ppm}$, pH=6, $I=0.1$.

Figure 20 shows the effect of pH on the values of α and first order rate for the same system as the previous figures. The change in pH has had very little effect upon the distribution of α values, and virtually none on the first order rates. At first sight, this may seem strange, since the humic species will have higher charges at pH 11, and one might expect a similar Coulomb effect to that observed with ionic strength (Figure 19). In fact, the raw electrophoretic mobility data (Figure 9) help to explain this result. As pH increases from pH=6 to pH=11, the electrophoretic mobility remains virtually constant, even though the charge increases. The explanation is that the humic structure expands, maintaining an almost constant charge density, due to electrostatic self-repulsion. Here, the Coulomb term does not increase dramatically, because the expansion (and hence, constant charge density) produces only a very modest increase in the magnitude of the surface potentials, and hence a small decrease in α . The values of the first order rates are dominated by the variation in particle concentration with mass (see above), and hence, the k' distribution appears almost unaffected.

3.3.5 Discussion

There are certain characteristics of the metal ion-humate non-exchangeable interaction that any proposed mechanism must be able to explain (Keepax et al 2002; King et al 2001; unpublished data):

1. All metal ions show very similar rates of transfer from exchangeable to the longest lived non-exchangeable fraction and similar rates of desorption.

2. The rates are insensitive to total metal ion concentration and humate/metal ion ratio.
3. The relative occupations of the exchangeable and non-exchangeable fractions do vary: the non-exchangeable is maximised for metal ions of the highest valency, and also for the lower metal ion concentrations.
4. Batch experiments at 10 and 100ppm have shown that, although the absolute amount entering the non-exchangeable fraction does increase, there is no significant change in rate with humic concentration.
5. In batch experiments, the maximum occupation of the non-exchangeable site is at an intermediate ionic strength. However, the rate of desorption is virtually independent of ionic strength, except at $I=1$ where there is a slight decrease, e.g. from 5×10^{-7} to $2 \times 10^{-7} \text{ s}^{-1}$.
6. There is very little effect of pH on either association or desorption rates.
7. Although there is a distribution of fast and intermediate desorption rates, there is a distinct long lived fraction which accounts for a significant amount of the non-exchangeable metal, and which has a discrete, single first order desorption rate constant.

We should now compare the predicted rates with these **real** observations. Unfortunately, given the state of the modelling, we are only able to examine the association (exchangeable → non-exchangeable) rates.

In some cases, the behaviour predicted for the self-association mechanism is consistent with the experimental data. For example, very little effect of pH is predicted by the model. Similarly, at low to moderate metal loadings, where the total charges of the humic species are still significant, we would not expect a very significant change in the rates, because the electrophoretic mobility experiments show that the mobility of the samples remains constant as metal binds, analogous behaviour to that observed when the humic charge is affected by pH. Further, the origin of the rates is entirely 'physical' in nature and the chemical identity of any bound metal would not have any effect, and therefore, at least for metal ions of the same charge, there would be no difference in predicted rates.

Beyond the expected very small difference due to the variation in neutralisation, the current model would predict that valency would not affect the rates significantly, which is consistent with experiment. As for the observation that valency affects the distribution of metal ions between the exchangeable and non-exchangeable fractions, the current model is unable to comment. If the self-association process is responsible for the non-exchangeable interaction, then it may be that there is some difference in the binding of metal ions to the 'monomer' units, which might affect the amount that is trapped by the aggregation.

There are a number of discrepancies between the predicted rates and experiment. In real systems, there is a single, discrete, longest-lived fraction, which accounts for a significant fraction of the non-exchangeable metal, and may be described by a single pair of forward and backward first order rate constants. However, the calculations predict that the first order rates of aggregation will vary greatly across the distribution of particle masses. There is certainly no evidence for a single, consistent aggregation rate, and it is hard to see how these theoretical rate distributions can tally with the real behaviour.

The effect of humic concentration on the predicted rates is also anomalous: the model predicts increases in rates, where none is observed. The ionic strength effect is also problematic. A very large effect is predicted for aggregation rates, but no significant change is observed in experiments. Also, the model predicts a consistent and sustained change in behaviour with ionic strength: the Coulomb term will be highest at the lowest ionic strength, and it could never explain maximum population at an intermediate value.

The final problem is that the predicted rates are too high. Only at the lowest ionic strength do the self-association rates start to approach those of the non-exchangeable fraction.

Therefore, in some ways, the self association rates predicted by the model are consistent with the metal ion non-exchangeable fraction rates. However, in other ways they are not. In order for the self-association mechanism to be responsible for the non-exchangeable behaviour, at least in the absence of some other, additional mechanism, then it must be consistent with **all** of the experimental data.

The model predicted rate constants derived from the electrophoretic mobility data are not reproducing the behaviour seen in the metal ion desorption batch experiments, and the conclusion must be that for these systems, the self-association mechanism does not seem to be responsible for the observed metal ion kinetics. However, it would be useful to know whether it is possible, given the appropriate potentials/charges etc., for the self association process ever to show rates of the correct order. The requirement is that two particles have a potential interaction profile with a Coulomb barrier, which retards aggregation sufficiently to give a first order rate of approximately $1 \times 10^{-7} \text{ s}^{-1}$ **and** a potential well at short separations, so that the doublet will be stable.

Figure 21 shows the potential energy profile for two mass 50k colloids with surface potentials of -87mV. At this surface potential, the predicted first order rate is $1 \times 10^{-7} \text{ s}^{-1}$ and the model also predicts a stable doublet. Therefore, under the right conditions it would be possible for the self-association process to result in rates of the correct order. The problem is that although ultracentrifugation measurements show that particles of mass 50k do exist in the sample, the electrophoretic mobility experiments strongly suggest that their surface potentials cannot be -87mV.

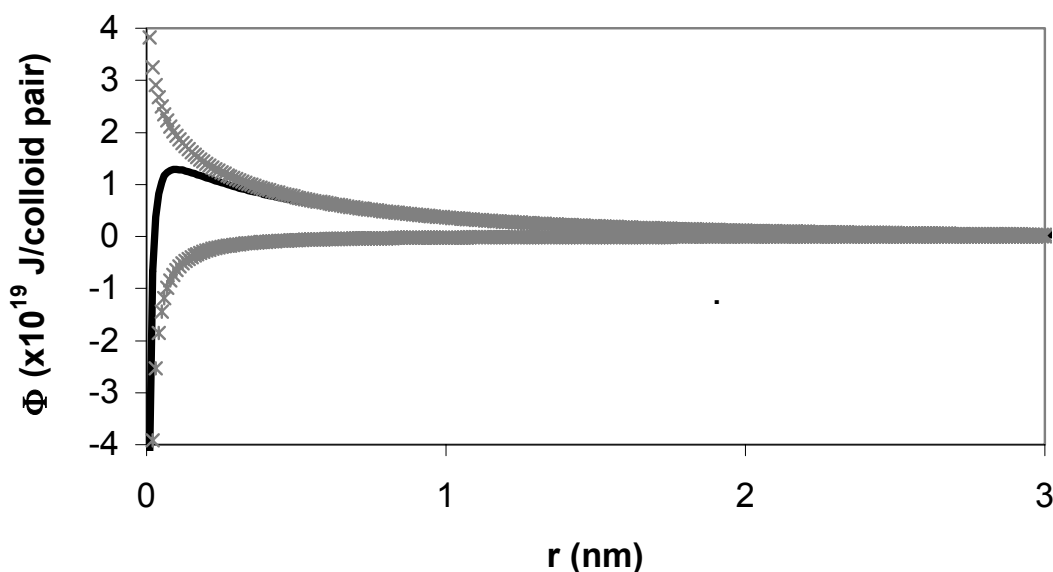


FIGURE 21: calculated potential energy plot, $I = 0.1$, $M_1 = M_2 = 50k$, $\psi_1 = \psi_2 = 87$ mV $R_{S1} = R_{S2} = 2.53 \times 10^{-9}$ m.

For other particle masses, it is much more difficult to construct systems that generate the correct conditions. For example, for two mass 500 species, at any realistic surface potential, the rates are far too fast. Figure 22A shows a profile for two particles of masses 500 and 50k with surface potentials of -2 and -400mV respectively. This combination of parameters does give a first order aggregation rate of $1 \times 10^{-7} \text{ s}^{-1}$. However, there is no potential well, and so the doublet would dissociate immediately. More than this, the surface potential required for the large particle is hardly realistic. Figure 22B shows the predicted profile for the mass 500 particle interacting with the same $M=50k$, -87mV species that produced the correct rate in Figure 21. However, when this particle interacts with the $M=500$ species, the figure shows that there is no Coulomb barrier at all, and the rate is predicted to be diffusion limited, i.e., $k' = 1 \times 10^6 \text{ s}^{-1}$. Hence, even if certain members of a mass distribution do aggregate at the correct rate, then other aggregations will have rates that are either much higher or lower.

It seems that, although it is possible in theory for processes of this type to have aggregation rates of the correct magnitude, in the case of humic substances, a single rate across the population is not likely due to the polydisperse and highly unequal mass distribution, and also variations in surface potential.

The conclusion must be that regardless of whether the model is constrained by the electrophoretic mobility data, or arbitrary parameters are used, it seems unlikely that the self-association mechanism can be responsible for the metal ion non-exchangeable behaviour. However, it is important to appreciate that although the modelling suggests no link between aggregation and non-exchangeable behaviour, it certainly does not imply that the self-association process itself will not take place. On the contrary, the model predicts that

aggregation of the 'monomer' units within the mass distribution should take place. Hence, if the non-exchangeable behaviour occurs as a result of the collapse of the humic structure around a metal ion and the formation of a hydrophobic zone, then it may be that self-association provides the large species for this mechanism.

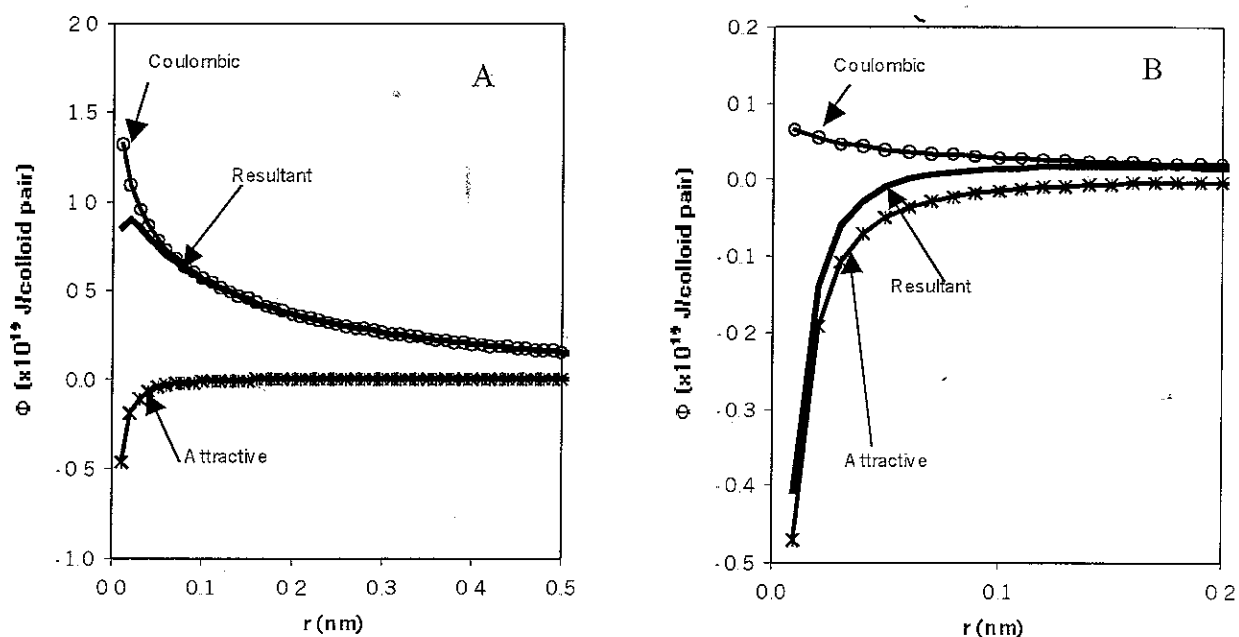


FIGURE 22: calculated potential energy plots: A - $I = 0.1$, $M_1 = 50k$; $M_2 = 500$, $\psi_1 = 400$; $\psi_2 = 2$ mV; B - $I = 0.1$, $M_1 = 50k$; $M_2 = 500$, $\psi_1 = -87$; $\psi_2 = -2$ mV

4 Natural kinetics (Natural anthropogenic analogue study)

4.1 Introduction

Most kinetic studies to date have involved ‘synthetic’ metal-humate complexes. That is, metals and humics are mixed in the laboratory, and allowed to equilibrate, before the desorption kinetics are measured. However, it is important to study the desorption of metal ions incorporated via natural processes to determine whether parameters determined in synthetic experiments may be applied with validity in the field.

A soil sample was collected from the bank of the Esk Estuary, West Cumbria, UK National Grid Reference SD113964. Sites adjacent to BNFL Sellafield provide a rare opportunity to study the kinetics of a humic acid sample ‘naturally’ enriched with anthropogenic actinides, for example Am and Pu. Essentially, all the Am and Pu in the soil in the area around the site arise from radioactive waste disposals from Sellafield, 10-12 miles away.

The soil sample (approximately 50 cm x 15 cm) was sectioned into five portions, and analysed using gamma ray spectrometry to measure the activity of ²⁴¹Am. The activity of ²⁴¹Am was found to be constant throughout the sample.

4.2 Experimental

Extraction of the Humic Acid

The soil sample was sieved through a 2.0 mm mesh. A suitable amount of undried soil was placed in a beaker (2000.0 ml). NaOH (0.5 M) was added, in the ratio 5.0 g soil (wet weight): 10.0 ml NaOH. The pH of the mixture was checked, to make sure that it was above pH = 10. The mixture was stirred overnight at room temperature, covered, and allowed to settle for 24 hours. The solution was decanted, centrifuged for 45 minutes (3000 rpm), and the supernatant collected.

In these experiments, the term ‘natural’ corresponds to the Am and Pu already present in the soil from the Sellafield discharges. The radiotracers added to the humic acid in the laboratory (Am and Eu) are defined as ‘artificial’.

Desorption of the ‘Natural’ Americium

The resulting humic acid solution (400.0 ml) was adjusted to pH = 6 ± 0.1 using AnalaR HNO₃. Cellulose phosphate sodium salt (25.0 g) was added to the humic acid solution in a sterile 1000 ml container. The sample was laid on its side and left to shake at 25°C in a thermostated water bath. Aliquots of the solution (100.0 ml) were removed and analysed using gamma ray spectrometry to measure the concentration of solution phase ²⁴¹Am.

To test for reproducibility, the experiment was repeated using a different soil sample taken from the same site.

Desorption of Radiotracer Americium and Europium

A spike of radioactive tracer, either ^{241}Am (2.0 kBq) or ^{152}Eu (4 kBq) was added to the same humic solution, which had already been used in the previous natural desorption experiment, and allowed to equilibrate for 7 days (Note, most of the 'natural' ^{241}Am had already been removed during the preceding experiment. Cellulose phosphate sodium salt (25.0 g) was added to the solution and the desorption experiment described above was repeated. Aliquots of the solution (25.0 ml) were removed and analysed using gamma ray spectrometry to measure the concentration of solution phase ^{241}Am or ^{152}Eu .

Desorption of the 'Natural' Plutonium ($^{239,240}\text{Pu}$.)

Cellulose phosphate sodium salt (25.0 g) was added to the humic acid solution ($\text{pH} = 6 \pm 0.1$, 400.0 ml) in a sterile 1000 ml container. The sample was laid on its side and left to shake at 25°C in a thermostated water bath. Aliquots of the solution (3.0 ml) were removed at regular intervals and kept for analysis. This time, the aliquots were not returned to the experiment.

Plutonium Chemical Separation

Pyrex glass columns (10.0 cm x 0.6 cm) were used for the standard separation. The column was prepared by plugging with glass wool and packing with Bio-Rad AG1-X8 anion exchange resin (100-200 mesh) to a depth of 4.0 cm. The column was pre-conditioned with 20.0 ml of 9 M HCl prior to sample elution.

Each humic sample (3.0 ml) was added to a 20.0 ml pyrex glass beaker. To each beaker, 16 M HNO_3 (10.0 ml) (to destroy the organic matter), ^{242}Pu (0.04 Bq) (to monitor the efficiency of the chemical separation), and NaNO_3 (80.0 mg) (to fix the oxidation state of Pu to Pu(IV)) were added, and the samples heated on a hotplate at 60°C . Each solution was evaporated to dryness, followed by the addition of a further 10.0 ml of 16 M HNO_3 . This process was repeated, until the solution became clear. A total of 50.0 ml of 16 M HNO_3 was used for each sample.

12 M HCl (5.0 ml) was added to each sample which was then evaporated to dryness to destroy the HNO_3 . 9 M HCl (10.0 ml) and 16 M HNO_3 (0.4 ml) were added and the solutions left to reflux gently ($40\text{-}50^\circ\text{C}$) for 45 minutes. The resultant solutions were left to cool for 20 minutes and then passed through a preconditioned column on which plutonium was retained as the anionic $[\text{Pu}(\text{NO}_3)_6]^{2-}$ complex. The column was washed successively with 9 M HCl (15.0 ml), 8 M HNO_3 (15.0 ml), and 12 M HCl (15.0 ml) to eliminate the other actinides from the column whilst retaining the Pu in anionic form. Finally, the Pu was eluted from the column by reduction to neutral PuCl_3 with a mixture of 11.5 M HCl/0.2 M HI (15.0 ml).

The final eluent was evaporated to dryness in the presence of KHSO_4 (10% w/v) carrier solution (1.0 ml). A few drops of 16 M HNO_3 were added in order to oxidise the iodine and the sample evaporated to dryness again. Finally, the sample was converted back to chloride

form with a few drops of 12 M HCl, and taken to dryness. The residue was dissolved in electrolyte solution (4% ammonium oxalate w/v dissolved in 0.3 M HCl) (12.5 ml) and transferred to a prepared electrolysis cell.

The electrolysis cell consisted of two threaded glass tubes (SV 30, Orme Scientific, Manchester) held together with a SV 30 plastic joint. A highly polished stainless steel planchette (cathode) was held in place by a recessed brass planchette mount supported by the lower electrode. The cell was sealed with a Teflon 'o' ring. A length of Pt wire (anode), encased in narrow glass tubing, was inserted through a rubber bung into the electrolyte solution to complete the cell. Electrodeposition was carried out at a current of 0.5 A, and a potential of 15-20 V for 2 hours. 2 minutes before removing the planchette, concentrated ammonia solution (2.0 ml) was added to the electrolyte. The cell was washed with deionised water (250.0 ml), dismantled, and the planchette removed. The source was rinsed with a small amount of deionised water (10.0 ml) and then acetone (5.0 ml) to remove any traces of electrolyte. The sample was allowed to dry in air before analysis for $^{239,240}\text{Pu}$, using a solid state α -particle spectrometer. Note, the technique does not allow resolution of ^{239}Pu and ^{240}Pu , and therefore, the activity is the sum of the two, $^{239,240}\text{Pu}$.

4.3 Results

The $(C/C_0)_{t=0}$ values quoted below correspond to the relative amount of isotope bound in the longest lived non-exchangeable fraction before any desorption takes place. $(C/C_0)_{t=0}$ values are given as percentages of the total initial concentration.

The desorption of the natural Am from the sample was repeated twice, starting from scratch with two separate aliquots of soil, and proceeding through two separate extraction and desorption series. The results are shown in Figure 23. The results from the two experiments are clearly concordant both in terms of $(C/C_0)_{t=0}$ and rates, despite the fact they are based upon separate samples of soil. Therefore, even if there is some inherent heterogeneity in the soil from the site, it does not seem to affect the desorption kinetics.

Generally, the form of the plots is very similar to those for completely synthetic batch experiments (metal ion and humate mixed in the lab). There is a sharp drop at the start as any exchangeable isotope is removed, followed by a period when isotope fractions with intermediate rates desorb, and finally the plots show the linear shape that is typical of the longest lived, non-exchangeable fraction. Figure 24 shows the desorption data for the natural $^{239,240}\text{Pu}$ (one experiment only). Once again the same general exchangeable, intermediate and slow non-exchangeable behaviour is evident. The fitted first order desorption rate constants and $(C/C_0)_{t=0}$ values for the natural isotopes are given in Table 3.

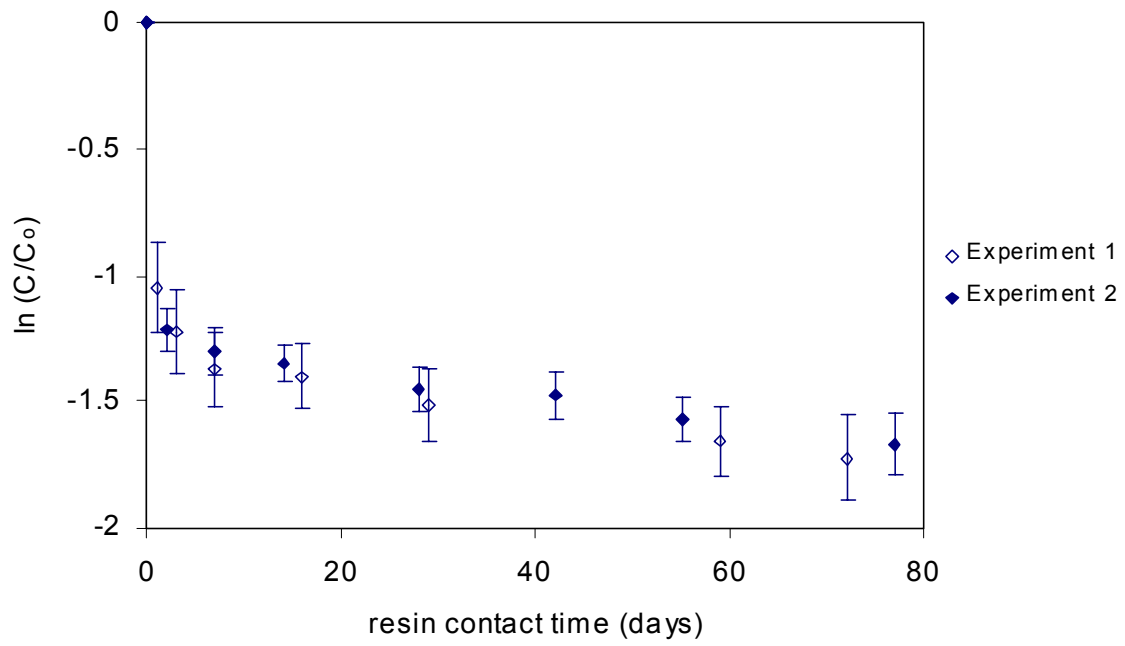


FIGURE 23: Desorption of natural ²⁴¹Am from Esk humic acid at pH = 6 ± 0.1.

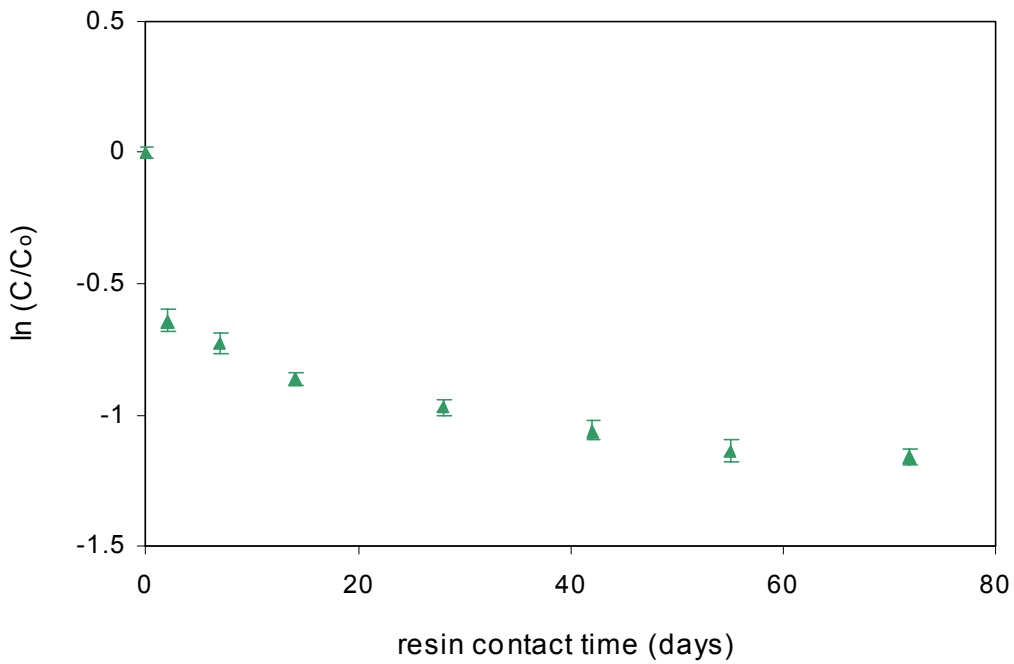


FIGURE 24: Desorption of natural ^{239,240}Pu from Esk humic acid sample at pH = 6 ± 0.1.

TABLE 3: Total atom concentrations and kinetic data for Esk humic systems. N.B. there is a range of atom concentrations for the $^{239,240}\text{Pu}$ system*, because the two isotopes have different half-lives, but the relative concentrations of the two are unknown. Therefore, the concentration of Pu lies in this range

Isotope (system)	Total atom concentration (mol dm ⁻³)	First order rate (s ⁻¹) (2σ error)	(C/C ₀) _{t=0} (%) (2σ error)
‘natural’ ^{241}Am	1.8×10^{-12}	5.9×10^{-8} (18 %)	28 (1 %)
‘natural’ $^{239,240}\text{Pu}$	$5.3 - 19.4 \times 10^{-11}$ *	6.1×10^{-8} (40 %)	44 (10 %)
‘artificial’ ^{241}Am	1.6×10^{-10}	4.9×10^{-8} (11 %)	14 (3 %)
‘artificial’ ^{152}Eu	1.0×10^{-11}	4.9×10^{-8} (26 %)	7 (2 %)

Figure 25 shows the artificial Am and Eu desorption data compared with the mean result from the two natural Am experiments. The rates and (C/C₀)_{t=0} values are given in Table 3.

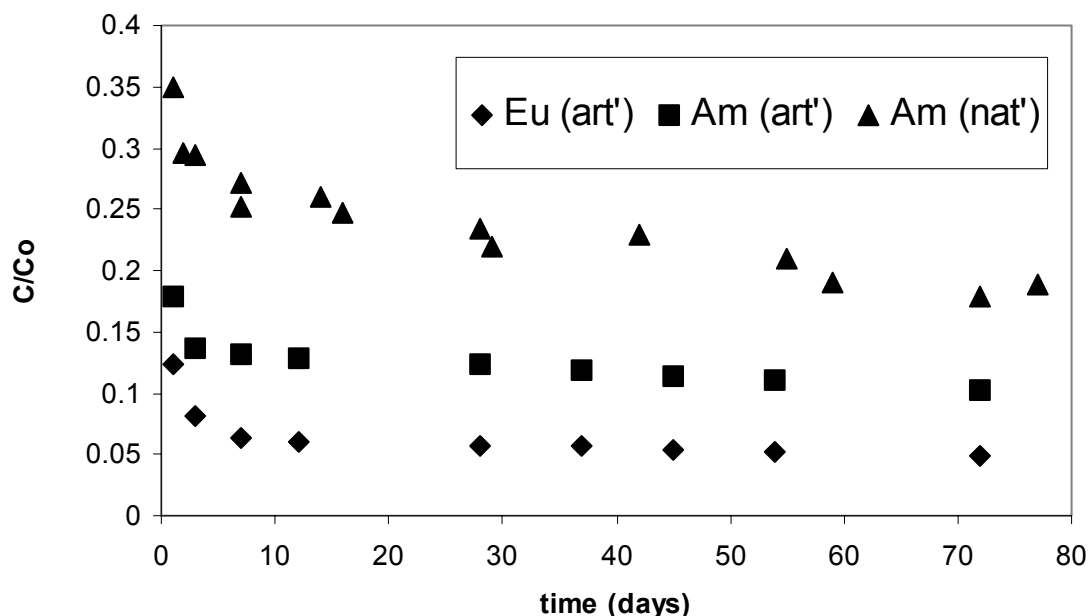


FIGURE 25: desorption of natural (nat') Am and artificial (art') Am and Eu from Esk humic.

The natural desorption rates are significantly lower than those obtained from standard synthetic batch experiments, which are typically of the order of 10^{-7} s^{-1} (King et al 2001), compared with 10^{-8} s^{-1} here. The automatic assumption might be that the very long equilibration time is responsible. However, the desorption rates for isotopes only equilibrated for a few days are the same. The only other significant difference between these experiments and the synthetic batch experiments is the humic concentration, 300ppm, compared to 10ppm typically. It is possible that this is responsible for the difference. In fact, all of the isotopes regardless of the origin (natural or artificial) or chemistry (Eu, Am, Pu) show the same desorption rates. This would suggest that it is some property of the humic itself that is

responsible for the magnitude of the desorption rate, and more than that, it must be some process that operates on a timescale of days rather than years, at least in this particular case. No evidence has yet been found for any 'irreversible' or pseudo-irreversible behaviour.

The $(C/C_0)_{t=0}$ values are different for the various systems. There are several possible factors that could explain the difference: the very different equilibration times; the different atom concentrations; the different chemistries. The two natural systems have higher values, and this may be due to the long equilibration time. However, it is hard to separate the influences of the various possible factors. The artificial Am has a lower $(C/C_0)_{t=0}$ value than the natural Am. However, it also has a much higher atom concentration. Batch experiments have shown that changing metal atom to humic concentration ratios do affect $(C/C_0)_{t=0}$ (King et al 2001). Therefore, the difference may just be due to the metal/humic ratio rather than the equilibration time. The natural Pu $(C/C_0)_{t=0}$ value is higher than the natural Am value, although it has a higher atom concentration. Therefore, it seems likely that this difference at least must be due to their different chemistries.

These are preliminary findings, and experiments are continuing.

References

Bartschat, B.M., Cabaniss, S.E. and Morel, F.M.M. (1992) Oligoelectrolyte model for cation binding by humic substances. *Environmental Science and Technology*, 26, 284-294.

Benedetti, M.F., Van Riemsdijk, W.H. and Koopal, L.K. (1996) Humic substances considered as a heterogeneous donnan gel phase. *Environmental Science and Technology*, 30, 1805-1813.

Bryan, N.D., Jones, D.M., Appleton, M., Livens, F.R., Jones, M.N., Warwick, P., King, S.J. and Hall, A. (2000) A Physicochemical Model of Metal-Humate Interactions. *Physical Chemistry Chemical Physics*, 2, 1291-1300.

Bryan, N.D., Jones, M.N., Birkett, J. and Livens, F.R. (2001a) The application of a new method of analysis of ultracentrifugation data to the aggregation of a humic acid by cupric ions. *Analytica Chimica Acta*, 437, 281-289.

Bryan, N.D., Jones, M.N., Birkett, J. and Livens, F.R. (2001b) Aggregation of humic substances by metal ions measured by ultracentrifugation. *Analytica Chimica Acta*, 437, 291-308.

Cacheris, W.P. and Choppin, G.R. (1998) Dissociation kinetics of thorium-humate complex. *Radiochimica Acta*, 42, 185-190.

Chakrabati, C.L., Lu, Y., Gregorie, D.C., Back D.C. and Schroeder W.H. (1994) Kinetic studies of metal speciation using chelex cation exchange resin: application to cadmium, copper and lead speciation in river water and snow. *Environmental Science and Technology*, 28, 1957-1967.

Choppin, G.R. (1988). Humics and radionuclide migration. *Radiochimica Acta*, 44/45, 23-28.

Choppin, G.R. and Clark, S.B. (1991) The kinetic interactions of metal ions with humic acid. *Marine Chemistry*, 36, 27-38.

Conte, P. and Piccolo, A. (1999) Conformational arrangement of dissolved humic substances. Influence of solution composition on association of humic molecules. *Environmental Science and Technology*, 33, 1682-1690.

Dierckx, A., Hall, A., De Canniere, P., Warwick, P., Put, M. (1998) Stability of I-125 and C-14 labelled boom clay organic matter. *Radiochimica Acta*, 82, 379-384.

Engbretson, R.R. and Von Wandruszka, R. (1998) Kinetic aspects of cation-enhanced aggregation in aqueous humic substances. *Environmental Science and Technology*, 32, 488-493.

Hayes, M.H.B. and Swift, R.S. (1978) The chemistry of soil organic colloids. In Greenland, D.J. and Hayes, M.H.B. (eds.) *The Chemistry of Soil Constituents*, (179-320), Wiley, London.

Hayes, M.H.B. and Swift, R.S. (1990) Genesis, isolation, composition and structures of soil humic substances. In de Boodt, M.F., Hayes, M.H.B. and Herbillon, A. (eds.) *Soil Colloids and Their Association in Aggregates*, (245-305), Plenum, New York.

Hiemenz, P.C. and Rajagopalan, R. (1997) *Principles of Colloid and Surface Chemistry*. Marcel Dekker, New York.

Hogg, R., Healy, T.W. and Fuerstenau, D.W. (1966) Mutual coagulation of colloidal dispersions. *Trans. Faraday Soc.*, 62, 1638-1651.

Jones, M.N. and Bryan, N.D. (1998) Colloidal properties of humic substances. *Advances in Colloid and Interface Science*, 78, 1-48.

Keepax, R.E., Jones, D.M., Pepper, S.E. and Bryan, N.D. (2002) The effects of humic substances on radioactivity in the environment. in Keith-Roach, M. and Livens, F.R. (eds.) *Microbes and Radionuclides* (pp 143- 177), Elsevier, Amsterdam.

King, S.J., Warwick, P., Hall, A. and Bryan, N.D. (2001) The dissociation kinetics of dissolved metal-humate complexes. *Physical Chemistry Chemical Physics*, 3, 2080-2085.

Lassen, P., Carlsen, L., Warwick, P., Randall, A. and Zhao, R. (1994) Radioactive labelling and characterization of humic materials. *Environment International*, 20, 127-134.

McCarthy, J.F., Czerwinski, K.R., Sanford, W.E., Jardine, P.M. and Marsh, J.D. (1998) Mobilization of transuranic radionuclides from disposal trenches by natural organic matter. *Journal of Contaminant Hydrology*, 30, 49-77.

Moulin, V., Reiller, P., Amekraz, B., Moulin, C. (2001) Direct characterization of iodine covalently bound to fulvic acids by electrospray mass spectrometry. *Rapid communications in mass spectrometry*, 15 (24), 2488-2496.

Piccolo, A. (1997) New insights on the conformational structure of humic substances as revealed by size exclusion chromatography. In Drozd, J., Gonet, S.S., Senesi, N. and Weber, J. (eds.) *The Role of Humic Substances in Ecosystems and in Environmental Protection*, IHSS, Wroclaw, Poland.

Piccolo, A., Nardi, S. and Concheri, G. (1996) Macromolecular changes of humic substances induced by interaction with organic acids. *European Journal of soil science*, 47, 319-328.

Plancque, G., Amekraz, B., Moulin, V., Toulhoat, P. and Moulin, C. (2001) Molecular structure of fulvic acids by electrospray with quadrupole time-of-flight mass spectrometry. *Rapid communications in mass spectrometry*, 15 (10), 827-835.

Read, D. and Falck, W.E. (1996) *CHEMVAL 2: A Coordinated Research Initiative for Evaluating and Enhancing Chemical Models in Radiological Risk Assessment* A Commission of the European Community Report, Contract number: FI2W-CT91-0065, Report No. EUR 16648 EN, ISBN: 92-827-8988-8.

Schulton, H.R. and Schnitzer, M. (1993) A state of the art structural concept for humic substances. *Naturwissenschaften*, 80, 29-30.

Schussler, W., Artinger, R., Kienzler, B., Kim, J.I. (1998) Modelling of humic colloid mediated transport of americium (III) by a kinetic approach. In Buckau, G. (ed.) *Effects of Humic Substances on the Migration of Radionuclides: Complexation and Transport of the Actinides*. (pp 91-101) . Wissenschaftliche Berichte (FZKA 6124, ISSN 0947-8620), Forschungszentrum Karlsruhe Technik und Umwelt, Karlsruhe, Germany

Schussler, W., Artinger, R., Kim, J.I., Bryan, N.D. and Griffin, D. (1999). Modelling of Humic Colloid Borne Americium (III) Migration in Column Experiments Using the Transport/Speciation Code k1-D and the KICAM Model, Paper presented at MIGRATION 99, Chemistry and Migration Behaviour of Actinides and Fission Products in the Geosphere, Lake Tahoe, California, September 26 - October 1, 1999

Schussler, W., Artinger, R., Kim, J.I., Bryan, N.D. and Griffin, D. (2001) Numerical modeling of humic colloid borne americium(III) migration in column experiments using the transport/speciation code K1D and the KICAM model. *Journal of Contaminant Hydrology*, 47, 311-322.

Swift, R.S. (1999) Macromolecular properties of soil humic substances: Fact, fiction, and opinion. *Soil Science*, 164, 790-802.

Tanford, C. (1961) *Physical Chemistry of Macromolecules*. John Wiley and Sons Inc.

Tipping, E. and Hurley, M.A. (1992) A unifying model of cation binding by humic substances. *Geochimica et Cosmochimica Acta*, 56, 3627-3641.

Von Wandruszka, R., Ragle, C. and Engebretson, R., (1997) The role of selected cations in the formation of pseudomicelles in aqueous humic acid. *Talanta*, 44, 805-809.

Warwick, P., Hall, A., Pashley, V., Bryan, N.D. and Griffin, D. (2000) Modelling the effect of humic substances on the transport of europium through porous media: a comparison of equilibrium and equilibrium/kinetic models. *Journal of Contaminant Hydrology*, 42, 19-34.

Wershaw, R.L. (1986) A new model for humic materials and their interactions with hydrophobic chemicals in soil-water or sediment-water systems. *Journal of Contaminant Hydrology*, 1, 29-45.

Wershaw, R.L. (1993) Model for humus in soils and sediments. *Environmental Science and Technology*, 27, 814-816.

Wiese, G.R. and Healy, T.W. (1970) Effect of Size on Colloid Stability. *Trans. Faraday Soc.*, 66, 490-499.

Annex 9

**Electrophoretic Determination of the Degree of Eu Complexation by Humic Acid:
Analysis and Assessment of Experimental Error**

J. Mizera, P. Benes and G. Masnerova

Technical University of Prague (CTU)

Electrophoretic determination of the degree of Eu complexation by humic acid: Analysis and assessment of experimental error

J. Mizera, P. Beneš, G. Masnerová

Czech Technical University in Prague, Faculty of Nuclear Sciences and
Physical Engineering, Department of Nuclear Chemistry
Břehová 7, 115 19 Praha 1, Czech Republic

Abstract

The degree of complexation of Eu with Aldrich humic acid (HA) was determined by the free liquid / moving boundary electrophoresis used in combination with the radiotracer method. Electrophoretic mobilities of Eu in 10 mg/L HA solutions were measured in a broad range of Eu total concentration (10^{-8} - 10^{-5} M), at pH 4 and 6, ionic strength 0.01 and 0.1 (NaClO₄). The Eu mobilities in the cathodic direction were used to calculate the degree of complexation. Its dependence on the total Eu concentration was curve-fitted and values corresponding to 1%, 10%, and 50% of PEC/3 (one third of the HA proton exchange capacity) were interpolated for a comparison with other experimental methods. Uncertainty of the determination given by sorption losses of Eu in the apparatus has been estimated. The effect of kinetic lability of the Eu-HA complexes is discussed.

Introduction

Electromigration methods have been used to study complexation equilibria in solution (Shvedov 1971, Rösch 1987) since several decades. Although these methods have been often used for separation and characterization of humic substances (HS) according to their size and charge, they became a useful tool for analysis of the interaction of metal ions with HS only recently (Duxbury 1989). Among the variety of the electromigration techniques, capillary zone electrophoresis (Dabek-Zlotorzynska 1998, Pacheco 2001) and continuous electrophoretic ion focusing (Marquardt 1996) are most frequent in the metal-HS complexation studies.

The free liquid / moving boundary electrophoresis combined with the radiotracer method was directly designed to analyse speciation of trace elements in natural water (Beneš 1979). Recently, the method has been employed at equilibrium and kinetic studies of Eu complexation with HS (Mizera 2001a, 2001b). In this work, Eu-humic acid complexation data obtained by the method are completed for a direct comparison with the data being currently collected by several independent experimental methods (ultrafiltration, dialysis, ion exchange, and potentiometric titration) under comparable experimental conditions. Performance of the method, source and extent of experimental error are critically assessed.

Principle of the method

When a substance (metal, e.g.) is present in solution as a mixture of different species its migration in the electric field can be described by a mean, or effective electrophoretic mobility expressed as

$$u = \sum_{i=0}^n u_i \cdot x_i \quad (1)$$

where u_i is mobility, and x_i molar fraction of a given species. In case that establishment of equilibrium among the different species is slower than their separation by electrophoresis, cathodic and anodic mobility can be distinguished.

In the arrangement of the free liquid / moving boundary electrophoresis, the electrophoretic cell (Fig. 1) consists of three parts (anodic, central, and cathodic) and is filled with an analyzed solution identical in all three cell compartments but for radiolabelling applied in the central compartment. From redistribution of the radiolabelled boundary caused by migration of charged species in the electric field, the mobilities can be calculated. It is possible to determine the degree of complexation of metal by HA from the decrease of its effective cathodic mobility observed in the presence of the complexing agent, while the anodic mobility is indicative of the negative charge of the metal-HA complexes formed. Provided Eu^{3+} is the only positively charged species present, the percentage of Eu bound to HA ($\%EuHA$) can be determined based on the electrophoretic mobilities measured in the cathodic direction as

$$\%EuHA = 100 \cdot \frac{[EuHA]}{[Eu] + [EuHA]} = 100 \cdot (1 - u_+ / u_0) \quad (2)$$

where u_+ is the observed effective cathodic mobility characterizing the mixture of Eu species present in solution, and u_0 is the mobility of Eu^{3+} (calculated from its limiting molar conductivity with correction for the non-zero ionic strength, or better directly measured in the experimental arrangement used).

The effective electrophoretic mobility is determined as

$$u_{+(-)} = \frac{\kappa \cdot V}{i \cdot t} \cdot \frac{A_{+(-)} + A'_{+(-)}}{A + kA' + A_+ + A'_+ + A_- + A'_-} \quad (3)$$

where $u_{+(-)}$ is the electrophoretic mobility towards cathode (anode) [$\text{cm}^2\text{V}^{-1}\text{s}^{-1}$], κ is specific conductivity [S cm^{-1}] of the solution analyzed, V is volume of the central part of the apparatus [mL], i is the mean electric current in the circuit throughout an experiment [A], and t is duration of the experiment [s]. A_+ and A_- are activities [cpm] in solutions sampled after experiment from side compartments (cathodic and anodic, respectively), A'_+ and A'_- are their sorption losses, A is activity from the central part and A' its sorption loss. The sorption losses are determined as activities of 1 M HCl solution used to recover the adsorbed metal. The denominator of the right hand part of the fraction containing the activities represents the mean activity (or concentration $[\text{Eu}]_0$) of Eu in the middle compartment which was free (not adsorbed on the walls) during the electrophoresis, so that it was available for electromigration. Its value depends on kinetics of the adsorption, which is described by the parameter k (see the discussion in the results section).

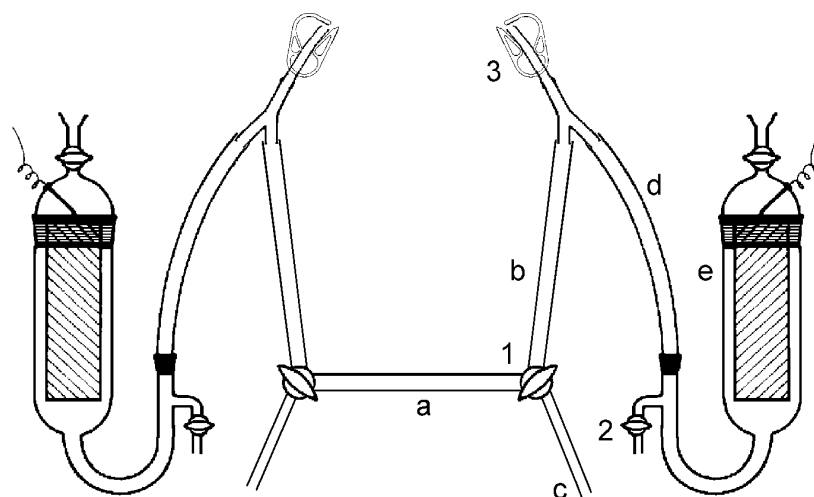


Fig. 1. Electrophoretic apparatus: a – central compartment, b – cathodic/anodic compartment, c – filling tube (to solution), d – connecting tube, e – electrode (AgCl/Ag in 1 M NaCl), 1 – 2-way valve, 2 – stopcock, 3 – filling tube, clamped (to syringe).

Experimental

Reagents and sample preparation

All the stock and working solutions were prepared from analytical reagents without further purification, and ultrapure water (Millipore Milli-Q 50). Humic acid (HA) was purchased from Aldrich (Na salt, tech., LOT No. 01816-054) and purified/protonated according to a procedure described in Kim 1990. It consists in removal of mineral impurities soluble in NaF solution, HA precipitation in acidic solution (HCl, pH~1), and washing the centrifuged precipitate by the HCl solution until a negative flame test for Na presence. The sequence was repeated three times, resulting HA suspension was lyophilized (freeze-dried). The product obtained is HA in protonized form with low content of mineral matter. In the course of the project, two batches of the purified/protonated Aldrich HA were prepared. The first batch used has been thoroughly characterized, for the other one only the proton exchange capacity (PEC) has been determined. The PEC was determined with back titration of excess Ba(OH)₂ equilibrated in suspension with the insoluble HA (Perdue 1985). Dissociation of HA acidic functional groups was characterized by potentiometric titration. TG analysis determined content of water and mineral matter. The HA structure was further characterized by FTIR spectroscopy.

HA stock solutions (0.5 g/L) were prepared periodically by dissolution of purified/protonated HA in 0.1 M NaOH under nitrogen, and refrigerated with pH adjusted at ~ 6. Working solutions of HA (10 mg L⁻¹) were prepared by dilution of the stock solutions. Eu was added from stock solutions of appropriate concentration (Eu³⁺ in 0.01M HClO₄) to reach a required total metal concentration. Additional stock solutions spiked with radiotracer were prepared. The radiotracer, ¹⁵²Eu with minor admixture of ¹⁵⁴Eu, was transferred from the original preparation in chloride form into perchlorate to give a stock solution of 3.4×10⁻⁶ M

Eu in 0.01 M HClO₄. Sample pH was adjusted by addition of NaOH / HClO₄ solutions, samples at pH 6 were buffered by MES, 1×10⁻³ mol L⁻¹. Constant ionic strength (*I*) of 0.1 and 0.01 (mol L⁻¹) was maintained by NaClO₄. Freshly prepared samples in closed polyethylene vials were left for a certain time (typically for two days except for the experiments designed to study the effect of contact time between Eu and HA; see below) in dark prior to running an experiment. Before filling the electrophoretic cell, pH was checked and readjusted, and an aliquot sample for activity measurement was taken. Correction on Eu sorption loss on the vial walls was made by measuring aliquot activity desorbed from emptied vials by 1 M HCl solution.

Instrumentation and procedures

Dissociation of the HA functional groups was investigated by a continuous potentiometric titration performed with an automatic titration station (Radiometer Titrilab 80) using a glass combined electrode (Radiometer GK2401C). A 30 mL solution of HA (15 mg HA dissolved under nitrogen in 0.1 M NaOH standardized by KHP) containing an excess HClO₄ to drop pH to ≈ 2.5, and NaClO₄ to maintain the ionic strength at ≈ 0.1, was titrated with 0.1 M NaOH under nitrogen atmosphere, thermostated at 25 °C. The progress of titrant addition was controlled by stability of the electrode signal (0.1 mV/s) limited by maximum time allowed to elapse between two additions (150 s).

The electrophoretic experiments were carried out in the above described arrangement using the apparatus depicted in Fig. 1 (volume of the central tube is ca. 3.5 ml). They were run at constant current of 2.2 mA at *I* = 0.1, 1 mA at *I* = 0.01, with corresponding voltage of 250-350 V, at ambient temperature, for 1 hour at *I* = 0.1, 2 hours at *I* = 0.01. An electrophoretic experiment was carried out in duplicate with each batch of working solution. Activity of all samples collected in the experiments was counted in glass vials using a well-type NaI(Tl) crystal with a single-channel analyzer. In a special series of experiments, besides measuring activity of the samples from the cell compartments, electromigration of HA and/or Eu-HA complexes was followed also by measuring absorbance of the samples (in quartz cuvettes at 365 nm). To be able to measure the absorbance changes in the cell compartments, a modification of the above mentioned experimental arrangement was necessary, which consisted in omitting HA from the solutions in the cathodic and anodic compartments.

Results and discussion

Characterization of humic acid

By TG analysis, water content 4.3 weight % was determined at 105 °C, and ash content 1.8 weight % at 535 °C. PEC of 7.00±0.01 mol/kg (8.615± 0.105 mol/kg for the 2nd batch) was found by the Ba(OH)₂ method. The titration curve of HA (0.5 g/L) was modeled assuming two types of carboxylic groups C_S and C_W with pK_a's 3.30 and 5.80, with respective site concentrations 2.42 and 2.14 mol/kg, and phenolic hydroxyl groups C_P with pK_a 10.98 and concentration 2.44 mol/kg. At the curve fitting, the PEC value was used as a constraint. The results (titration curve and distribution diagram) are depicted in Fig. 2.

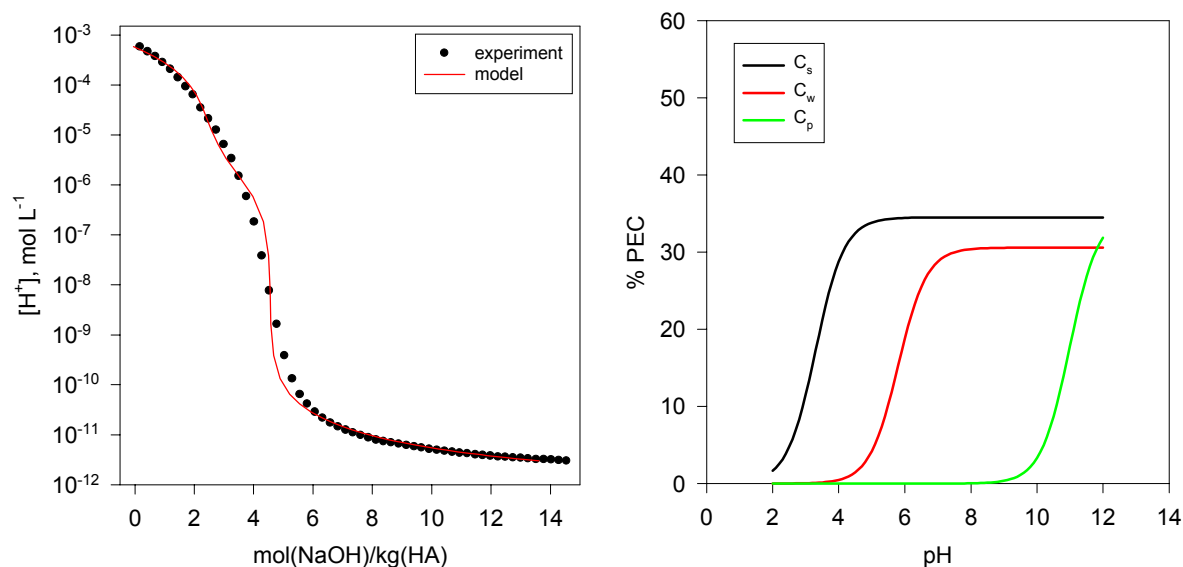


Fig. 2. Dissociation of the acidic functional groups of Aldrich HA; experimental and modeled titration curves (left), and distribution diagram for a 3-site model (right).

The FTIR spectrum (see Fig. 3), taken on a HA film prepared by evaporation on a silicon window, shows a typical humic acid pattern with the most pronounced carboxylate ($-\text{COO}^-$) bands at 1595 and 1381 cm^{-1} , carboxyl ($-\text{COOH}$) bands at 1706 cm^{-1} , the broad phenolic hydroxyl band at ~ 3300 cm^{-1} , and the sharp methyl and methylene bands at ~ 2900 cm^{-1} . The lack of spectral bands of the OH stretch modes of clays between 3800 and 3600 cm^{-1} as well as minor Si-O-Si bands around 1000 cm^{-1} point to substantial removal of mineral admixtures.

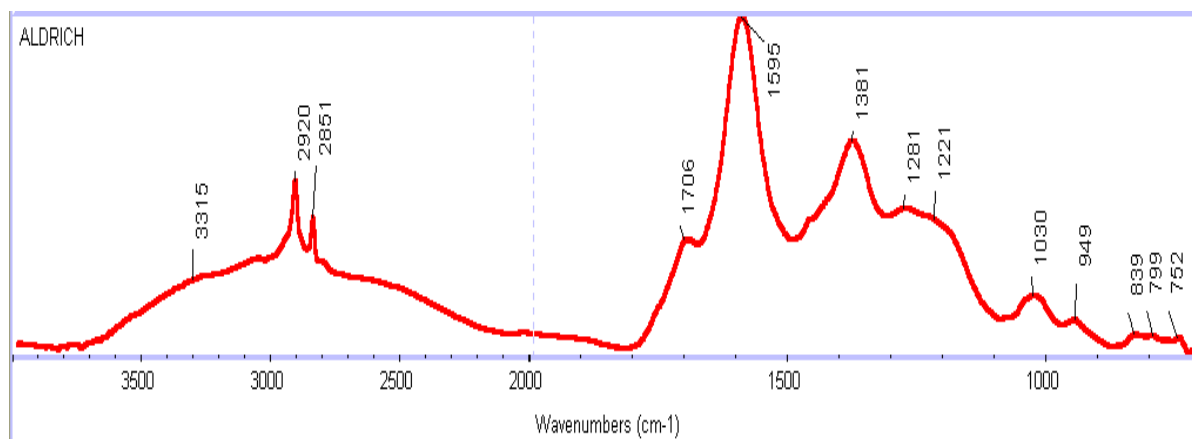


Fig. 3. FTIR spectrum of Aldrich HA.

Eu-HA electrophoretic / complexation data

Electrophoretic behavior of Eu in the presence of HA and the derived information about the degree of complexation (i.e., percentage of Eu bound to HA, $\%EuHA$) are illustrated by Fig. 4 and Tab. 1. Electrophoretic mobilities of Eu in 10 mg/L HA solutions were measured as function of Eu total concentration (10^{-8} - 10^{-5} mol L^{-1}), at pH 4 and 6, ionic strength 0.01 and

0.1. At the %EuHA calculation by Eq.(2), u_0 (the Eu^{3+} mobilities) values of 5.74×10^{-4} and $4.58 \times 10^{-4} \text{ cm}^2 \text{V}^{-1} \text{s}^{-1}$ at $I = 0.01$ and 0.1 , respectively, were used as determined in the absence of HA at $[\text{Eu}]_0 = 10^{-4} \text{ mol L}^{-1}$ and $\text{pH} = 3$. The errors given in the table and depicted by error bars in the graph for both variables represent estimated uncertainty of the determination due to sorption losses of Eu in the central part of the apparatus. In the above presented Eq.(3) used for determination of electrophoretic mobility, the parameter k accounts for kinetics of Eu sorption. If the sorption is slow with linear time dependence, k is set to 0.5. In case of rapid sorption (i.e., with sorption equilibrium reached before starting an experiment), k approaches zero. Thus, the mobilities have been calculated from the duplicate measurements assuming both sorption kinetics modes, the resulting set of four values averaged and characterized by standard deviation. In the same manner, $[\text{Eu}]_0$ values calculated from the sum of activities in Eq.(3) are presented as an interval corresponding to the two sorption kinetic modes.

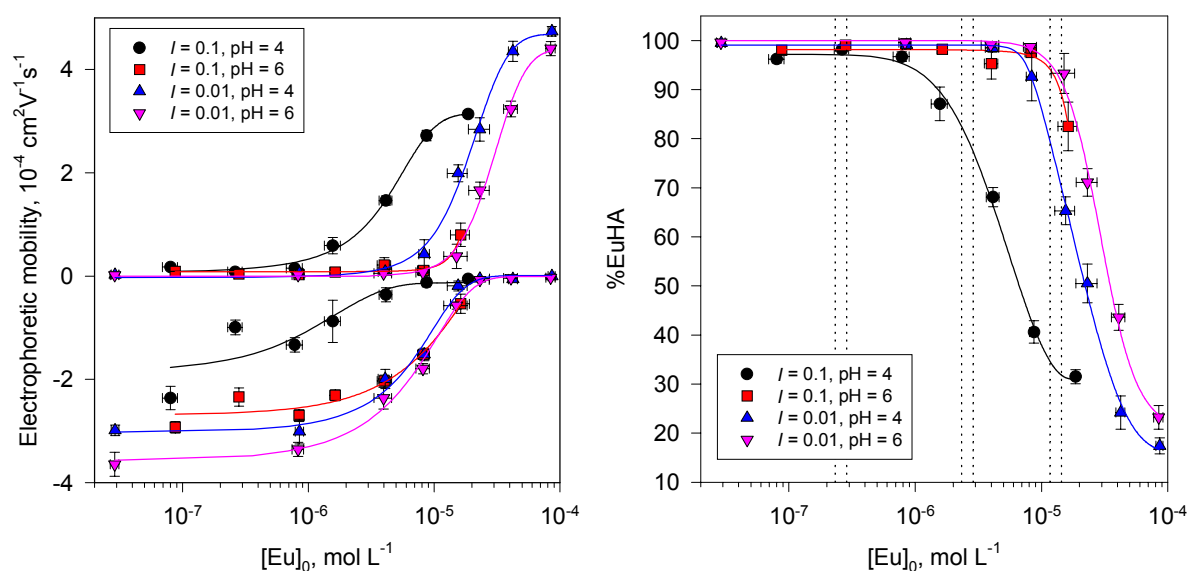


Fig. 4. Electrophoretic mobilities of Eu in 10 mg/L Aldrich HA solutions (left) and the derived percentage of Eu bound to HA (right), as function of Eu concentration, pH, and ionic strength. Vertical dashed lines values correspond to 1%, 10%, and 50% loading of one third of the HA proton exchange capacity.

The sigmoid dependencies %EuHA vs. $\log [\text{Eu}]_0$ were curve-fitted, and the values corresponding to 1%, 10%, and 50% of PEC/3 (one third of the HA proton exchange capacity) were interpolated for a future comparison with results of other experimental methods. Results of the interpolation, indicated by the vertical dashed lines in Fig. 4, are given in Tab. 2 (two sets of values are presented for the two HA batches). At $\text{pH} = 6$ and both ionic strengths, binding of Eu seems to be almost complete below 50% loading, as indicated by the absence of migration to cathode. At the same time, significant anodic mobilities can be observed. These mobilities decrease with increasing loading and disappear when cathodic mobilities become significant. This may simply reflect a high degree of neutralization of HA charge by complexed Eu. However, it could also point to a kinetic lability of the weaker complexes formed in this region which would favor fast isotope exchange, and consequent disappearing of anodic mobilities in prevailing cathodic migration. At $\text{pH} = 4$ compared to $\text{pH} = 6$, lower

%EuHA at higher loading is consistent with lower degree of dissociation of the acidic functional groups of HA. Significant suppression of complexing ability can be noticed with the ionic strength increase, pointing to reduction of the non-specific interaction of Eu^{3+} with the negative surface charge of HA and/or increased kinetic lability of the complexes.

Table 1. Electrophoretic mobilities (cathodic u_+ , anodic u_-) of Eu in HA solution (10 mg/L) as function of Eu concentration, ionic strength I , and pH, used for calculation of the percentage of Eu complexed with HA, *%EuHA* (see the text for explanation of errors given)

$[\text{Eu}]_0, \text{mol L}^{-1}$	$u_+, 10^{-4} \text{ cm}^2 \text{V}^{-1} \text{s}^{-1}$	$u_-, 10^{-4} \text{ cm}^2 \text{V}^{-1} \text{s}^{-1}$	<i>%EuHA</i>
$I = 0.1, \text{pH} = 4$			
$8.0\text{E-}8 \pm 1.1\text{E-}8$	0.18 ± 0.03	-2.36 ± 0.23	96.2 ± 0.7
$2.6\text{E-}7 \pm 3.4\text{E-}8$	0.08 ± 0.03	-0.99 ± 0.14	98.2 ± 0.7
$7.8\text{E-}7 \pm 1.1\text{E-}7$	0.15 ± 0.04	-1.33 ± 0.14	96.7 ± 1.0
$1.6\text{E-}6 \pm 2.3\text{E-}7$	0.59 ± 0.16	-0.87 ± 0.41	87.1 ± 3.4
$4.1\text{E-}6 \pm 4.8\text{E-}7$	1.46 ± 0.09	-0.36 ± 0.14	68.1 ± 2.0
$8.7\text{E-}6 \pm 6.6\text{E-}7$	2.72 ± 0.10	-0.12 ± 0.01	40.6 ± 2.3
$1.9\text{E-}5 \pm 6.7\text{E-}7$	3.14 ± 0.06	-0.05 ± 0.03	31.5 ± 1.4
$I = 0.1, \text{pH} = 6$			
$8.8\text{E-}8 \pm 6.2\text{E-}9$	0.09 ± 0.01	-2.93 ± 0.11	98.0 ± 0.2
$2.8\text{E-}7 \pm 2.0\text{E-}8$	0.04 ± 0.02	-2.34 ± 0.17	99.1 ± 0.3
$8.4\text{E-}7 \pm 7.1\text{E-}8$	0.03 ± 0.02	-2.70 ± 0.11	99.3 ± 0.4
$1.6\text{E-}6 \pm 1.5\text{E-}7$	0.08 ± 0.01	-2.31 ± 0.10	98.2 ± 0.2
$4.0\text{E-}6 \pm 4.9\text{E-}7$	0.21 ± 0.15	-2.03 ± 0.12	95.3 ± 3.2
$8.3\text{E-}6 \pm 8.7\text{E-}7$	0.11 ± 0.01	-1.52 ± 0.08	97.6 ± 0.1
$1.6\text{E-}5 \pm 2.8\text{E-}6$	0.80 ± 0.23	-0.54 ± 0.19	82.5 ± 5.0
$I = 0.01, \text{pH} = 4$			
$2.9\text{E-}8 \pm 2.0\text{E-}9$	0.03 ± 0.02	-2.99 ± 0.10	99.5 ± 0.4
$8.5\text{E-}7 \pm 6.4\text{E-}8$	0.05 ± 0.04	-3.01 ± 0.24	99.1 ± 0.8
$4.1\text{E-}6 \pm 4.9\text{E-}7$	0.09 ± 0.05	-1.99 ± 0.19	98.5 ± 0.9
$8.4\text{E-}6 \pm 8.0\text{E-}7$	0.43 ± 0.28	-1.52 ± 0.12	92.6 ± 4.9
$1.6\text{E-}5 \pm 2.8\text{E-}6$	1.99 ± 0.16	-0.19 ± 0.10	65.3 ± 2.9
$2.3\text{E-}5 \pm 4.4\text{E-}6$	2.84 ± 0.23	-0.05 ± 0.01	50.5 ± 3.9
$4.2\text{E-}5 \pm 3.5\text{E-}6$	4.35 ± 0.19	-0.06 ± 0.02	24.2 ± 3.4
$8.6\text{E-}5 \pm 5.5\text{E-}6$	4.74 ± 0.09	0.00 ± 0.00	17.4 ± 1.6
$I = 0.01, \text{pH} = 6$			
$2.9\text{E-}8 \pm 2.2\text{E-}9$	0.02 ± 0.02	-3.65 ± 0.23	99.6 ± 0.3
$8.3\text{E-}7 \pm 8.6\text{E-}8$	0.02 ± 0.01	-3.36 ± 0.13	99.6 ± 0.3
$4.0\text{E-}6 \pm 6.3\text{E-}7$	0.05 ± 0.03	-2.36 ± 0.21	99.1 ± 0.4
$8.2\text{E-}6 \pm 9.9\text{E-}7$	0.07 ± 0.02	-1.79 ± 0.10	98.7 ± 0.4
$1.5\text{E-}5 \pm 3.2\text{E-}6$	0.38 ± 0.23	-0.57 ± 0.07	93.3 ± 4.1
$2.3\text{E-}5 \pm 4.3\text{E-}6$	1.66 ± 0.16	-0.07 ± 0.04	71.1 ± 2.8
$4.1\text{E-}5 \pm 5.0\text{E-}6$	3.24 ± 0.15	-0.04 ± 0.01	43.6 ± 2.7
$8.5\text{E-}5 \pm 7.1\text{E-}6$	4.41 ± 0.14	-0.03 ± 0.01	23.2 ± 2.4

Table 2. %*EuHA* values corresponding to 1%, 10%, and 50% loading of one third of the HA proton exchange capacity, as function of ionic strength and pH

%PEC	[Eu] ₀ , mol L ⁻¹	<i>I</i> = 0.1, pH = 4	<i>I</i> = 0.1, pH = 6	<i>I</i> = 0.01, pH = 4	<i>I</i> = 0.01, pH = 6
1	2.3E-7	97	99	99	100
	2.9E-7	97	99	99	100
10	2.3E-6	83	98	99	99
	2.9E-6	78	98	99	99
50	1.2E-5	35	94	79	95
	1.4E-5	32	89	70	92

Effect of kinetic lability of the Eu-HA complexes

Since a change in the isotopic composition of metal studied is the only change caused by electromigration in the arrangement used, the method essentially does not disturb the equilibria in solution. Calculation of %*EuHA* based on the electrophoretic data using Eq.(2) is based on several assumptions. First, it neglects the effect of pseudocolloids and of Eu non-humic complexes on the measured effective mobility. This has been justified by working in the pH range where hydrolysis and formation of the carbonate complexes are negligible, while the effect of pseudocolloids must be strongly suppressed by the formation of the EuHA complexes. Second, Eq. (2) presumes that the EuHA complexes formed are neutral or, if (negatively) charged, they move independently on Eu³⁺ and do not influence the effective mobility observed in the cathodic direction. This is true when separation of all the Eu species by electromigration is more rapid than the isotopic equilibrium among all the ¹⁵²Eu-labelled and unlabelled species is established, otherwise the mobilities measured in either direction would be retarded by the mobilities of the oppositely charged species. The %*EuHA* calculated using Eq. (2) thus represents the maximum possible abundance of EuHA complexes.

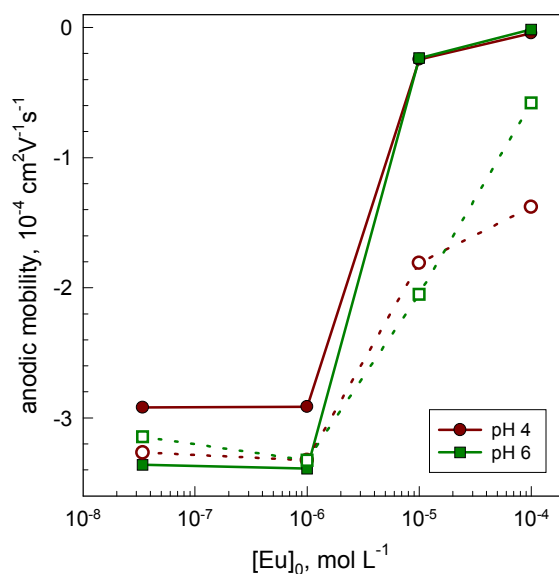


Fig. 5. Electrophoretic mobilities of Eu / Eu-HA in Aldrich HA (10 mg/L) measured at *I* = 0.1 with simultaneous radiometric (filled symbols) and spectrophotometric (open symbols) detection, as function of Eu loading and pH.

To reveal a possible effect of dissociation of the Eu-HA complexes on the electrophoretic determination of %EuHA, simultaneous measuring activity and spectrophotometric detection of the migrating $^{152}\text{Eu}/\text{Eu-HA}$ complex was used. Results are illustrated by Fig. 5. Differences between anodic mobilities determined from ^{152}Eu counting and those given by absorbance measurement rise with decrease of pH and increase of Eu concentration. This can reflect dependence of the lability of Eu-HA complexes on pH and the degree of metal loading. At low loading / high pH conditions, the good agreement of the radiometry- and spectrophotometry-based mobilities confirms the kinetic stability of the complexes formed. At high loading / low pH conditions, fast dissociation of kinetically labile complexes results in lower radiometry-based mobilities and higher spectrophotometry-based mobilities, as part of Eu leaves the negatively charged complex before entering the anodic compartment. Thus, overestimation of the degree of complexation at higher loading can be expected.

With respect to the possible sensitivity of the electromigration method to the kinetic lability of Eu-HA complexes, the effect of the pre-equilibration time (i.e., time of the contact of Eu with HA before running an experiment) was investigated. For this purpose, experimental conditions were chosen so that both cathodic and anodic mobilities could be observed at the same time. The Eu-HA systems at pH = 4, $I = 0.01$, and initial Eu concentration 1×10^{-5} and 2×10^{-5} mol L $^{-1}$ ($[\text{Eu}]_0 = 8.4 \times 10^{-6}$ and 1.6×10^{-5} mol L $^{-1}$, respectively; cf. Fig. 4 and Tab. 1) are best suitable for this purpose. Among the experiments run after pre-equilibration times <1 h, 2 h, 24 h, 7 d, 1 and 3 months, differences in both mobilities did not exceed a typical error associated with the method (see Tab.1), and did not follow any clear trend. Thus, the complexation equilibrium (amount of Eu complexed with HA) must be reached quite rapidly. Changes in quality of the complexes upon their aging, if any, cannot be observed by the method.

References

- Beneš,P., Glos,J.: J. Radioanal. Nucl. Chem. **52**, 43 (1979).
- Dabek-Zlotorzynska,E., Lai,E.P.C., Timerbaev,A.R.: Anal. Chim. Acta **359**, 1 (1998).
- Duxbury, J. M.: Studies of the Molecular Size and Charge of Humic Substances by Electrophoresis. In: *Humic Substances II*, (Hayes et al., eds.), John Wiley and Sons Ltd, New York, 593 (1989).
- Kim,J. I., Buckau,G., Li,G.H., Duschner,H., Psarros,N.: Fresenius J. Anal. Chem. **338**, 245 (1990).
- Marquardt,C., Herrmann,G., Trautmann,N.: Radiochim. Acta **73**, 119 (1996).
- Mizera,J., Beneš,P., Hvoždová,I., Jansová, A.: Radiochim. Acta **89**, 785 (2001a).
- Mizera,J., Dolanský,J., Beneš,P.: Radiochim. Acta **89**, 529 (2001b).
- Pacheco,M.L., Havel,J.: J. Radioanal. Nucl. Chem. **248**, 565 (2001).

Perdue, E.M.: Acidic Functional Groups of Humic Substances. In: *Humic Substances in Soil, Sediment, and Water: Geochemistry, Isolation, and Characterization*, (Aiken, G.R. et al., eds.), John Wiley and Sons Ltd., New York, 493 (1985).

Rösch, F., Milanov, M., Hung, T.K., Ludwig, R., Buklanov, G.V., Khalkin, V.A.: *Radiochim. Acta* **42**, 43 (1987).

Shvedov, V. P.: *Electromigration Method in Physicochemical and Radiochemical Research* (in Russian), Atomizdat, Moscow, 78 (1971).

Annex 10

**Preliminary Results for Determination of Conditional Stability Constant for Pu(IV)-
Humate using Immobilized Humic Acid on Silica Gel**

G. Szabo, J. Guzzi, T. Miyajima and A. Bulman

**Fodor Jozsef National Center of Public Health, Frederic Joliot-Curie National Research
Institute of Radiobiology and Radiohygiene (FJC)**

Preliminary results for determination of conditional stability constant for Pu(IV)-humate using immobilized humic acid on silica gel

Gyula Szabó¹, Judit Guenzi¹, Tohru Miyajima² and Robert A. Bulman³

¹"Frédéric Joliot-Curie" National Research Institute for Radiobiology and Radiohygiene, PO Box 101, Budapest, H-1775, Hungary

²Department of Chemistry, Faculty of Science and Engineering, Saga University, 1-Honjo, Saga 840-8502, Japan

³National Radiological Protection Board, Didcot, United Kingdom, OX11 ORQ

Abstract

To facilitate investigations of the influence of humic substances on the migration of plutonium in and around nuclear waste repositories we have immobilized humic acid on silica gel. It is anticipated that this material might serve as geochemical models of the humate-coated minerals that are likely to be present in the vicinity of the repositories. The binding of plutonium by the immobilized humic acid was examined at pH 4 in 0.02, 0.05, 0.10, 0.20, 0.50 and 1.00 M NaClO₄ by titration method. Pu(IV)-humate conditional stability constants have been evaluated from data obtained from these experiments by using non-linear regression of binding isotherms. The results have been interpreted in terms of complexes of 1:1 stoichiometry.

Key words: humic acid, plutonium, conditional stability constant (β)

Introduction

Extensive research over the years has established that humic substances play an important role in the geochemical cycling of metal ions and radionuclides. By the chemical nature of humic acids it was anticipatable that they would influence the speciation of plutonium in the environment, Choppin and Allard, 1985; Choppin, 1992; Moulin at al., 1992. Although several investigations have confirmed the suppositions, the chemistry of the interactions of plutonium with humic substances needs to be understood in fine detail especially with the humic matter sorbed on solid phases so that humate-mediated movement of this transuranic element through the environment can be predicted, Livens and Singleton, 1991; Bulman and Szabó, 1991; Moulin and Moulin, 1992. The main objectives of this work are to provide equilibrium complexation data for plutonium humic interaction by laboratory

experiments on designed controlled systems because scientifically proved data for Pu-humate complexes are rare in the literature.

Experimental

Materials and methods

Silica gel (Polygoprep Si-300, 20 μm , BET surface area 100 m^2/g) was obtained from Macherey-Nagel. Humic acid was purchased from Aldrich Chemical Co. Ltd. and purified by the method of Kim et al., 1990. 3-Aminopropyltriethoxysilane and 1-(3-Dimethylaminopropyl)-3-ethylcarbodiimide hydrochloride were purchased from Aldrich Chemical Co. Ltd. Humic acid was immobilized on silica gel ($\text{SiO}_2\text{-HA}$) by using previously described procedure (Szabó et al., 1992; Koopal et al., 1998; Bulman et al., 1997). The specific surface area of the prepared solid phase was determined by BET method and are given in Table 1. C, H and N analyses of HA-SiO_2 were conducted on an automatic CHNS-O analyzer (see Table 1). The IR spectra of the prepared silica gel was recorded using a NICOLET 5PC FT-IR Spectrometer and is showed in Figure 1. The KBr pellet technic was applied. ^{239}Pu was determined by liquid scintillation counting in a Packard Tri-Carb 2550 liquid scintillation counter. The proton exchange capacity of the immobilized HA was determined by potentiometric titration (see Table 1).

The citrate of ^{239}Pu was prepared from stock solutions of the nitrates dissolved in 4 M HNO_3 . An aliquot of the stock solution was evaporated to dryness and the residue dissolved in 0.01 M HNO_3 to which was added an equal volume of 2% trisodium citrate. The resulting solution was adjusted to pH 4 and passed through a membrane of porosity 25 nm (Millipore Ltd.) to minimize the presence of polynuclear transuranic species. ^{239}Pu were determined by liquid scintillation counting in a Packard Tri-Carb 2550 liquid scintillation counter.

The binding of plutonium by the immobilized humic acid was examined at pH 4 in 0.02, 0.05, 0.10, 0.20, 0.50 and 1.00 M NaClO_4 containing 4.2×10^{-8} M concentration of plutonium by titration method.

Table 1. Characteristics of the used $\text{SiO}_2\text{-HA}$

	$\text{SiO}_2\text{-HA}$
Substrate content (mg g^{-1})	14.3 ± 1.2
Proton exchange capacity (meq/g solid matter)	0.0482
BET surface area ^a ($\text{m}^2 \text{g}^{-1}$)	74 ± 8

^aThe surface area of the parent silica gel is 100 $\text{m}^2 \text{g}^{-1}$

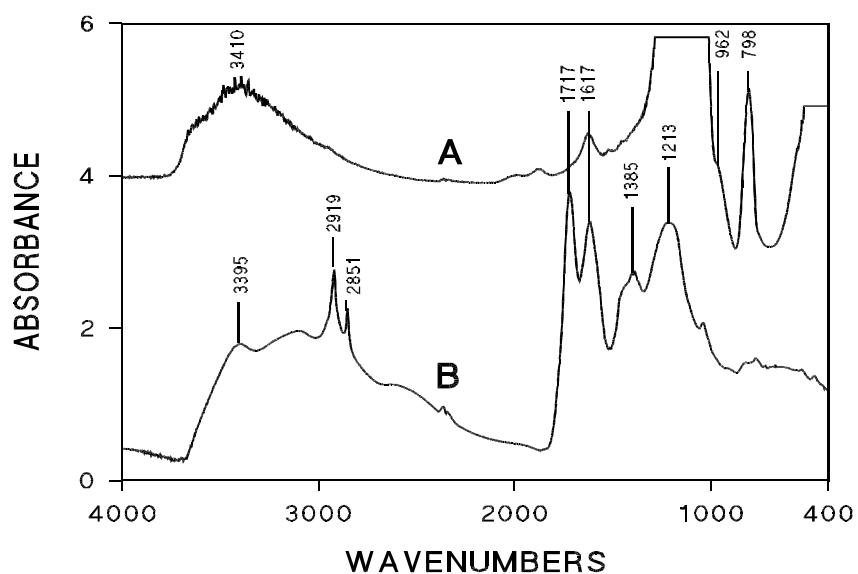


Figure 1. IR spectra of SiO₂-HA (A) and the parent humic acid (B)

Calculation of conditional interaction constants (β) from binding isotherm

The conditional interaction constant (β) is relative to the following equilibrium:



$$\text{with } \beta = \frac{[MHA(z)]}{[M^{z+}]_f [HA(z)]_f} \quad (2)$$

where:

M^{z+} : the metal cations

$HA(z)$ the concentration of humic acid

$[MHA(z)]$: the concentration of the metal humate complex

$[M^{z+}]_f$: the concentration of the free metal ion

$[HA(z)]_f$: the concentration of the free humic acid

The assumption is made that the macromolecule is the central group and the complexation can be described in terms of Langmuir-type adsorption equation. The free ligands concentration can be calculated in Eq. 2 with introducing B_{\max}

$$[\text{HA}(z)]_f = [\text{B}_{\text{max}}] - [\text{MHA}(z)] \quad (3)$$

where:

B_{max} : complexing capacity of humic acid

A combination of Eqs. 2 and 3 gives the relation that could be used for calculation of conditional interaction constants:

$$\beta = \frac{[\text{MHA}(z)]}{[\text{M}^{z+}]_f ([\text{B}_{\text{max}}] - [\text{MHA}(z)])} \quad (4)$$

or after alteration

$$[\text{MHA}(z)] = \frac{\beta [\text{M}^{z+}]_f \text{B}_{\text{max}}}{1 + \beta [\text{M}^{z+}]_f} \quad (5)$$

In sorption experiment it is necessary to introduce another factor to get the specific binding

$$[\text{MHA}(z)] = \frac{\beta [\text{M}^{z+}]_f \text{B}_{\text{max}}}{1 + \beta [\text{M}^{z+}]_f} + \text{NS} [\text{M}^{z+}]_f \quad (6)$$

where:

NS the nonspecific binding proportional with $[\text{M}^{z+}]_f$

Result and discussion

Determination of complexing capacities of humic substances immobilized on silica gel

Typical binding isotherms (solid phase concentration vs. liquid phase concentration in equilibrium) of plutonium by SiO_2 -HA at different ionic strength at pH 4 are presented on Fig. 2. As seen from the Fig. 2, a high reproducibility in the isotherms is obtained. From these binding isotherms it has been possible to calculate, see Table 2, the complexing capacity (B_{max}) expressed in $\text{mol} \cdot \text{g}^{-1}$ solid phase. As seen in Table 2 the binding capacities of the immobilized humic acid on silica gel decrease with increasing ionic strength. From an examination of Fig. 3, it is apparent that the values of the maximal binding capacity (B_{max}) of the immobilized humic acid on silica gel are related linearly to the logarithmic ionic strength ($\log I$) expressed in $\text{mol} \cdot \text{l}^{-1}$. A similar phenomenon has been reported by others (Czerwinski, 1996).

Table 2. Binding capacity (B_{\max}) of humic acid immobilized on silica gel with plutonium as a function of ionic strength.

Ionic strength	B_{\max} (10^{-8} mol/g gel)	B_{\max} (10^{-8} mol/g gel)
	on 10 mg gel	on 20 mg gel
0.02	78.6 ± 20.2	-----
0.05	56.9 ± 8.6	55.7 ± 14.3
0.10	43.1 ± 3.9	46.8 ± 12.2
0.20	26.9 ± 2.9	18.7 ± 2.1
0.50	13.8 ± 1.8	10.1 ± 1.1
1.00	8.1 ± 0.6	6.8 ± 0.4

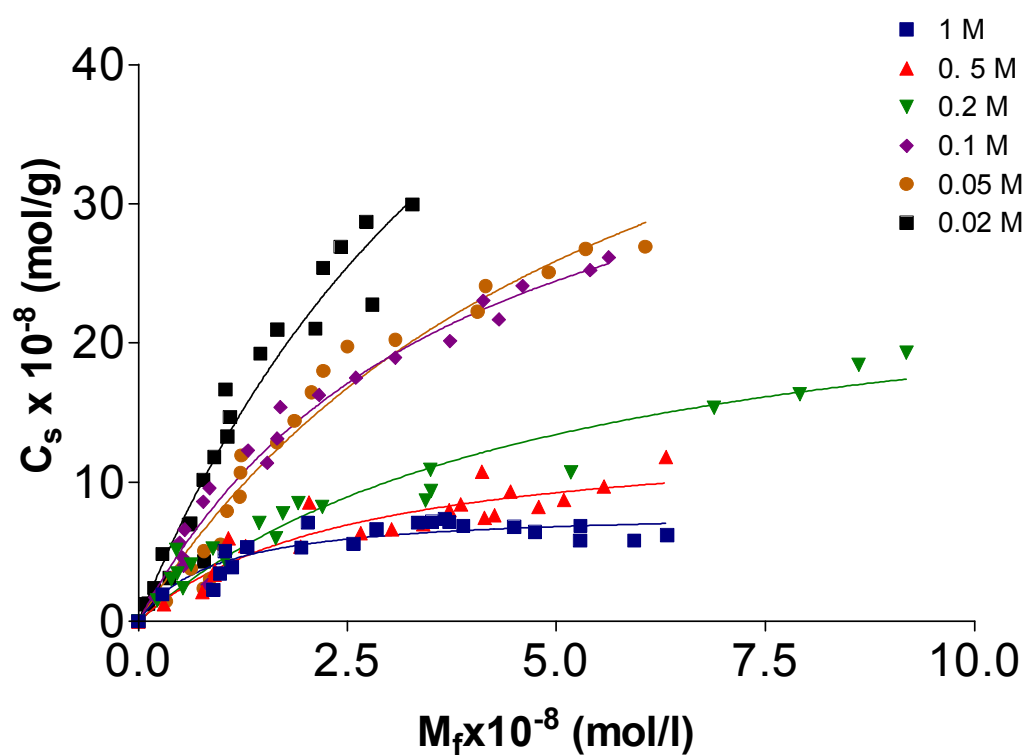


Figure 2. Binding isotherms of plutonium on $\text{SiO}_2\text{-HA}$ in different ionic strengths at pH 4

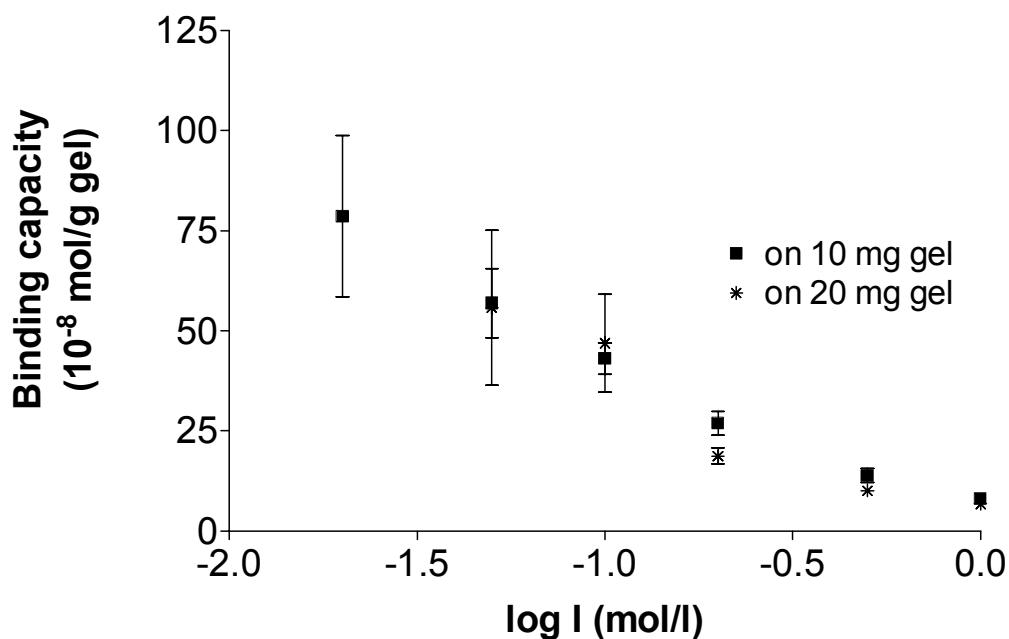


Figure 3. Effect of ionic strength on the maximal binding capacity (B_{\max}) of $\text{SiO}_2\text{-HA}$

Effect of ionic strength on conditional interaction constants ($\log \beta$)

From the data of sorption studies the conditional interaction constants can be calculated by using Eq. 4. The calculated values of conditional interaction constants of plutonium-humate on $\text{SiO}_2\text{-HA}$ from different ionic strength perchlorate solutions at pH 4 are presented in Table 3 and Fig 4. Additionally Table 3 contains the $\log \beta$ values obtained from binding isotherms (Eq. 6). The nonspecific binding on the silica gel matrix and on the wall of the centrifuge tube can be calculated by use of Eq. 6. The calculation has been shown that 2-7 % of plutonium adsorbs on these nonspecific binding places. From Fig. 4 it is apparent that the conditional interaction constants slightly increase with increasing ionic strength. In the literature, the ionic strength effect on the interaction constants has been debated. In some cases, conditional interaction constants appears increasing with ionic strength as shown by Fukushima et al., 1994, with Cu(II) , in other cases decreasing with increasing ionic strength as observed for Am(III) (Czerwinski, 1996). It should be also emphasized that the technique and calculation method used may greatly affect the variation of the interaction constants with ionic strength.

Table 3. Conditional interaction constants ($\log \beta$) of humic substances immobilized on silica gel with plutonium as a function of ionic strength.

Ionic strength	Log β	Log β
	Calculated from titration data use of Eq. 4	Calculated from binding isotherms data use of Eq. 5
0.02	7.25 ± 0.13	7.28 ± 0.44
0.05	7.16 ± 0.17	7.22 ± 0.63
0.10	7.40 ± 0.14	7.42 ± 0.77
0.20	7.35 ± 0.14	7.29 ± 0.67
0.50	7.60 ± 0.17	7.61 ± 0.51
1.00	8.01 ± 0.27	8.05 ± 0.56
Mean	7.47 ± 0.33	7.44 ± 0.32

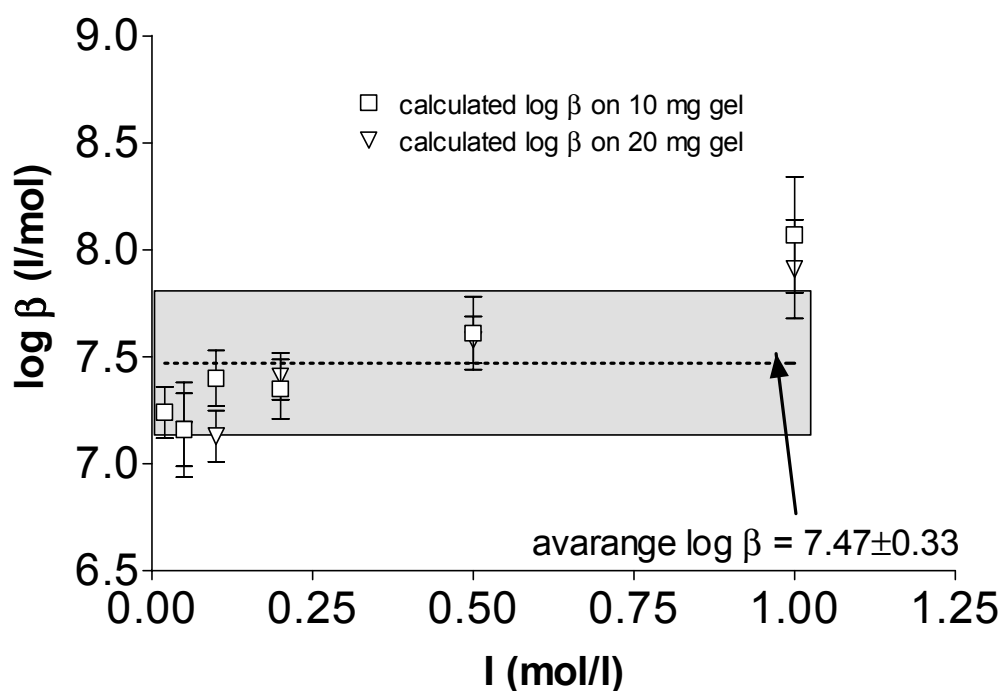


Figure 4. Effect of ionic strength on the calculated conditional stability constant ($\log \beta$) of plutonium-humate

Acknowledgments

This work was supported by European Commission, EC Contract No. FIKW-CT-2001-00128.

Literature

Bulman, R. A., Szabó, Gy.:

Investigations of the interactions of transuranic radionuclides with humic and fulvic acids immobilized on silica gel, *Lect. Notes Earth Sci.*, **33** (1991) 329

Bulman, R.A., Szabó, Gy., Clayton, R.F., Clayton C.R.:

Investigation of the uptake of transuranic radionuclides by humic and fulvic acids chemically immobilized on silica gel and their competitive release by complexing agents, *Waste management*, **17** (1997) 191

Choppin, G.R., Allard, B.:

Handbook on the Physics and Chemistry of the Actinides (Freeman, A.J., Keller, C. Eds.) Amsterdam 1985, **Vol 3**, Chap 11.

Choppin, G.R.:

The role of natural organics in radionuclide migration in natural aquifer system. *Radiochimica Acta*, **58/59** (1992) 113

Czerwinski, K.R., Kim, J.I., Rhee, D.S., Buckau, G.:

Complexation of trivalent actinide ions (Am^{3+} , Cm^{3+}) with humic acid: The effect of ionic strength, *Radiochimica Acta*, **72** (1996) 179

Fukushima, M, Tanaka, S., Taga, M.:

Effect of ionic strength on complexing equilibrium between copper(II) and humic acid, *Inter. J. Environ. Anal Chem.*, **56** (1994) 229

Kim, J.I., Buckau, G., Li, G.H., Duscher, H., Psarros, N.:

Characterization of humic and fulvic acids from Gorleben groundwater. *Fresenius J. Anal. Chem.* **338** (1990) 245

Koopal, L.K., Yang, Y., Minnaard, A.J., Theunissen, P.L.M., Van Riemsdijk, W.H.:
Chemical immobilisation of humic acid on silica, *Colloid Surfaces A: Physicochem. Eng. Aspects*, **141** (1998) 385

Livens, F.R., Singleton, D.L.:
Plutonium and americium in soil organic matter, *J. Environ. Radioact.*, **13** (1991) 323

Moulin, V., Moulin, C.:
Fate of actinides in the presence of humic substances under conditions relevant to nuclear waste disposal, *Appl. Geochem.* **10** (1992) 573

Moulin, V., Tits, J., Ouzounian, G.:
Actinide speciation in the presence of humic substances in natural water conditions, *Radiochimica Acta*, **58/59** (1992) 179

Szabó, Gy., Farkas, Gy., Bulman, R.A.:
Evaluation of silica-humate and alumina-humate HPLC stationary phases for estimation of the adsorption coefficient, K_{OC} , of soil for some aromatics, *Chemosphere*, **24** (1992) 403

Annex 11

Alkaline Conversion of Clay Organic Matter as a Potential Additional Source for Humic Substances

**F. Claret, Th. Schaefer, A. Bauer and
G. Buckau**

Marie-Curie Grant MCFI-2001-01983

Alkaline Conversion of Clay Organic Matter as a Potential Additional Source for Humic Substances under High Alkaline Conditions

Francis Claret, Thorsten Schäfer, Andreas Bauer and Gunnar Buckau

Forschungszentrum Karlsruhe, Institut für Nukleare Entsorgungstechnik, D-76021 Karlsruhe, Germany

Abstract

Clay from four different depths (447 to 516 m) of the Meuse Haute Marne (MHM) site is investigated for the potential conversion of hydrophobic clay organic matter into humic substances under alkaline conditions expected from cement dissolution in the near-field of a nuclear waste repository. Original organic material in the clay consists mainly of aliphatic hydrophobic compounds basically without oxygen containing functional groups. After contact with “solid young fluid” (mimicking cement dissolution, initial pH 13.22) for around one and a half years, high concentrations of hydrophilic organic matter are found (243 to 355 mg DOC/L). Characterization by solubility behavior, UV/Vis absorption and IR and spectroscopy show that the dissolved hydrophilic organic matter has the characteristic features of humic and fulvic acids. Estimation of humic and fulvic acid content via UV/Vis spectroscopy results in 97.5 (± 9.7) % of DOC being humic and fulvic acid. The results show that this is a potential additional source of humic substances that may need to be regarded in evaluation the safety function for radioactive waste disposal in presence of clay and cement.

Introduction

The Meuse Haute Marne (MHM) in the eastern Paris basin is under investigation for disposal of radioactive waste. The sedimentary host formation is an approximately 130 m thick clay-rich Callovo-Oxfordian formation at about 350 to 550 m depth below ground surface in the selected area. Cement is foreseen both as waste form and as material for the engineered barrier system. In case of water intrusion, cement dissolution will, amongst others, lead to high pH values. Preliminary investigations show that originally hydrophobic clay organic matter is converted to hydrophilic organic matter that shows typical properties of humic and fulvic acids. The present paper presents the initial results on the outcome of this conversion process.

Experimental material

Clay samples are from four different depths of the borehole EST 104. Sampling depth and experimental conditions of experimental solutions, after about 540 days of contact with alkaline solution expected from cement dissolution, are shown in Table 1. The total organic carbon content in the four clay samples is around 1.3 wt % (Claret et al. 2002). Several parameters suggest a low maturity level of the organic matter and samples are characterized by the presence of unsaturated biomarkers (Elie et al. 2000).

Table 1: Sampling depth of MHM site clay samples, and pH, Eh, DOC and sulfate concentration of final solutions after around 540 days of contact time with "solid young fluid".

Sample No.	Sampling depth (m)	pH	Eh (mV)	DOC (mgC/L)
1	447	12.3	13	299
2	"	12.4	12	260
3	490	13.2	-29	243
4	"	13.2	-29	267
5	494	13.3	-36	270
6	"	13.3	-28	252
7	516	13.2	-35	355
8	"	13.3	-28	324

*: "Solid young fluid" to mimic conditions expected for cement dissolution; NaOH: 65.2 mmol/L; KOH: 161 mmol/L; Ca(OH)₂: 2.24 mmol/L. Initial pH is 13.2.

Results and discussion

The pH values dropped from 13.2 to 12.4 and 12.3 in the samples from 447 m depth whereas the pH values of the other samples scatter around the value of the initial solution (Table 1). The generation of hydrophilic organic matter becomes obvious from the high DOC concentrations in the supernatant solutions. Humic acid is isolated by acid precipitation. Fulvic acid remains in the supernatant solution. The IR spectra of acid precipitate and supernatant fractions of the clay organic matter conversion products are shown in Fig. 1. On top of the figure,

regions are given for bands found in humic and fulvic acids as well as bands typical for silica clay contaminants in the supernatant sample. The IR-spectra show the typical features of humic and fulvic acids as well as the expected silica clay contaminant.

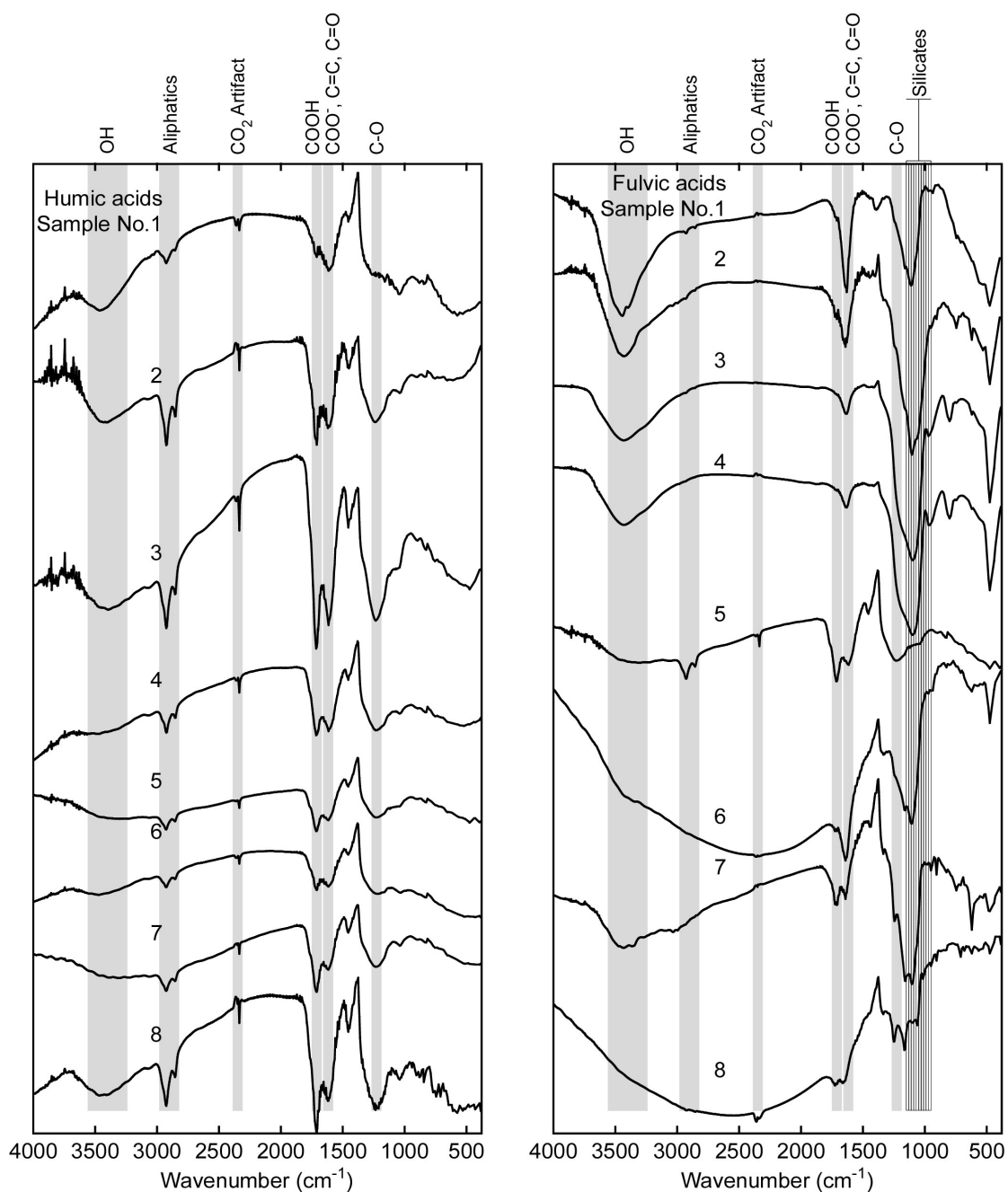


Fig. 1: IR spectra of acid precipitate and supernatant solution fractions of clay organic matter alkaline conversion products. Typical bands for humic and fulvic acids, as well as silica clay contaminants, are given as gray vertical lines.

UV/Vis absorption spectra of humic and fulvic acids show no specific features but a strong steady increase with decreasing wavelength, as also found for the spectra of the clay organic matter conversion products in the present investigation (Fig. 2). The fulvic acids were not

separated and purified from inorganic contaminants, resulting in the sharp increase in absorption at wavelengths below 300. Due to the small amount of sample, the fulvic acid samples were not isolated and purified but are measured in a matrix of high concentrations of silica and various salts. Consequently, below 300 nm a sharp increase in absorption is seen in all fulvic acid samples. Investigations on a large number of humic and fulvic acids of different origin has shown that this absorption ratio (E3/E4) correlates with the specific absorption at a given wavelength (Kim et al. 1995). This finding is based on investigation of 49 aquatic humic and fulvic acids from four different aquifer systems and 12 samples isolated from respective sediments. This empirical relationship cannot be generalized without caution. Nevertheless, this relationship is used for estimation of the specific absorption of the clay organic matter conversion products.

Applying the deduced specific absorptions of individual samples, the resulting calculated humic and fulvic acid concentrations are calculated. In Table 2, the sum of humic and fulvic acid in individual samples is compared with the measured DOC values. A mean value of 97.5 ± 9.7 % of DOC is evaluated to consist of humic and fulvic acids. Despite the required caution in the approach used, this result allows the conclusion that DOC consists mainly of humic and fulvic acids generated during contact of the clay with the alkaline “solid young fluid”.

Table 2: Sum of generated humic and fulvic acid estimated from UV/Vis spectroscopy, measured DOC content and the fraction of DOC identified as humic and fulvic acid.

Clay horizon (No.)	Sum of HA and FA from estimation by UV/Vis spectroscopy (mg C/L)	DOC (measured) (mg C/L)	Fraction of DOC as HA+FA (%)
1	349	299	116.9
2	219	260	84.3
3	222	243	91.3
4	242	267	90.8
5	266	270	98.4
6	258	252	102.5
7	342	354	96.7
8	322	324	99.4
			Mean value: 97.5 ± 9.7

Summary and conclusions

The original organic matter in the clay material is mainly hydrophobic and with a low solubility in aqueous solution. Under conditions expected for cement dissolution in the near-field of a nuclear waste repository, high concentrations of hydrophilic organic substances are generated by conversion of the original organic matter. The dissolved organic matter is shown to be dominated by humic and fulvic acids. These humic and fulvic acids may significantly

change the solubility and mobility of radionuclides. The results show that this is a potential additional source of humic substances that may need to be regarded in evaluation the safety function for radioactive waste disposal in presence of clay and cement.

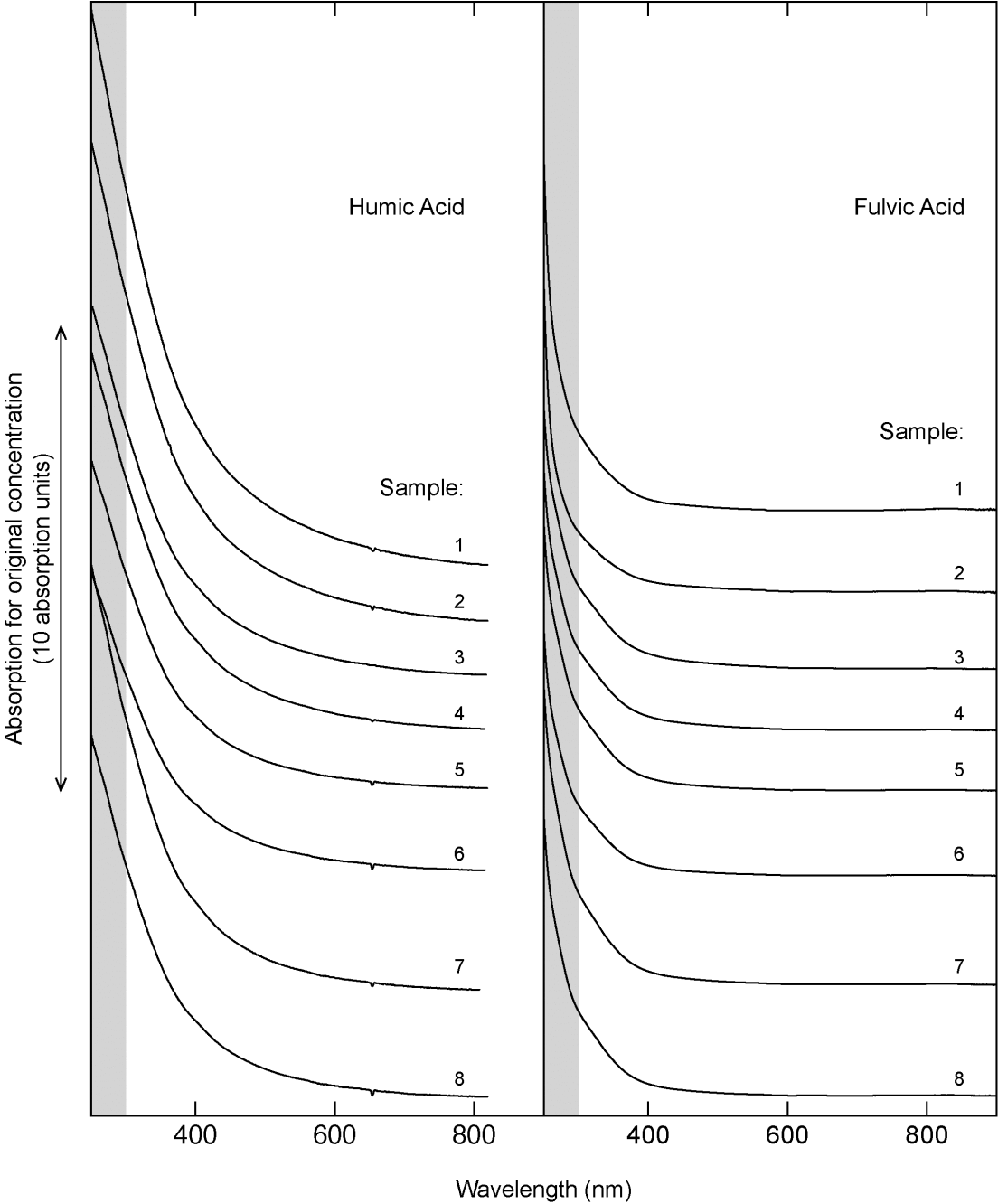


Fig. 2: UV/Vis absorption spectra of MHM site clay organic matter alkaline conversion products.

References

- Claret F, Bauer A, Schäfer T, Griffault ., Lanson B. Experimental investigation of the interaction of clays with high pH solutions: A case study from the Callovo-Oxfordian formation, Meuse - Haute Marne underground laboratory (France). *Clays Clay Minerals* 2002; 50: 632-645.
- Elie M, Faure P, Michels R, Landais P, Griffault L. (2000) "Natural and Laboratory Oxidation of Low-Organic-Carbon-Content sediments: comparison of Chemical Changes in Hydrocarbons", *Energy and Fuels* 2000; 14: 854-861.
- Kim J I, Artinger R, Buckau G, Kardinal Ch, Geyer S, Wolf M, Halder H and Fritz P. Grundwasserdatierung mittels ¹⁴C-Bestimmungen an gelösten Humin- und Fuvinsäuren. Report: RCM 00895, Technical University Munich, 1995, 221 pp.